AFRL-AFOSR-UK-TR-2011-0010

High Power, Pulsed, RF generation from Nonlinear Lumped Element Transmission Lines (NLETL's)
2nd Year Proposal

Paul W Smith

Oxford University
Engineering Science
Parks Road
Oxford, United Kingdom OX1 3PJ

EOARD GRANT 09-3102

May 2011

Final Report for 19 July 2009 to 19 July 2010

Air Force Research Laboratory
Air Force Office of Scientific Research
European Office of Aerospace Research and Development
Unit 4515 Box 14, APO AE 09421

REPORT DOCUMENTATION PAGE

Form Approved OMB No. 0704-0188

1. REPORT DATE *(DD-MM-YYYY)*	2. REPORT TYPE	3. DATES COVERED *(From – To)*
02-05-2011	Final Report	19 July 2009 – 19 July 2010

4. TITLE AND SUBTITLE

High Power, Pulsed, RF generation from Nonlinear Lumped Element Transmission Lines (NLETL's) - 2nd Year Proposal

5a. CONTRACT NUMBER

FA8655-09-1-3102

5b. GRANT NUMBER

Grant 09-3102

5c. PROGRAM ELEMENT NUMBER

61102F

6. AUTHOR(S)

Professor Paul W Smith

5d. PROJECT NUMBER

5d. TASK NUMBER

5e. WORK UNIT NUMBER

7. PERFORMING ORGANIZATION NAME(S) AND ADDRESS(ES)

Oxford University
Parks Road
Oxford, United Kingdome OX1 3PJ

8. PERFORMING ORGANIZATION REPORT NUMBER

N/A

9. SPONSORING/MONITORING AGENCY NAME(S) AND ADDRESS(ES)

EOARD
Unit 4515 BOX 14
APO AE 09421

10. SPONSOR/MONITOR'S ACRONYM(S)

AFRL/AFOSR/RSW (EOARD)

11. SPONSOR/MONITOR'S REPORT NUMBER(S)

AFRL-AFOSR-UK-TR-2011-0010

12. DISTRIBUTION/AVAILABILITY STATEMENT

Approved for public release; distribution is unlimited.

13. SUPPLEMENTARY NOTES

14. ABSTRACT

This report results from a contract tasking Oxford University as follows: The capabilities of the Oxford Pulsed Power group, in using NLETLs to generate high power soliton bursts, is well established and documented in earlier reports and papers.
This proposal now seeks to establish a continuation programme from that which has been running for the last 7 months. The new package of proposed investigations is based not only on the existing programme but also new developments in the general field of NLETLs reported elsewhere.
It is emphasised that the work proposed above is in addition to that which was proposed in our first proposal and which is still "on going" with 5 months left of the first years funding.
Since the amount of work will increase the additional effort in the group will be supported by 3 additional students who will start 3 research projects based on specific topics from the above programme.

1. A.M.Belyantsev and A.B.Kozyrev, " Influence of local dispersion on transient processes accompanying the generation of rf radiation by an electromagnetic shock wave",Tech.Phys.43(1) pp 80-85,1998
2. N.Seddon, C.R.Spikings and J.E.Dolan, "RF Pulse Generation in Nonlinear Transmission Lines" Presented at the IEEE Pulsed Power Conference, 2007, Albuquerque. Conference Proceedings pp.678-681.
3. P.W.Smith, 'Transient Electronics'. John Wiley. Published July 2002 ISBN : 0-471-97773-X
4. A.B.Kozyrev and D.W.van der Weide, "Trains of envelope solitons on nonlinear left-handed transmission line media", A.P.L. 91, 254111,2007

15. SUBJECT TERMS

EOARD, Solitons

16. SECURITY CLASSIFICATION OF:			17. LIMITATION OF ABSTRACT	18. NUMBER OF PAGES	19a. NAME OF RESPONSIBLE PERSON
a. REPORT	b. ABSTRACT	c. THIS PAGE			A. GAVRIELIDES
UNCLAS	UNCLAS	UNCLAS	SAR	52	19b. TELEPHONE NUMBER *(Include area code)* +44 (0)1895 616205

by CNLR than by nominal unstressed capacitance and inductance according to simulation data . Higher voltage pulsed input capabilities may need to be provided via a thyratron switched generator and a matched high voltage transmission line transformer

5. Each NLTEL system will undergo tests to investigate the effects of varying line lengths (number of sections), varying terminations (high power resistors), and varying inductances. Extraction efficiency from the lines will be studied on single, double parallel, triple parallel and asymmetric parallel line (ASP) systems. Very long lines, not less than 100 stages but ideally several hundred, will be tested, because simulation data implies that interesting and promising effects may be observable on the extension of pulsed soliton burst duration and extraction efficiency.

6. The lines will also tested with an applied DC bias voltage to study the effectiveness of bias control over frequency of operation

7. Investigation of scalability. Because a line with low nominal capacitance values will probably require extra inductance to facilitate optimum soliton-like oscillation, the increase in capacitance inherent in the move to higher voltages may not be a significant problem. This is because increasing the line capacitance reduces the minimum limit on line inductance for oscillation, and thus the line inductance can be reduced. The extent of this compensation will be investigated further. It has recently become clear that driving a given CNLR too hard leads to a loss of oscillation amplitude, which can eventually become complete. Similarly, not driving a given CNLR hard enough leads to a lower than possible maximum frequency of oscillation. Therefore, simply driving a given line harder cannot make up for a lower CNLR. So, a thinner dielectric block will have an optimal driving voltage that is lower than its thicker counterpart, in terms of generating oscillation. These two points are powerful indicators that the NLETL approach to pulsed soliton burst generation may be relatively easy to scale in voltage.

8. Materials technology. Ferroelectric ceramic tiles will be used to build the lumped element lines. Specific dimensions for the tiles will be subject to change, and this results in the major cost of this project. A large number of tiles (hundreds) will be required, though if cutting facilities are available, larger tiles commissioned from the manufacturer may be cut down to smaller sizes. As stated CNLR is vitally important whilst dielectric strength (voltage stand-off) may not be so critical, since driving the CNLR too hard is not desirable (as noted above), and isn't a feasible means of increasing power levels. Although the current plan is to source the tiles commercially, the option exists to attempt to manufacture certain ceramics in-house as has been done in the past.

9. Flashover suppression on the surface of the tiles will be looked at to see if coating the surfaces or machining them in particular shapes can reduce the tendency of the tiles to surface track at high applied voltages.

10. If possible some basic propagation tests would be attempted by connecting some NLETLs to, for example, horn or monopole array antenna systems. This is feasible in Oxford as appropriate shielded facilities exist in another research group within the Department.

It should be noted that the design process for NLETL soliton generating systems has been found to be both complex and sensitive to various parameters. Under very high voltage conditions, simulated data may not prove to be sufficiently accurate for the design process, and as such, some degree of experimentation and modification is expected to be required. These experiments will concentrate on establishing the feasibility of generating very long (hundreds of cycles), very high voltage (mid-line peaks in excess of 100 kV) soliton pulse bursts. The impact of the "extraction problem", and the effectiveness of the ASP configuration method are also important to investigate at very high voltage levels. Power achieved will be taken as the peak power averaged over the first three cycles

1. James D.C. Darling and Paul W. Smith," High Power Pulsed RF Extraction from Nonlinear Lumped Element Delay Lines" Accepted for publication in IEEE Trans Plasma Science. 2008.
2. M.P.Brown and P.W.Smith, ' High Power, Pulsed Soliton Generation at Radio and Microwave Frequencies', Invited Paper Presented at the 11th IEEE Pulsed Power Conference, 1997, Baltimore,MA. Conference Proceedings pp.346-354.
3. P.W.Smith, 'Transient Electronics'. John Wiley. Published July 2002 ISBN : 0-471-97773-X
4. C.R.Wilson, M.M.Turner and P.W.Smith.,' Pulse Sharpening in a Uniform LC Ladder Network Containing Non-linear Ferroelectric Capacitors ' IEEE Trans Electron Devices, Vol.38 (4), pp767-772, 1991

C. FACILITIES/EQUIPMENT:

The pulsed power group in Oxford was established in 1991 and consequently has many facilities/equipment and resources that will be required in this project. However major items of equipment that will be need to be purchased to upgrade existing facilities include a 500 MHz oscilloscope, an updated computer facility and a wide bandwidth 100kV probe.

D. QUALIFICATIONS OF PERSONNEL:

Mr Jamie Darling who will take the major role in this research will be in his 3rd year of research leading to a D.Phil. degree. He already has an M.Eng. degree form Oxford (1st Class). Dr Paul Smith has worked predominantly in the field of pulsed power since 1972, is Reader in the Department of Engineering Science and a Fellow of Pembroke College. His book "Transient Electronics"3 describes much of the work in which he has been involved.

E. SCHEDULE OF REPORTS:

We would anticipate delivering summary progress reports on a three monthly basis and a final full report together with copies of Mr Darlings D.Phil. thesis. With permission of our sponsors we would anticipate publishing several conference and journal articles on this work.

15. SUBJECT TERMS
EOARD, Solitons, Nonlinear Circuits

16. SECURITY CLASSIFICATION OF:			17. LIMITATION OF ABSTRACT	18, NUMBER OF PAGES	19a. NAME OF RESPONSIBLE PERSON
a. REPORT	b. ABSTRACT	c. THIS PAGE			A. GAVRIELIDES
UNCLAS	UNCLAS	UNCLAS	UL	250	19b. TELEPHONE NUMBER *(Include area code)* +44 (0)1895 616205

Introduction

This research project studies the generation of high power bursts of solitons/nonlinear oscillations at radio frequencies from nonlinear lumped element transmission lines (NLETLs) where the nonlinear elements are ferroelectric capacitors or metallised tiles of ferroelectric ceramic. This work leads on from an existing programme where nonlinear tuning diodes or varactors have been used in NLETLs to study and model these phenomena. Earlier work in our laboratories has already demonstrated the feasibility of constructing NLETLs using both strontium and barium/strontium titanates to generate soliton bursts at power levels of tens of MW at frequencies up to 50MHz. This project will study the feasibility of increasing this power to 500MW and above at frequencies of 500 MHz.

The main difficulty with this technology has been one of coupling the RF soliton burst efficiently into a resistive load. Several ways of addressing this problem have been identified using experimental, low power NLETLs constructed using varactor diodes and also from a comprehensive computer model of the behaviour of such lines. This model has been exhaustively tested by comparison with experimental results.

This project draws on these results to move to high voltage NLETLs built mainly using nonlinear ferroelectric ceramics in the form of capacitors or metallised blocks which should be able to deliver high power RF bursts efficiently into resistive loads and antenna's.

This technology has enormous potential in defence. The NLETLs should be able to be developed into highly compact, frequency agile RF sources that could be used in applications such as high power, beam steerable, radar sources, DEWs, and particle accelerators.

Report

The thesis of Jamie Darling is submitted as the report on the first year's activity on the project finishing in September 2009. Again this should be read in conjunction with the other reports already submitted on this project. This thesis provides a complete description of not only the work carried out, but also the background and history to this project. Copies of this thesis have already been sent to AFOSR, Washington, and AFRL, Kirtland who are project sponsors/monitors.

Current work

Work continues on this project thanks to a second year's funding provide by EOARD. As such work is being carried out on nonlinear magnetic, capacitive and hybrid NLETLs and a soliton oscillator. The later has been successfully made to work at

power levels of a few 10's of Watts and is only the second time this type of working system has been demonstrated.

In addition further work on the theory and understanding of the way in which NLETL's of all types operate is under active study. A new modelling system, which supercedes that described in the thesis, has been developed. This will be used to study the effect of loss in the NLETLs as well as the load reflection process seen on capacitive NLETLs. Different NLETL types are also under study to try to find better structures whose ability to generate efficient, high power RF at high frequencies exceeds that of current technologies.

Paul W. Smith
April 2010

High Power Pulsed RF Generation by Soliton Type Oscillation on Nonlinear Lumped Element Transmission Lines

Jamie Darling

Pulsed Power and Plasma Physics Group

Department of Engineering Science

A thesis submitted in partial fulfilment of the requirements for the degree of Doctor of Philosophy in the University of Oxford.

HIGH POWER PULSED RF GENERATION BY SOLITON TYPE OSCILLATION ON NONLINEAR LUMPED ELEMENT TRANSMISSION LINES

D.Phil. Thesis

Jamie Darling

St John's College

Michaelmas Term, November 2009

Abstract

Nonlinear Lumped Element Transmission Line (NLETL) technology has potential value as a source of high power pulsed RF waveforms. Applications include radar and directed energy systems where established pulsed power generators are typically based on vacuum tube or solid state devices.

Simulation data and experiments based on low voltage BB212 varactor diodes have enabled a comprehensive analysis of key trends relevant to the design of such lines, and an enhanced understanding of the phenomenon by which the input pulse to a suitable NLETL may break into a train of high frequency oscillations. The nonlinear–dispersive Korteweg de Vries (KdV) equation has on occasion been associated with electrical transmission lines incorporating dielectric nonlinearity, and the individual pulses in the past identified as soliton waves accordingly. The type of oscillation under consideration has been found here to be directly reliant upon the discrete nature of the transmission line, and mathematically distinct from other continuous soliton solutions. There are, however, indications that the combination of nonlinearity and spatial discreteness leads to wave trains of a solitonic nature, most closely related to the discrete breathers arising from certain theoretical models of nonlinear lattices.

The problem of extracting RF energy, whereby a significant loss of oscillation occurs in the vicinity of a resistive load, has been noted. In order to tackle this important issue several novel ideas are suggested, the most noteworthy of which are the asymmetric parallel (ASP) and periodic loading configurations. High voltage experiments using nonlinear ferroelectric ceramics based on barium titanate have demonstrated good pulse burst generation and improved extraction following encouraging results at low voltage. The success of the periodic loading arrangement supports an alternative approach which would incorporate propagating antenna components directly into the transmission line structure. NLETL pulse bursts have been generated at frequencies of 250 MHz at low voltages and 90 MHz on barium titanate lines operating at several tens of kV, where implied mid-line peak power levels have approached 200 MW. The maximum peak power extracted from a high voltage NLETL to a resistive load is approximately 60 MW. Certain limitations of the ferroelectric ceramic materials currently available have been identified, primarily dielectric loss and electrical strength. Progress made on solving the extraction problem offers motivation for addressing these issues in the near future.

Acknowledgements

The supervision and expert guidance of Dr Paul Smith during this work are gratefully acknowledged. In addition, thanks are due to Luis Caballero and Anthony Dyson of the Pulsed Power and Plasma Physics Group for many helpful discussions and advice. The project has been supported with funding from the United States Air Force Office of Scientific Research and MBDA UK, and it has been a pleasure to work with these establishments. Many individuals at these organisations, and at the Pulsed Power department of BAE Systems in Bristol, have been friendly and supportive. I am particularly indebted to Nigel Seddon of MBDA for working to get me involved with the wider pulsed power and high power RF communities. The D.Phil. itself was enabled by EPSRC funding, and other helpful sources of financial support for conference travel include the Royal Academy of Engineering, the Department of Engineering Science and St John's College.

Nomenclature

ASP
- asymmetric parallel, a specific configuration of NLETLs designed to enhance delivery of RF energy to resistive loads.

BB212
- a common-cathode twin-packaged varactor tuning diode whose capacitance decreases with increasing reverse bias voltage.

CNL
- capacitive nonlinearity, typically referring to a dependence of capacitance on voltage.

CNL ratio
- specific reference to the ratio of nominal (unstressed) to saturated capacitance values where the CNL characteristic may be considered approximately exponential in nature, quantified by the value of cnl_a as defined in equation 5.1.

CNL steepness
- specific reference to the rate at which the capacitance changes (typically decreasing) with increasing voltage, quantified in turn by the value of cnl_b as defined in equation 5.1.

ESR
- equivalent series resistance.

FFT
- fast Fourier transform.

KdV
- Korteweg de Vries equation, a nonlinear and dispersive partial differential equation of interest to NLETL modelling.

NLETL
- nonlinear lumped element transmission line, the adopted term where strong dielectric nonlinearity is combined with a discrete electrical transmission line.

Number of stages, N
- reference to the number of capacitive elements to a given NLETL, which will be one less than the number of inductors and two less than the total number of voltage waveforms measurable from Stage 0 (input) to Stage $N + 1$ (output).

Parallel
- reference to the use of multiple NLETLs connected at input and output to deliver improved oscillation at a resistive load.

Periodic Loading
- an effective method of extracting RF energy from a NLETL to multiple resistive loads.

PFN
- pulse forming network.

PTP
- peak-to-peak quantity.

Soliton
- a specific mathematical wave solution to certain partial differential equations exhibiting nonlinearity and dispersion.

TLT
- transmission line transformer.

VMD
- voltage modulation depth, used to quantify the quality of a given pulse burst in terms of the ratio of peak to trough voltage values, typically averaged over the leading three pulses.

Contents

Chapter 1

Introduction

High power waveforms, in the region of 100 MW and beyond, at radio frequencies (RF) to the order of 100 MHz, have several important applications. For example, certain radar and emerging military systems, industrial processes and particle accelerators rely on bursts of RF energy at substantial power levels. The thesis describes the development of a novel source of high power pulsed RF waveforms to which the term nonlinear lumped element transmission line (NLETL) has been assigned. The circuit under consideration is a uniform electrical transmission line incorporating discrete components, with linear series inductors and strongly nonlinear shunt capacitors. That a wide input pulse may under certain circumstances decompose into a train of many narrow pulses at a much higher frequency has been known for several decades, and explained on the basis of soliton generation by virtue of a delicate counter-balance between nonlinear (concentrating) and dispersive influences. The soliton is a self-reinforcing nonlinear dispersive wave which has several unusual characteristics, and these may be observed in the behaviour of pulses generated on a NLETL.

If the technology could reliably be used to generate trains of solitons at useful frequencies and at high power levels, and the RF energy thus generated delivered to practical loads, this novel technique for pulse burst generation would be of value. Although various issues and limitations quickly became apparent, these have been analysed and tackled quite successfully by several new ideas proposed here. At the time of writing the technology is considered feasible for application if these new concepts are employed, subject to further research into certain limiting aspects of dielectric materials science which have now been clarified (including loss, electrical strength and lifetime).

Chapter 2 offers background and motivation by introducing the capabilities and limitations of established sources of RF pulsed power. Relevant applications and their requirements are also discussed; high power and high frequency waveforms are applicable to an increasingly wide range of tasks and their generation in a given application environment is often technically chal-

lenging. As such, there is a keen interest in developing alternatives to the currently available vacuum and solid state devices, where they might offer advantages such as lower cost, simplicity and compactness. Indeed, research activity on nonlinear transmission lines (in the past referred to generally as NLTLs) has been active for several decades, initially for the curiosity of generating electrical solitons and also for pulse compression and the production of RF energy. That past research is summarised in some detail in chapter 3—progress has been sporadic with a repeated emphasis on the potential value of the concept but poor or at best mediocre practical demonstrations of waveforms, and no published system based on this specific NLETL topology capable of delivering useful RF energy levels to resistive loads.

A revised understanding of the phenomenon is now offered, on the basis of several key design trends and issues which have arisen through work on this project. In chapter 4 the mathematics of nonlinear dispersive soliton waves is reviewed, and solutions to a suitable continuous wave equation derived analytically for study. On the basis of the discrete nature of NLETL oscillation, apparently not previously appreciated, the review extends further into soliton theory to consider discrete lattice breathers. An updated explanation from a rather abstract perspective results, and is complemented by a more physical mechanism of oscillation proposed in chapter 7.

A numerical tool based on the NLETL circuit model has been developed and proved invaluable in supporting experimental work. Chapter 5 briefly introduces its implementation and ability to rapidly test new ideas and to investigate a wider range of design parameters than those reasonably available for experimental demonstration. A significant emphasis has been placed on experimental work on a wide range of lines, with chapters 6 and 8 covering design, construction and testing at low and high voltages respectively. The most immediate issue to be solved was that of extracting RF energy from the NLETL to a resistive load without severely disrupting the oscillation. New line configurations with this in mind have been developed and successfully demonstrated at both low and high voltages. The two most significant of these will be termed

the asymmetric parallel (ASP) and periodic loading configurations, the latter of which is introduced in chapter 7 alongside the discussion of the nature of oscillation mentioned above, which probably underlies its effectiveness.

Concluding remarks are made in chapter 9 in the form of a summary of work completed and of the further research which is considered necessary. Results are encouraging and now suggest feasible application of the technology, but to create a robust system possessing a reasonably long lifetime will require developments in materials science to ensure electrical strength and reduce dielectric loss and, ideally, increase the nonlinearity (ratio of nominal to saturated capacitance values). References are listed at the end prior to the appendices which include code listings and some mathematical derivations.

The work reported in the thesis was presented at the following conferences, and in the journal and proceedings papers referenced here:

- The 16$^{\text{th}}$ IEEE Pulsed Power and Plasma Science Conference,
  17$^{\text{th}}$ through 22$^{\text{nd}}$ June 2007, Albuquerque, New Mexico [1] [2]
- The 2$^{\text{nd}}$ Euro-Asian Pulsed Power Conference,
  22$^{\text{nd}}$ through 26$^{\text{th}}$ September 2008, Vilnius, Lithuania [3]
- The 17$^{\text{th}}$ IEEE International Pulsed Power Conference,
  29$^{\text{th}}$ June through 2$^{\text{nd}}$ July 2009, Washington, DC [4]
  (receiving IEEE Arthur H. Guenther Pulsed Power Student Award)

Chapter 2

Pulsed Power Technology

2.1 High Frequency Waveforms and Applications

The present chapter offers a selective review of RF pulsed power technology: the devices that are currently capable of meeting the requirements of contemporary applications and the extent of their capabilities. Awareness of these applications and associated devices is of direct relevance to the development of NLETL technology, whose deployment potential is attracting increasing interest in the pulsed power RF community. The process of discussing this technology will also introduce the characterisation of important devices and some common terminology used in defining and assessing their performance. As a review of such a complex and wide ranging field the contents of this chapter is inevitably limited in scope, and a wealth of further information will be found via further reading starting with the chosen referenced material. For example, details of constituent parts, such as high voltage power supplies, electron guns and the like, and cutting edge aspects of design should be sought elsewhere.

2.1.1 RF Generation

Prior to considering the technology resulting from a century's worth of research and development in high power RF engineering, the defining nature of RF waveforms will be explored alongside some of their most important and interesting applications. The pulsed power engineer is in general seeking to deliver appreciable quantities of electrical energy on very short time scales. Often a generator will be required to deliver single pulses with specified peak power and leading edge characteristics (indeed, a non-abstract interest in nonlinearity and transmission lines began with the possibility of pulse sharpening as described in section 3.1). High frequency bursts, typically sinusoidal but essentially comprising many pulses, are of more relevance to the present study, and this type of pulsed power waveform will be considered exclusively throughout the remainder of the chapter.

The pulsed power source may provide high frequency energy continuously, or for reasonably

extended periods of time, in which case its output is said to be continuous-wave (CW). Alternatively the application may demand pulses of energy, with each pulse containing a burst of oscillations, and often issues such as electrical breakdown and thermal management will limit the generator to some specified duty cycle at elevated power levels. In such circumstances factors of merit such as pulse duration and pulse repetition frequency (PRF) become important in matching a given technology to its application scenario. In respect of the title of this thesis, the term 'high power' is often taken in this context to signify power levels exceeding 100 MW [5], and the RF spectrum covers frequencies of 30 kHz through 300 MHz. NLETL capabilities also extend tentatively into the lower end of the microwave (MW) regime, which takes the spectrum to 30 GHz [6]. With the ongoing evolution of suitable technologies, and the development of sophisticated new techniques, higher power waveforms at millimetre wavelength frequencies are also emerging.

2.1.2 Wave Propagation

RF waveforms can exist in many forms: in the flow of conventional electrical current, as electromagnetic waves in free space or waveguide structures, by virtue of space charge effects along a corrugated slow wave structure, by spatial density variations in an electron beam and in the amplitude modulation of a laser beam, to give a few examples. Nonetheless it is universally important to establish the elementary definitions of phase and group velocity for an arbitrary wave, especially so in circumstances where a dispersive medium causes their values to differ and their propagation characteristics to be frequency dependent. A forward sinusoidal wave in V propagating over space z and time t is defined in equation 2.1 where A is a measure of amplitude and α, β and ω follow standard notation to indicate attenuation, phase shift and angular frequency respectively.

$$V(z,t) = Ae^{-(\alpha+j\beta)z}e^{j\omega t} \tag{2.1}$$

The nature of wave propagation is characterised by the wave number $k = \alpha + j\beta$, and thus the speed at which a fixed point on the wave progresses through space can be defined as the phase velocity v_p,

$$v_p = \frac{\omega}{k} \tag{2.2}$$

An alternative measure of propagation speed is the group velocity v_g, indicated by the instantaneous relationship between frequency and wave number (equation 2.3). The distinction is relevant to a frequency dependent medium where, for example, the envelope of a wave packet might travel at this lower speed relative to the modulated wave due to dispersive effects.

$$v_g = \frac{\partial \omega}{\partial k} \tag{2.3}$$

2.1.3 RF Engineering Applications

The generation of RF waveforms at elevated power levels is motivated by several key applications which continue to demand simultaneous increases in power and frequency. Increasing range and channel bandwidth of communication systems is a familiar example, although other military and industrial applications are perhaps more aligned with the potential capabilities of NLETL technology discussed in chapter 3. Historically an important application, radar has developed considerably over recent decades to incorporate higher frequencies and ultra-wide band (UWB, [5] [7]) capabilities. A radar pulsed power source will deliver sufficient power to meet range requirements along with the high frequencies necessary to maximise resolution and to minimise antenna dimensions. In addition, by possessing frequency agility a radar system potentially becomes less susceptible to clutter and jamming and capable of reducing ambiguities in target size caused by changing reflection coefficients [6]. UWB radar systems generally place stringent requirements on the quality of propagated waveforms in terms of jitter and frequency stability (discussed for NLETL systems in section 6.2) in order to establish accurate ranging [8]. Furthermore, some processes such as pulse compression are reliant upon more complicated

excitation signals, typically in the form of chirps whereby the instantaneous frequency is increased or decreased over each pulse burst duration (see section 7.4). Short pulse impulse radar utilises a high power pulse with a very quick rise time and wide bandwidth which can offer higher resolution without the need for the signal correlation and complex processing associated with pulse compression. These enhanced radar capabilities open up many new application scenarios including, for example, the line of sight detection of objects on the periscope scale, the characterisation of space debris down to 1 cm dimensions and environmental monitoring [9].

An emerging and relevant application for pulsed power technology is presented by the latest directed energy devices and concepts. Terms such as nonlethal weapons (NLW) and directed energy weapons (DEW) are becoming familiar in defence engineering in relation to offensive capability against electronic equipment, alongside electronic counter-measures (ECM) and explosive ordnance disposal. Often, peak power is preferenced over finesse in these situations [6], although many measures rely on some degree of frequency agility. The application can exploit the high power capability of generators offering frequencies around 100 MHz to 5 GHz [5], which may then also be employed in susceptibility testing of electrical equipment.

Further established and novel requirements for pulsed power generation might also prove to be within the scope of NLETL technology. These include industrial processes such as the surface modification of materials [10] and plasma fragmentation of waste concrete [11] [12] and environmental decontamination. Magnetically confined plasmas involved in controlled nuclear fusion experiments require significant heating which is typically achieved at one of several plasma resonant frequencies, the lowest of which is around 100 MHz [13], although often work in this area is concentrated on much higher frequencies in the millimeter wave spectrum. Also of scientific interest, linear accelerators have in the past played a significant role in shaping the development of several RF devices discussed in the following sections—where heavier particles are involved frequency specification may be below 1 GHz.

Primary interest in this work at this time has related to directed energy and radar applications and it is anticipated that the novel approach to pulse burst generation could compare favourably with alternative systems. In addition to fundamental capability, a realistic application is likely to make further specifications in terms of lifetime, robustness, expected failure mechanisms, packaging requirements and operational efficiency. The latter inevitably becomes increasingly important at higher power levels, although acceptable values of efficiency vary widely between devices depending on requirements and the nature of operation [13]. The economics of manufacture may also prove decisive, either for small one-off batch production or in the case of predictable long term demand. There are interesting comparisons to be made in this respect between the two main classes of RF pulsed power technology: solid-state power amplifiers (SSPAs, section 2.2) and microwave vacuum electron devices (MVEDs, section 2.3).

2.2 Solid-State Power Amplifiers

One approach to RF pulsed power generation which is increasingly popular is the use of solid-state electronic devices for switching and signal amplification. A typical power semiconductor device is the gallium arsenide (GaAs) field effect transistor (FET), although various semiconductor materials have attracted interest, most recently silicon carbide (SiC) and gallium nitride (GaN). A fundamental and important limitation of solid-state power amplifiers (SSPAs) is the fact that electron transit times mean the interaction region has to be small at high frequencies. To avoid breakdown at high power levels, the maximum operational voltage is limited accordingly and so, to develop a given power, the current flowing through the device has to be quite high. Wide band-gap semiconductor materials such as SiC and GaN break down at a higher voltage and are hence able to operate with lower currents for a specified power [6]. As the high current of a SSPA flows through a solid medium, losses and heating reduce efficiency and place significant requirements on cooling the small interaction region area and on packaging design.

SSPA devices may then struggle to meet the demands of some high power applications, but with minor modification it is possible to power-combine many transistors if a stable arrangement with minimum jitter can be realised. This is an approach well suited to driving electronically steered phased array antennas and at moderate power levels each amplifier can be suitably compact. The PRF of SSPAs tends to be low because the turn-on time for a transistor to establish its active junction depletion layer is quite long, typically close to a millisecond. But once up and running their bandwidth can be large, perhaps covering 100 MHz to 1 GHz [6] giving them appreciable wide band capability. Cost is variable with specifications and often the complexities of cooling and packaging dominates the expense of manufacture, but they can be relatively cheap to produce in large numbers if based on existing processes. Conversely, the vacuum devices discussed in section 2.3 are slow and complex to assemble and rarely benefit so heavily from the savings of batch production. A bespoke SSPA design subject to a one-off or fluctuating market for demand may become prohibitively expensive due to the nature of semiconductor manufacturing techniques.

The SSPA option has several benefits including high bandwidth and flexibility, although a further disadvantage of note is their susceptibility to radiation and extremes of temperature without adequate protection. Solid-state amplification is often used for CW operation at low or moderate power levels, up to 10 kW or so, and frequencies below about 1 GHz.

2.3 Microwave Vacuum Electron Devices

The microwave oven 2.45 GHz magnetron presents an unusual manufacturing scenario for microwave vacuum electron devices (MVEDs), in that the market has proved sufficient to justify very cheap, automated and fast production. More generally, high power vacuum devices are quite specialised and time consuming to manufacture, but for applications demanding uncompromised power and frequency performance the MVED route is usually preferenced over the solid-state alternative. In this section the fundamental principles behind MVED operation are

first presented, and from this introduction some benefits for handling high power and high frequency quickly become apparent. Three types of radiative process associated with moving electrons are also introduced, along with some of the most important corresponding MVED approaches to RF generation and amplification.

Effective conversion of DC input energy to output RF energy is achieved using a high current, high mobility, beam of electrons subject to velocity modulation by a small signal input waveform. The density micro-bunching of charged electrons resulting from this interaction involves high levels of RF power which may be extracted prior to a separate electron collector and necessary cooling arrangement. Electrons might radiate in a spontaneous and uncorrelated manner by the processes of transition, Cherenkov or Bremstralung radiation, but the necessary requirement for a useful RF output is coherent radiation in phase achieved with, for example, localised bunches of electrons.

2.3.1 Transition Radiation

Transition radiation occurs when moving electrons experience a change in material refractive index, or some perturbation in propagation medium such as a conducting grid or, as in the case of the klystron amplifier, a short gap resonant cavity [14]. A high voltage power supply is used to generate a high current electron beam whose velocity is modulated in a 'buncher' cavity by the input signal. A second 'catcher' resonant cavity is placed so as to pick up the beam at the point where this velocity modulation has led to fully developed bunching of electrons, and to select the harmonic frequency of the impulsive beam. Initial work was carried out on this technology around 1939 [15] and since that time the fundamental principles have been maintained, subject to some increasingly sophisticated modifications and enhancements. The klystron MVED is inherently fairly narrowband and has delivered stable high power amplification to GW power levels at frequencies from 200 MHz to 100 GHz for certain applications [6]. High

frequency operation is, as ever, subject to certain limitations, and in this case the width of the cavity gaps must be comfortably less than the operational wavelength to maintain a coherent waveform. Thus limitations on power are enforced by electrical breakdown, and so modified klystrons were duly developed with multiple interaction cavities and enhanced electron beam arrangements. Their performance for narrowband high power applications is undoubtedly impressive, although a further issue is generally weak coupling of the RF field to the electron beam with individual cavities. Another class of linear beam MVED, utilising what is termed a slow wave structure (SWS), is perhaps therefore a logical development in being based on a continuous interaction process.

2.3.2 Cherenkov Radiation

In fact, both linear beam SWS and crossed field devices (magnetrons for example [14]) can be associated with an alternative emission process, termed Cherenkov or Smith-Purcell radiation, with the latter name sometimes specifically attributed to the MVED situations of interest here. The necessary interaction is found to occur when the phase velocity v_p of an electromagnetic wave is less than that of the travelling electrons. This is clearly an unusual situation requiring a large wave number, at least greater than unity even for relativistic electrons (travelling near to the speed of light), and is achieved by subjecting the wave to a periodically loaded transmission medium to bring its phase velocity down to that of a co-propagating electron beam [16]. The travelling wave tube (TWT) is built around a corrugated helix slow wave structure which achieves Smith-Purcell interaction and energy transfer with a concentric electron beam, once again of high mobility due to vacuum conditions. Upon being coupled into the input end of the helix, a small input RF signal initiates electron bunching and subsequent to this a continuous interaction process rapidly builds up the electron densities and electromagnetic wave amplitude [17].

Whereas in a TWT the group velocity of the slow propagating wave and the electron beam are in the same direction, an alternative but closely related device is the backward wave oscillator, or BWO, which operates under the different condition of a negative group velocity such that the RF output is delivered from the electron gun end of the SWS having built up in the opposite direction [13]. The operation of a BWO can in some sense be considered a feedback process [17] but in any case both the TWT and BWO are best summarised on a dispersion diagram (figure 2.1), where the dispersion curve high k region of interaction represents a backwards wave [18].

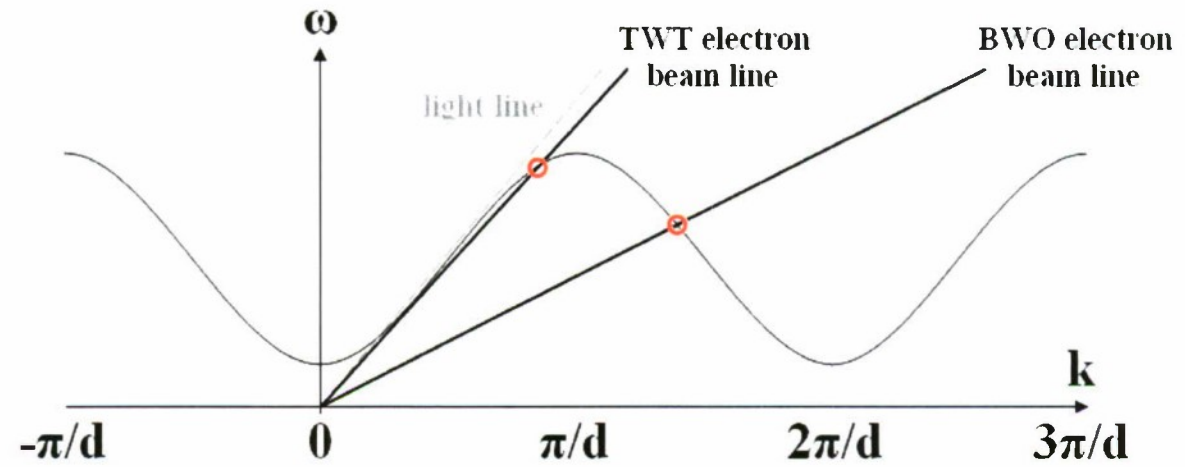

Figure 2.1: Illustrative periodic dispersion diagram for a slow wave structure (SWS) superposed with the dispersion characteristics of the electron beams utilised in TWT and BWO devices. A positive gradient corresponds to a positive group velocity (equation 2.3) and visa versa. The SWS dispersion pass band can be quite large, meaning wide bandwidth operation is feasible.

The TWT and the BWO are potentially wide bandwidth amplifiers and have found extensive use in communications and associated applications accordingly. The high frequency and power issue in this case is the requirement on the SWS period to be substantially less than a whole wavelength, and on small clearances for good coupling effects. As such, new material microfabrication techniques are playing an important role in developing the latest MVED technology [6].

2.3.3 Bremsstrahlung Radiation

A third type of radiation, Bremsstrahlung, is applicable to several important MVEDs [13] such as the cyclotron resonance maser (CRM) and the free electron laser (FEL), and results from the motion of electrons in a constant or periodically varying magnetic field respectively. Transitions between kinetic energy levels have associated with them a specified cyclotron frequency [19], and an electromagnetic wave whose frequency is close to a harmonic of a characteristic electron oscillation frequency can partake in a cumulative interaction process [6].

In summary, the MVED approach often benefits from the ability to handle very high power levels in small interaction volumes, due in part to the high electrical strength of the electron beam vacuum space but thanks also to the presence of a separate collector and larger cooling area. The vacuum also leads to good immunity against ionising radiation, and impressive lifetimes before any failure in the space environment have been repeatedly demonstrated by SWS MVEDs in satellite communications. Typical vacuum components have the disadvantage of being more noisy than their SSPA equivalents however, with noise figures in excess of 20 dB versus perhaps 2-5 dB [6]. Furthermore, almost all pulsing MVED devices often suffer from pulse shortening when stretched to their working limits [13], whereby the output RF burst duration is shorter than that of the driving voltage pulse. This may be due to a build up of space charge (decelerated electrons), plasma generation within the high frequency circuits or at the collector, or general RF breakdown effects, and limits single pulse energy delivery. Nonetheless, at the highest power levels and frequencies, the application customer will usually look to vacuum options over solid-state. In recent years a hybrid option has been conceived and is mentioned in the following section.

For a comprehensive review and detailed information on the latest vacuum devices and capabilities the 2005 book by Barker et al is highly recommended [6].

2.4 Hybrid and Alternative Technologies

In principle, high power electrical switches such as spark gaps [20] may be switched at high repetition rates in the pursuit of high frequency pulsed power waveforms, and good switching characteristics at very high voltages are feasible with carefully designed compact spark gaps operating with sulfur hexafluoride (SF_6) gas, transformer oil or even some solid materials for example. However, this approach is overshadowed by dedicated solid-state or vacuum electron oscillators and amplifiers for the frequencies and applications of interest. Issues quickly arise at high repetition rates due to poor repeatability and lifetime, and multiple gaps are inevitably subject to some jitter which degrades combined performance. The effective speed of a spark gap switch transition is linked to its unavoidable inductance and a resistive phase time [21], and of course directly related to the highest achievable switching rate.

Another completely different approach has been developed and successfully marketed by BAE Systems [1] in recent years. A nonlinear transmission line, distinct from that considered in this work by its magnetic rather than dielectric nonlinearity, and incorporation of alternate stage linking capacitors, generates 30 ns pulse bursts at up to 20 MW peak power and GHz frequencies [22]. Operation is based on conceptual work carried out by Kozyrev et al in Russia in the 1990s [23] [24], whereby the stated nonlinear line configuration is used to realise a 'multi-layer heterostructure' supporting the creation of a high frequency monochromatic wave (not of soliton nature). Analysis of this process is complex [23], but concedes the fact that a wide propagating drive pulse may develop oscillations, one at a time in a progressive manner, from its sharpened leading edge. The resulting train of oscillations grows and moves back through the main pulse at a relative speed which is the difference between the shock front velocity and the group velocity of the generated monochromatic wave. The BAE Systems generator was developed in their Pulsed Power group in Bristol, UK, and through careful design is capable

[1] BAE Systems plc. Advanced Technology Centre, Sowerby Building (20R), FPC267, PO Box 5, Filton, Bristol, BS34 7QW. http://www.baesystems.com.

of producing good quality RF waveforms with some amplitude droop but useful pulse burst durations of perhaps 30 oscillations, and at a PRF of 1 kHz. Efficiency is limited by the reliance on quite a large number (hundreds) of stages in the nonlinear transmission line in order to facilitate full development of the high frequency waveform, and on the magnetic materials involved. A controllable bias current offers frequency variability and due to good phase stability several units may be power combined if necessary. Recent further work by Belyantsev and Kozyrev [25] [26] has been published which features a numerical and theoretical study of a millimetre wave RF generator in the 100-300 GHz regime based on a microfabricated multi-layer heterostructure. The study is of interest, specifically in its predication of sufficiently low loss to reach such high frequencies, but relates to much lower power levels. Low power high frequency electronics is a distinct field in itself, serviced by a wide range of different technologies such as Schottky diodes and Gunn devices, and outside the scope of this current work.

The 1991 'tri-service US Department of Defence vacuum electronics initiative' [27] resulted in the Northrop Grumman Corporation [2] development of a high power microwave approach combining a SSPA driver and a high efficiency reduced gain TWT [6]. The resulting microwave power module (MPM) avoids reliability issues associated with higher gain travelling wave tubes and has in practice realised a noise figure of 10 dB compared to the 30 dB expected from a comparable stand alone TWT. CW RF output has been delivered in this way at 50–200 W over 2–40 GHz and individual units may feasibly be power combined; for context a directly relevant application has been suggested to be towed decoys for fast jet electronic counter-measures [28].

The above devices, SSPAs, MVEDs and various alternatives, are in many cases elegant and highly capable solutions to the current demands of the RF pulsed power community. They are often found to be rather specialised, expensive and inevitably subject to some performance com-

[2]Northrop Grumman Corporation. 1840 Century Park East, Los Angeles, California, 90067–2199. http://www.northropgrumman.com.

promise when exposed to the most demanding applications; there exists a keen interest within the RF pulsed power community in novel approaches to work alongside established technology. The generation of soliton–type oscillations on nonlinear lumped element transmission lines is a case in point, and has indeed attracted renewed and intense attention during the past few years [29].

2.5 Pulsed Power Antennas

The process of efficiently radiating and receiving an RF signal as a free space electromagnetic wave is reliant upon some form of antenna. The state of the art in impulse and microwave antenna design [5] [30] is of direct relevance to several application scenarios mentioned in section 2.1 but falls outside the scope of the current work. In anticipation of the experimental work covered in section 6.6 some more elementary aspects of microwave antenna operation are discussed briefly here.

The dipole element establishes a standing wave according to the relationship between its electrical length and the wavelength of interest, and is in principle quite suited to microwave frequencies [31]. The necessary condition of resonance, and corresponding stability in radiated electric and magnetic field components, is only achieved satisfactorily within a relatively small range of wavelengths. Stray reactances and end effects influence the optimal length and in practice cause the centre and end feed impedances of a half-wave dipole, ideally zero and infinite, to be around 70 Ω and 2.5 kΩ respectively. The antenna is resistive under good resonant conditions whereas a short dipole becomes capacitive and a long one inductive—in both cases its efficiency is reduced. Loops tend also to radiate an RF signal by virtue of their magnetic field component, although with generally low efficiency even when tuned appropriately. Larger antennas will typically have a null in the plane of the loop whereas smaller loops, of conductor length less than $\lambda/10$, have a directional pattern perpendicular to this [30].

Issues with an electrical current oscillating at very high frequencies, such as the skin effect, dielectric loss and leakage radiation, lead to the use of waveguides for moving signals around as electromagnetic waves. These are typically hollow tubes and the arrangement is conceptually similar to an infinite number of quarter wavelength shorted stubs across a central conductor, each of which is ideally of infinite input impedance. Coupling to free space may then be achieved, for example, by tapering the end of a waveguide to create a horn antenna, perhaps for use in conjunction with a reflecting dish.

The effective bandwidth of a given antenna tends to be limited by adverse effects on either its impedance or its gain pattern, and many configurations have been developed in order to achieve more broadband operation. Specific designs include the log-periodic and discone antennas (section 6.6), and during construction measures such as increasing the cross sectional area of conductors may also enhance bandwidth somewhat. Applications often benefit from antenna directionality, or gain, which typically results from interference effects between radiated wave components. An array of dipoles or waveguide slots will present an end-fire gain pattern when fed in anti-phase and separated by a quarter or half wavelength free space propagation delay, whereas an array of elements excited in phase will tend to have a perpendicular gain pattern, or array factor (figures 2.2 and 2.3). In the latter case there isn't the same requirement on element spacing, since the sideways pattern results simply from constructive superposition, although the use of very small spacing leads to super-conductive effects and a drop in efficiency and is not ideal for predictable operation [30]. Arrays tend to have reasonable bandwidth [31] and in practice are sometimes stacked or combined with some form of reflective surface for improved gain characteristics [32].

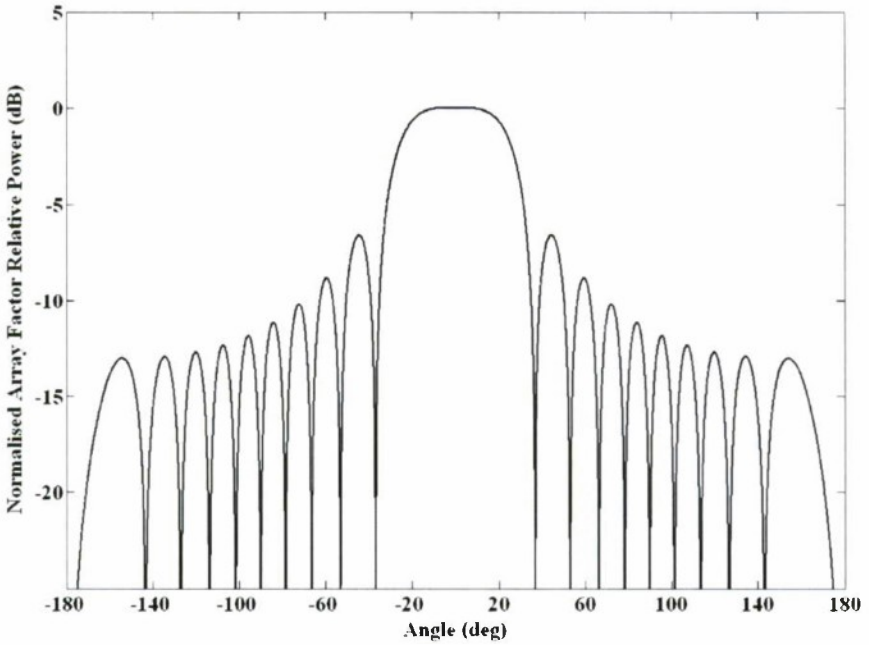

Figure 2.2: Superposition array factor calculated for an end-fire series of 20 arbitrary antenna elements. Multiplication by the directional pattern of each element results in that of the total field, but in the case of dipoles which are approximately omnidirectional in the plane perpendicular to their axes, the array factor is an accurate representation of overall directivity in this plane. Here, the elements are fed subject to a $\pi/2$ phase shift and the inter-element spacing is $\lambda/4$, an arrangement offering maximum gain in just one direction. A π phase shift and $\lambda/2$ spacing would result in end-fire gain in both the forward and backward directions.

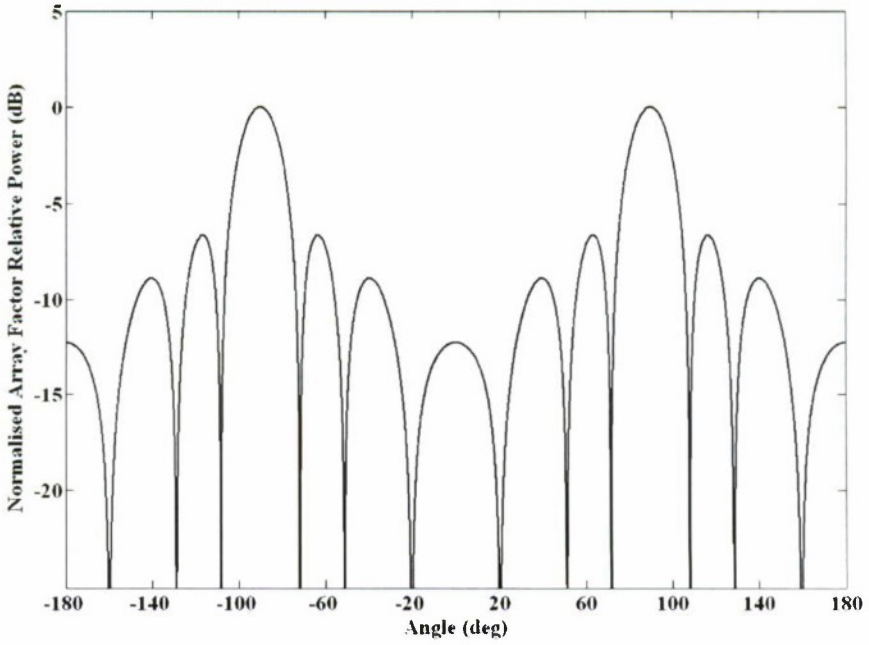

Figure 2.3: The broad-side array factor corresponding to 40 antenna elements receiving phase matched excitation signals, with a $\lambda/12.5$ spacing equivalent to 8 cm between elements operating at a frequency of 300 MHz, or free space wavelength of 1 m.

Chapter 3

The Nonlinear Lumped Element Transmission Line

3.1 Background to the NLETL Concept

The current work is concerned with the generation of RF signals, potentially at high frequencies and power levels, by using a length of nonlinear lumped element transmission line (NLETL) to convert a relatively long input pulse into a wave train at much higher frequency. Some discussion on how a NLETL operates may be found in chapter 7, and more detailed information on soliton waves is presented in chapter 4 which includes some of the relevant analytical work carried out. This chapter will first introduce the nonlinear lumped element transmission line and associated notation adopted throughout the thesis. The discrete NLETL will be compared and contrasted with the approximately continuous nonlinear distributed shock lines employed to reduce leading edge rise times for certain pulsed power applications. The 1970s saw electrical transmission lines used to create special pulse-like waveforms thought to be solitons, an approach apparently inspired by the analytical work of Toda in 1967 on nonlinear one dimensional lattice waveforms. In due course, the motivation of potential application to RF systems was added to what had previously been a scientific curiosity. A summary of that research is provided in section 3.2, prior to a review of the type of dielectric material used in the experiments of chapter 8 to realise the necessary NLETL nonlinearity at high voltage.

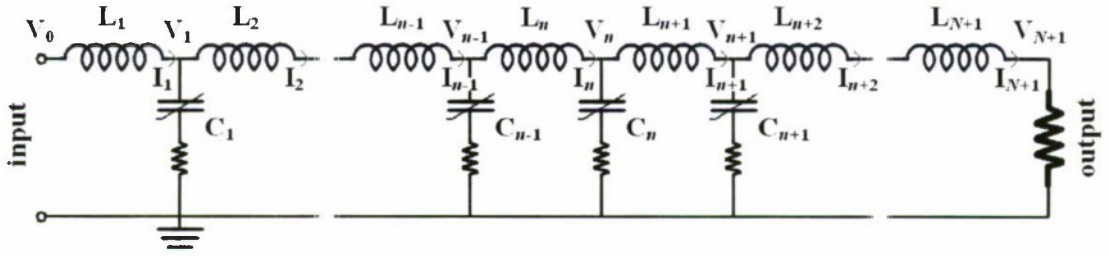

Figure 3.1: The standard nonlinear lumped element transmission line circuit configuration, illustrating the stage and component numbering conventions used throughout, with linear inductors, nonlinear capacitors and ESR resistive loss. The line is N stages (capacitors) in length; the input and output ends are shown along with some interim stages.

Figure 3.1 illustrates the concept: a lumped element transmission line is shown consisting of series inductors, which are taken (in most cases) to be linear, and shunt capacitors which

are strongly nonlinear. The capacitive nonlinearity (CNL) may for practical purposes be approximated by an exponential decrease in capacitor value with increasing voltage (section 8.3). Capacitor voltage measurement points relating to the discrete sections of the line will be referred to as 'stages', with the input labelled stage 0, the waveform at the first capacitor stage 1 and so on up to the output stage $N + 1$ where N is the length of the line, defined here as the number of capacitive elements. With reference to the numerical model detailed in chapter 5, the inductors are nominally identified numerically from input to output as 1 through $N + 1$ and the capacitors from 1 through N. The stage 0 voltage is that developed at the input to the NLETL by the pulse generator source subsequent to the influence of its output impedance. Also included in figure 3.1 are resistors representing the loss induced by capacitor equivalent series resistance (ESR), and isolation capacitors at the input and output of the line which allow a DC bias voltage to be established prior to additional pulse propagation (section 6.2).

A nonlinear electrical circuit is one whose component parameters depend on instantaneous voltage or current values. Important points are the fact that whilst a linear circuit does not broaden the frequency spectrum of a propagating signal, the introduction of nonlinearity can lead to energy being shifted in frequency, and that Kirchoff's conservation laws still hold subject to the nonlinear dependencies being taken into account [33]. The numerical model of chapter 5 is reliant on Kirchoff's laws, and a frequency up-shift effect is evident in NLETL behaviour. It is also interesting to note that nonlinear damping properties in a physical system may under certain circumstances lead to self-sustained oscillation and periodic motion from a constant input energy flow [34]. This may be compared to any linear system which would require a periodic source of energy to sustain any kind of periodic motion.

3.1.1 Continuous and Discrete Transmission Lines

Before considering the specific form of nonlinear transmission line illustrated in figure 3.1, it is instructive to review the preceding use of nonlinear pulse propagation for pulsed power ap-

plications. Where a requirement exists for the delivery of a high power pulse front within a very short time period, a nonlinear line can be used to steepen the leading edge of the pulse if the nonlinearity acts to increase velocity with amplitude [35]. The first such lines were 'magnetic' in that they were based on saturating inductors [36], as opposed to nonlinear dielectrics (in addition to shock lines, the total duration of a pulse may be reduced, and its amplitude increased, by use of the Melville magnetic line whose tapered component values progressively compress the pulse [20]). The formation of a shock front is subject to a minimum limit on rise time, set either by discrete line characteristics or, if the line is effectively continuous, by material properties. A typical state of the art system in 1988 was able to deliver 70 kV pulse rise times of 350 ps to 50 Ω, and also demonstrated 95 kV in 380 ps [37]. Sub-nanosecond pulses are extremely fast in this context, but attention was also subsequently paid to the development of 'dielectric' shock lines incorporating nonlinear capacitance instead of inductance. This approach has demonstrated, for example, a reduction in 20 kV rise time from 500 to 120 ns [38], 28 kV from 280 to 50 ns [39] on lumped element lines, which were sometimes found to also generate the high frequency oscillations of immediate interest. Similar work on more continuous distributed lines reported no such oscillations [40], only the formation of a steady state shock front.

The distinction between a continuous transmission line, or a discrete network tending to the continuous limit, and a discrete lumped element transmission line is extremely important in the context of the current research, and yet has not been clearly made in the literature prior to this work. Good NLETL pulse burst generation is now understood to be reliant both on a suitable CNL characteristic and on line discreteness. As such, the term nonlinear lumped element transmission line (NLETL) has been introduced to distinguish soliton generators where the resulting pulses are bound to the discrete stages of the line from other nonlinear transmission line (NLTL) systems, which behave more as nonlinear continuous media, with dispersion (section 2.4).

3.1.2 Soliton Type Oscillation

The high frequency oscillations just mentioned were noted at around 15 MHz during dielectric shock experiments at the University of St Andrews in the late 1980s, and this stimulated further interest in the phenomenon within the Pulsed Power and Plasma Physics Group. The individual pulses generated in this way on a NLETL were concluded to be solitons as early as 1973 by Hirota and Suzuki [41] amongst others, the soliton being a stable pulse-like wave created and sustained out of a delicate counter-balance between nonlinear (concentrating) and dispersive (spreading) effects. Chapter 4 provides an insight into the fascinating nature of these unique waveforms from a mathematical perspective, and may be consulted along with chapter 7 for several new ideas on the true solitonic nature of NLETL oscillations.

Under suitable conditions (section 6.3) a reasonably narrow arbitrary pulse applied to the NLETL of figure 3.1 will be reformed fairly quickly into a smooth symmetrical pulse somewhat sharper in profile, and propagate down the line as such thereafter (figure 3.2). The line capacitive nonlinearity, and the dispersion associated with it being discrete, are thought to result in a physical realisation of the nonlinear–dispersive soliton wave. In itself, this is useful where pulse compression is required, since both the rise and fall times are reduced by propagation along the NLETL and the resulting pulse typically has a reduced total time duration, as well as amplified peak voltage. Increasing the input pulse width will initially lead to an increase in soliton amplitude. But a fundamental property of solitons is that their width decreases with amplitude, and at some point a sufficiently wide input pulse is seen to form two solitons (figure 3.2). As the driving pulse width is further extended more and more of the narrow pulses are generated, and the effect is simultaneous throughout the pulse although it typically takes several stages for the modulation to become fully developed. In this way, only a few stages, perhaps 10–15, are required for a NLETL to create a high frequency RF waveform of amplified peak voltage, good voltage modulation depth (VMD) and hence peak-to-peak power, as seen in figure 3.3. It will be subsequently noted that more line stages can be beneficial for the generation of longer

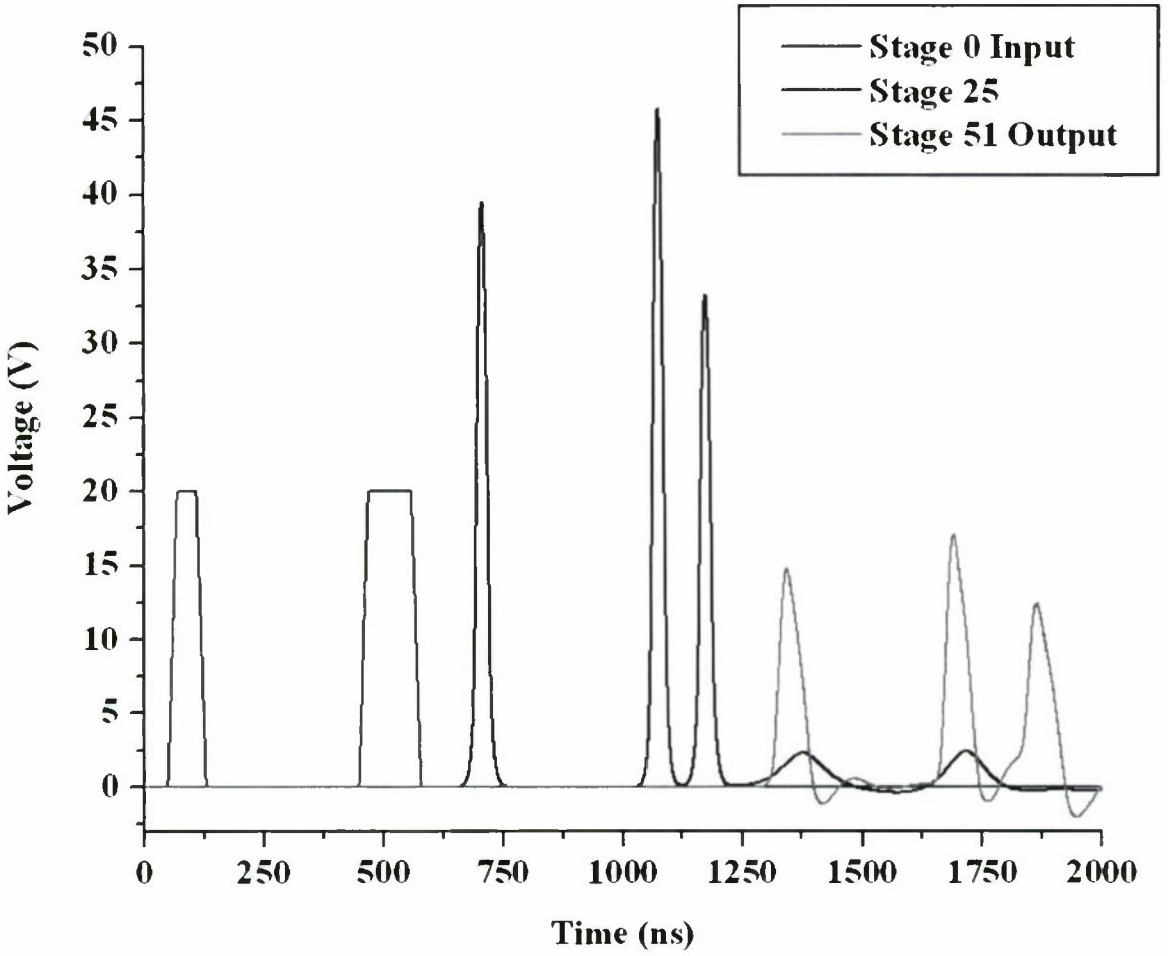

Figure 3.2: Simulation results for a 50 stage 2 μH 600 pF NLETL with a short input pulse followed after a slight delay by a wider input pulse. The first pulse evolves into a single soliton while the second forms two. Extraction of each individual soliton pulse to the resistive load (80 Ω in this case) is typically accompanied by a reduction in amplitude and corresponding increase in width.

pulse burst durations due to the disrupting influence of the inevitable reflections which occur at a linear termination. The frequency shifting effect is clearly illustrated in the spectrum information of figure 3.4 obtained by Fourier transform.

The NLETL pulse burst generator is thus a very simple but high performance RF source in principle, which may be scaled to high voltages to service the high pulsed power requirements of several applications (chapter 2). There are, however, reasons why the technology has yet to find deployment despite the many benefits summarised in section 3.4 and several decades of awareness of the phenomenon. These have become clear during the course of work on this project, and include for example the problem of extracting the high frequency energy to a resistive termination, which may be seen in figure 3.3. There has also been a clear need to carry out a comprehensive characterisation of the influence of several different parameters on the quality and properties of pulse burst waveforms generated in this way. Progress in this area, along with an improved understanding and interpretation of NLETL behaviour, has revealed several key design trends (section 6.3) and has led to various ideas for addressing issues such as the extraction problem.

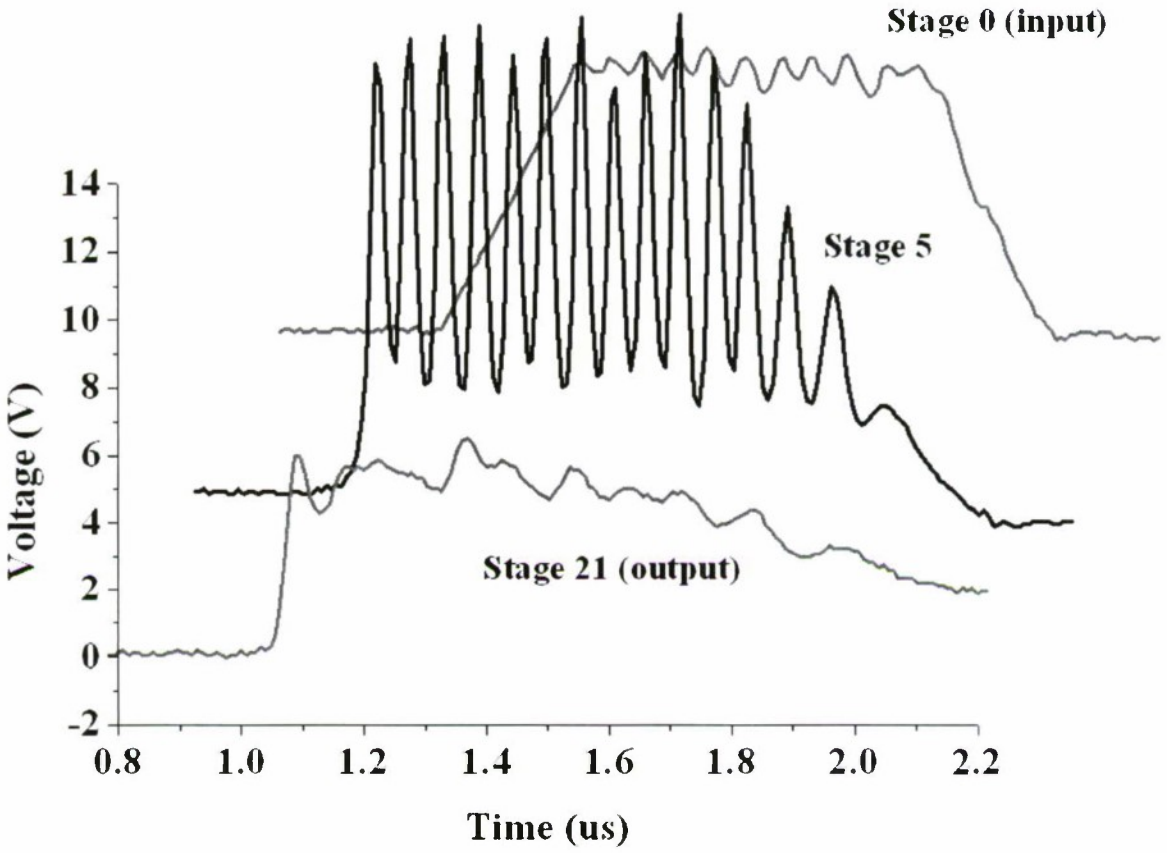

Figure 3.3: Extended pulse burst generation via a wide input pulse on an experimental low voltage NLETL.

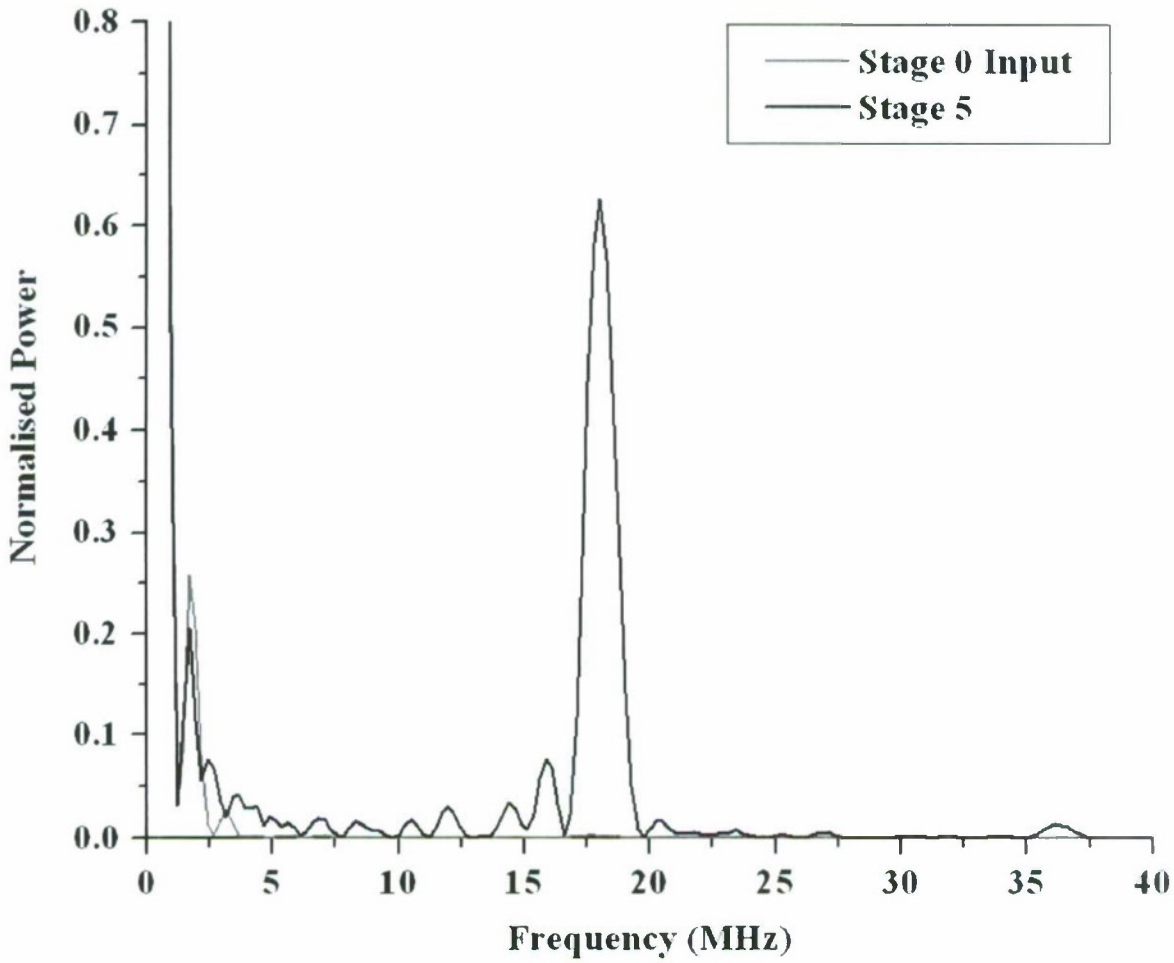

Figure 3.4: Fourier transform data corresponding to the input and stage 5 voltage waveforms of figure 3.3.

3.2 Review of Research 1970 to 2006

The creation of electrical solitons on nonlinear transmission lines has been researched around the world over the past few decades and continues to attract widespread interest. The following review of published literature on the subject will summarise the state of this research at the time the current project became involved in efforts to match the technology to RF applications. Certain aspects of the materials science behind achieving strong dielectric nonlinearity at high voltages are considered separately in the following section—it will become clear in subsequent chapters that material properties play an important role in the design and operation of NLETL systems. As previously mentioned, interest at the University of Oxford originated from pulse sharpening work with dielectric shock lines [42] which was followed by specific work investigating the RF application potential [43]. It should be noted that some of the analysis of early work on the topic doesn't always tie in with the latest understanding developed from the current project, which has evolved to take into account a broader review of solitonic wave theory (chapter 4) and several previously unrecorded observations (chapter 6 and chapter 7). The subject is more complex than perhaps implied by first impressions however, and the detailed and careful work by the authors referenced in this section should be recognised. The review will exclusively consider what has now been termed the nonlinear lumped element transmission line (NLETL), i.e. the dielectric lines associated in the early 1970s with solitons. Throughout this period, soliton theory was rapidly developed and applied to mathematical and physical systems in fields such as biology, plasma physics and optics. Having laid dormant as a fascinating but largely irrelevant mathematical curiosity, the soliton was thus becoming quite topical in many areas of science and engineering (see chapter 4).

Two papers were published by Toda in 1967 [44] [45] and are universally referenced by the first few authors who presented work on nonlinear transmission lines. These papers provided detailed analytic solitary wave solutions to the equations of motion of a one dimensional lattice with nonlinear interaction forces, and the concept of doing something similar with an electrical

system appears to have been inspired by them. Toda demonstrated, amongst other things, that a discrete system with nonlinear coupling between neighbouring particles can support normal modes such that each particle may oscillate with similar amplitude and frequency, and considered the resulting vibration to be a train of solitary waves. Soon after, in 1973, Hirota and Suzuki [41] observed the key properties defining soliton behaviour on a NLETL, including the curious nature of interactions. There were some relevant ideas relating to interactions in that work, which are noted in section 4.2. These first experiments were conducted at low voltages, with the transmission line considered to offer a means of investigating the unusual properties of real solitons in a physical system rather than for any specific application. The following year Kolosick et. al. [46] published results from a 50 stage NLETL based on the Western Electric F54837 varactor diode which was found to be sufficiently nonlinear under reverse bias voltages. Similar results were obtained, with more properties demonstrated for single soliton pulses, such as the relationship between amplitude and velocity of propagation. At the time the phenomenon was considered to provide a "direct analogy" to the solitons recently observed in ion-acoustic plasmas, a point considered further in chapter 7. Numerical modelling work was carried out by Daikoku in 1975 [47] using the Runge-Kutta-Gill method, and although this didn't offer any remarkably different results it reinforced the preceding experimental work by demonstrating properties and interactions. Further developments were made by Nagashima and Amagishi in 1978 [48], with another low voltage NLETL based on commercially available diodes and a theoretical study which addressed the issue of dissipation and loss in some detail. Motivation was still provided by the opportunity to create a physical realisation of the solitary waves associated with Toda's lattice, and results thus far focused on the generation and propagation of single pulses. These early electrical soliton-type waves were just a few volts in amplitude and not particularly sharp due to high line inductance values (tens of μH) and CNL characteristics which were probably relatively poor (chapter 6).

A 1977 paper by Lonngren [49], a co-author of Kolosick's 1974 paper, presented a wide ranging

study of the concept, once again as a model for other physical soliton phenomena. Experimental waveforms clearly showed the generation of multiple solitons from longer input pulse durations on this occasion. The nonlinear dispersive Korteweg de Vries (KdV) equation has been variously attributed to the NLETL system, and in itself this has served in part to justify the labelling of NLETL pulses as solitons since the KdV equation is known to support such solutions. An assessment of the published derivations culminating in the KdV equation is carried out in some detail in section 4.2, but Lonngren at this time, amongst several others since, makes the link on the basis of a long wavelength assumption. Whilst the latest work may cast doubt on the direct relevance of the KdV equation, this is not to suggest the NLETL waveforms are not solitonic in nature (chapter 7), and indeed Lonngren also investigated several characteristics specific to solitons, including both overtaking and head on collision interactions and the Fermi-Pasta-Ulam recurrence phenomenon [50]. Contributions by Jäger in 1978 and 1982 [51] [52] were also based on low voltage diodes, this time the BB142 varactor tuning diode, with the KdV equation introduced under the assumptions of weak nonlinearity and dispersion. The physical nature of the generation of solitons was discussed and associated with a delicate counter-balancing of nonlinear and dispersive effects resulting in a steady state wave of permanent profile. Pulses were generated at quite high frequencies, around 100 MHz, but only singularly or in pairs once again. The second of these papers considered the limitations imposed by losses at higher frequencies and mentioned work on a 500 stage BB142 line.

The scene was set in June 1988 for the application of the concept to high power RF generation with the first of four papers published by Ikezi et. al. over the following two years [53] [54] [55] [56]. During this period an initial feasibility study considered using extended bursts of many soliton pulses to provide a source of RF energy, and scaling previous low voltage experiments to much higher power levels by using a nonlinear ferroelectric in ceramic form as capacitor dielectric material. Some low voltage work was also carried out with the Motorola MV209 varactor diode, investigating soliton properties and specifically the temporal contraction of individual

pulses via tapered inductance values. But experimental progress and proof of concept was made with a high power NLETL based on barium strontium titanate (BST) ceramic tiles operating at room temperature. The waveforms so obtained were fairly poor in terms of duration (just a few pulses), modulation depth and uniformity, but implied a peak RF power in excess of 10 MW at frequencies exceeding 250 MHz. A wide ranging study of ferroelectric materials and various aspects of high power NLETL design was carried out at the University of Oxford during the 1990s [57] along with efforts to increase power levels. A carefully designed NLETL based on the good nonlinearity of strontium titanate operating at liquid nitrogen temperature demonstrated oscillation at up to 200 MHz peaking at 60 MW but, by comparison with extended pulse bursts such as that of figure 3.3, the quality of waveform was still relatively poor. Whilst the fundamental issue of extracting to resistive (i.e. power consuming) loads had yet to be fully acknowledged or addressed the work was progressive and well received in the pulsed power community.

Several theoretical and experimental studies have since been carried out on the behaviour of NLETL systems, such as the possibility of inducing chaotic behaviour [58]. Interesting work at Harvard University in the USA led to the development of a low voltage high frequency oscillator, with a nonlinear transmission line forming a closed loop containing a specially designed amplifier [59]. The amplification system is quite complicated and possibly has to regenerate the soliton on each pass due to the extraction problem, and the approach isn't scalable to power levels exceeding a few volts. A useful device offering sub-nanosecond width single pulses at a repetition rate of 130 MHz has been demonstrated however. At higher power levels, a potential use outside of shock and RF pulse burst formation that has been considered is a nonlinear bandpass filter which strongly attenuates large amplitude signals and could provide circuit protection in addition to filtering [60].

In recent years there has been a renewed interest in using NLETL systems for high power

RF pulse burst generation, perhaps thanks in part to the success, and limitations, of the BAE Systems alternative magnetic transmission line approach. Within France and the United States and quite possibly other countries, many resources are actively engaged in efforts to develop the technology, motivated by its potential benefits alongside existing options which are summarised in section 3.4, and by emerging defence applications to which it is potentially well suited. The work presented in this thesis has played a key role in this ongoing development, with both analytical work and experimental results leading the process according to published literature and discussion within the community.

3.3 Materials Science of Capacitive Nonlinearity

3.3.1 Barium Titanate and Ceramic Capacitors

In this section special attention is paid to ferroelectric materials manufactured in a ceramic form, because this is currently considered the most effective way of achieving high power NLETL oscillation, and the high voltage experiments of chapter 8 used capacitor ceramic discs based on barium titanate. Information on the characteristics of varactor tuning diodes, preferred for low voltage experiments, may be found in section 6.1. Commercial capacitors need a high permittivity dielectric material between the capacitor electrodes in order to offer a large capacitance value in a relatively small volume and to avoid having to work with small tolerances in electrode spacing. It turns out that the ferroelectric materials which have been exploited in recent decades for this purpose are suited to high voltage applications but often possess a strong nonlinearity, causing the permittivity to fall with increasing electric field strength. This nonlinearity is a well known disadvantage of ceramic capacitors and not surprisingly manufacturers have strived to minimise it by adding various dopants to their ceramic compositions. Today, almost all commercially available barium titanate capacitor materials offer insufficient nonlinearity for high frequency NLETL application, but a small minority, alongside a few obsolete capacitors, are still particularly poor in the conventional sense and retain most of the

nonlinearity potentially associated with pure barium titanate. In addition they have been modified to shift and broaden the temperature range of maximum permittivity; this coincides with maximum nonlinearity and the effect is convenient for NLETL operation at room temperature. The decision to use the dielectric discs from carefully selected commercial capacitors for high voltage NLETL experiments was taken on the understanding that the bespoke tailoring of a barium titanate ceramic would be unlikely to result in a stronger nonlinearity. It is likely that, for NLETL technology to be used in practice, an alternative approach to ferroelectric ceramic dielectrics may have to be found, one offering ultra-low loss at high frequencies, increased strength and lifetime under pulsed conditions, and perhaps even a significantly larger ratio of nominal to fully stressed capacitance values. That ratio, as distinct from the steepness of the capacitance–voltage curve, is now understood to be the most important indicator of a good CNL characteristic for this application (section 6.3.3).

3.3.2 Ferroelectric and Ceramic Materials

A dielectric, or non electrically conducting medium which can be polarised, may be piezoelectric in which case an applied electric field E will induce a mechanical strain as well as a polarisation P. Certain piezoelectric materials are termed polar, if a permanent polarisation remains in the absence of any applied field. Ferroelectric behaviour was discovered around 1920 and the name applied to a specific class of polar materials whose electrical behaviour was analogous to the magnetic behaviour associated with ferromagnetism [61]. In a ferroelectric dielectric, the direction of its spontaneous polarisation, the property which makes it polar, can be changed by the application of an appropriately oriented electric field. The behaviour of a ferroelectric changes markedly at temperatures beyond its Curie temperature, at which point a phase transition leads to paraelectric behaviour [62]. Figures 3.5 and 3.6 serve to further explain ferroelectric and paraelectric behaviour, by reference to polar piezoelectric dielectric properties and in terms of the energy barriers presented to atomic displacement.

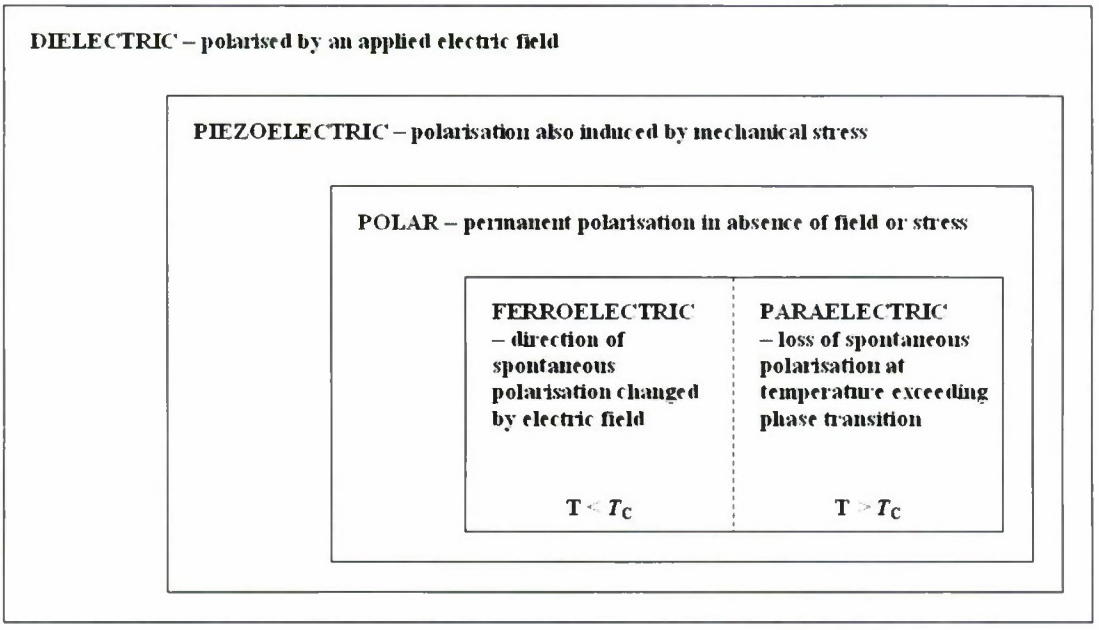

Figure 3.5: Dielectric material classifications. T_C refers to the Curie temperature of a ferroelectric material.

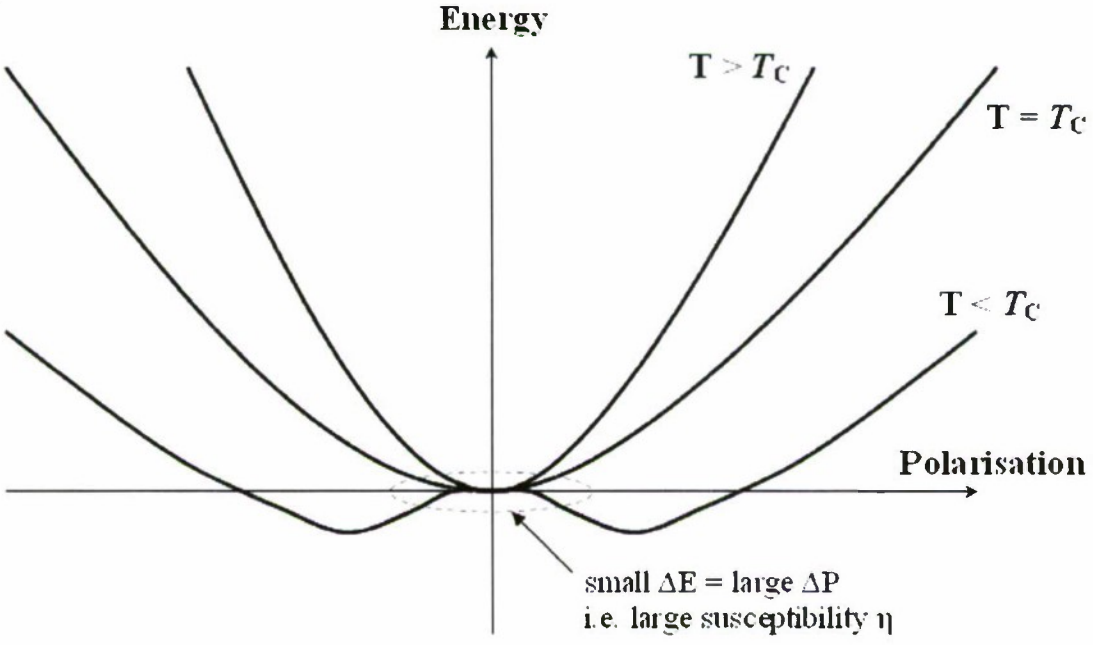

Figure 3.6: Energy barrier between ferroelectric states leading to permanent polarisation, with its reduction and the transition to paraelectric behaviour at increased temperatures.

The classic atomic model can explain polarisation in terms of ionic displacements to an asymmetric crystal structure which by superposition result in a net dipole moment per unit volume, as in a spatial separation of positive and negative charge. Ferroelectrics have found application in capacitor manufacture because they exhibit a very large polarisation under a given electric field, and so have a large relative permittivity ε_r according to the equation $\varepsilon = \varepsilon_0\varepsilon_r = \varepsilon_0(1+\eta)$ where the susceptibility $\eta = P/E$. In figure 3.6 there is a clearly defined transition from low temperature ferroelectric behaviour, with the potential wells maintaining some remnant polarisation on removal of the electric field, to the paraelectric phase, which is no longer ferroelectric but still highly polar. By reference to the graphical relationship between energy and polarisation, it is apparent that the largest polar displacement occurs under a given field when the material is at its Curie temperature and so this is the region of greatest relative permittivity ε_r. Hysteresis in the PE loop also decreases approximately to zero under paraelectric conditions, helpfully removing this contribution to dielectric loss. As polarisation of the material is increased, the additional energy required to further increase atomic displacement increases according the to changing gradient of the curves in figure 3.6 and this is the nonlinear nature of the dielectric, with η and ε_r decreasing with a rising E. Operation near the Curie temperature is desirable since capacitance per unit volume is highest and hysteresis loss minimised, but also nonlinearity is strongest and there will be maximum atomic displacements associated with high polarisation (section 3.3.4).

Reported in 1945, barium titanate ($BaTiO_3$) was one of the first few ferroelectric materials to be discovered along with, for example, potassium dihydrogen phosphate [61] and Rochelle salt (potassium sodium tartrate). The latter quickly found application to crystal microphones and electrical record pick-ups, offering various advantages over the existing carbon granule, condenser (capacitor), moving coil and ribbon designs [63]. It is quite stable and has a relatively simple atomic structure and as such its unique ferroelectric properties have led it to be well studied and understood. The Curie temperature of pure barium titanate is around 120 °C

but the region of transitional behaviour can be shifted and broadened if other dopant materials are introduced to the lattice. The properties of pure barium titanate are also altered in this way by its manufacture in a more convenient ceramic form as opposed to in a single crystal structure. A ceramic is a polycrystalline aggregate of particles, placed under high pressure to form a 'green body' which is then fused together by sintering. Typical sintering temperatures for a barium titanate ceramic would be around 1350 to 1450 °C, but the details of the grain preparation and process followed can have a large impact on the dielectric and mechanical properties of the resulting ceramic [64]. Strontium is often added to a barium titanate mix in a 60:40 ratio of barium to strontium, the resulting BST ceramic possessing a room temperature phase transition with reasonably stable properties. Although information is not released by manufacturers, it is likely that the high voltage capacitors referred to in chapter 8 are based on a BST composition designed to achieve maximum permittivity and stability at room temperature along with, helpfully in this context, a large nonlinearity if steps haven't been taken to reduce it.

Commercially available barium titanate ceramic disc capacitors are termed "high k" if they use the highest permittivity dielectric materials in order to offer larger capacitance values in smaller packages. It has been found elsewhere [43] and during this work (section 8.3) that these high k capacitors can potentially offer the strongest nonlinearity, although most of those available are relatively linear over their working voltage range due to tailored ceramic compositions. High power nonlinear materials research has primarily considered what is achievable with BST and its alternatives. The field of ferroelectrics has also been advanced by low voltage applications utilising the remnant polarisation of lead zironate and lead titanate for memory devices [62]. The degree of materials research necessary to make a significant step forward from ferroelectric ceramics, as NLETL dielectrics, falls outside the scope of this work. However, the characterisation of a wide range of capacitors detailed in section 8.3 uncovered a few which exhibit the full nonlinearity ratio that may be expected from a barium titanate structure.

3.3.3 Electrical Strength

BST ceramic can sustain relatively high electric fields, perhaps to the order of 20 kV/mm depending on composition and manufacture, and is commonly found in high voltage capacitors. The requirements on NLETL capacitive elements are demanding however, because it is necessary for the input pulse amplitude to exceed the point of saturation and certain line configurations are ideally driven somewhat harder (chapter 6). Peak voltages on the generated wave train are often around twice that of the input pulse and a sufficiently strong dielectric material is an important factor in achieving good quality oscillation in this way. With this in mind, the measurements presented in section 8.3 are of particular relevance to the latest high voltage experiments given the variance expected between different ceramic compositions.

Structural failure of a dielectric under voltage stress occurs either as a partial discharge within the material or as a complete breakdown, and the former often leads through channel growth to the latter [65]. It is important to avoid microscopic disturbances which lead to the formation of space charges and premature breakdown, and to minimise opportunities for field enhancement where conductive material is introduced. A ceramic structure incorporates many grains and inter-grain boundaries and it is understood that large amounts of voltage stress are concentrated at the relatively high impedance boundaries which may also create points of failure [42]. The high voltage strength testing carried out during this work found that surface tracking flashover often occurs prior to any structural failure; a suitable surface coating is generally required to inhibit tracking.

The ability of these ceramics to withstand high voltage stress is also probably subject to an ageing process and measured permittivity has been found in some cases to drop off significantly after relatively little use [39]. A recent study reported the delivery of 10^6 shots before failure of a barium titanate based ceramic specimen [42]. The 15 kV pulse applied in that case was sufficient to drive fully the nonlinearity which had also been measured, but for realistic application it

would appear that lifetime is likely to present a significant issue with these dielectric materials. It is also relevant to note that certain forms of radiation may have a detrimental effect on permittivity and lifetime of barium titanate [61].

3.3.4 Electrostrictions and Piezoelectricity

The piezoelectric nature of ferroelectric materials has been established in section 3.3.2 and may be expected to mechanically stress a dielectric subject to high electric field strengths. Piezoelectric deformation is approximately linear with applied field, but an alternative process leads to a strain in ferroelectrics which increases quadratically with polarisation (and field) and is much more significant than piezoelectric effects under higher fields [66]. This electrostrictive force is applicable to all dielectric materials, unlike the piezoelectric effect, and is not reversible in that a strain does not induce an open circuit potential difference by electrostriction. Regardless of field orientation, the strain acts to compress a block of dielectric, and has been reported to have limited the exploitation of ferroelectric ceramics in high voltage applications [64]. In the course of detailing progress on high power soliton generation with ceramic lines Ikezi also considered the problem of electrostrictions and suggested that mechanical waves originating from the metal–dielectric boundaries could be most significant. In addition to strain induced microcracking leading to field enhancement and dielectric breakdown, the work investigates the damping of a high frequency signal by mechanical strain, but concludes the latter effect to be negligible.

Electrostriction is a fundamental property of ferroelectric materials, and is unfortunately strongest when the temperature is such that nonlinearity, permittivity and hence maximum polarisation are at a maximum. Dielectric failures were quite frequent during the high voltage experiments of chapter 8. These may have been caused primarily by the mechanical strain associated with electrostrictive forces, but it is difficult to draw conclusions from a test subject because it is generally completely fragmented. There is a slight indication from this work that

the provision of shock absorption layers may permit a slightly higher peak pulsed voltage before failure.

3.3.5 High Frequency Response

The process of relaxation in a dielectric material has been noted in the formation of shock fronts of limited rise time on nonlinear transmission lines for pulse sharpening applications. A finite time is required for the material to switch from an uncharged to a charged state and the maximum permitted frequency of oscillation for a signal of meaningful dielectric response is termed its relaxation frequency. Relaxation effects are unlikely to be an issue at the lower end of the microwave spectrum, but for the materials of interest the value has yet to be accurately established, particularly at high levels of stress. Opinion differs quite widely, and they are possibly significant as low as 500 MHz, although some have suggested that relaxation effects are not present up to 50 GHz [61].

The addition of strontium to form barium strontium titanate should act to increase the relaxation frequency because strontium atoms are lighter than barium [29]. Whilst relaxation effects are potentially relevant to millimetre-wave RF applications, these are optimistic frequencies for a NLETL system fundamentally reliant on discrete lumped element behaviour to reach, and they are not expected to influence results at this time. In addition, simulation results have implied that even very small non-reactive components associated with loss, such as a non-zero capacitor ESR, can have a serious damping effect on high frequency oscillation. The relaxation process can itself be modelled by a series resistance [42], presumably taking a very low value. If dielectric ESR loss is not extremely low, the implication is that relaxation effects are likely to be irrelevant, since the two effects may be represented in the same way and the resistance value used to model the former is almost certainly going to take a much larger value.

3.3.6 Alternative Nonlinear Dielectric Materials

A ferroelectric ceramic based on barium titanate is suited to the current application with regards its nonlinearity and availability but does have some disadvantages which are likely to result in short lifetime. At this time alternative materials offering significant improvements for NLETL use have not been identified, but materials science is a large and complex field and as such there is scope to carry out further dedicated research into NLETL dielectric requirements. It is, for example, possible that other ferroelectric crystal structures and ceramic compositions could usefully be explored [61], and perhaps the case that completely different materials even in liquid form be worth investigating.

Certain unusual polymers such as polyvinyldene fluoride, or PVDF, are strongly piezoelectric and ferroelectric when poled correctly [67], lightweight, tougher and less brittle than ceramics. PVDF is a semi-crystalline polymer with three different crystal structures, of which the β form is the most piezoelectric and presumably the most nonlinear [62]. It should be able to sustain an electric field of 13 kV/mm but disadvantages include its high cost, low melting point and, critically, its very low relative permittivity. Compared to a value of about 3000 for a typical BST ceramic, the permittivity of less than 10 would necessitate very large area capacitors, unhelpful for high frequency lumped element behaviour, and would limit the maximum nonlinearity ratio. New research is underway on metamaterials, which gain properties from their structure rather than their chemical composition and are noted for being capable of realising unusual properties. In addition, high energy densities for a Blumlein pulser have recently been demonstrated via nano-scale titanate particles embedded in a polymer resin capable of withstanding over 200 kV/mm [68]. In that instance, reducing nonlinearity was a specific design aim achieved at the expense of relative permittivity which was around 30 to 60, but the manufacturing approach to high voltage dielectric materials is of interest.

3.4 Summary of Application Potential

The specific capabilities of NLETL pulse burst generators and their potential advantages for certain applications will become clear through the review of numerical and experimental results which follow. Typical mid–line waveforms are encouraging and extraction of RF energy to resistive loads has been demonstrated. A general summary of advantages and disadvantages associated with the concept provides motivation for the work, and also a clear indication of certain areas which would benefit from further dedicated research in the future.

By its fundamental nature, the NLETL is a pulse burst generator without the ability to amplify RF signals, and is not obviously applicable to communication systems. Higher frequency lines have been found to support quite long pulse durations (number of cycles per burst), although even the latest approaches to extraction introduce some pulse shortening if energy is required at a single load. Chapter 7 contains information relating to the suitability of antenna array construction for applications requiring propagation; this suitability is an advantage in certain situations for its simplicity and efficient extraction of longer net pulse durations (section 8.6.2). Indeed, relative simplicity of design, construction and operation is a major benefit in comparison with established but costly high power RF technology. Neglecting issues of extraction to a single resistive load, DC to RF conversion efficiency can be high because the NLETL does not have to be particularly long and overall losses could be minimised by air-cored linear inductor design and low hysteresis loss at the ferroelectric–paraelectric transition temperature. Efficiency is, of course, especially important where high pulse repetition rates occur at high power levels. Specific cooling requirements would then require further investigation and implementation, perhaps by flowing air or insulation oil.

Several design factors which influence the maximum achievable frequency and power are subject to limitations imposed by currently available dielectric material properties. As such the materials science of capacitive nonlinearity in this context is hugely important and should now be

the specialist focus of the next phase of NLETL research. Frequency may inevitably be limited by dielectric relaxation effects, a property fundamental to a polar material which responds to an applied field with the physical displacement of charge. This is not a limit which has yet been reached and is likely to greatly exceed that imposed by ESR–type loss, and the reliance on discreteness (chapter 7) anyway. Important material properties are the lowest possible conduction loss to minimise damping of high frequency signals and a good nonlinearity in terms of nominal to saturated capacitance ratio. This parameter has a strong influence on frequency according to the nmerical work of chapter 5 and some of the high voltage test line results of chapter 8. A material which permits a very low saturated capacitance under full stress, or a large CNL ratio well exceeding current values of around 10 would, it is now thought, allow significantly higher frequencies to be reached. Also relevant is the power handling capability of any potential new material, since it is necessary to be able to physically saturate the nonlinearity consistently without compromising lifetime. The important influence of the CNL steepness, as distinct from CNL ratio, and the potential for it to be too high or low, is also considered in section 6.3.2.

A final note is made here of the frequency tunability available by applying a variable DC bias voltage to the line (section 6.2). This is a key requirement of most realistic applications, certainly for wide bandwidth operation and also to enable reliable frequency stability. Overall the NLETL approach compares favourably to equivalent SSPA and MVED alternatives within its capability range, and this latest work has enabled its practical use by overcoming the extraction problem by, for example, the asymmetric parallel (ASP) and periodic loading configurations. But dielectric material issues, relating primarily to loss and lifetime under pulsed conditions, remain unsolved at this time and have currently limited frequency and peak power to 250 MHz and 175 MW.

Chapter 4

The Soliton

4.1 Historical Review of Solitary Wave Theory and the Soliton

A soliton is in essence a solitary travelling wave which emerges unaltered from a collision [69]. In this context the term solitary refers to a localised travelling wave, either of pulse profile or a transition between two asymptotic values. Of course, many forms of localised disturbance are encountered in wave theory, but the unusual properties which follow are unique to solitons and are often taken to be their defining characteristics. For a given soliton of pulse profile travelling at a velocity v, possessing an amplitude a and a characteristic width w:

- $v \propto a$; in the same propagation scenario, a larger soliton travels with a greater velocity than a smaller one
- $w \propto 1/\sqrt{v}$; a soliton which has greater amplitude, and therefore velocity, tends to have a narrower profile
- v, a and w are unaltered by interaction with another wave of the same kind, from which the individual solitons emerge with their original profiles

The soliton is a nonlinear wave whose stability with respect to interactions is surprising given the chaotic and random behaviour usually associated with nonlinear systems [70] [50]. The interaction may be a head-on collision, or alternatively an overtaking event due to the amplitude dependent velocities of individual solitons. Despite the waves emerging with unaltered shape they are typically subject to a phase shift, although it has been shown mathematically that the total phase change is zero, i.e. if one soliton gains velocity during the period of interaction the other is slowed down and the resultant phase disturbances are equal and opposite [47]. Behaviour during head-on collisions and overtaking interactions is unusual and discussed further in section 4.4, with specific relevance to the extraction of soliton pulse trains from a NLETL for example.

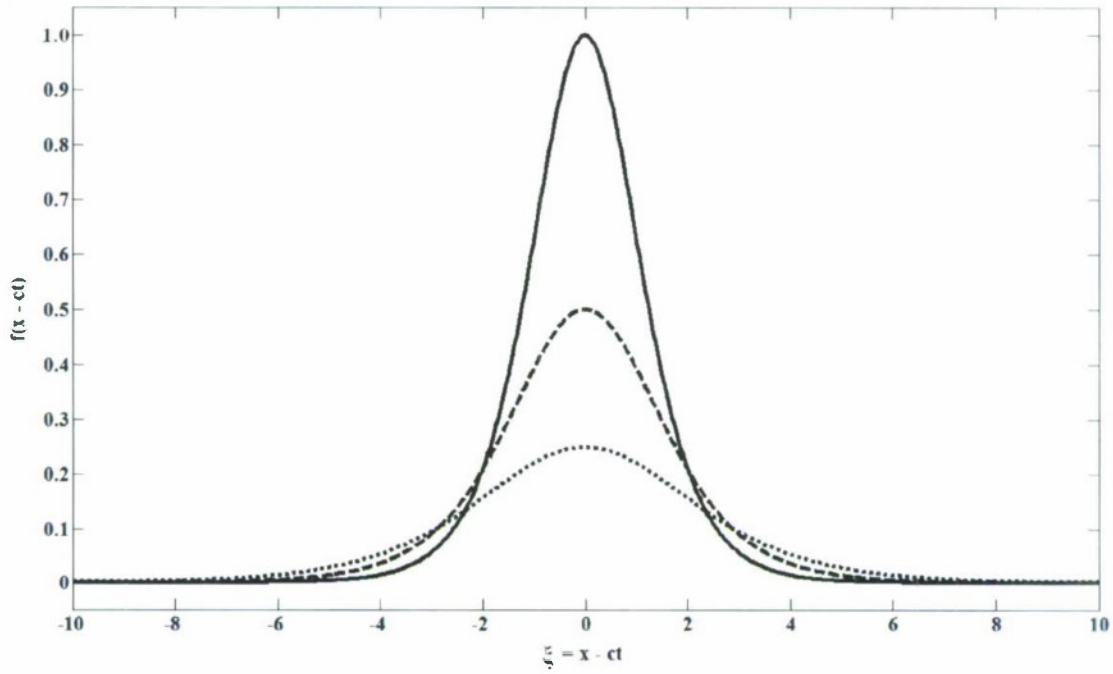

Figure 4.1: The instantaneous profiles of three stable travelling solitary waves of soliton form, at different amplitudes.

The three fundamental properties as listed above were noted at the time of the first documented encounter with the "great wave of translation" reported by John Scott Russell first in 1838 [71] and then in more detail in his 1844 Report on Waves [72]. Scott Russell was an acknowledged expert on wave theory in the mid 19th century and this comprehensive work was intended to "determine the varieties, phenomena and laws of waves" but he was especially concerned with the "velocity and characteristic properties of the solitary wave". Much experimental work was carried out at the time on water waves in tanks up to 30 feet in length, but the author claims to have first observed this form of wave on the Union canal at Hermiston, Edinburgh in 1834. He noticed a well defined elevation of water initiated by the disturbance of a boat which formed a "rounded, smooth and well-defined heap of water, which continued its course along the channel apparently without change of form or diminution of speed". The fact that this type of wave motion leads to the physical translation of water, unlike more familiar sinusoidal waves, was also determined experimentally at the time.

A subsequent 1895 paper by Korteweg and de Vries [73] evaluated some of the theoretical aspects of the phenomenon, with reference once again to water waves, and emphasised the role of nonlinearity in the formation of the peculiar stable wave pulses, where its influence is countered by that of dispersion. One of the most well known nonlinear dispersive partial differential equations which was introduced in their paper is hence known as the KdV equation after the authors. On this occasion the term cnoidal was also first used to describe a periodic train of solitary wave pulses adhering to the defining soliton properties, due to the elliptic integral function cn$[f, m]$ used in its mathematical derivation. Periodic solutions to the KdV equation 4.3 are found by this method in section 4.4 and compared qualitatively with numerical and experimental NLETL voltage waveforms. The term 'soliton' was not actually applied to this type of wave entity until 1965, when it was used by Kruskal and Zabusky during their numerical work [74].

$$\frac{\partial \psi}{\partial t} + \alpha\psi\frac{\partial \psi}{\partial x} + \beta\frac{\partial^3 \psi}{\partial x^3} = 0 \tag{4.1}$$

Both nonlinear (concentrating) and dispersive effects act independently to continuously alter the shape of a propagating wave since the wave component velocities have a dependence on the wave number k (equation 2.1). A delicate counter–balance is intuitively possible, however, with their combined influences acting to sustain stable pulse like waves. Several nonlinear–dispersive PDEs are well established, such as the sine-Gordon, nonlinear Schrodinger (NLS) and the KdV of equation 4.1. In section 4.3 it will be shown that the KdV equation has soliton solutions, and waveforms incorporating up to four individual soliton pulses are found and illustrated graphically. With reference to equation 4.1, where ψ represents an arbitrary wave function over space x and time t, and α and β are constants, first order nonlinearity is evident in the second term. The third term, a third order differential in x, contributes dispersion. The dissipation, or exponential loss, that would be associated with an even order differential term is not taken into account by the KdV equation and is neglected at this time. Finding exact multiple–soliton

solutions to nonlinear-dispersive PDEs is generally difficult (section 4.3) but the mathematical form of an individual soliton can be found relatively easily [69], via a suitable integrating factor, to be a sech^2 profile:

$$\psi(x-ct) = \frac{3c}{\beta}\text{sech}^2\left\{\sqrt{\frac{c}{\alpha}}(x-ct-x_0)\right\} \tag{4.2}$$

An outline summary of that method may be found in [43]. The defining properties associated with the soliton wave velocity, amplitude and width may be confirmed by inspection of equation 4.2, and figure 4.1 illustrates this typical soliton form for three different values of amplitude. An alternative derivation of the sech^2 solution, also subject to simplification and various assumptions but coincidentally exactly correct for a single soliton, is suggested by Hirota [75]. This method matches low and peak amplitude velocities to find a steady state stable pulse like wave solution, making use of exponentially decaying wave components in the low amplitude region instead of the superposition of plane wave components. It is interesting to note here for the nonlinear dispersion relation $\omega = \alpha k + \beta k^3$ which results: the frequency is dependent on wave number k and amplitude β and the corresponding phase velocity will have a quadratic dependence on wave number. Further progress and the more rigorous exact solution of the KdV equation relies on the use of the inverse scattering transform [69], Backlund transformations [76] or the Direct Method which is considered further in section 4.3.

Interest in nonlinear dynamics, and specifically in the formation and unique behaviour of soliton waves in nature and engineered systems, has attracted much interest in the past few decades. Originally a mathematical curiosity observable in water, an example in nature being tidal bores on certain river channels under specific conditions, the theory has interfaced with various other branches of mathematics. For example, the motions of certain surfaces, those which admit Backlund transformations, may generate solitonic equations [76]. This aspect of soliton theory is quite abstract but closely related to a certain type of periodic solution known as a breather, which is considered relevant to the pulsed behaviour of NLETL systems (section 4.4, section

7.1). In addition, developments in fibre optic communications have made use of a dependence of refractive index on light intensity to generate envelope solitons which may be described by the NLS equation. The self–sustaining nature of the resulting signal, with inevitable dispersive effects conveniently counter–balanced by the nonlinearity, has proven value for coherent high bandwidth long distance communication. In 1958 soliton theory was applied to the theoretical plasma physics of magnetised plasmas subject to rapid compression [77] [78] and recent solid state oscillators have exploited the nonlinear Gunn effect in certain semiconductor materials [50]. Medical diagnostics and condition forecasting could soon also make use of the nonlinear dynamics associated with soliton type waveforms. It is becoming understood that issues in health are sometimes associated with a loss of nonlinear complexity and the development of periodicity and resonances, as tremors or in monitored output [79].

In summary, whilst a specific definition of the soliton wave is hard to establish, the defining characteristics have been noted and make the phenomena somewhat unusual, both from a mathematical perspective and where it might exist in physical systems. In a general sense, the term soliton can be applied to any solution of a nonlinear wave equation which (i) represents a wave of permanent form, (ii) is localised in the travelling coordinate $x - ct$, (iii) retains its identity after interacting strongly with other solitons [69].

4.2 Connection Between NLETL Oscillation and Solitons

Approximately continuous nonlinear transmission lines have been used to reduce high power pulse rise times (section 3.1), clearly demonstrating a nonlinear influence, and any form of lumped element ladder network is dispersive to some extent. The dielectric nonlinearity, whereby effective capacitance per stage reduces with increasing voltage, causes larger amplitude wave components to propagate faster and form, by a 'catch-up' effect, a shock front at the pulse

leading edge. A nonlinear dispersion relation, where characteristic frequency has a dependence on amplitude, is the intuitive result. Conversely, dispersion has the effect of spreading wave components apart and the necessary nonlinear dispersive requirements for soliton formation are potentially present.

On first glance, and considering the material of the preceding section, the phenomenon described in chapter 3 may be understood as a mathematical inevitability given the NLETL system of propagation, and can be physically interpreted as the result of a delicate balance between nonlinearity and dispersion. The presence of both nonlinearity and dispersion, and the nature of pulse decomposition into a train of high frequency pulses, behaving in accordance with the properties of soliton waves, led to them being identified as solitons. Indeed, the first published works on nonlinear electrical transmission lines served only to report on the potential to use them as a physical means of observing the unusual behaviour of solitons (section 3.2).

The KdV equation has been derived from the circuit model of a lossless lumped element transmission line with capacitive nonlinearity on a few occasions [49] [48] [43], and this implies that electrical soliton waves should be supported by such lines. Other than the required relationships between amplitude, velocity and width previously mentioned, several distinctive characteristics may be observed of NLETL waveforms which have also been identified with soliton behaviour. During the period of a head-on collision event between two individual soliton type pulses on a NLETL (figure 4.2 and figure 4.3) the resultant pulse is of large amplitude, sometimes greater than the sum of their individual amplitudes. Mathematical and numerical work published on soliton waves often investigates interactions such as this, and results agree with this observation [76]. This may be coincidental however, and as noted by Hirota and Suzuki in 1973 [41], is to be expected in practice since during the overlap period the net current flow must be very low and accompanied by a corresponding increase in voltage. After the collision the two original pulses emerge with their original shapes even, according to simulation results, when their ampli-

tudes were different. This preservation of identity, in accordance with soliton behaviour, is also evident after an overtaking interaction. Overtaking solitons would be expected to form a wide, low amplitude resultant pulse during the interaction, which is indeed the case on a NLETL as illustrated in figure 4.4. Under these conditions, where co-propagating soliton type pulses temporarily coincide due to different propagation velocities, the net current would be expected to increase which once again offers some physical explanation for this soliton like behaviour.

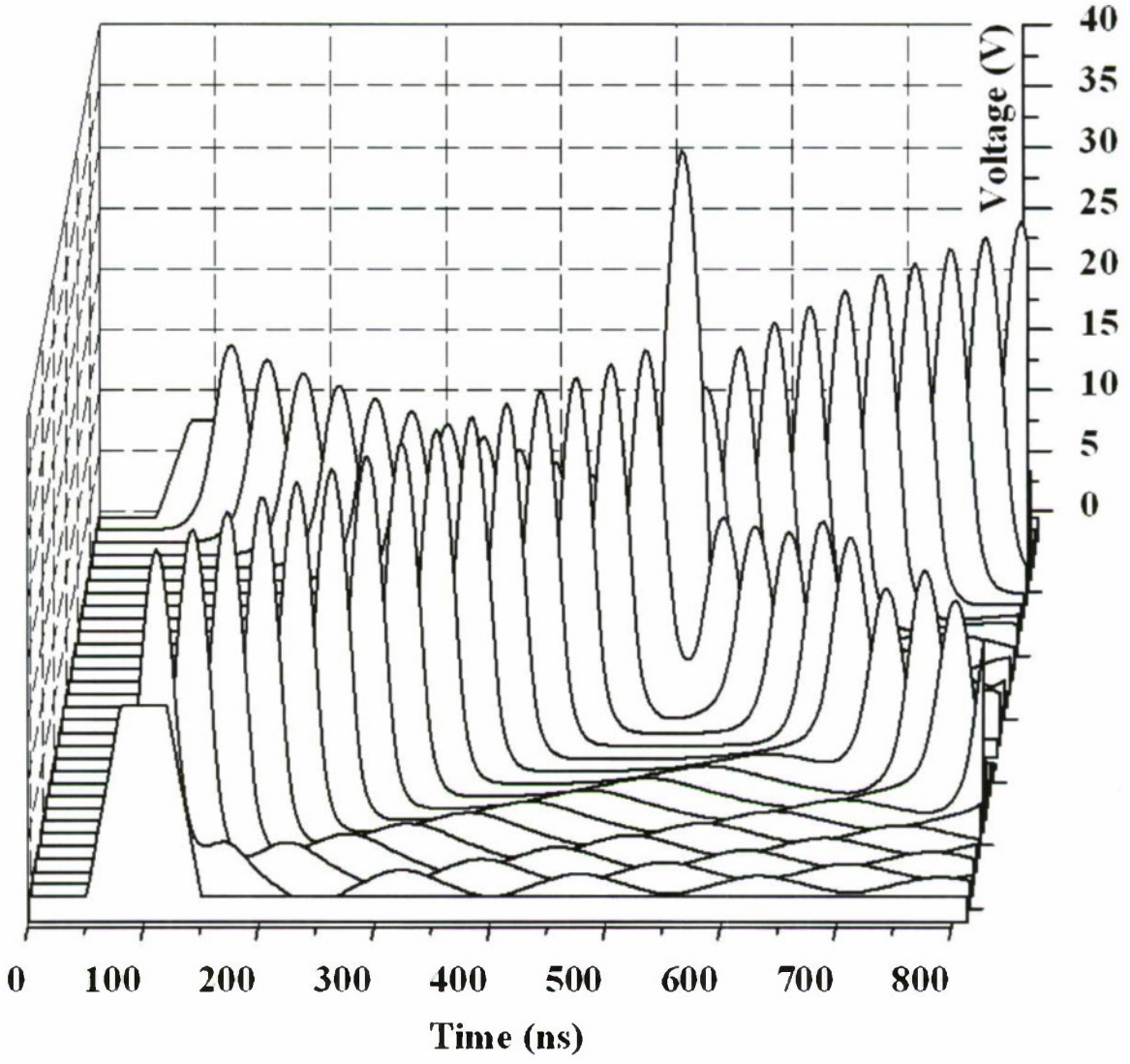

Figure 4.2: The head-on collision of two single solitons is demonstrated on a 30 stage simulated NLETL, with narrow input pulses of different amplitudes applied to each end of the line. During this type of interaction the resultant amplitude is large, and in this case where the two solitons are of different form they are seen to regain their original identities after emerging from the collision.

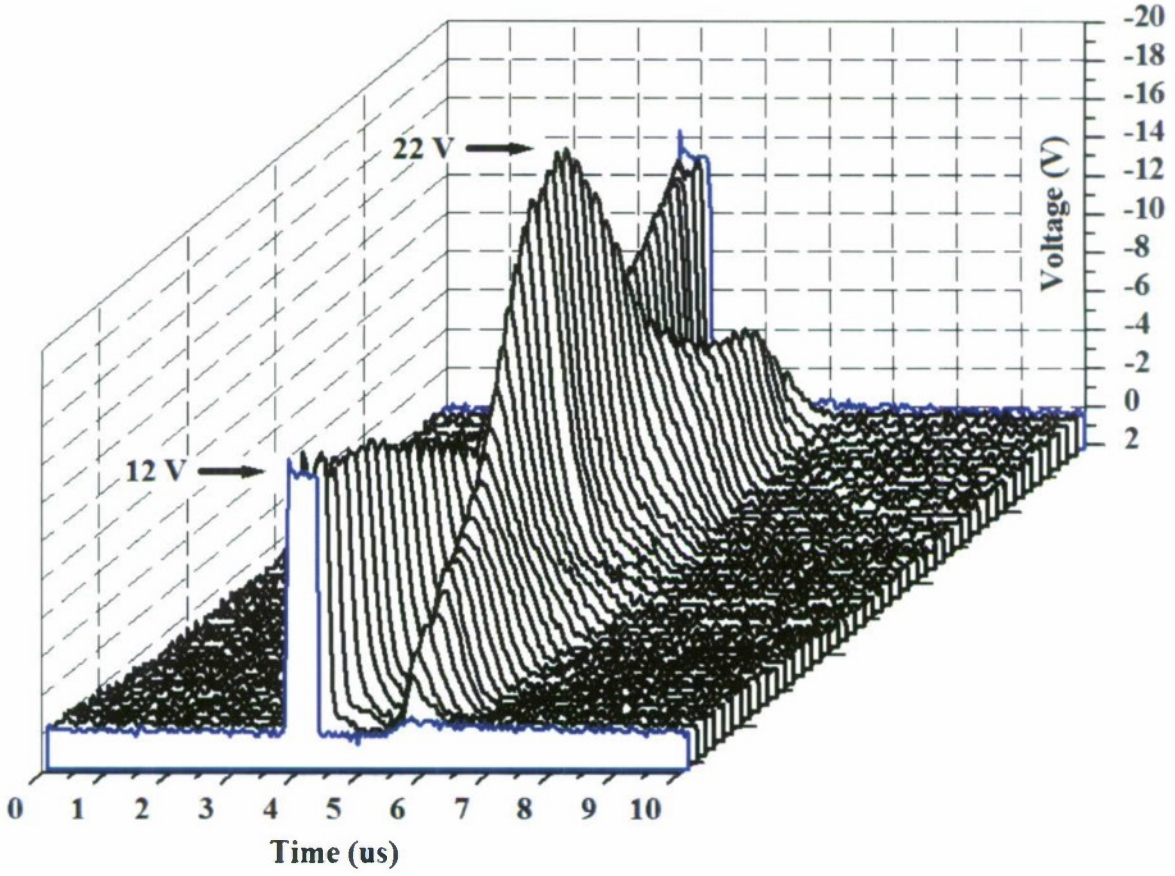

Figure 4.3: A similar head-on collision to that of figure 4.2, here on an experimental line and with equal amplitude inputs to both ends.

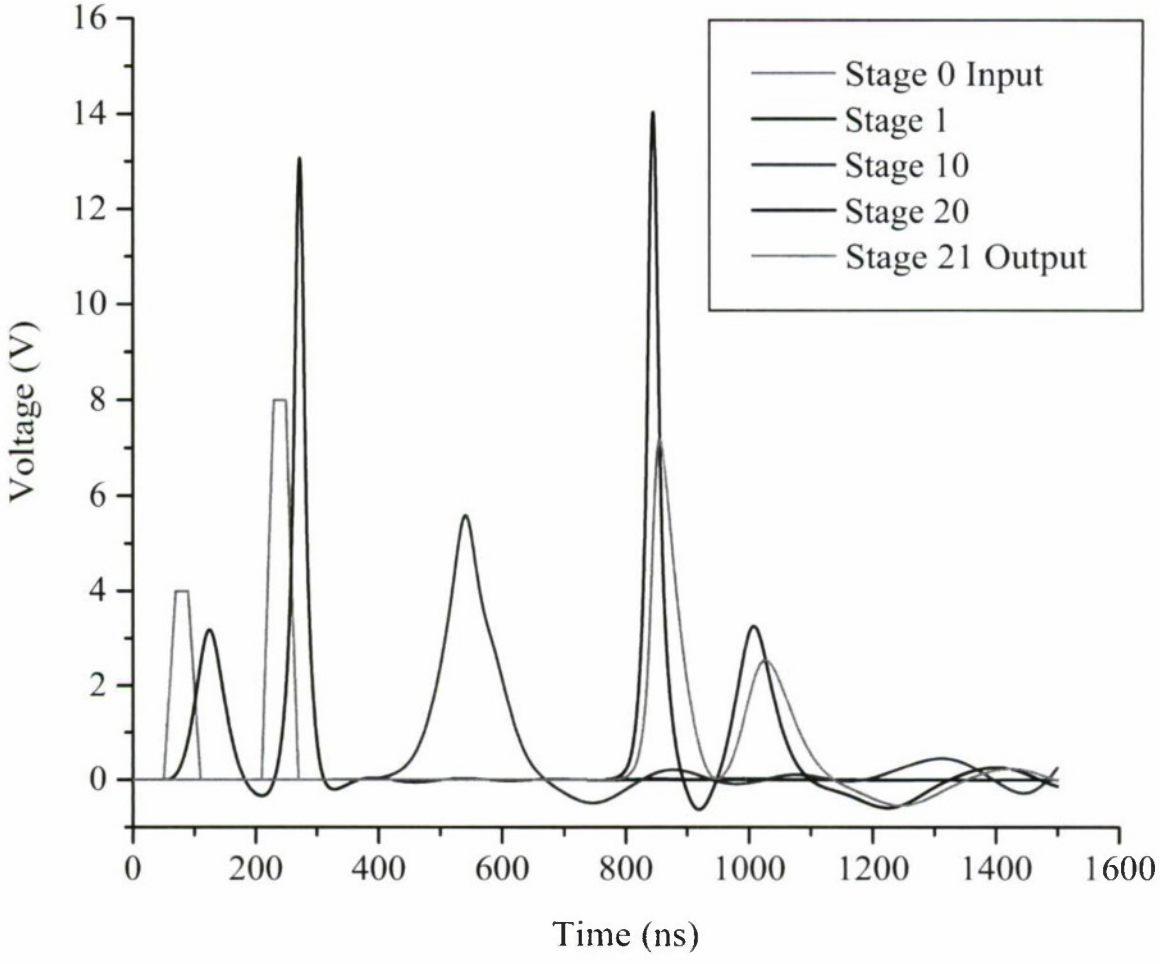

Figure 4.4: A simulated overtaking interaction is arranged by an input comprising two narrow single soliton generating pulses, the first of smaller amplitude than the second. The larger soliton catches up with its smaller counterpart at the middle of the 20 stage NLETL, where the resultant amplitude is low. Once again both solitons emerge from the interaction with their original profiles. Extraction from the NLETL is typically accompanied by a reduction in individual soliton amplitude, as seen here.

Further interesting similarities, including reference to the structure of periodic cnoidal wave trains, are discussed in section 4.4. Despite all this, there are certain issues which call the true solitonic nature of NLETL oscillations into question. An important aspect of work on this project has been bringing these to light and attempting to consolidate several new insights with the accepted soliton explanation. The nonlinear dispersive wave theory called upon to explain the formation of high frequency pulses on electrical transmission lines has to this point been continuous in space and time, and the important step of deriving the KdV equation is reliant on effecting the transition from a discrete system of current and voltage to a continuous partial differential equation. The long wavelength assumption has to be made in the KdV derivation, specifying each pulse wavelength to be much greater than that of the individual stages along the discrete line. A key point not noticed by those employing the KdV derivation, or indeed by published work on nonlinear electrical transmission lines prior to this time, is the stage to stage anti-phase property always adhered to by NLETL oscillations, which are in fact fundamentally reliant on line discreteness. It should be noted that a pulse period is always two discrete stages and in this way an extended burst of oscillation progresses in a see-saw fashion down the NLETL, where adjacent stage waveforms maintain anti-phase with one another (figure 4.5). As such, any assumption of the continuous limit is obviously mathematically inappropriate, and the association with the KdV equation must be considered to be flawed. In fact, a further inconsistency is clear in the form of a low amplitude, or weak nonlinearity, limit assumption which has been made on occasion in accordance with analysis applied to water surface waves. This is despite the NLETL requirement of a strong nonlinearity and its full exertion, to and beyond saturation, for good oscillation (section 6.3).

Extensive numerical and experimental results have been obtained on a wide range of NLETL systems and these will be presented throughout the following chapters. Consistent indications that the electrical pulses on such lines behave and interact as per established soliton theory may be seen in these results. It is now thought (section 4.4, chapter 7) that the soliton mathematical

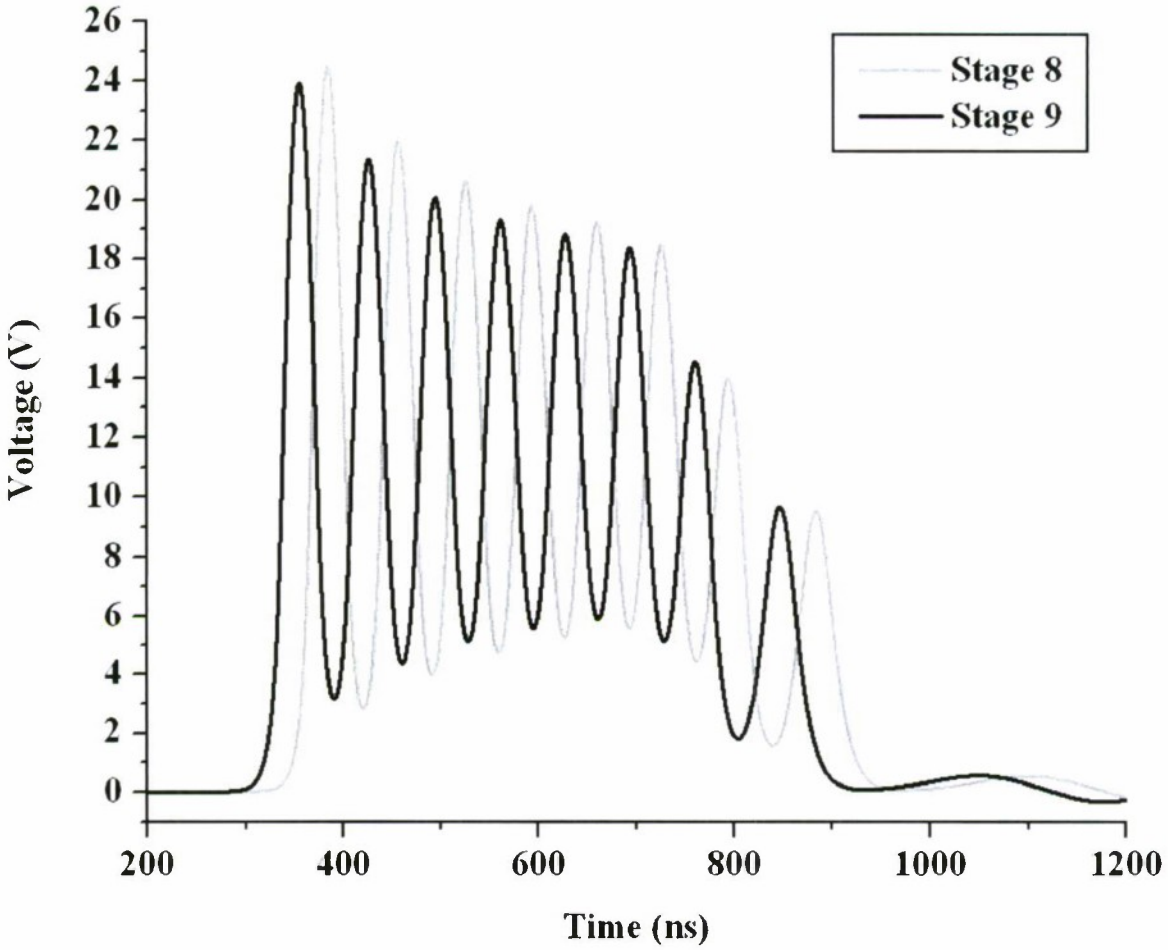

Figure 4.5: Voltage waveforms at two adjacent stages on a simulated NLETL.

model is applicable to the NLETL system, but the intrinsic dependence on discreteness does mean care needs to be taken when designing the lines, and in drawing direct parallels between these oscillations and the established soliton phenomena of other continuous media.

The following section investigates soliton properties further by solving the KdV equation exactly for an unlimited number of solitons, and illustrates graphically the resulting wave functions of up to four solitons over space and time. The chapter concludes by considering some further aspects of nonlinear dispersive wave theory which have been found to be relevant, including the nature of discrete lattice soliton solutions.

4.3 Solving Nonlinear–Dispersive Wave Equations

Largely following the method of Hirota [75] [80], the analysis of this section is concerned with obtaining and graphically interpreting exact multiple soliton solutions to the continuous KdV equation. The purpose is to investigate soliton properties with an arbitrary wave function u over space x and time t without reference to any specific NLETL but for that noted in previous work with the KdV equation. Soliton behaviour would appear to be relevant to the generation of RF waveforms on electrical transmission lines (section 6.2) and various ideas on the extraction problem (section 6.4.2) were developed with these analytical results in mind. The KdV is one of the most simple equations incorporating nonlinearity and dispersion but such partial differential equations are in general very hard to solve exactly. Several methods have become established and on this occasion the 'direct method' proposed by Hirota is applied to the KdV equation in the following form

$$\frac{\delta u}{\delta t} + 6u\frac{\delta u}{\delta x} + \frac{\delta^3 u}{\delta x^3} = 0 \tag{4.3}$$

In the surveyed literature the direct method was found to be the most accessible and widely applicable, with elegant solutions which lend themselves to computer graphing. The analysis proceeds by applying the following steps to the KdV equation 4.3:

1. a dependent variable transformation from u to f
2. conversion to a Hirota bilinear form (see equation 4.12) according to the 'D–operator'
3. a perturbation expansion of f in a small parameter ε
4. analysis of the bilinear form equation at each order of ε

The key motivation behind the direct method, and its special D–operator defined below, is the fact that a perturbation expansion to $f = 1 + \varepsilon f_1 + \varepsilon^2 f_2 + \varepsilon^3 f_3 + ...$ truncates exactly when subject to the Hirota bilinear form for f. It will shortly be demonstrated that the number of non-zero terms in this expression for f corresponds to the number of solitons which may be found in the solution, and this number is determined by the choice of f_1.

It turns out [75] that a suitable expansion of the wave function is in terms of exponential wave components rather than conventional plane wave components. Here, an exponential wave component is written $f \sim e^{\eta}$ where $\eta = Px + \Omega t$. P and Ω are used to represent the quantities normally identified as wave number k and angular frequency ω to distinguish from actual space and time dependencies when under the necessary transformation.

The direct method is accompanied by a binary differential operator, the D–operator, which acts on a pair of functions a and b as per the defining equation 4.4, with respect to space x. Equation 4.5 extends the operation over two variables x and t. The variables s and y do not feature in the result; they simply control the application of conventional differentiation to the pair of functions.

$$\mathrm{D}_x^n(a.b) = \mathrm{D}_x^n a \bullet b = \left(\frac{\partial}{\partial x} - \frac{\partial}{\partial y}\right)^n a(x)b(y)|_{x=y} = \frac{\partial^n}{\partial y^n} a(x+y)b(x-y)|_{y=0} \tag{4.4}$$

$$\mathrm{D}_t^m \mathrm{D}_x^n a \bullet b = \frac{\partial^m}{\partial s^m}\frac{\partial^n}{\partial y^n} a(t+s, x+y)b(t-s, x-y)|_{s=0,y=0}; \text{ for } m, n = 0, 1, 2, ... \tag{4.5}$$

If equation 4.4—the D–operator applied to a pair of differentiable functions a and b with respect to a single variable (in that case x)—is subject to careful consideration the following example cases may be verified. These are noted here because they will be used in expressing the KdV equation in D–operator notation.

$$\mathrm{D}_t a \bullet b = a_t b - a b_t \tag{4.6}$$

$$\mathrm{D}_x a \bullet b = a_x b - a b_x \tag{4.7}$$

$$\mathrm{D}_x^3 a \bullet b = a_{xxx} b - 3 a_{xx} b_x + 3 a_x b_{xx} - a b_{xxx} \tag{4.8}$$

and where $a \equiv b$:

$$\mathrm{D}_x^2 a \bullet a = 2(a_{xx} a - a_x^2) \tag{4.9}$$

It is interesting to note at this point the subtle difference between this operation and a normal function product derivative, this being a reversed sign on terms having an odd number of derivatives on the second function. Having introduced the D–operator, it is now necessary to apply the dependent variable transformation to the KdV equation

$$u = 2(\log f)_{xx} \tag{4.10}$$

The resulting bilinear form in f of the KdV equation originally given in terms of u in equation 4.3 is then

$$f_{xt} f - f_x f_t + f_{xxxx} f - 4 f_{xxx} f_x + 3 f_{xx}^2 = c f^2 \tag{4.11}$$

This may be written neatly using the definition of the D–operator as per equations 4.6 and 4.9 in the Hirota bilinear form (taking $c = 0$)

$$(\mathrm{D}_x \mathrm{D}_t + \mathrm{D}_x^4) f \bullet f = 0 \tag{4.12}$$

$$\text{or } (\mathrm{D}_x (\mathrm{D}_t + \mathrm{D}_x^3) f \bullet f = 0 \tag{4.13}$$

The function f is now subject to the perturbation expansion mentioned earlier, in a parameter ε whose value is assumed to be small

$$f = 1 + \varepsilon f_1 + \varepsilon^2 f_2 + \varepsilon^3 f_3 + ... \tag{4.14}$$

and some further properties of the D–operator are noted

$$\mathrm{D}_x\mathrm{D}_t f \bullet 1 = \mathrm{D}_x\mathrm{D}_t 1 \bullet f = f_{xt} \tag{4.15}$$

$$\mathrm{D}_x^4 f \bullet 1 = \mathrm{D}_x^4 1 \bullet f = f_{xxxx} \tag{4.16}$$

$$\mathrm{D}_x^m\mathrm{D}_t^n \mathrm{e}^{\eta_1} \bullet \mathrm{e}^{\eta_2} = (P_1 - P_2)^m(\Omega_1 - \Omega_2)^n \mathrm{e}^{\eta_1+\eta_2} \tag{4.17}$$

The final statement above is a key property which ensures the direct method converges on an exact solution, in that the perturbation expansion of f contains a finite and manageable number of non-zero terms. Specifically, it is equal to zero when $\eta_1 \equiv \eta_2$, where $\eta_i = P_i x + \Omega_i t + \eta_i^0$.

If the equation 4.14 expanded form of f is inserted into the bilinear form of the KdV equation 4.12 and the integer orders of ε considered individually a series of equations is obtained which may be simplified by use of the results in 4.15. In this way the equation

$$\mathrm{D}_x(\mathrm{D}_t + \mathrm{D}_x^3)(1 + \varepsilon f_1 + \varepsilon^2 f_2 + \varepsilon^3 f_3 + ...) \bullet (1 + \varepsilon f_1 + \varepsilon^2 f_2 + \varepsilon^3 f_3 + ...) = 0 \tag{4.18}$$

is considered for the orders of ε, ε^2, ε^3 to give a series of equations in f_1, f_1 and f_2, f_1 and f_2 and f_3 and so on. For example, solving equation 4.18 for the second order ε gives

$$\mathrm{D}_x(\mathrm{D}_t + \mathrm{D}_x^3)(f_2 \bullet 1 + f_1 \bullet f_1 + 1 \bullet f_2) = 0 \tag{4.19}$$

The method concludes by noting that, having chosen the solution for $f_1 = \mathrm{e}^{\eta_1}$, f_2 is equal to zero by reference to equation 4.19, and all higher order components of f are also equal to zero according to their equivalent equations. So, the solution in terms of f for this choice of f_1 is

actually remarkably simple, $f = 1 + f_1$, although it turns out that this results in a single soliton solution to the KdV equation, since

$$u = 2(\log f)_{xx} = 2(\log(1 + e^{\eta_1}))_{xx} = \frac{2P_1^2 e^{\eta_1}}{(1 + e^{\eta_1})^2} = \frac{P_1^2}{2} sech^2 \frac{P_1 x + \Omega_1 t + \eta_1^0}{2} \tag{4.20}$$

This result for the original wave function u is in agreement with the established sech^2 soliton profile, already known to be a valid solution to the KdV equation.

On the basis that assigning the single exponential wave component to f_1 led to a single soliton solution, it is perhaps intuitive to choose $f_1 = e^{\eta_1} + e^{\eta_2}$ in looking for a two soliton solution to the KdV equation by this method. The result is a non-zero value for f_2 in the perturbation expansion of f, which truncates for all higher order terms according to the properties of the D–operator. Thus, the above analysis is extended to give a two-soliton solution which is

$$u = 2\log(1 + \varepsilon(e^{\eta_1} + e^{\eta_2}) + \varepsilon^2 a_{12} e^{\eta_1 + \eta_2})_{xx} \tag{4.21}$$

To visually interpret this result the logarithmic transformation needs to be carried out by some appropriate method. Figure 4.6 was generated from equation 4.21 in Matlab and is plotted where the values of $P_{1,2}$ and $\Omega_{1,2}$ have been chosen to generate two solitons of different amplitude. The analysis may be extended further to incorporate in the solution as many solitons as might be required; the inclusion of one more exponential component in f_1 leads to one more non-zero term in the series expansion of f and one more soliton in the resulting solution for u. The continuing convergence of f is due to the nature of the D–operator definition, and were conventional function product derivatives to have been used instead the solutions would contain an infinite number of terms and need to be approximated.

An initial problem is the rapidly increasing complexity of the solution for f as the number of solitons increases to three or more. Fortunately, Hirota's direct method is concluded by a

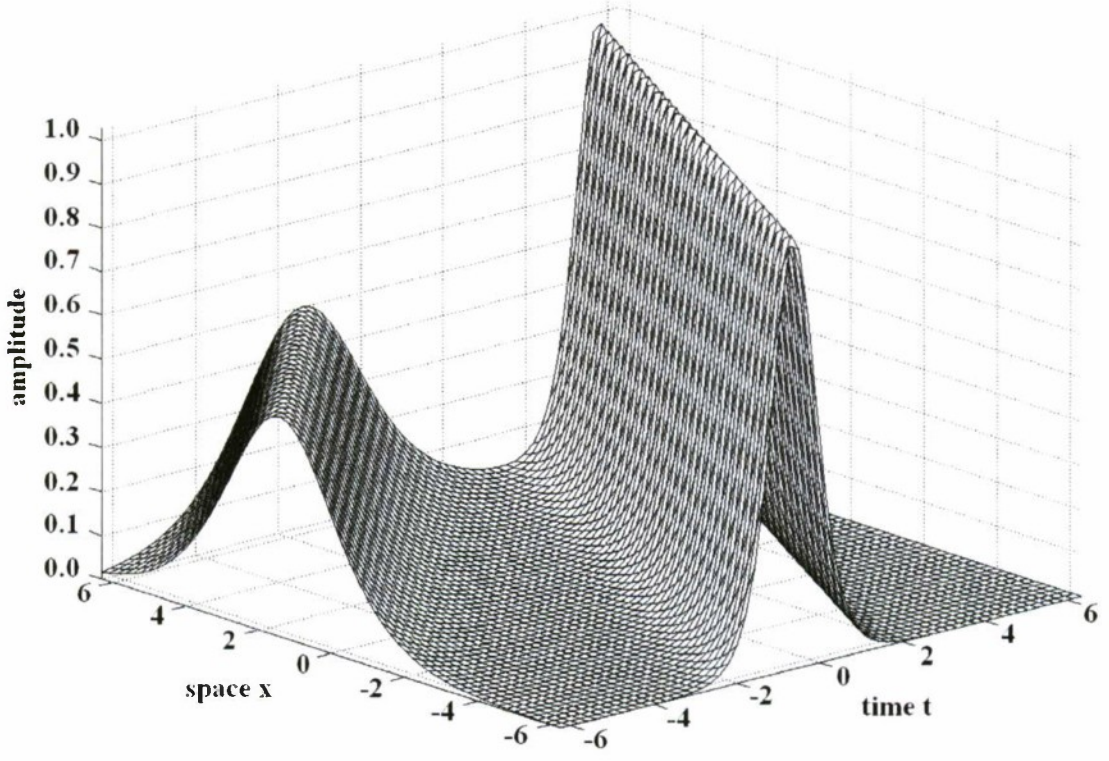

Figure 4.6: Two solitons of different amplitudes derived from the KdV equation are seen here to travel at different velocities whilst maintaining their individual profiles.

remarkably concise equation for f representing N solitons which is suited to computer implementation and given by equation 4.22.

$$f = \sum \exp\left(\sum_{i=1}^{N} \mu_i \eta_i + \sum_{i<j}^{(N)} A_{ij}\mu_i\mu_j\right) \quad \text{where } a_{ij} = e^{A_{ij}} \tag{4.22}$$

In this equation, the first exponent summation is over all combinations of $\mu_i = 0, 1$ for $i = 1, 2, \ldots, N$ whilst the second summation is over the pairs (i, j) from the set $1, 2, \ldots, N$, that satisfy the condition $i < j$. Application of the logarithmic dependent variable transformation once again returns the actual wave function result for u. It is time consuming but reasonably straightforward to verify equation 4.22, for example with an initial choice of $f_1 = e^{\eta_1} + e^{\eta_2} + e^{\eta_3}$ and a three soliton solution. At this point, the important result is demonstrated with up to four solitons and a range of interesting interaction phenomena. Appendix A contains the m file code used to generate these waveforms, making use of the powerful Matlab tool that is symbolic algebra.

For example, an interaction between four solitons generated by the KdV equation each with distinct but arbitrary parameters is depicted in figure 4.7. The graphs of figure 4.7 through figure 4.10 plot the evolution of the amplitude of the wave function u over the two variables space x and time t. The two–soliton solution of figure 4.6 was also generated by the preceding direct method and clearly demonstrates some key properties of the soliton wave, namely that a larger amplitude corresponds to a faster speed of propagation and a sharper profile.

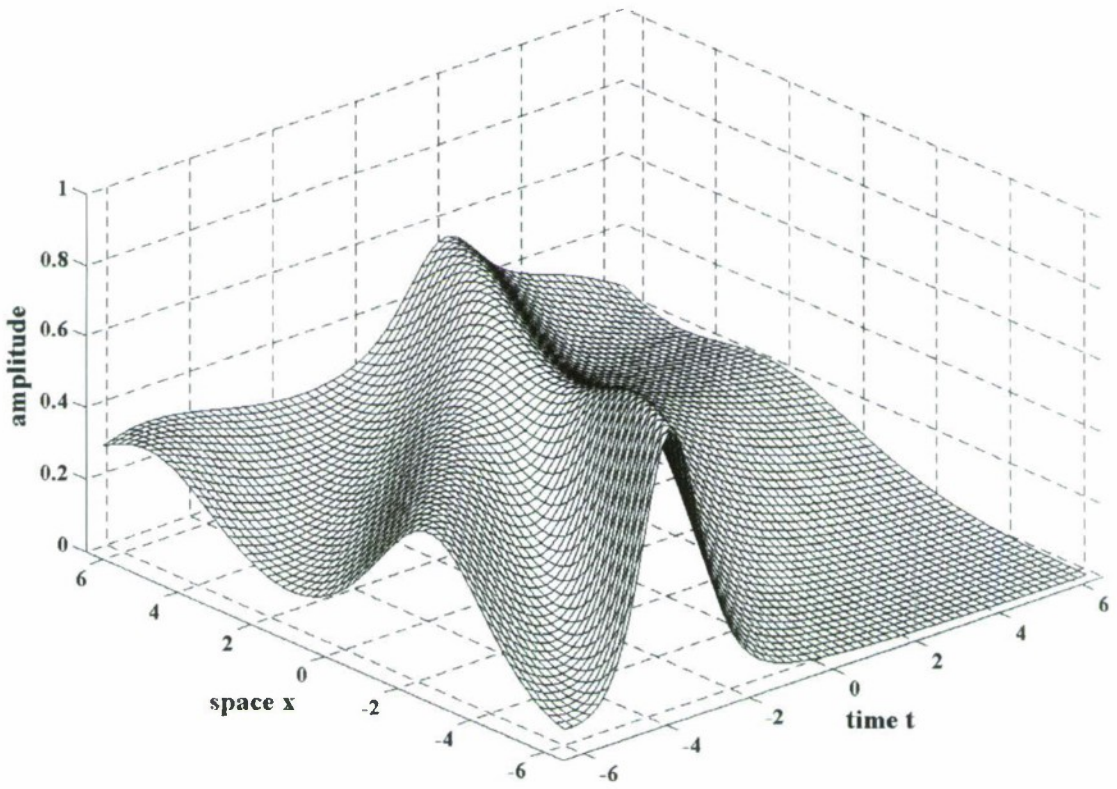

Figure 4.7: A four soliton solution to the KdV equation generated by the direct method solution of equation 4.22, where the individual soliton parameters are arbitrary but distinct.

The opportunity was taken to consider the effects that neighbouring co-propagating solitons might have on one another, with potential relevance to the extraction problem discussed further in due course. Due to the nonlinear nature of the waves a simple superposition would not be appropriate, but it is now possible to visualise the loss of modulation depth when a

train of originally independent solitons are drawn closer together (figure 4.8). The effect is also accompanied by a reduction in amplitude of the individual pulses which may be seen in figure 4.9, where each of the three solitons are nominally of the same amplitude but the two on the left are effectively undergoing an eternal interaction over time as they propagate very close to each other. The right hand soliton is further displaced from any neighbours and retains more of its original identity. The influence of co-propagating solitons on one another was found to be quite strong, with only small changes in position leading to appreciable changes in profile and resulting modulation depth of the wave train as a whole. These results are of course in arbitrary continuous units and may not be quantitatively related to any physical NLETL system, but the fundamental effects and general patterns are useful to note (section 6.4). It is, for example, interesting that in general the extraction of a single soliton from a NLETL to a resistive load is accompanied by a reduction in its amplitude which, for a pulse train, could be expected to significantly compromise modulation depth according to direct method results such as these.

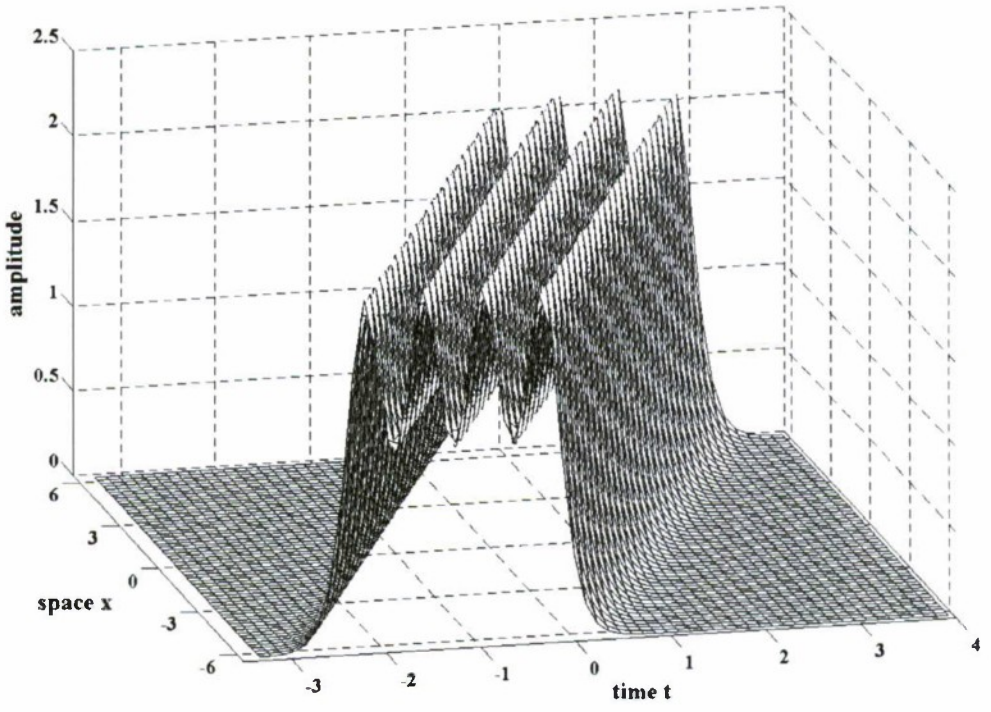

Figure 4.8: Four co-propagating solitons in close proximity to one another.

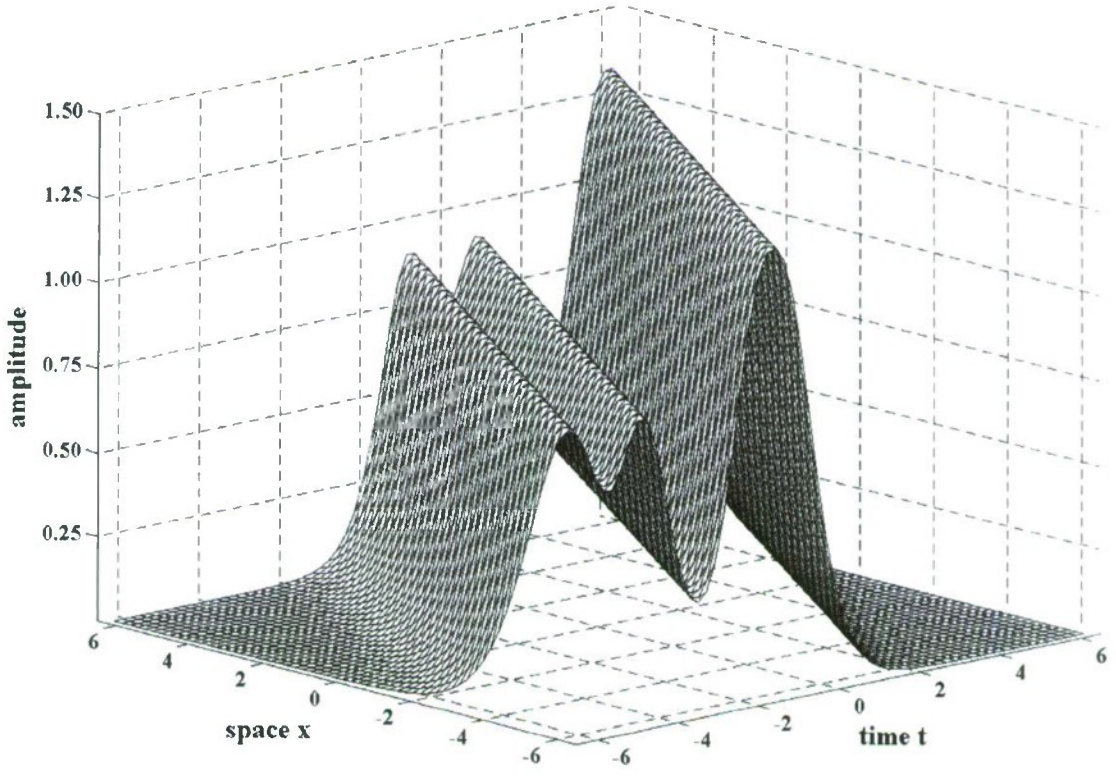

Figure 4.9: Three co-propagating solitons all of the same nominal amplitude and velocity but with closer spacing between the left hand pair.

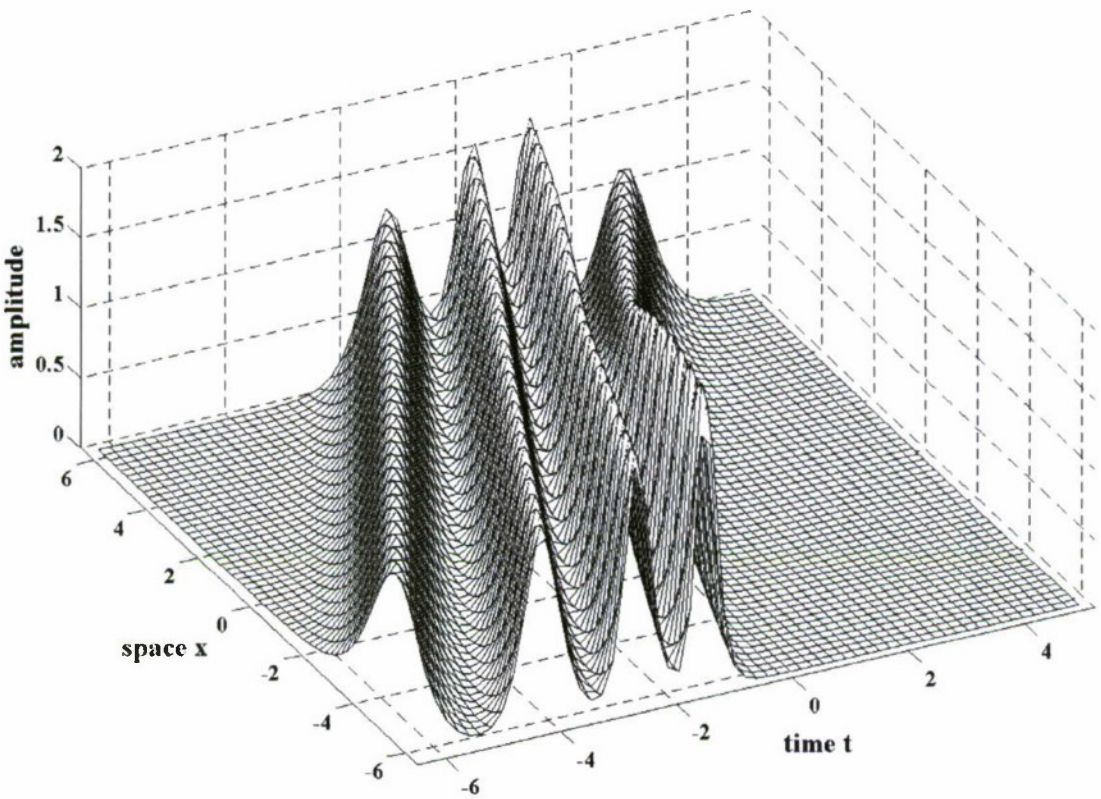

Figure 4.10: Four solitons of different but similar amplitudes featuring an exchange interaction between the right-hand pair, whose knock-on effect is also perceptible in the other trajectories.

Experimenting with the KdV solution parameters which determine soliton properties, and thus establishing the nature of various interactions, leads to some other curious results. What appears to be a deflection of the right hand of four co-propagating solitons in figure 4.10 is in fact a valid example of an exchange interaction between solitons where their difference in velocities is small [81]. Under certain conditions and with large amplitude solitons of similar velocities the smaller one actually reverses its polarity on the crest of the overtaking interaction, before regaining its identity on the other side of the larger one which cut through its path.

4.4 Further Aspects of Soliton Theory

It has been suggested [50] that a group of several solitons should over time arrange themselves in height order with the tallest at the front, and it is interesting to note that the steady state type III NLETL pulse burst envelope shape (section 5.3) is of this form. Similarly, the spreading which is clearly evident on longer lines (section 6.3.1) is to be expected from general soliton theory, even in regions of similar amplitude pulses of matching nominal velocities. Furthermore, a soliton wavetrain sometimes splits in two for no apparent reason [50] and a 400 stage simulation has indicated the initiation of this curious effect. The Fermi-Pasta-Ulam recurrence phenomena, whereby a sinusoidal excitation applied to a nonlinear dispersive system may break in to soliton component waves before eventually reforming its original profile [76], is claimed to have been demonstrated on a NLETL system [49]. Such unusual and quite specific behaviours are reassuring to note if NLETL oscillations are to be considered solitonic in nature. The term dark soliton has been used to describe the solution to wave equations of reversed nonlinearity, whereby the excitation acts to reduce the nonlinear exertion. Both numerical and experimental (figure 4.11) transmission lines have been arranged to support the generation of dark solitons, with a reversed polarity input pulse applied in addition to an equal DC bias voltage.

Figure 4.12 illustrates a periodic cnoidal soliton solution which was derived from the KdV equation with the use of elliptic integrals [69] [82]; figure 4.13 indicates the cnoidal nature

of a typical high voltage NLETL experimental waveform. This nonlinear wave train result is of particular relevance in comparing the NLETL oscillations with soliton waves since they are typically generated in extended bursts. Mathematical details of the method employed are included in appendix B, where the value of constant m determines period and, effectively, the degree of nonlinearity, which can be strong [69] [82]. In equation 4.23 the solution is stated here in accordance with the terminology described in the appended material.

$$f(\zeta) = f_2 - (f_2 - f_3)\mathrm{cn}^2\left[(\zeta - \zeta_3)(\frac{f_1 - f_3}{2})^{1/2}, m\right] \tag{4.23}$$

The amplitude dependence of wave frequency associated with a nonlinear dispersion relation such as that described in section 4.1 is indicated by the clear difference in sharpness between peaks and troughs. This disappears for the limiting case of $m = 0$, when the function cn becomes sinusoidal, and is also typically visible on numerical and experimental NLETL pulse burst waveforms (figure 4.12 and 4.13). For $m = 1$ the solution is no longer periodic but gives the familiar single soliton sech^2 profile.

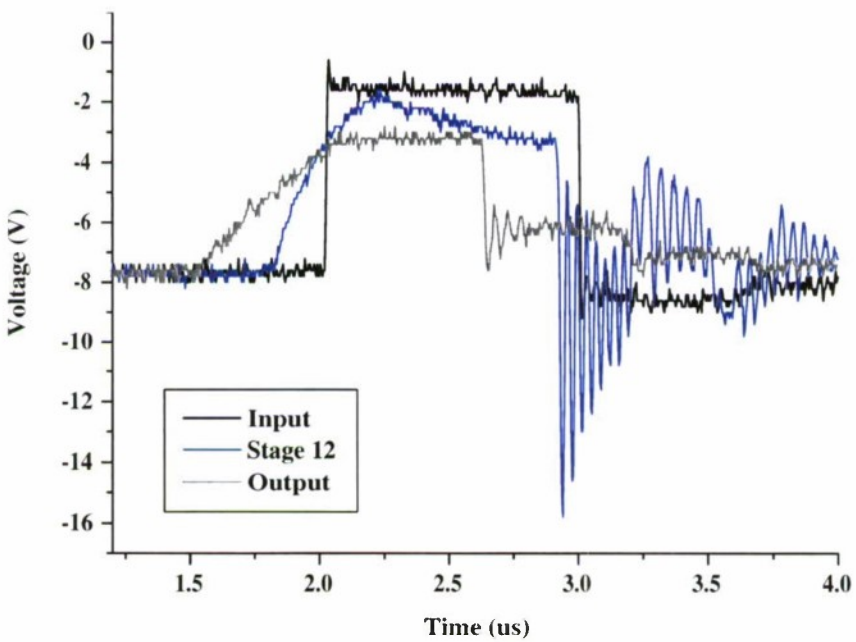

Figure 4.11: Input, mid-line and output voltage waveforms on an experimental NLETL arranged with the necessary DC bias and input pulse polarity to demonstrate the generation of dark solitons by the reversed nonlinear effect.

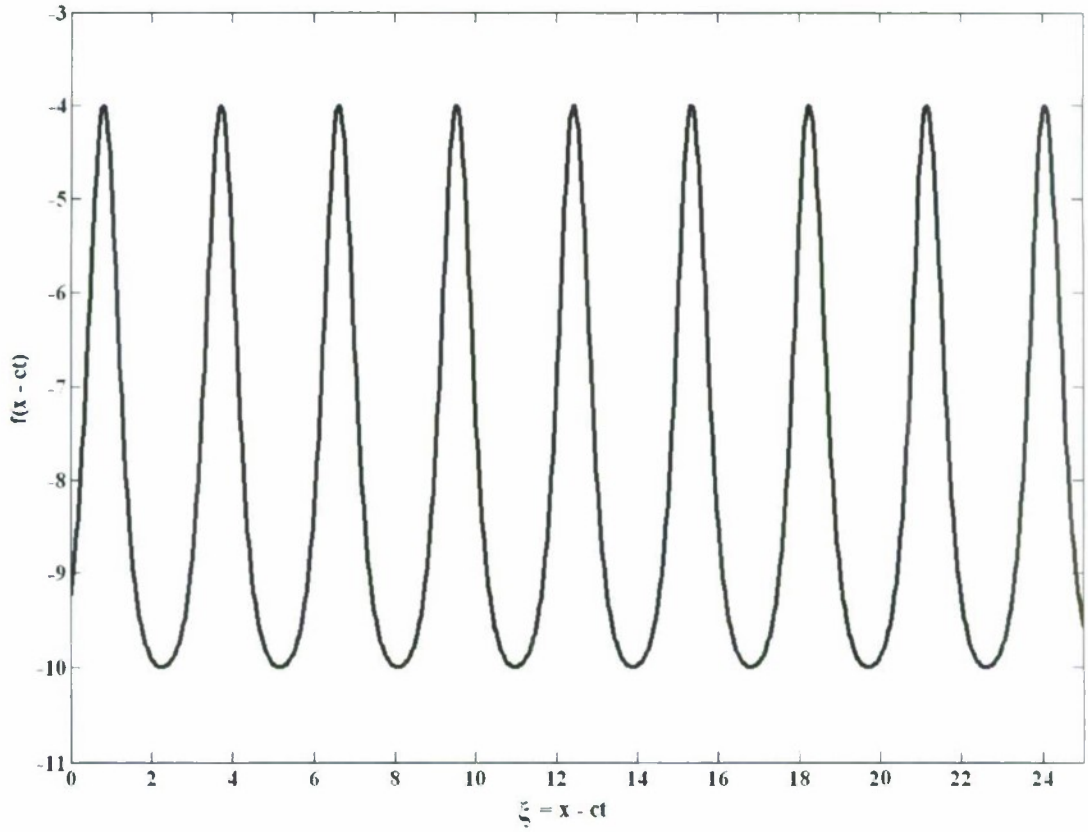

Figure 4.12: A nonlinear soliton wave train, where m of equation 4.23 takes the value 0.95.

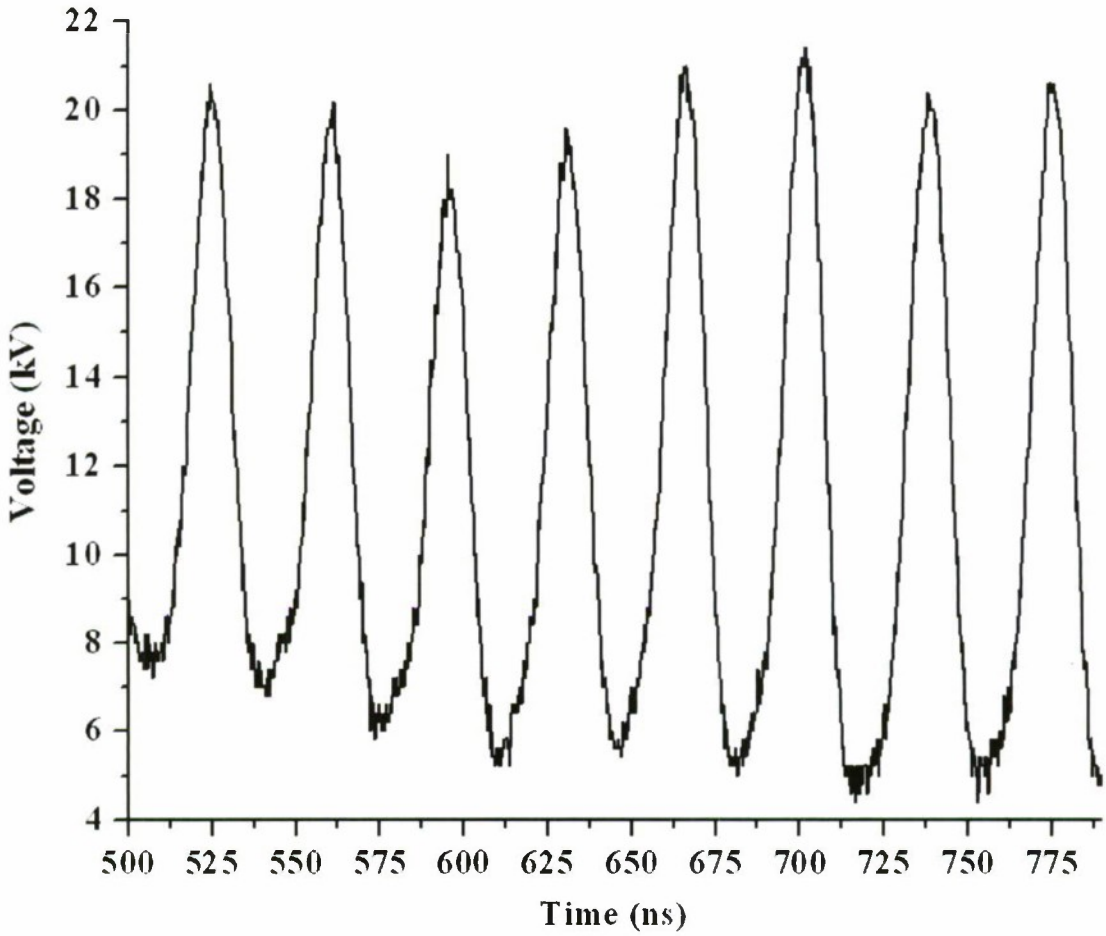

Figure 4.13: A typical experimental pulse burst wave train on a high voltage NLETL (chapter 6).

It is important to consider the discrete nature of the NLETL propagation medium, and also of the associated nonlinear oscillation, and ultimately to question how reasonable it is to label the pulses as solitons. Following the results presented in chapters 5 and 6, this discussion is continued in chapter 7, but note is made here of the 2003 book by Remoissenet [82]. This book pays specific mathematical attention to developing many different aspects of soliton wave theory including that associated with discrete nonlinear systems. In the case of a discrete, but linear, electrical transmission line the characteristic current and voltage equations are subject to a transformation which gives expressions based on a wavelength in unit cells and a velocity in cells per second. A dispersion relation is then obtained, in terms of a normalised wave number $\kappa = \delta k$ where δ represents a unit cell physical length. The relationship so obtained, between κ and angular frequency ω which takes into account spatial dispersion associated with the discrete structure of a line, is given by

$$\omega^2 = \omega_c^2 \sin^2 \frac{\kappa}{2} \tag{4.24}$$

where $\omega_c = 2/\sqrt{LC}$. As expected this curve is clearly dispersive and dictates that pulse profiles will be subject to spreading on a linear discrete line. Furthermore, it implies that the group velocity becomes zero when κ reaches the value π, and that the corresponding cut-off frequency is ω_c. This extreme is termed the Brillouin limit by Remoissenet after the corresponding Brillouin zone described by models for atomic lattices, and implies low pass filter action. Following on from that work, it is interesting to consider the situation where a nonlinear discrete line forces neighbouring stages to oscillate in anti-phase such that the wavelength is necessarily equal to twice δ. It is thus straightforward to write

$$\kappa = \delta \frac{2\pi}{\lambda} = \delta \frac{2\pi}{2\delta} = \pi \tag{4.25}$$

The implication of this statement is that the strong oscillation occurring on an appropriately designed NLETL is occurring at the Brillouin limit, at a maximum frequency whose value is

presumably set by that of the saturated capacitance.

Toda, the originator of the NLETL concept for the investigation of soliton properties, did in fact, it seems, appreciate to some extent the value of the one dimensional lattice model, whereby nonlinear interaction forces are associated with equations of motion, as may be generated by an equivalent mechanical system [45]. Whilst this idea did not feature notably in future reports on the matter, a wider study of the field reveals that several forms of solitons exist in principle, other than those generated by a counter–balance between nonlinearity and dispersion in a continuous medium. Breathers, or "entrapped periodic solutions" [76], are basically oscillatory localised excitations which may be standing or travelling, and are considered to be solitonic in nature. A form of discrete breather soliton has been identified on certain lumped element transmission lines incorporating very high loss in the form of capacitor series resistance. This 'diffusive soliton' forms a single transition, or kink, between voltage levels courtesy of a diffusion–loss power balance [82] at resistances of a few hundred ohms. However, the circuit is not comparable with that of NLETL systems currently under consideration, where capacitor ESR is typically far lower and will in fact inhibit oscillation if of any significant value (section 5.4).

An alternative form of soliton wave, the discrete lattice breather, is of immediate interest, although apparently rarely discussed in published literature. It has been associated with motions in atomic lattices where, critically, individual elements may sometimes oscillate in anti-phase with one another [82]. This anti-phase property is now considered a defining characteristic of the NLETL pulse burst waveforms of interest, which may perhaps be considered analogous to the motion of a one dimensional lattice subject to nonlinear interactive forces. A detailed mathematical study by Aubry in 1997 [83] investigated the spatially localised and time periodic structures (breathers) occurring at the anti-continuous limit on arrays of nonlinearly coupled oscillators. Certain solutions also exhibited the anti-phase property and were found to be very

robust to disturbances, but the coupling between elements was required to be reasonably small, a fact that could possibly be related to the practical limit on reducing the line inductance value (section 5.4). It falls outside the scope of this work to subject to rigorous proof the idea that electrical NLETL systems under consideration are generating discrete lattice breathers, but it is an interesting proposition. The suggestion offers a material link with soliton wave theory, and this is reassuring to note given the unusual waveform behaviour typically observed, despite the issues with previous associations which have now become clear. The term 'soliton-type' wave is often used here, to reflect the practical link with soliton theory which is subject to some uncertainty but remains relevant.

Chapter 5

Simulation

5.1 Motivation for Numerical Modelling Work

The generation of pulse burst waveforms on NLETL systems has been investigated from experimental, analytical and numerical perspectives. The practical development of experimental systems is the primary interest, with important insights and representative results to be gained and reported on. The analytical work introduced in the previous chapter has relevance to the interpretation of experimental waveforms and has led to some useful observations and ideas. In addition, a large quantity of information has been obtained from a comprehensive numerical study which models the voltage and current waveforms on a nonlinear electrical transmission line circuit.

The development time dedicated to the resulting computer tool, the implementation of which is detailed in the following section, proved to be justified for many reasons. In comparison with the process of designing, building and obtaining results from an experimental NLETL, results may be generated very quickly, typically in just a few minutes. This is particularly relevant to longer lines, which inevitably take considerable amounts of time and materials to construct and test. There is no direct expense associated with a given simulation run, whereas most of the nonlinear capacitive elements to be described in subsequent chapters are relatively costly to obtain, especially when required in large numbers. In fact, the range of suitable capacitor options available (both low and high voltage) proved to be quite limited and by simulation a wider range of parameters relating to the nonlinear characteristics may be considered. Various NLETL studies have in the past included some element of numerical modelling (for example [47] [41]) but with limited scope, reporting specific qualitative results on each occasion.

In this way, the simulation capability has contributed to the process of establishing the key trends summarised in section 6.3. Numerical results can sometimes be compared directly with experimental work, and have assisted in designing lines, in addition to enabling a wider comprehensive investigation of design parameters. It is anticipated that the results from this phase

of the work will be important design considerations for practical NLETL systems, an example being the emphasis on a large CNL ratio but modest CNL steepness when subject to a given drive voltage (section 6.3.3). The simulation tool has also made a contribution to the design of a large number of experiments, evolving alongside this aspect of the work to incorporate increasingly complex configurations and combinations of lines.

Initial simulated waveforms (section 5.3) were in good agreement with experimental results in terms of, for example, frequency, peak amplitude, modulation depth of oscillation and characteristics such as anti-phase, envelope modulation patterns and extraction. Appendix C should be consulted for code details and technical notes on the simulation; the following sections offer a brief introduction to the C++ implementation and a review of typical results. The opportunity is also taken in section 5.3 to make note of a few basic characteristics apparently fundamental to NLETL pulse burst waveforms.

5.2 Implementation of the NLETL Simulation Tool

Further to specific references made below, acknowledgement is made of the material in several textbooks on C and C++ [84] [85] [86] [87] which were used on many occasions during the development of the NLETL simulation tool. The Microsoft Visual Studio 6.0 C++ compiler was used to create a GUI interfaced application (figure 5.1) with an object oriented (OOP) data structure. An output ASCII file is created for current and voltage at the stages of each line with respect to discrete time steps, and each run has an associated information text file detailing all the relevant parameters at the time. It was earlier noted that, in a nonlinear circuit, Kirchoff's conservation laws still apply subject to the nonlinearity being taken into account, a fact used to generate generate nonlinear differential equations and associated difference equations suitable for numerical processing. The form of capacitive nonlinearity with respect to voltage V generally used throughout is given in equation 5.1, although other CNL curves have also been tried out

at times.

$$C = C_{nom}\left\{cnl_a + (1 - cnl_a)\exp(\frac{V}{cnl_b})\right\} \tag{5.1}$$

It is important to distinguish between the influences of constant values cnl_a, which determines the ratio of nominal to saturated capacitance, and cnl_b which relates to the steepness of the exponential curves illustrated in figure 5.2.

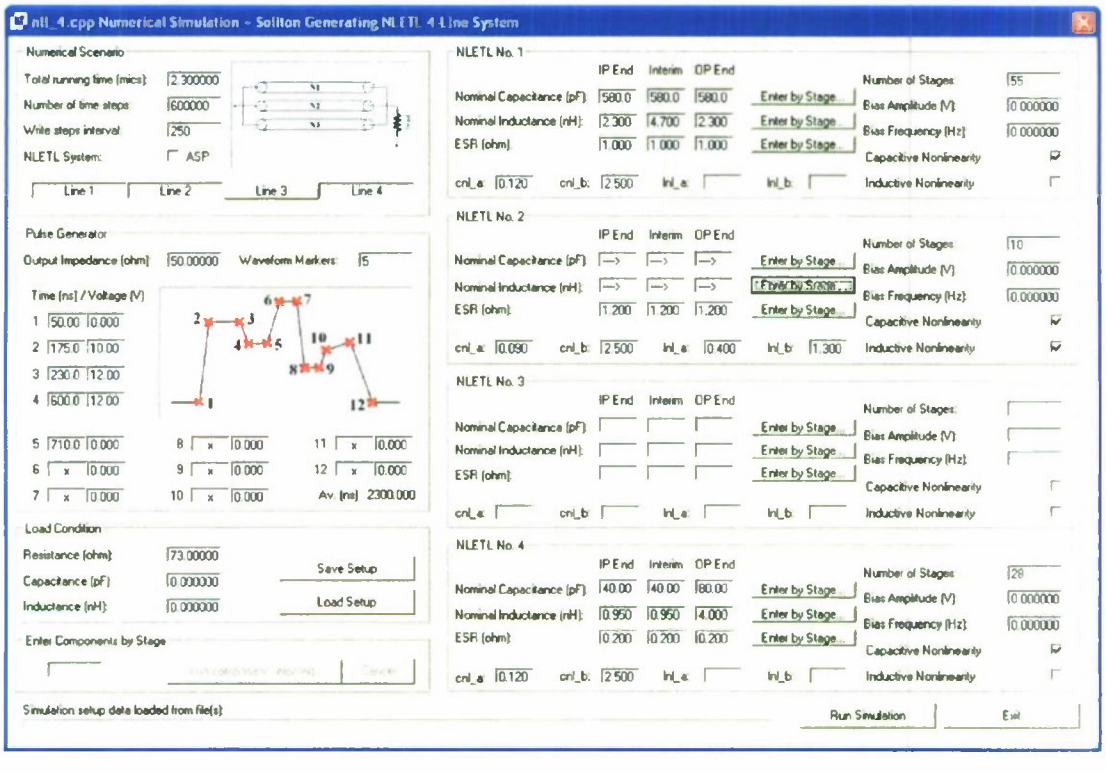

Figure 5.1: Graphical user interface developed with the four line NLETL simulation tool.

Using NLETL stage numbering and terminology in accordance with figure 3.1 it is straightforward [43] [49] to obtain the difference equations 5.2 and 5.3. The derivation is based on the capacitor charge equation $Q = CV$ and the fact that current $I = \frac{dQ}{dt}$, and also incorporates a capacitor ESR loss (no inductor loss was included) which causes the actual n^{th} capacitor vol-

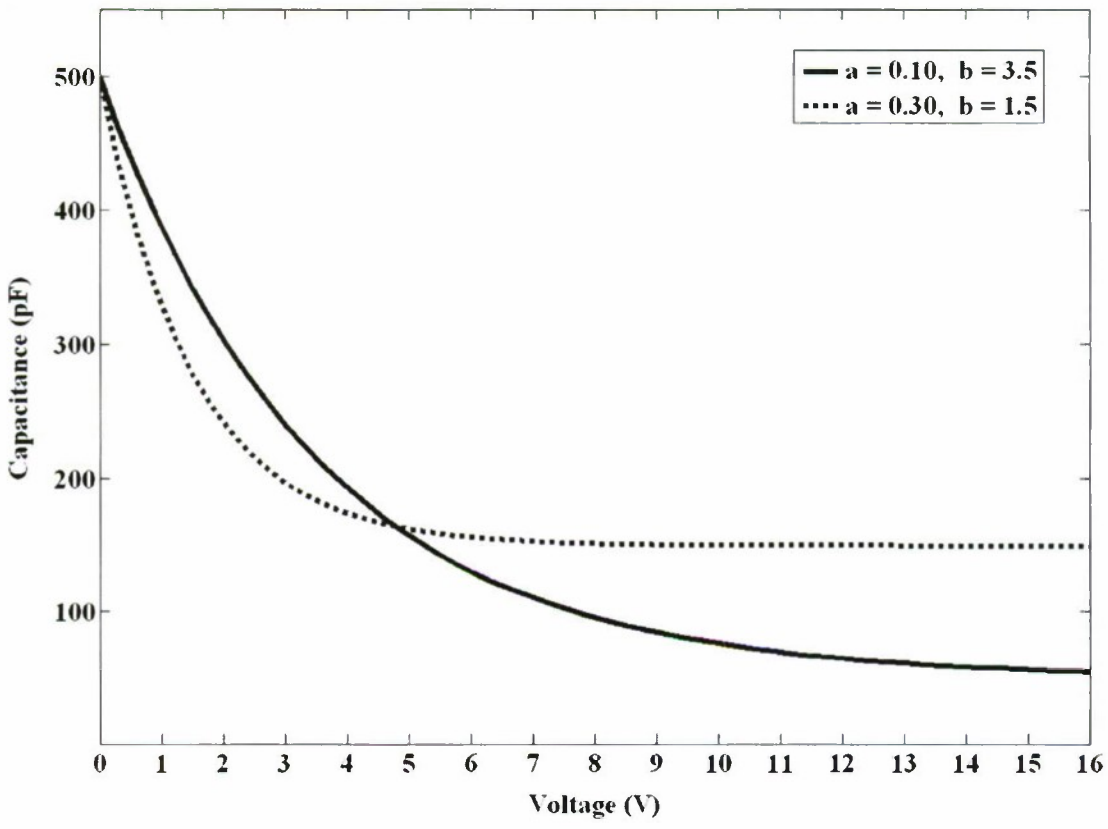

Figure 5.2: Two exponential CNL curves generated via equation 5.1, where a smaller value of cnl_a leads to a high ratio of nominal to saturated capacitance, and a smaller value of cnl_b corresponds to a steeper curve.

tage to take the value $V_{n,cap} = V_n - I_{n,cap}R_n$. With reference to the stage numbering previously illustrated in figure 3.1:

$$\frac{d}{dt}(C_n(V_n)V_n) + R_n\frac{d}{dt}(C_n(V_n)I_n) - R_n\frac{d}{dt}(C_n(V_n)I_{n+1}) = I_n - I_{n+1} \tag{5.2}$$

$$L_n\frac{dI_n}{dt} = V_{n-1} - V_n \tag{5.3}$$

The corresponding incremental changes in current and voltage values at the n^{th} stage during a time interval Δt are then written as

$$\Delta I_n = \Delta t\frac{V_{n-1} - V_n}{L_n} \tag{5.4}$$

$$\Delta V_n = \Delta t\left[\frac{I_n - I_{n+1}}{C_n(V_{n,cap})} - R_n\frac{V_n - V_{n-1}}{L_n} + R_n\frac{V_{n+1} - V_n}{L_{n+1}}\right] \tag{5.5}$$

Euler's well known method [88] for a discrete function $f(t_n, V_n)$ stipulates that the new value of voltage, V_{n+1}, may be approximated from the incremental change in time from t_n to $t_{n+1} = t_n + \Delta t$ as $V_{n+1} = V_n + \Delta t f'(t_n, V_n)$. The product of time step and first time differential of f is simply the incremental change in V_n given by equation 5.5. A more accurate method under similar conditions is given by the fourth order Runge–Kutta equations

$$V_{n+1} = V_n + \frac{1}{6}k_1 + \frac{1}{3}k_2 + \frac{1}{3}k_3 + \frac{1}{6}k_1 \tag{5.6}$$

where

$$k_1 = \Delta t f'(t_n, V_n) \tag{5.7}$$

$$k_2 = \Delta t f'(t_n + \frac{\Delta t}{2}, V_n + \frac{k_1}{2}) \tag{5.8}$$

$$k_3 = \Delta t f'(t_n + \frac{\Delta t}{2}, V_n + \frac{k_2}{2}) \tag{5.9}$$

$$k_4 = \Delta t f'(t_n + \Delta t, V_n + k_3) \tag{5.10}$$

The code used to implement this method and the application as a whole (called `nll_4`) may be found in appendix C. The complete system is based on an OOP (object oriented programming) object called `nl_line` corresponding to a single NLETL.

The OOP approach is suited to more complex data management and supports well organised ongoing development of functionality. For example, the subsequent incorporation of multiple NLETLs for the simulation of parallel and ASP configurations simply created additional instances of the standard `nl_line` class definition, albeit with some minor modifications enabling the appropriate interaction between lines. The various object definitions encapsulate the necessary functions for processing and a `nl_line` object will also contain the necessary data, or pointers to it. Due to the strong nonlinearity and algorithm used, a large number of calculations are generally carried out with a correspondingly large quantity of data to be dealt with, especially with longer lines. Pointers are used where possible for efficiency, and naming conventions used in the code to distinguish pointers, member variables etc. are outlined at the start of appendix C. Initial testing revealed certain issues with the large quantities of data generated, and a new data type `tba[501]` was defined, consisting of an array of 501 pointers such that blocks of processing steps may be carried out between saves to disc, avoiding the use of massive data arrays. This successfully achieved a balance between file write operations and memory stack usage and avoided instabilities or excessively long processing times. The `tba[501]` data type allowed the dynamic allocation of the pointer array for current and voltage at each stage of the line. Throughout the code, the de-reference notation used is as per `(*p(__line_voltage + S))[T]` for voltage data, where `S` indicates stage number and `T` the time step within the current time block.

Via the user interface illustrated in figure 5.1 it is possible to quickly define a wide range of parameters for a given simulation scenario. These include, for example, line inductance, nominal capacitance, CNL parameters and loss, in addition to numerical settings such as running time

and step length.

The large number of time steps required when frequencies are high are not necessary for representative data output, and to avoid excessive disc space usage it is possible to specify an interval between time steps at which to record data. The ASCII data files generated as output may be plotted and analysed with data analysis software.

5.3 Capabilities and Summary Results

Extensive testing during development, and comparison with experimental results where possible, indicate that the simulation tool functions correctly and generates largely accurate results. A comparison between typical experimental and equivalent numerical waveforms is made by figure 5.3 and figure 5.4. In each case the unusual behaviour of an appropriately designed NLETL subject to a wide input pulse is clearly demonstrated. The pulse immediately breaks up to form a train of high frequency pulses which after just a few discrete stages have developed almost full modulation throughout the input pulse duration. Individual pulses are symmetrical, as per the sech^2 soliton form, but the overall envelope develops a sharpened leading edge which is to be expected of a nonlinear transmission line. The tail is also extended according to the nonlinear effect and typically contains some oscillation at a lower frequency than that in the body of the pulse.

A key pattern which is followed by the shape of the modulating envelope is evident in figure 5.5, the three distinct forms of which are referred to here as type I, type II and type III waveforms. The overall modulation generally follows this pattern, although certain lines driven very quickly may immediately generate the type II or type III waveform, and the extended pulse bursts supported by higher frequency lines often develop periodic modulation envelopes (for example see figure 5.13) [82].

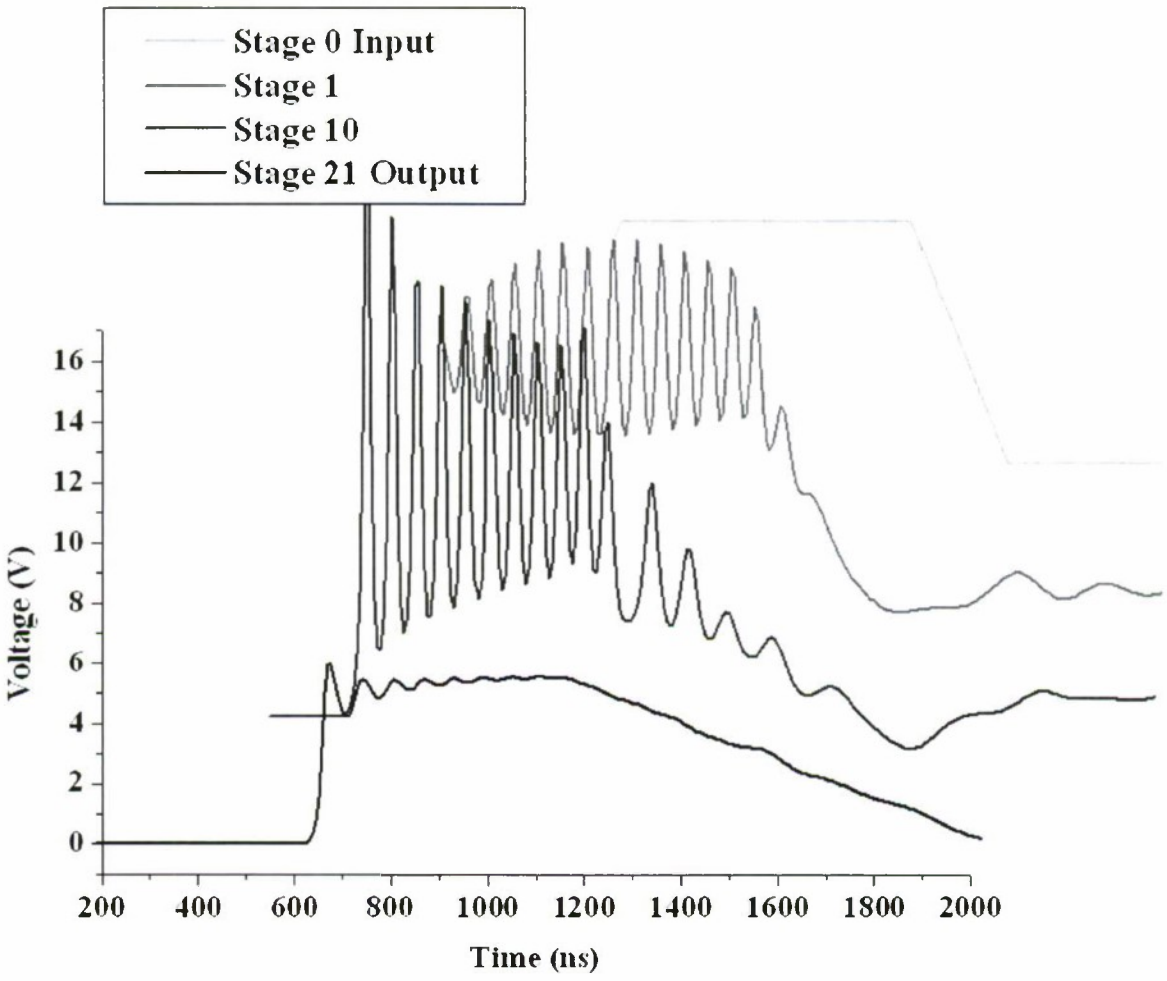

Figure 5.3: Selected stage voltage waveforms along a simulated NLETL.

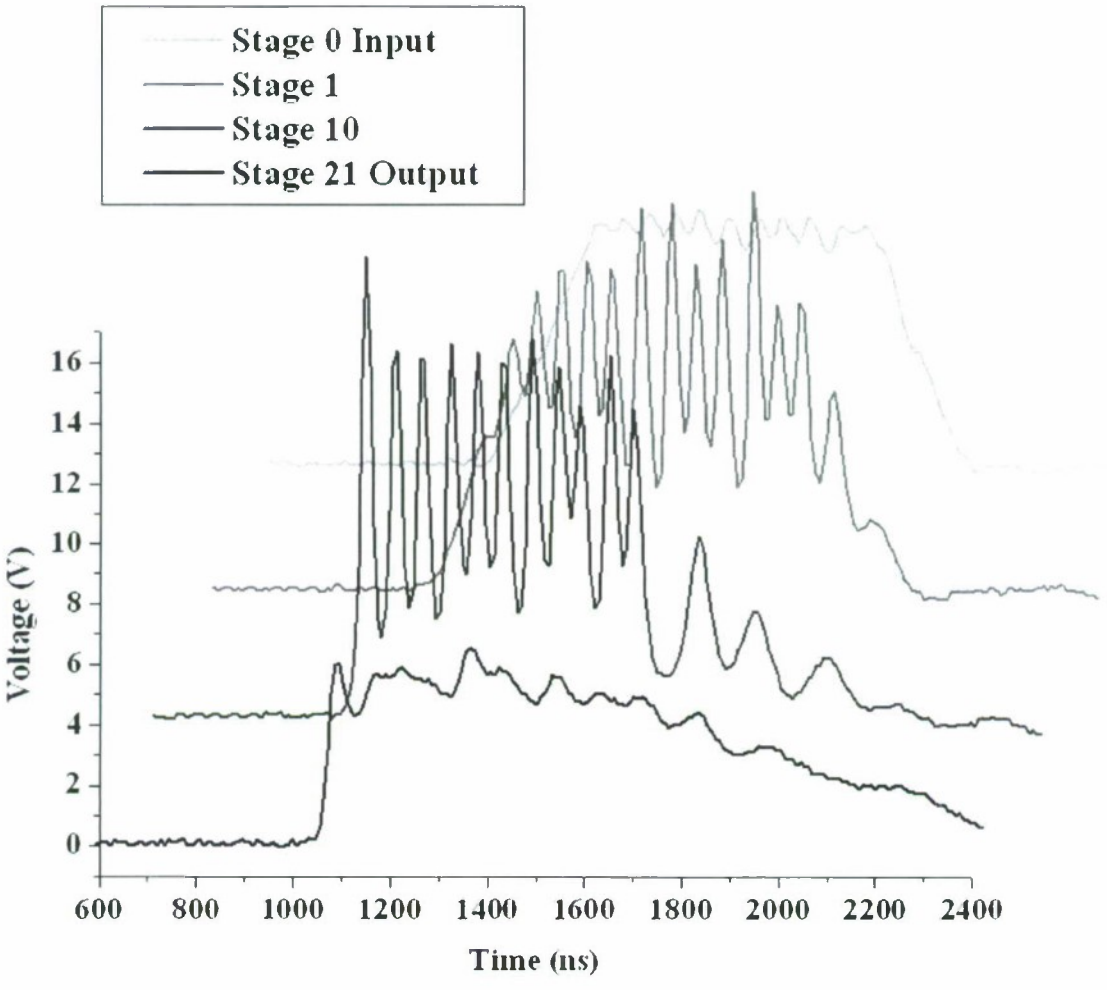

Figure 5.4: Selected stage voltage waveforms along an equivalent experimental NLETL.

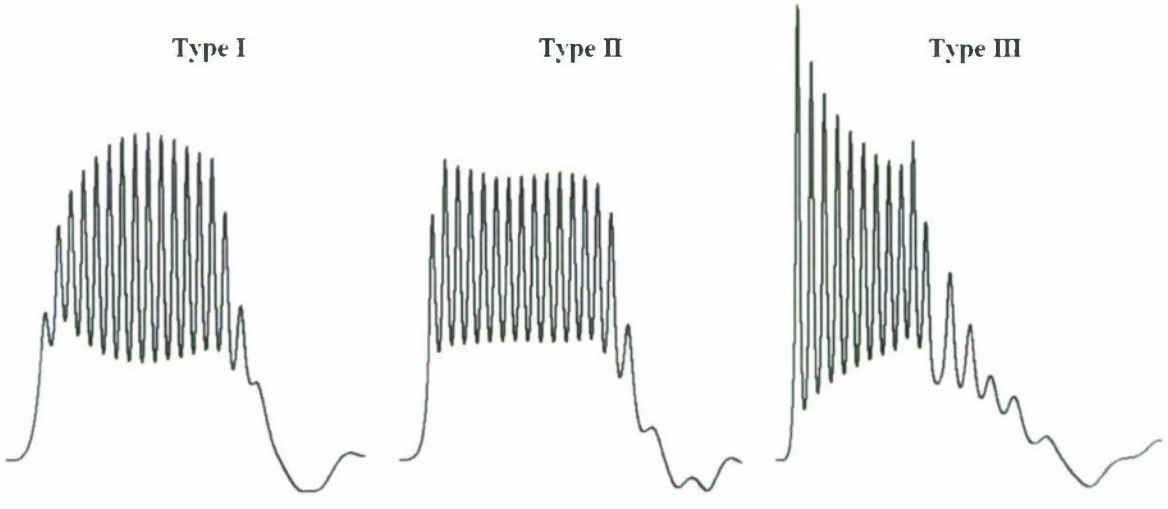

Figure 5.5: The three envelope shapes through which a typical NLETL pulse burst evolves over the initial few stages.

The voltage modulation depth (VMD) of oscillation, is severely weakened upon extraction from the NLETL to a linear load resistor. The extraction problem and potential means of achieving efficient extraction of RF energy to useful load impedances is central to much of this work. The lines of figure 5.3 and figure 5.4 were terminated by a resistance value approximately matching the (nonlinear) line impedance—the value of minimal reflection is judged to be around the nominal unstressed characteristic impedance of the NLETL—leading to a gradual and fairly uniform reduction in oscillation over the final few stages. Figure 5.6 illustrates the typical nature of extraction to a low value resistance termination. This is an interesting case for the loss of precisely one soliton pulse per stage backwards from the output end. The effect is also seen in the complete set of stage voltages from a representative 16 stage simulation, shown in figure 5.7. Similarly, a load which is significantly higher than the nominal line impedance leads again to the loss of one pulse per stage, replaced by a step up instead of step down in voltage. The extraction issue is discussed further in chapter 6, as indeed are many important trends identified in both experimental and simulated results.

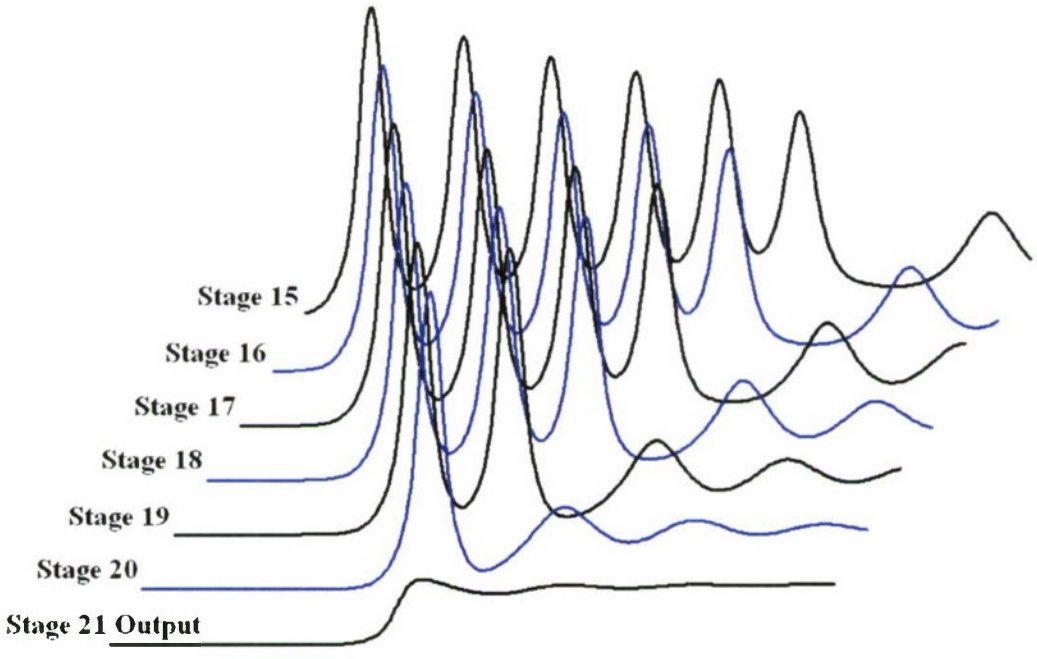

Figure 5.6: Output end stage voltage waveforms on a simulated NLETL of 100 Ω nominal characteristic impedance terminated by a 60 Ω resistor.

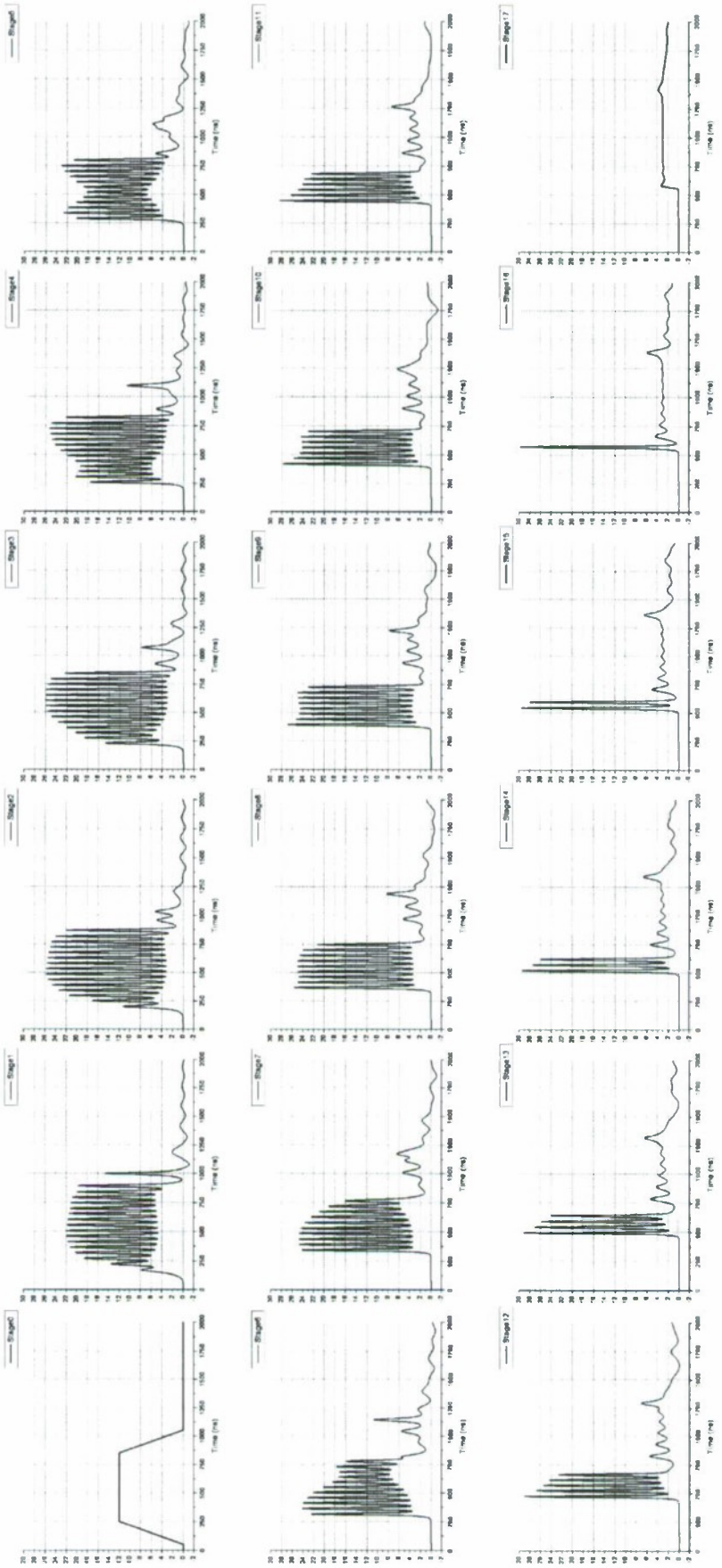

Figure 5.7: Typical progression of voltage waveforms on a simulated NLETL, showing the extraction problem and associated loss of one pulse per stage backwards from the load.

A specific aspect of NLETL design for which currently available experimental options are limited is the capacitive nonlinearity (CNL), in terms of its steepness with respect to applied voltage and its ratio of nominal to fully stressed capacitance values. Simulation results imply that increasing the CNL ratio, according to a small value of cnl_a in equation 5.1, leads to oscillation of improved modulation depth and higher frequency. Frequency on a given NLETL is plotted against a range of nominal and saturated capacitance values in figure 5.8, all other parameters remaining constant. Clearly the highest frequencies are reached via low values of both, but decreasing the saturated value for a given nominal capacitance—using a larger CNL ratio—has a strong influence on frequency in itself. A typical graph of frequency versus CNL ratio would be approximately exponential whereas the dependence on nominal capacitance, for a given CNL ratio, is more or less linear. This observation is also particularly valuable to note given the need to maintain reasonable discreteness and hence limiting values of capacitance and inductance for strong oscillation (section 5.4). Although unhelpful with low load impedances (figure 5.9), there are also indications that an exponential nonlinearity possessing a very low value of cnl_a could dramatically improve RF extraction to resistive loads (figure 5.10). However, such a large CNL ratio is far from that achievable with currently available and recognised materials or components.

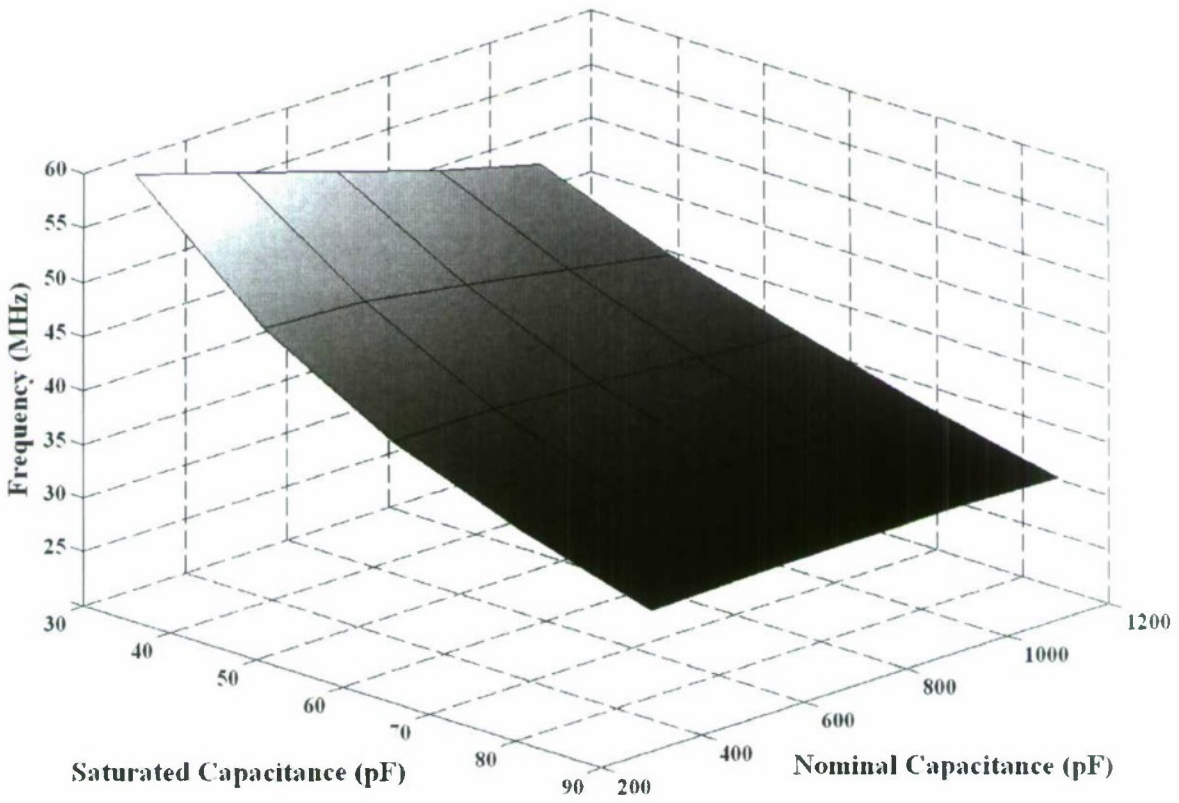

Figure 5.8: Frequency of oscillation recorded on a range of simulated lines of various nominal and saturated capacitance values, all other parameters remaining constant.

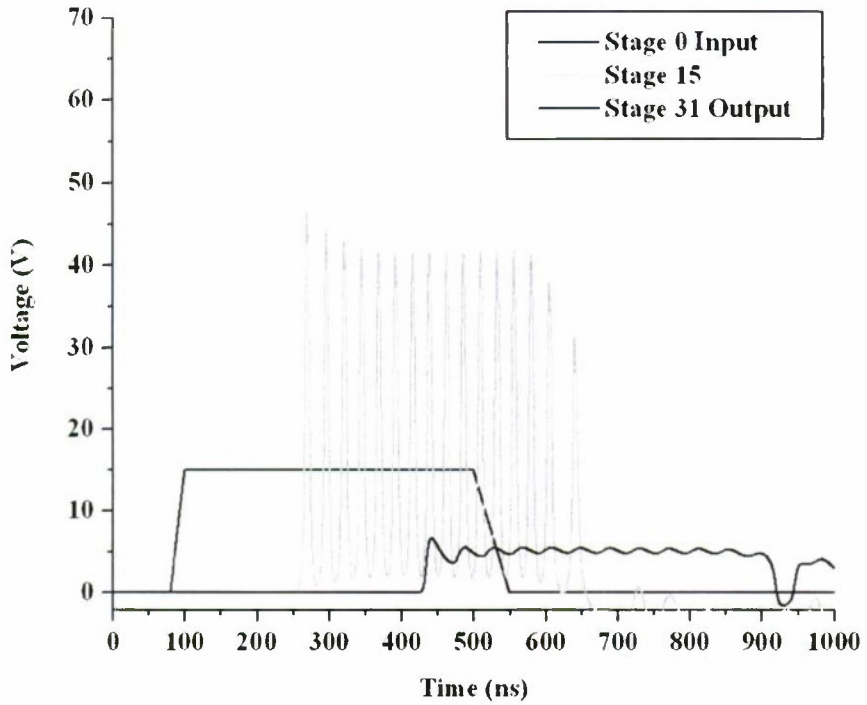

Figure 5.9: Simulation data for a 30 stage NLETL with an inductance of 1 μH, nominal capacitance of 600 pF and very large CNL ratio of 25 ($cnl_a = 0.04$; $cnl_b = 3.5$), terminated with a 30 Ω load.

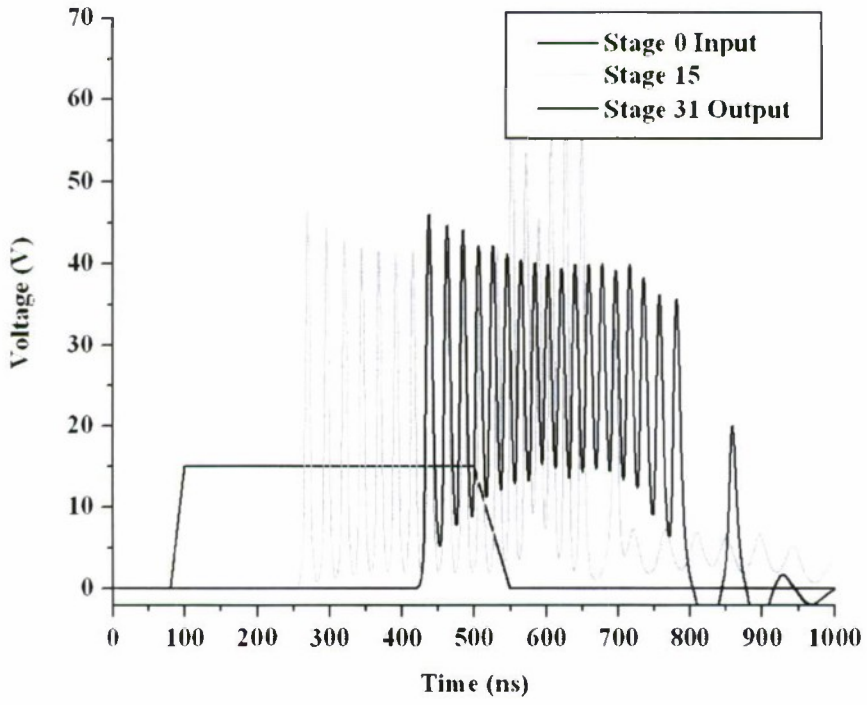

Figure 5.10: The simulation run as per figure 5.9 but with a larger 300 Ω load.

In addition to single uniform NLETLs, simulations have been run with tapered lines, multiple lines in parallel and ASP configurations and magnetic nonlinearity. An inductive nonlinearity may be crudely represented by an exponential decrease in inductance with increasing current flow; the addition of this property to a line already incorporating dielectric nonlinearity is not found to have a very significant effect. In itself, a magnetic line is still found to suffer from the extraction problem with pulse shortening and reduced output peak to peak amplitude, although arguably to a somewhat lesser degree. However, the extraction problem for a dielectric NLETL is not too severe at lower frequencies and the frequency of oscillation on a magnetic line is generally lower than its equivalent dielectric counterpart. The pulse train forms simultaneously, rather than one pulse at a time, but takes many more stages to fully form and appears to be more susceptible to the presence of ESR type loss. The anti-phase relationship between adjacent stage waveforms, utilised by the ASP and periodic loading concepts (section 6.4.3 and section 8.6), is not maintained, although the system is still very much in the discrete limit with a phase difference of around 120° between stages. There are disadvantages with using magnetic materials in this context, such as larger hysteresis loss, and magnetic lines have not been studied in any great detail on this occasion because the work is concerned primarily with lines incorporating dielectric nonlinearity.

The simulation tool described is subject to certain limitations and there is scope for further development and improvement. As the frequency of oscillation increases, so too must the number of time steps if instability is to be avoided, and at very high frequencies (exceeding around 500 MHz) it becomes impractical to complete the numerical process in a stable manner. This has not presented a significant limitation on single line simulations designed to support experimental work, results from which have not exceeded 250 MHz, but is a significant problem with the ASP scenario, which appears to be particularly unstable. In order to further extend the capabilities of the simulation tool, future work in this area would be based on a variable step length method designed to deal with strongly nonlinear systems which may fluctuate between

being 'stiff' and 'non-stiff' [89]. The problem with stiff equations occurs when solutions begin to contain components with very different growth parameters, but due to large compounded rounding errors a simple reduction in step length is problematical where the nonlinear solution temporarily becomes smooth.

5.4 Characterisation of Oscillation over $L - C$ Space

According to numerical results using this simulation, should the NLETL stage inductance or capacitance, or both, be too low then the generation of soliton–type pulse trains is severely compromised. In order to assess the general patterns and limits on frequency for a range of typical lines, the `nl_line` object was built into a special simulation tool designed to run over a matrix of inductance and nominal capacitance values. The simulation task required to generate output data such as figure 5.11 is time consuming and typically takes several days to complete, but this is not a significant problem since it was only required to run a few times. The lowest inductance and nominal capacitance values were limited by the ability to avoid instability with a reasonably large number of time steps.

It initially appears that at very low values of inductance and or capacitance the oscillation reduces appreciably, and at extreme values the simulation shows no indication of any soliton–type pulse generation. The limitation is perhaps understandable in practice, since the phenomenon is now understood to be reliant on NLETL discreteness (chapter 7). With very small component values, in the continuous limit, frequency would have to become infinitely large to maintain stage by stage anti-phase, and the discrete mechanism which induces this type of oscillation becomes less significant. It seems, looking at the left and lower edges of figure 5.11 that a very low inductance is more of a problem than a very low nominal capacitance. In general, however, both component values need to be reasonably high to initiate good quality oscillation. The example simulation presented here was run with a 'typical' capacitor ESR of 0.5 Ω; it was subsequently noted that much higher frequencies are achievable by reducing inductance and

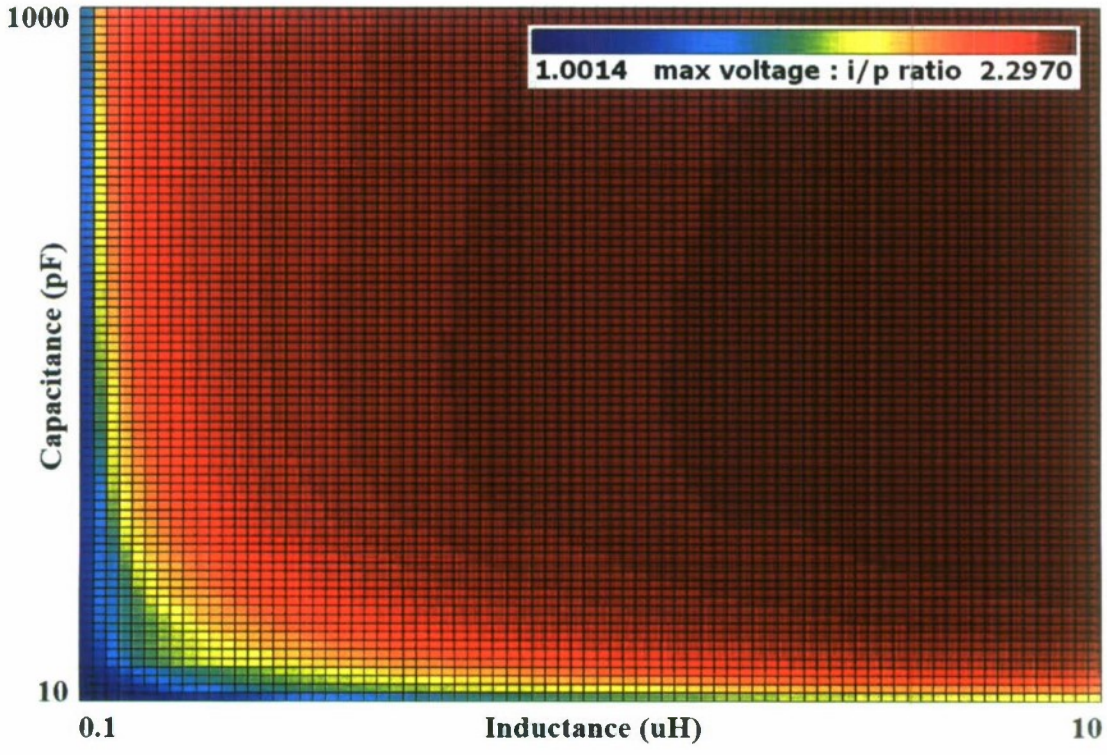

Figure 5.11: The degree of oscillation induced on a NLETL over a wide range of inductance and nominal capacitance values, implied by the ratio of peak amplified voltage to input pulse amplitude (scales are linear).

capacitance when the ESR is zero.

It may be reasonable to suppose NLETL operation could in theory be scalable in frequency without limit, and a subsequent analysis of the influence of loss has brought an important point to light. Simulations run at moderate frequencies (the order of 50 MHz) in support of earlier experimental work suggest that the actual value of ESR is not particularly relevant in terms of pulse burst generation up to several, if not tens of Ω. However, a simulated line designed to operate at frequencies within the microwave region is in fact very sensitive to the value of ESR, with quite moderate values leading to a dramatic reduction in oscillation compared with the lossless equivalent case. Figure 5.11 gives a general pattern in the presence of a typical loss value, but the actual frequencies which may be reached (by a reduction in inductance and nominal capacitance) before oscillation collapses are dependent on loss.

The relaxation frequency associated with an electrical dielectric (chapter 3) implies a limit on frequency which is of interest in this context. It turns out that one simplified model used to represent dielectric relaxation is in fact the addition of a series resistor [42] and resulting non-zero time constant. The presence of dielectric and connection loss, effectively in the form of an ESR resistance, thus presents an equivalent limitation on frequency response to that of dielectric relaxation, but at a much lower frequency. As such, some of the concern with relaxation effects may be better directed at the materials science of achieving ultra-low loss, since according to simulations the latter limitation is dominant.

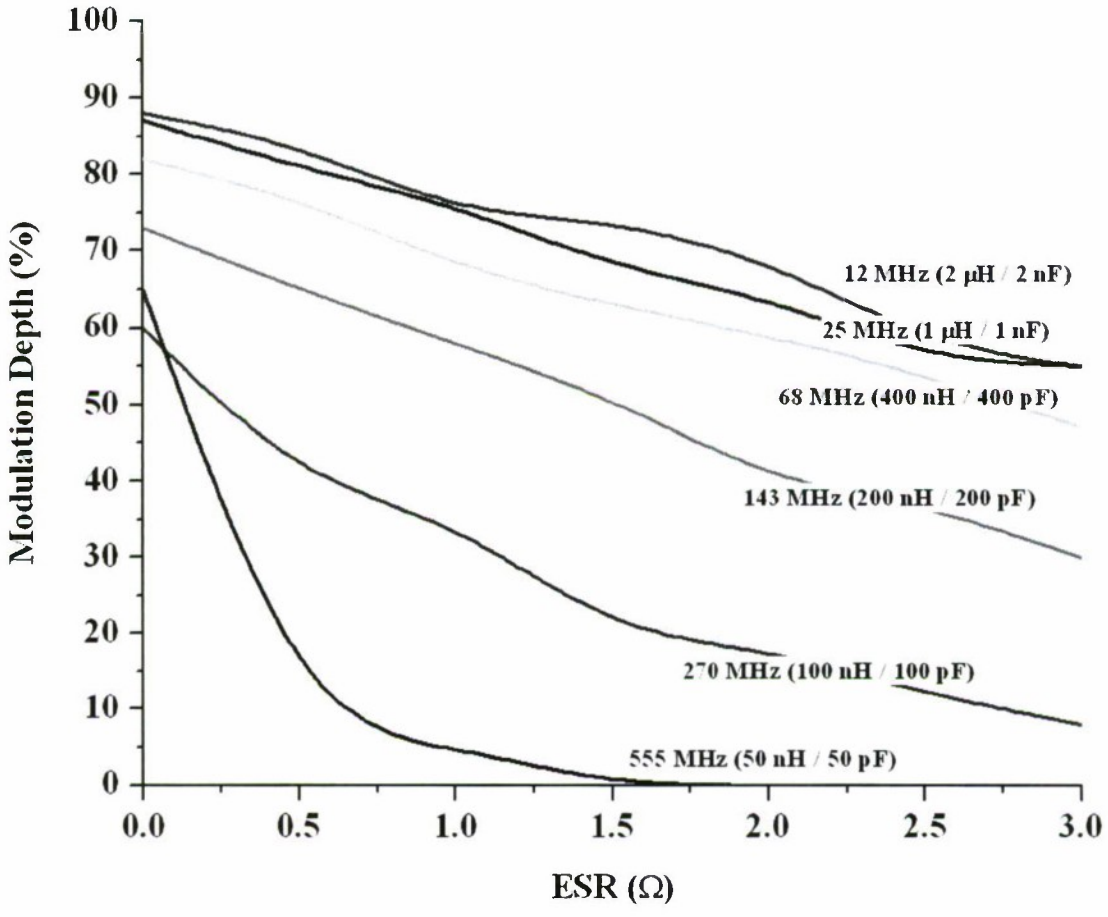

Figure 5.12: The reduction in percentage voltage modulation depth at stage 12 of a 20 stage NLETL as capacitor ESR loss is increased from zero to 3 Ω, measured on the fifth pulse. Simulation parameters are as figure 5.13, with design frequency controlled by inductance and nominal capacitance values.

The increasingly critical influence of ESR loss at higher design frequencies was analysed further over a range of inductance and nominal capacitance values, and some representative results are included in figure 5.12. A 30 stage simulated line was driven by a fast rising input pulse and the percentage modulation depth of the fifth pulse at stage 18 was noted where ESR values ranged from zero to 3 Ω. As inductance and capacitance were reduced the CNL ratio was kept constant, so as to be representative of a reduction in area of a dielectric slab under uniform electric field conditions. A compromised modulation depth generally occurs alongside a significant reduction in pulse duration, and the relative values of inductance and capacitance may also be relevant. The 200 MHz example of figure 5.13 demonstrates a slightly more severe loss of oscillation with 3 Ω of ESR than the 270 MHz line used to generate that data presented in figure 5.12. The former is relevant to the high voltage NLETL of section 8.5 and achieved 200 MHz with an inductance of 50 nH and a nominal capacitance of 500 pF, whereas the latter used values of 100 nH and 100 pF respectively. However, the basic trend is that the initiation of soliton–type oscillation at microwave frequencies is reliant upon very low loss as modelled by an ESR resistance.

All other factors remaining constant, reducing loss then raises the ceiling on frequency, but for a given loss simulation results have shown that a larger CNL ratio also increases frequency potential. The natural question to ask is whether there should be any limit on frequency if a zero loss NLETL were to be available, beyond the current numerical and experimental limits. Some physical explanations for the curious behaviour of NLETLs put forward during this work support the suggestion that there should indeed by a limit, according to the fundamental reliance on discreteness (chapter 7). The difficulty in realising discrete and distinct electrical components at very high frequencies has already been mentioned, as has the presence of a relaxation frequency beyond which a dielectric material will struggle to respond.

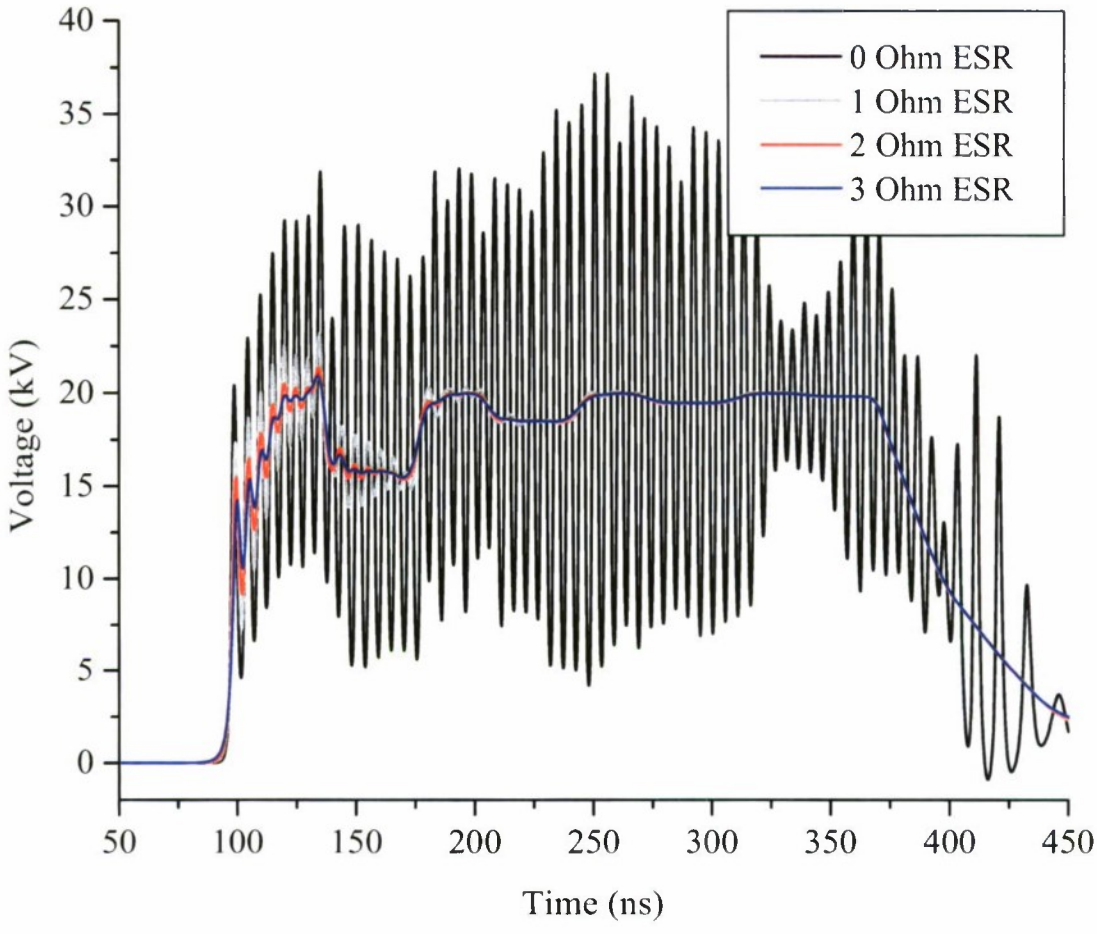

Figure 5.13: Mid-line voltage waveform on stage 12 of a 20 stage high frequency NLETL at different values of capacitor ESR from the lossless case to 3 Ω. The simulation was run with 50 nH of inductance, 500 pF nominal capacitance, $cnl_a = 0.12$, $cnl_b = 3500$ and a 12 Ω termination. The input pulse rise time was 50 ns, amplitude 20 kV and resulting frequency is around 200 MHz.

Chapter 6

Low Voltage Experiments

6.1 Introduction to Low Voltage NLETL Work

NLETL technology has practical value in the realm of high power RF applications, and consequently emphasis was put on the construction and testing of high voltage lines during the experimental work outlined in chapter 8. However, the initial phase of experimental work was at low voltage; in addition to the reduced cost of components, working on the transmission lines at low voltage has the advantage that a typical NLETL can be built in less time, with easier operation and means of accurate measurement. There was, of course, a clear motivation to also investigate and demonstrate successful implementation of the technology at high power levels. Prior to this, the construction and testing of the large number of low voltage lines described here generated many insightful waveforms and results which, alongside wide ranging simulation data, allowed several key design trends to be established (section 6.3). Furthermore, various limitations and issues, for example in achieving high frequencies and effective extraction of RF energy from the nonlinear lines, quickly became apparent. Low voltage NLETL configurations proved the ideal testing ground for several novel ideas to improve operation which arose from the careful analysis of preceding experimental and numerical results.

The results presented in this chapter correspond to the period of work with low voltage lines, which were built using varactor tuning diodes such as the BB133 and BB212 devices. The latter offered a better capacitive nonlinearity characteristic by far and was used almost exclusively, with around 900 obtained in total, each package containing two diodes. The BB212 design has unfortunately been out of production for a while and is difficult to get hold of, so a specialist obsolete component sourcing company was employed to locate the large quantity required.[1] A varactor diode under reverse bias presents a capacitance which decreases with applied voltage by virtue of a hyper-abrupt pn junction, behaving as per an ordinary diode when forward biased [32]. The devices used here were provided in a TO-92 twin package each containing two

[1]Kingsbeech Ltd, Unit 5, Querns Business Centre, Whitworth Road, Cirencester, GL7 1RT. 01285 657756, http://www.kingsbeechltd.co.uk/

matched diodes created from the same silicon wafer, which was coincidentally useful for certain multiple line NLETL configurations. Due to their sharing a common cathode, and the need to operate under a negative bias for the nonlinear response, the cathode was treated as earth and a negative voltage pulse used to drive each NLETL. According to its data sheet the BB212 is rated to 12 V and 100 mA but was found to survive substantially greater pulsed voltages during this work. The stated ratio of nominal to saturated capacitance values is around 10, and indeed measurements taken with a Sawyer-Tower circuit [43] suggested reduction from 570 pF to 50 pF over 11.2 V. An alternative diode which is currently commercially available, the BB133, has a much lower nominal capacitance at around 50 pF and, in accordance with simulation results, would only generate reasonable oscillation in a line of very high inductance. Combined with a relatively poor CNL ratio this limited BB133 lines to low frequency operation with short pulse durations (figure 6.1).

No other devices in production were found to come close to the BB212 for nonlinearity ratio and nominal capacitance, hence the time put into locating it, and various alternatives such as red LEDs (known to be relatively nonlinear) were also tried with poor results. Inductors were generally air cored and wound in-house to reduce loss although a few higher inductance low voltage lines used commercial ferrite inductors despite the increased cost. Nominal capacitance could be reduced and peak voltages approaching 200 V were reached by stacking several diodes per stage, and reasonably good voltage sharing was measured in such circumstances. A wide range of line designs, lengths and configurations (section 6.4) were built and tested, with frequencies ranging from a few MHz to 250 MHz. The necessary input waveforms were typically supplied by a range of pulse generators such as the Philips PM5715 (to around 20 V) and the KSM Type T16 (to around 50 V), although the higher voltage stacked diode lines were driven by a series of matched pulse forming lines in combination with a 400 V power supply and MOSFET switching circuit. General good practice in making high frequency measurements was adhered to during these experiments, particularly with respect to

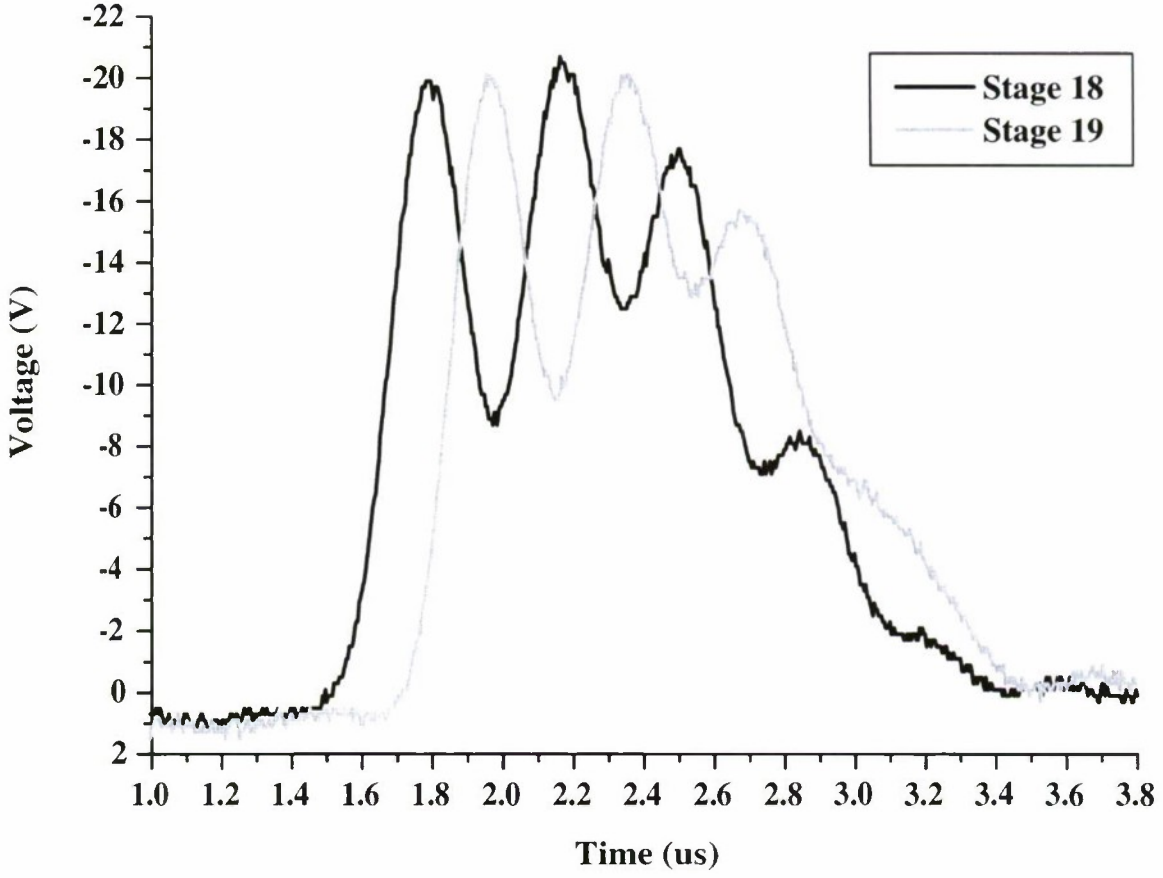

Figure 6.1: Experimental waveforms obtained from a BB133 low voltage NLETL, demonstrating soliton type oscillation with anti-phase maintained between the two adjacent stage voltages (section 4.2), but at the modest frequency of 2.8 MHz and with relatively poor modulation depth.

earthing and minimising stray inductances at points of measurement. Low inductance solid carbon resistors were preferred over helical or wire wound equivalents, and voltage waveforms measured as close to their terminals as possible where inferences of energy extraction are made. Sufficient bandwidth oscilloscopes (Tektronix 2440 to 500 MHz and Tektronix DPO 4104 to 1 GHz) and probes (for example PMK PMMG511 to 500 MHz and 600 V) were used throughout.

Motivation during this initial experimental phase of the work, and for the project as a whole, was partially provided by the clear need to carry out a more detailed characterisation of the phenomenon on a much wider range of lines, to investigate limiting factors and establish a context

for subsequent results and observations. Similar factors motivated the NLETL simulation code, which also enabled parameter values, such as those controlling CNL characteristics and loss, to be varied beyond those reasonably available in practice. Various NLETL design trends, often not previously appreciated, are summarised in section 6.3 and are valuable outcomes of the work which should be taken into account where good operation at specific frequencies and power levels is desired. The observation of fundamental discreteness and anti-phase was also made and first published during this work and, alongside these experimental, numerical and more abstract mathematical results forms the basis of many of the ideas discussed in chapter 7.

Low voltage experiments also enabled certain issues, such as the extraction of RF energy to resistive loads, to be investigated in practice. It was relatively convenient to test novel ideas using BB212 diodes, and improved extraction was indeed demonstrated via special line configurations.

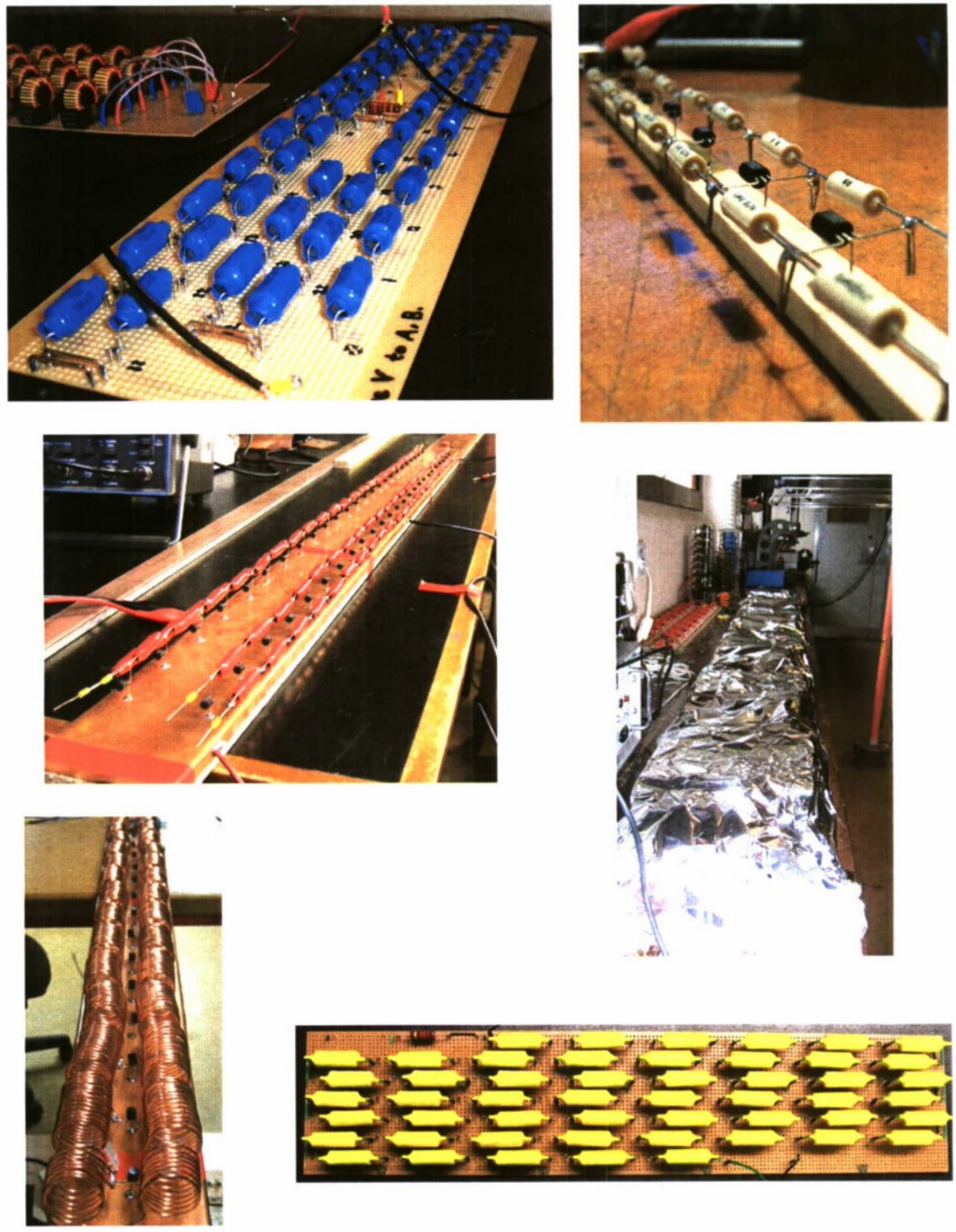

Figure 6.2: Some low voltage experimental lines based on BB133 and BB212 varactor diodes.

6.2 Experimental Pulse Burst Waveforms

The generation of single soliton pulses and extended pulse burst waveforms has been demonstrated successfully, with examples given here in figures 6.3 through 6.7. The results of a more detailed characterisation of the phenomenon on low voltage lines are summarised in the following section. That includes the conditions necessary to induce oscillation on a discrete transmission line incorporating capacitive nonlinearity.

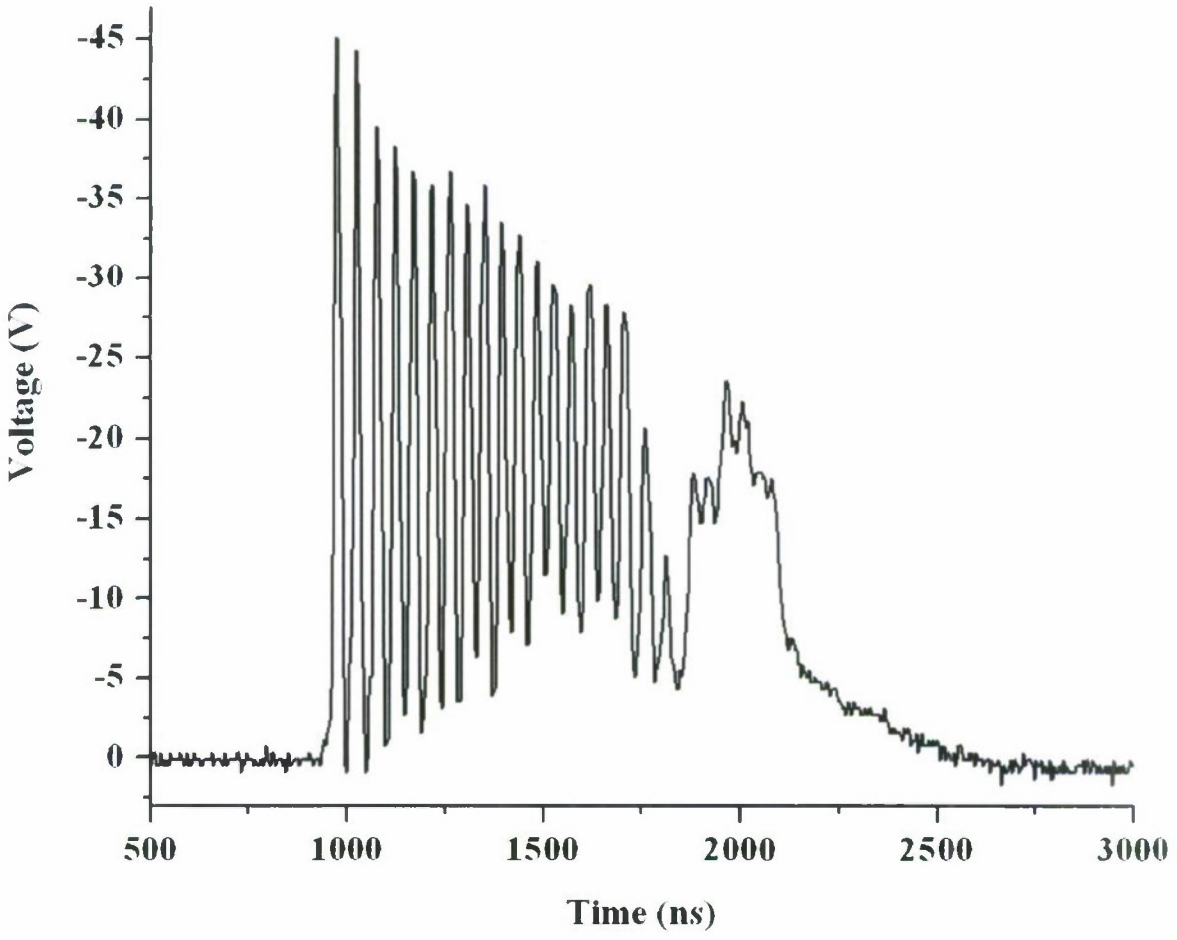

Figure 6.3: Steady state type III envelope shape on a 25 MHz low voltage NLETL. The line was 24 stages in length, with 560 pF BB212 capacitive elements, 10 μH of inductance and this is stage 10.

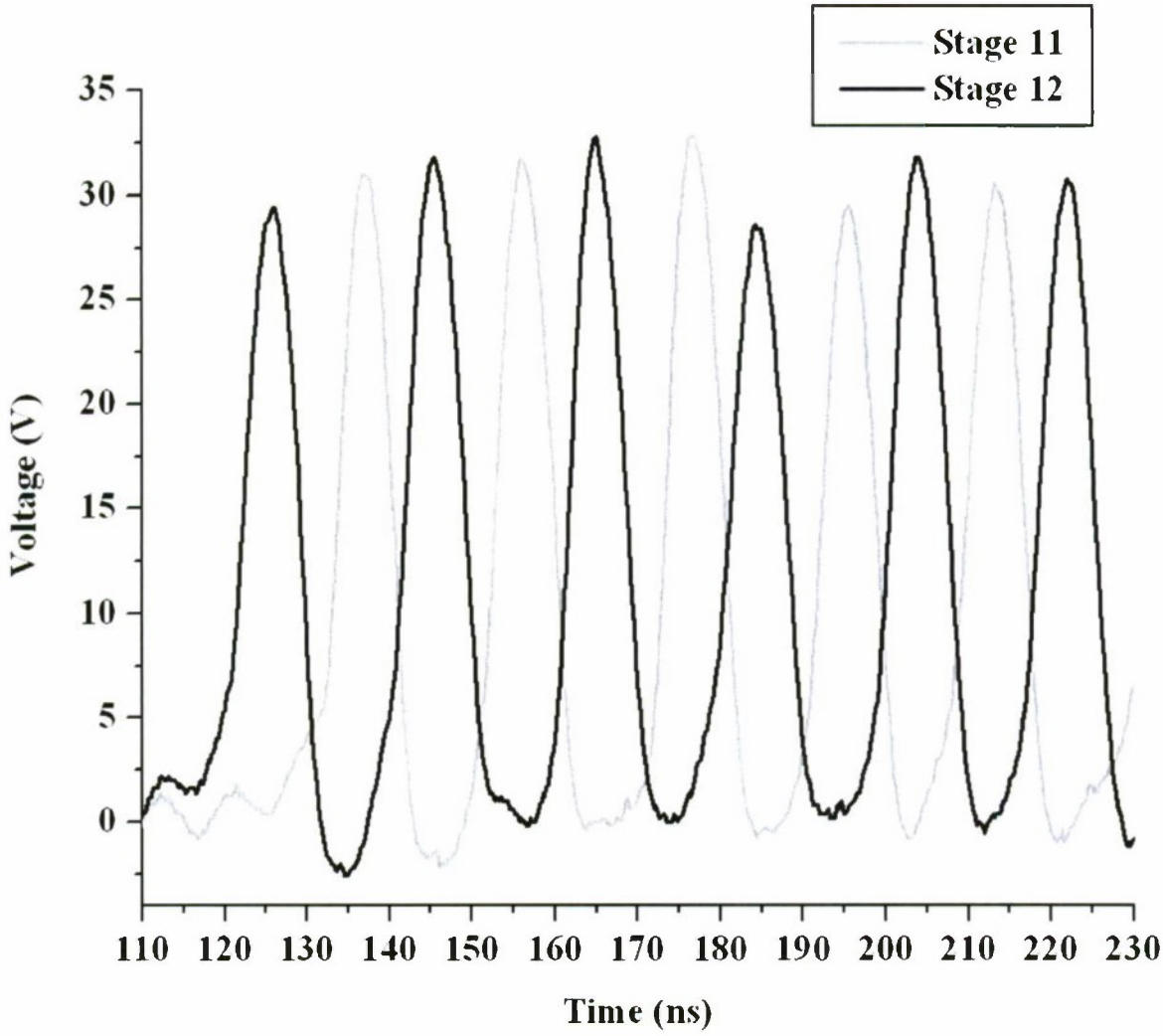

Figure 6.4: Low voltage NLETL mid-line voltage waveforms depicting good uniformity and modulation depth, with the characteristic anti-phase maintained between neighbouring stages.

Under a wide input pulse the burst of many solitons may take several stages to form fully but is developed fairly uniformly, rather than one pulse at a time as typically observed on the BAE Systems magnetic lines. The evolution of the three envelope modulation shape types, as previously mentioned in section 5.3, has been evident throughout. The type III envelope seen in figure 6.3, with a decreasing RF component amplitude, forms the typical NLETL steady state pulse burst waveform and may be generated sooner in the line by a faster input leading edge. However, with long pulse burst durations reflection effects can act to disrupt this relatively smooth profile unless the line is sufficiently long. The anti-phase property is now considered to

be an important defining characteristic of this type of oscillation on a NLETL and was observed in all numerical and experimental results (figure 6.4). The wavelength and propagation velocity of the high frequency component are always related such that the wavelength is equivalent to two discrete stages. Also illustrated in various results presented here is the extraction problem, whereby any kind of interference with a resistive load of reasonable value, or even termination by an open circuit, tends to severely disrupt the high frequency waveform. This issue is clearly important and, having become central to much of the work, is considered exclusively in sections 6.4 and 6.5.

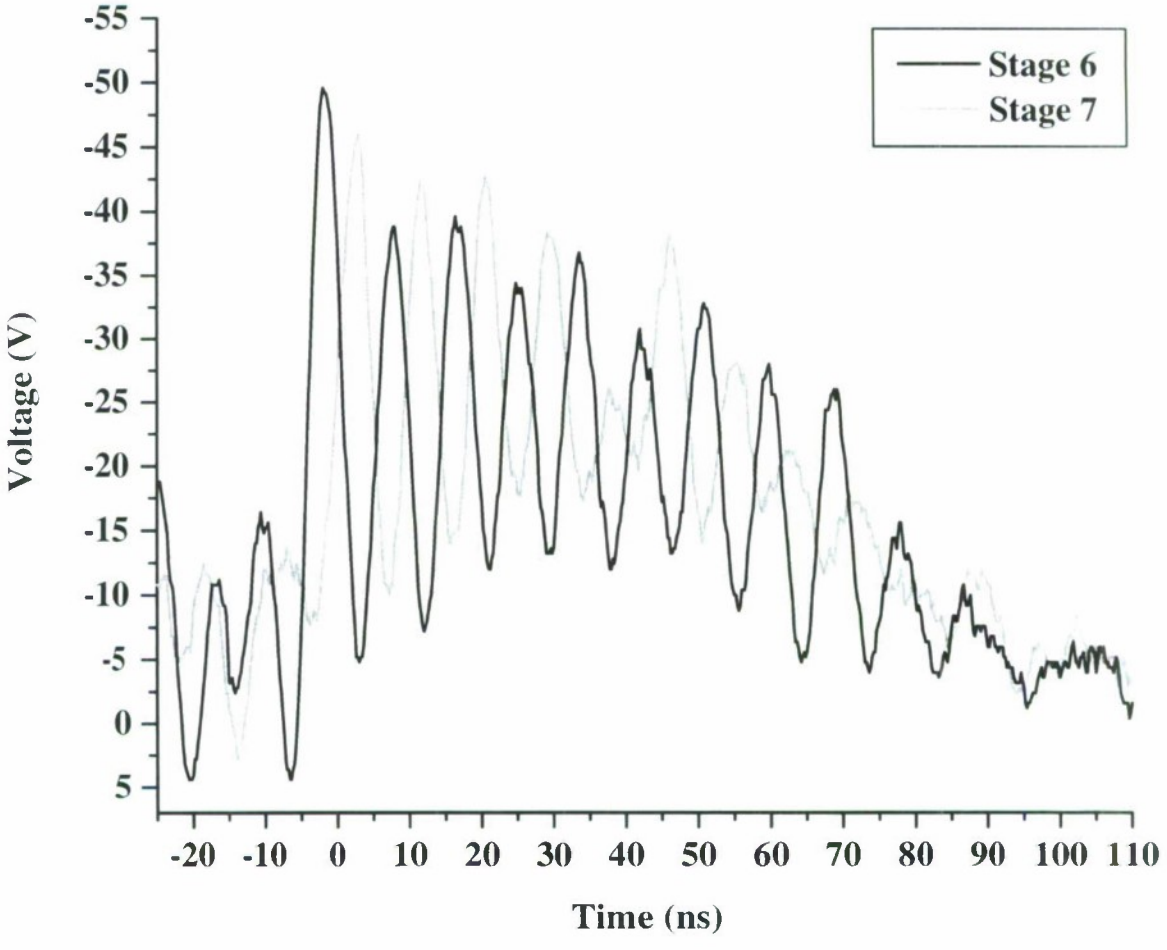

Figure 6.5: Higher frequency oscillation and anti-phase is demonstrated on a BB212 low voltage line with reduced inductance, at around 120 MHz.

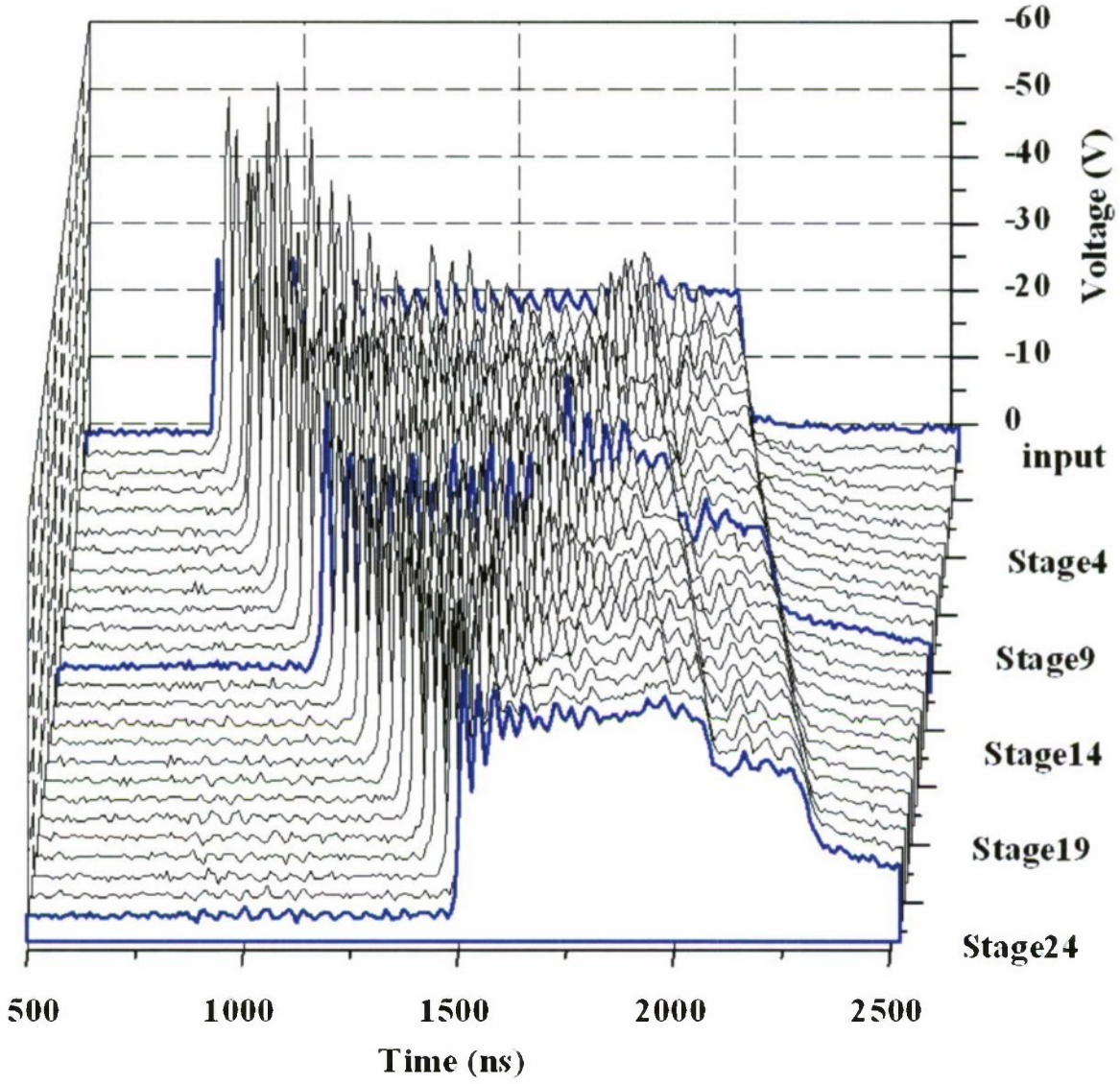

Figure 6.6: Line progression of voltage waveforms from input (rear) to output (front) of a low voltage experimental line terminated in a relatively high 680 Ω load.

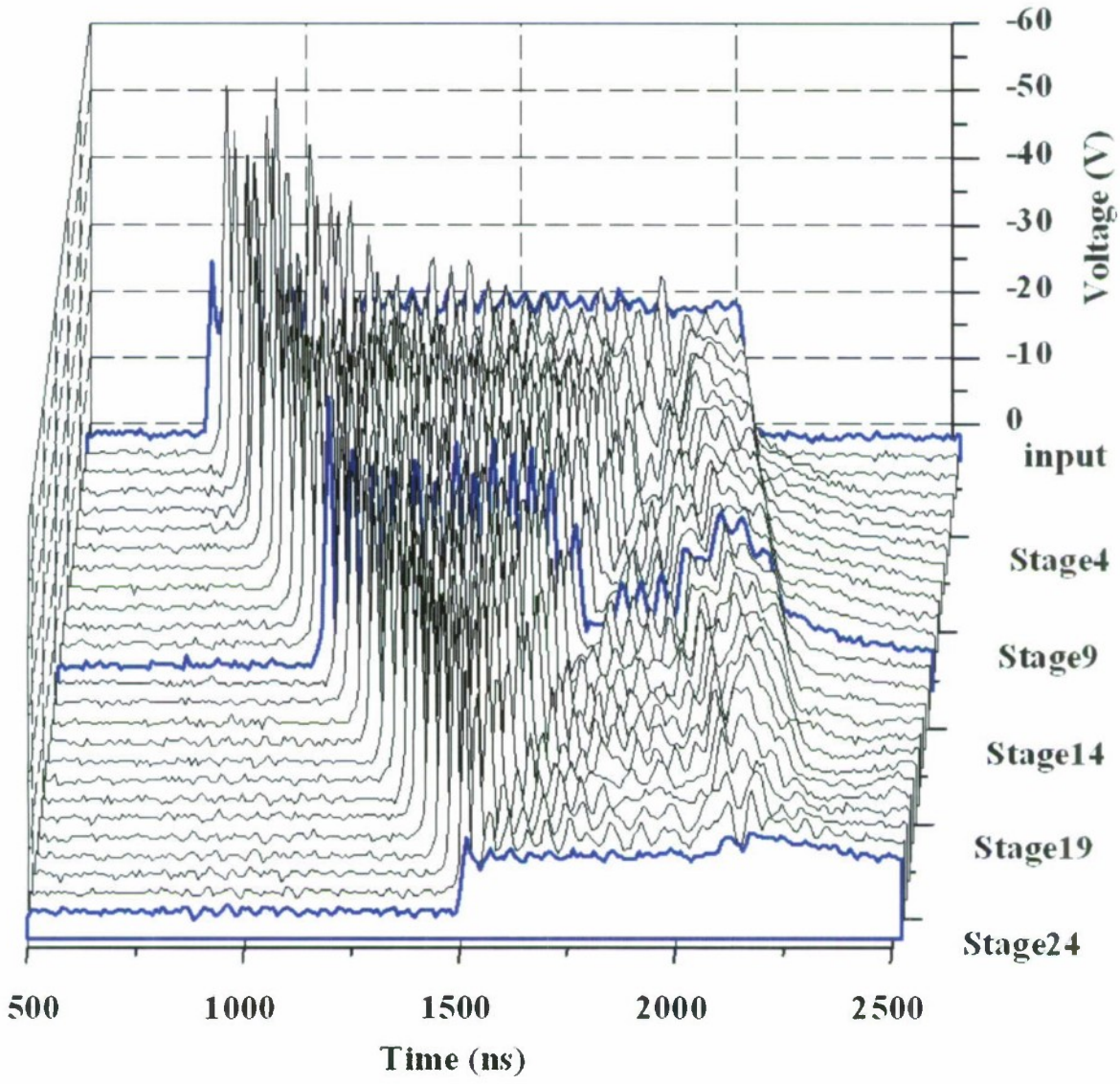

Figure 6.7: Data obtained under the same conditions as figure 6.6, with a relatively low 120 Ω load. The nominal NLETL characteristic impedance in this case is around 140 Ω.

Many different designs of NLETL were constructed and tested and on some occasions a complete 'line progression' of voltage waveforms measured at every stage was obtained (figure 6.6 and figure 6.7) which offers a complete impression of how a given pulse train and envelope shape develops, evolves and interfaces with the line termination. Most lines, and those which generated the best results, used the BB212 varactor tuning diode of nominal capacitance 570 pF and CNL ratio of around 10. In addition, a series of six NLETLs were built (figure 6.8), each comprising 20 stages (capacitive elements) with stacked diodes for operation at higher voltages. Using the twin package design, three pairs of diodes were stacked (six in total) per stage and good oscillation with peak voltages of around 200 V demonstrated. This also allowed a reduced nominal capacitance of approximately 380 pF to be tested, although the 800 nH of inductance built into these lines via 2.5 mm wound copper wire was fairly substantial.

Frequencies in excess of 80 MHz were achieved however, and the design was not aimed at testing the limits of frequency with low inductance values, rather at generating good quality oscillation comfortably within these limits. Keeping the NLETL characteristic impedance reasonable high also meant it could feasibly be driven with the pulse forming networks (PFNs) built to replace the pulse generators used on lower voltage single diode lines. This was particularly relevant to the driving of multiple NLETLs in parallel. Also, the six line segments could readily be connected in various different configurations to investigate the ideas proposed in section 6.4 as well as the operation of a single long 120 stage line. Representative mid-line waveforms, where useful pulse durations of over 20 cycles were sustained, may be seen for example in figure 6.9. These six lines were designed and built with the low voltage propagation experiments detailed in section 6.6 in mind, the requirements of which partly motivated the increase in operating voltage by stacked diodes.

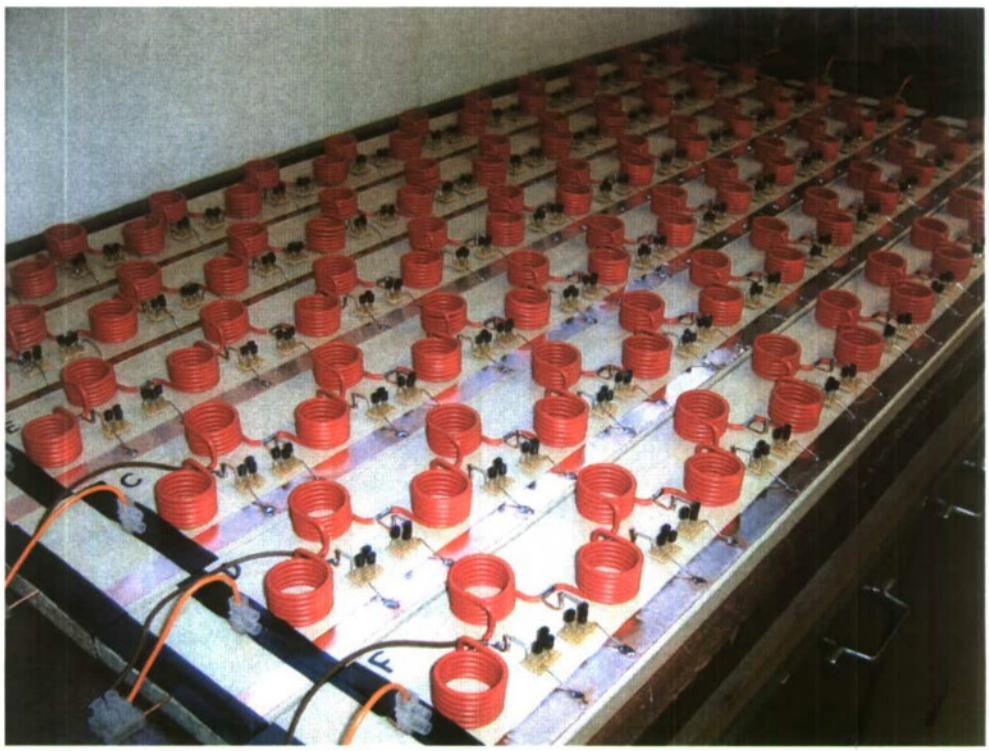

Figure 6.8: Six low voltage NLETLs each comprising 20 stages with stacked BB212 varactor diodes.

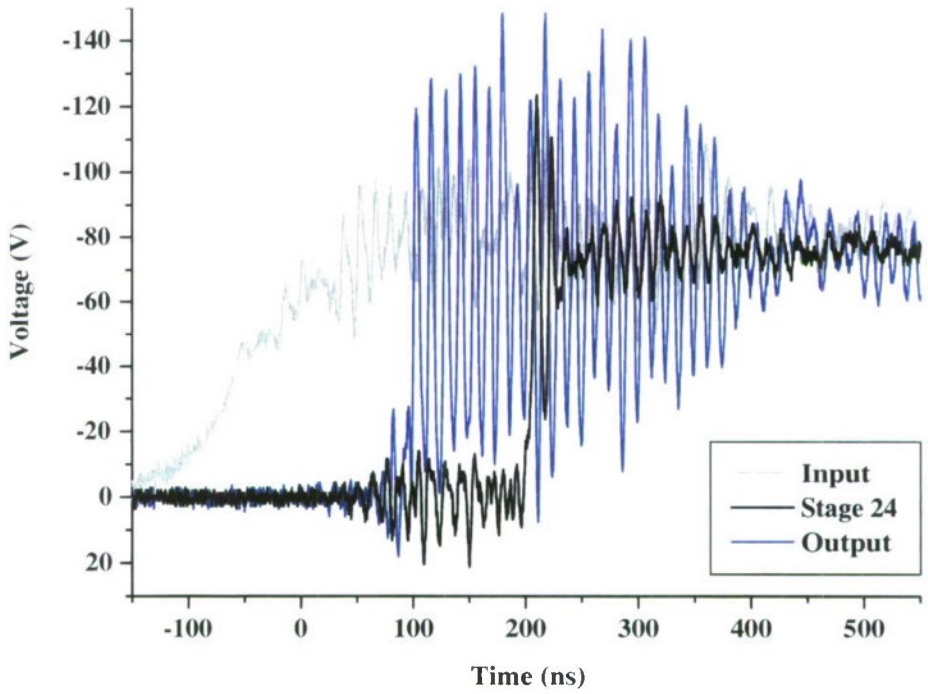

Figure 6.9: Input, interim and output voltage waveforms on 40 stages of the line depicted in figure 6.8, with an 80 Ω termination and peak to peak voltage around 120 V.

Another set of lines—also used during the low voltage propagation experiments—were designed to establish the maximum frequency of operation achievable with the BB212 CNL characteristic. A test NLETL was used to progressively reduce inductance until oscillation was found to disappear; with a single loop of 10 mm diameter waveforms such as that of figure 6.10 were obtained at frequencies up to 250 MHz. For comparison, three loops generated slightly better quality waveforms at 120 MHz (figure 6.5), two loops 180 MHz. Once again, quite thick solid copper wire was used for its rigidity and minimal resistive loss, and the single loop inductance was built into four line segments totalling 64 stages in length seen in figure 6.12.

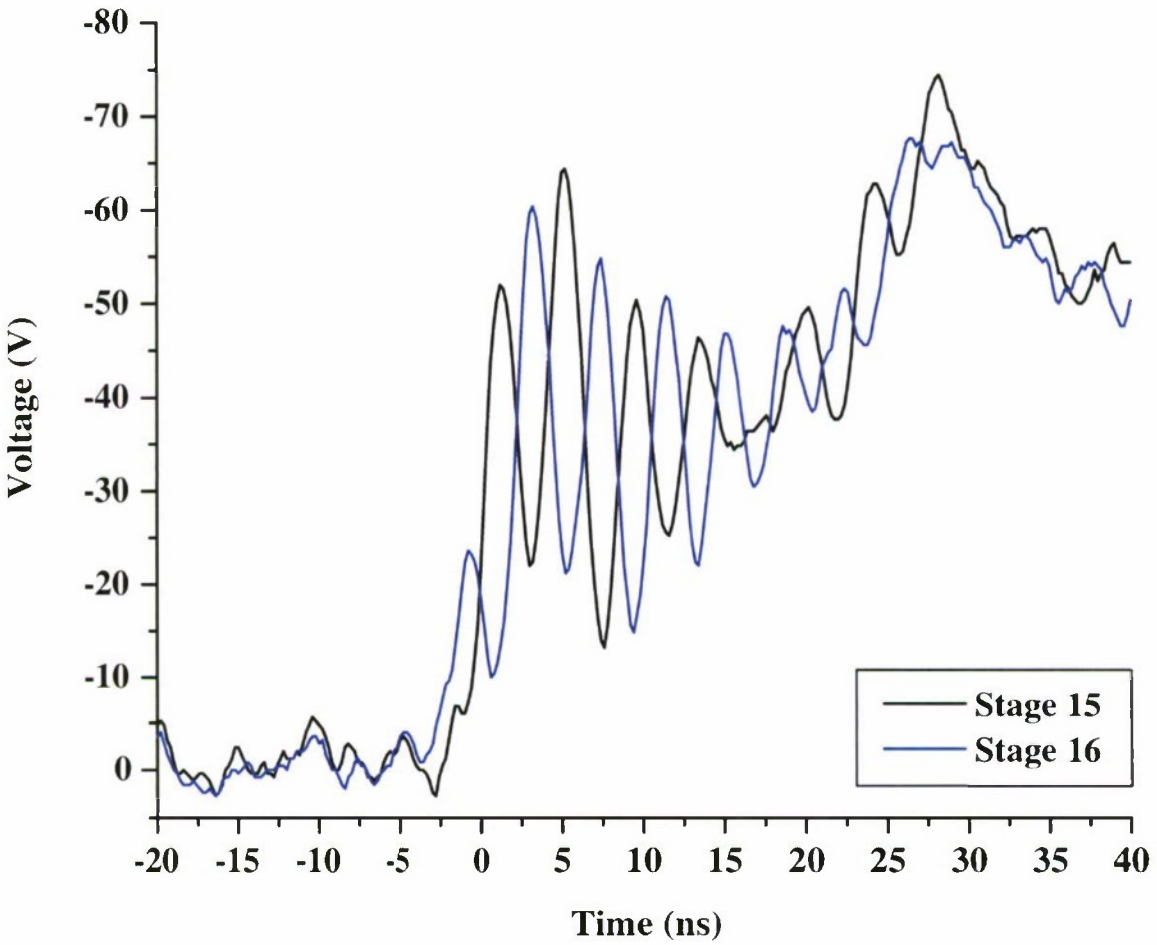

Figure 6.10: Mid-line waveforms at 250 MHz on the high frequency low voltage NLETL shown in figure 6.12, with reasonable oscillation and its defining anti-phase property.

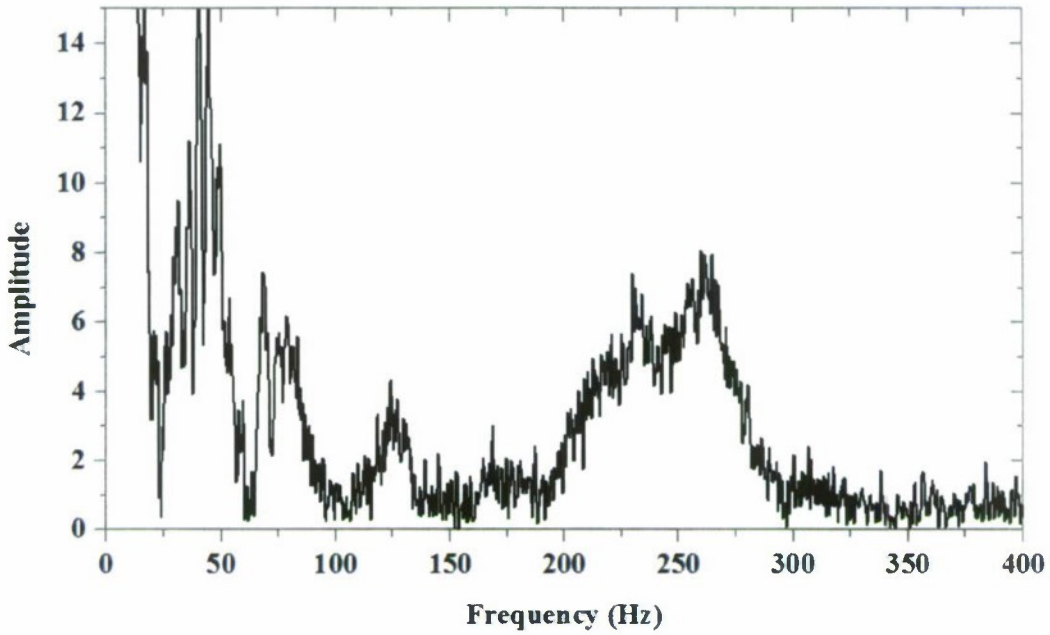

Figure 6.11: Fast Fourier transform applied to a typical mid-line waveform such as that of figure 6.10.

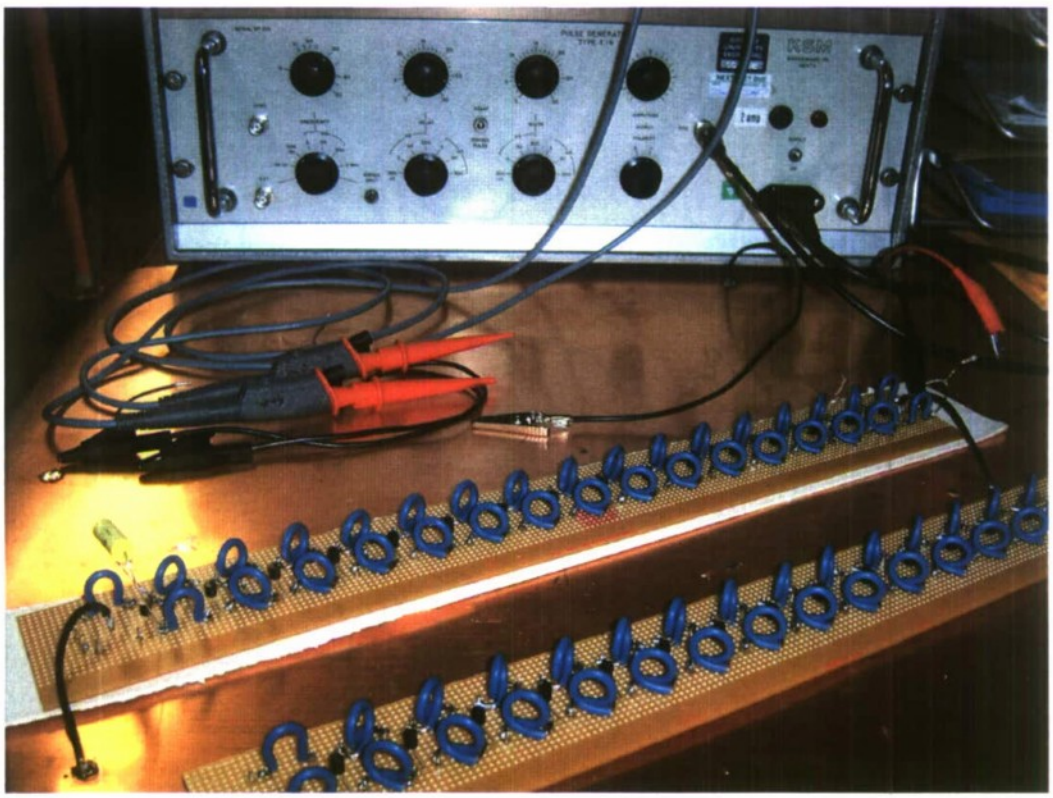

Figure 6.12: The high frequency NLETL operating on a low inductance earth plane with 50 V pulse generator visible in the background.

Many other NLETLs, in more than 10 distinct designs and incorporating around 900 BB212 diodes, generated insightful waveforms, a small sample of which will be seen in the following section in addition to those included above. Similar soliton type oscillation was generated on a low voltage nonlinear lumped element PFN, whereby the NLETL was DC charged before being switched to earth at one end by an IRF740 MOSFET with BJT gate drive circuit. Alternatively, using the standard input pulse excitation, by reversing the action of nonlinearity such that a DC saturation is reversed by an opposite polarity input pulse, it was shown that dark solitons [82] [50] may be produced on the tail of the propagating pulse and this effect was previously illustrated in figure 4.11. These alternative arrangements are still susceptible to the extraction problem and seem to be less effective pulse burst generators in terms of uniformity and duration.

The possibility of controlling frequency via a variable DC bias voltage has already been suggested, and with suitably placed isolation capacitors was demonstrated over the frequency range of 14.2 MHz to 24.7 MHz before oscillation started to drop off significantly. This ±25% bandwidth was a surprisingly good result and is illustrated in figure 6.13.

6.3 Key Trends Derived from Numerical and Experimental Results

6.3.1 Length of the NLETL

The relatively fast and simultaneous development of pulses on a suitable NLETL has been established and in many cases the line need not be particularly long to generate mid-line waveforms of good duration and modulation depth. In terms of optimising construction costs, size and also efficiency this may be advantageous; by comparison the magnetic NLTL systems described in section 2.4 typically constitute many hundreds of stages due to the slow emergence of an RF waveform from the driving pulse shock front. The number of stages should be kept reasonably

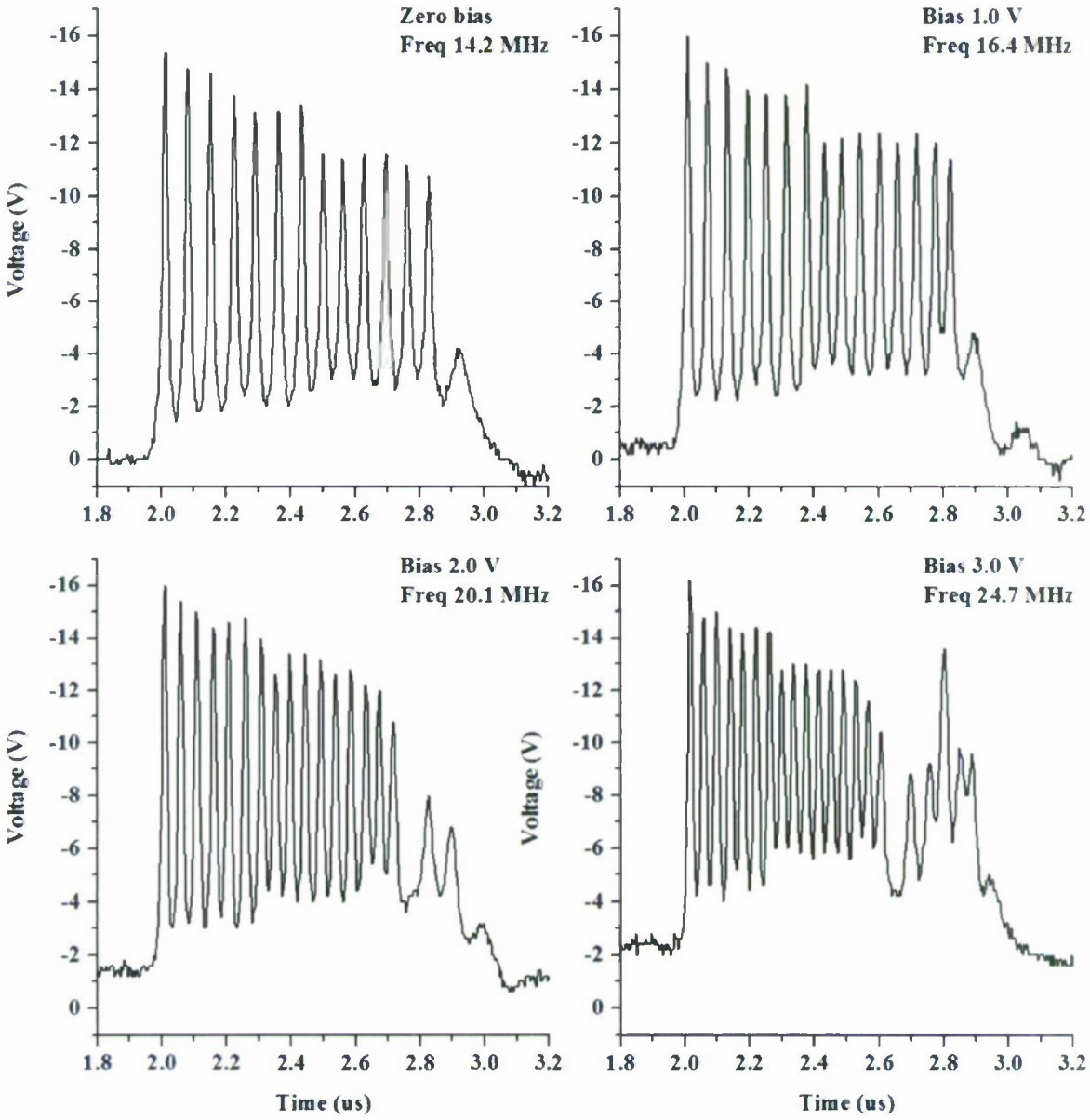

Figure 6.13: Pulse burst frequency agility is demonstrated on a low voltage NLETL.

low if possible because the soliton pulses tend to spread out and over the course of propagation along a very long line the resulting drop in frequency can be large. In a simulation example of a loss-less 200 stage NLETL frequency dropped from 15 MHz at stage 10 to 6 MHz at stage 190, and on a representative 80 stage experimental line 85 MHz decreased to 70 MHz. Spreading of periodic cnoidal waveforms is to be expected from soliton wave theory [50], and in results reported from past work on nonlinear transmission lines the effect may be observed to a similar degree [43] [48].

Pulse duration is an important figure of merit and line length does not have a direct influence over the number of pulses which may be generated per burst. This appears to be primarily related to frequency, with many more pulses sustainable at higher frequencies before the oscillation tails off. But extended pulse burst waveforms tend not to be generated on shorter lines due to the disruptive effects of reflections which may be avoided with a line of sufficient length. Alongside spreading and the design factors mentioned above this needs to be taken into account when designing a NLETL system for a given application and choosing the number of stages to build. A further issue which became apparent during the high voltage work of chapter 8, and may or may not be relevant depending on future progress in materials research, is the total risk of failure of any one capacitive element, which would be expected to rise with line length.

6.3.2 Frequency

The frequency of a generated pulse burst waveform is dependent in part on the values of inductance and nominal capacitance incorporated in a NLETL as would be expected and, if not cut off by a narrow input pulse width or reflection effects, more pulses are generated per burst at higher frequencies. But in addition, simulation data implies a stronger dependence of frequency on the relative value of fully saturated capacitance, as per figure 6.14 where frequency and maximum voltage amplification by virtue of soliton pulse formation are plotted at various values of CNL ratio.

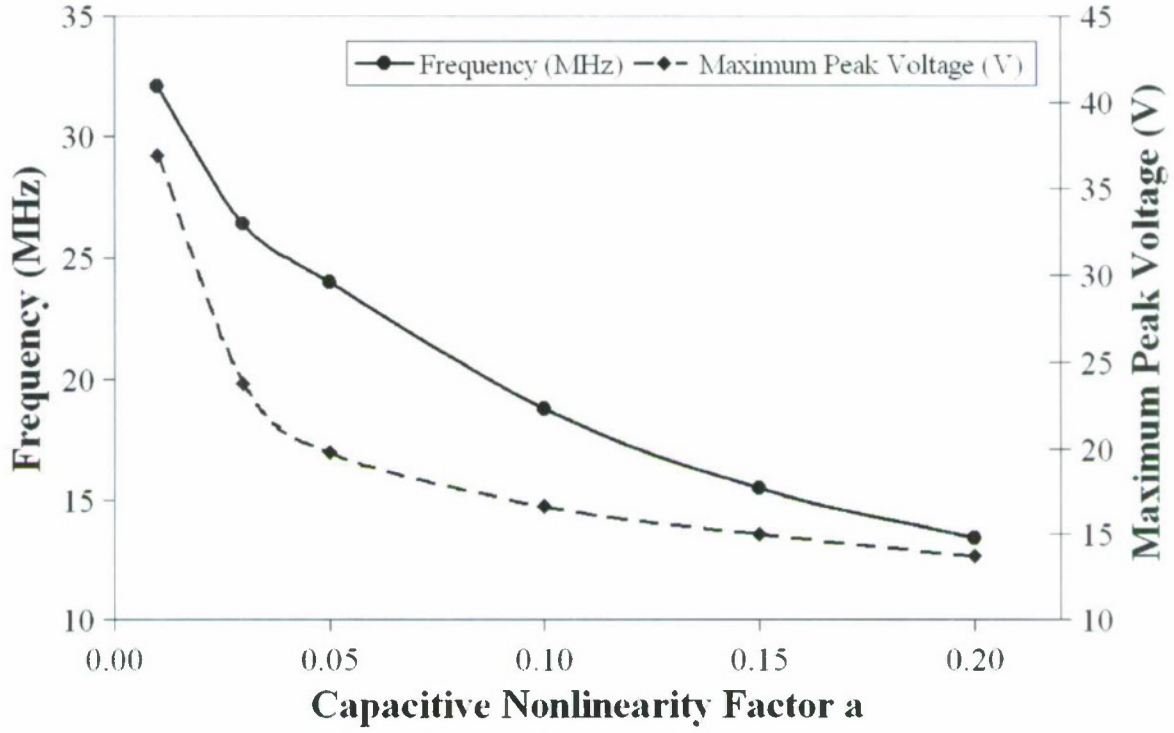

Figure 6.14: Simulation data indicating the strong influence of capacitive nonlinearity ratio on frequency and peak voltage amplification. A smaller value of a corresponds to a larger CNL ratio (equation 5.1).

The input pulse amplitude needs to be reasonably large to initiate any oscillation (figure 6.15 shows the approximately linear propagation of a small signal waveform on an experimental NLETL) and some influence on frequency is evident in figure 6.16. If frequency is to be controlled in this way, it should be noted that the quality of oscillation is relatively poor until a sufficiently high input amplitude is reached. An important observation made during this work is that it is possible to overdrive a given line, resulting in a complete loss of any oscillation (figure 6.17 and table 6.1). So for optimum operation at maximum frequency the range of permissible input amplitudes may be narrow, and for design at high power levels the CNL steepness should perhaps be relatively low but in any case taken into account.

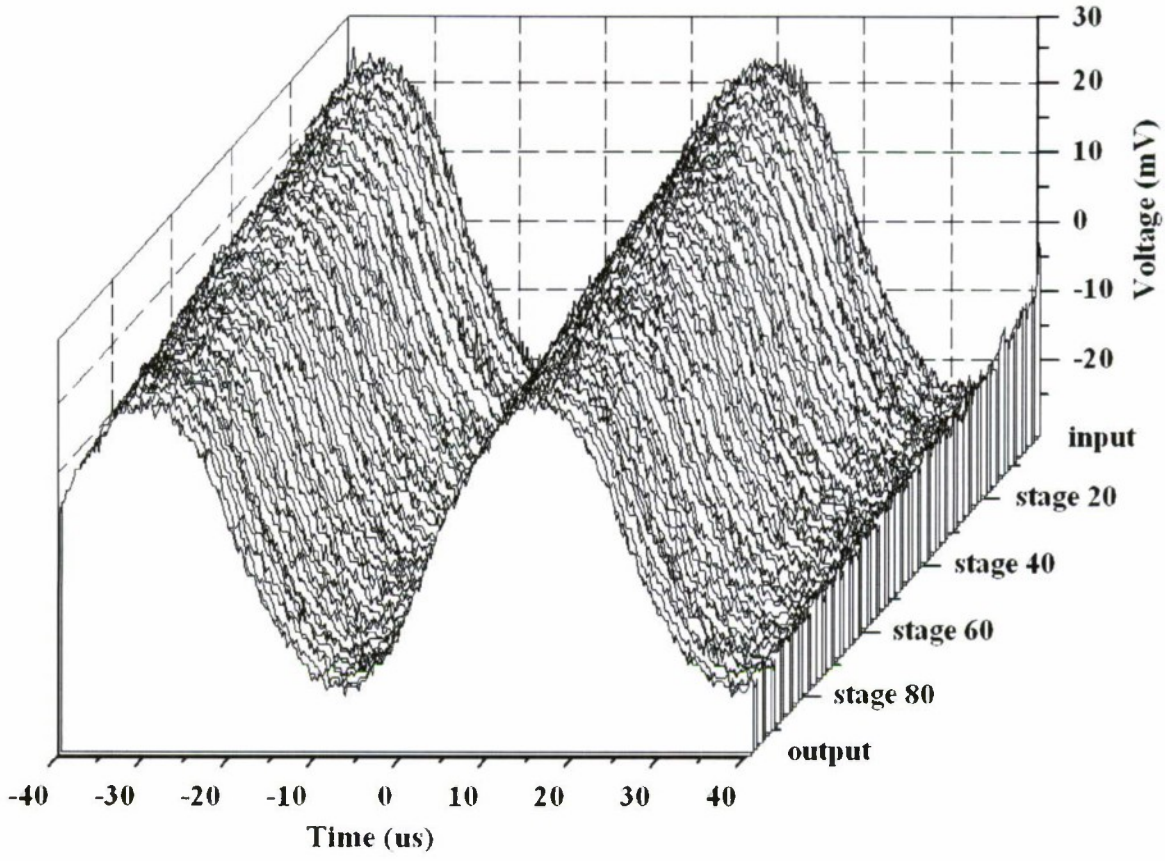

Figure 6.15: Very low amplitude sinusoidal signal on a strongly nonlinear transmission line remaining undistorted throughout propagation. To small signals the NLETL may be viewed as a continuous medium for low frequency waveforms such as this; a sufficient increase in amplitude would see the sinusoid break into a train of discrete soliton type pulses at much higher frequency.

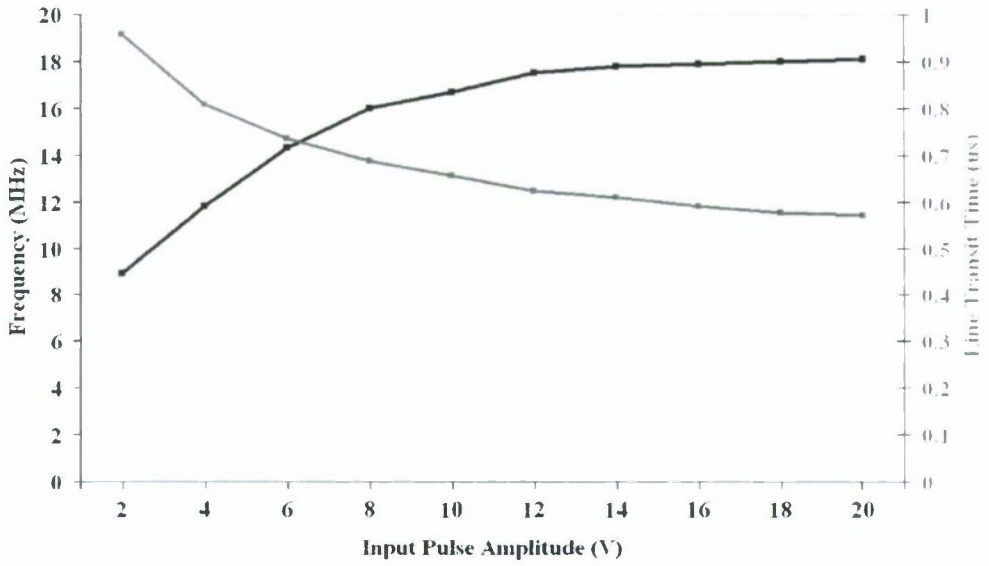

Figure 6.16: Frequency increases with input amplitude to a limiting value dependent on line design parameters. Narrower pulses tend to be of larger amplitude and hence progress along the line faster (section 4.1).

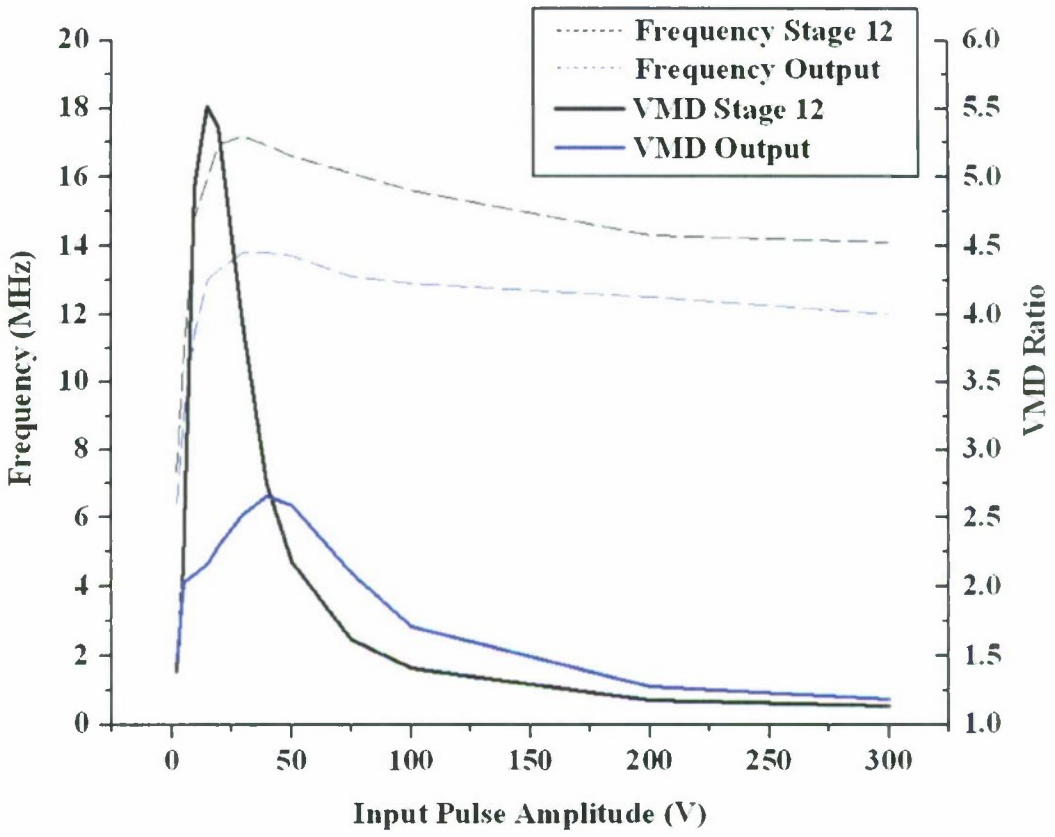

Figure 6.17: Further increases in input amplitude beyond the overdrive limit can lead to a complete loss of oscillation as illustrated by this simulation data.

PFN Charge (V)	Input Pulse Amplitude (V)	VMD Ratio	VMD %	Frequency (MHz)
75	45	62/7 = 8.9	88	47
100	55	82/14 = 5.9	83	68
125	75	94/17 = 5.5	82	68
150	95	106/18 = 5.9	94	81
200	130	116/40 = 2.9	65	83
300	180	129/60 = 2.2	53	80

Table 6.1: Whilst both low and high voltage experimental capacitive elements tend to fail before the overdrive limit is reached, some results do indicate the initiation of a similar reduction in oscillation and the slight drop in frequency seen in figure 6.17. This data comes from the stacked diode line described in section 6.2.

Varying the input pulse rise time has no effect on frequency, only on how quickly the pulse train develops. Indeed the driving pulse need not be very fast since the strong nonlinearity necessarily associated with this type of transmission line will sharpen its leading edge over the initial few stages. Several hundred ns is acceptable to beyond 100 MHz; at higher frequencies an input transient of more like 50 ns or less may be more appropriate if line length is to be minimised but this may quite reasonably be achieved with contemporary switching technology and is not expected to present a significant issue or limitation on system design.

6.3.3 Capacitive Nonlinearity Ratio and Steepness

Assuming an approximately exponential characteristic, the importance of distinguishing between the nonlinearity *ratio* of nominal to saturated capacitance values and its *steepness* with respect to voltage is now recognised. The phenomenon of soliton-type oscillation on this transmission line topology is reliant upon a sufficiently large CNL ratio and a poor nonlinearity in this respect cannot be overcome simply by driving it harder. Whilst the role of the 'fractional decrease' in capacitance in characterising the nonlinearity has been mentioned in passing on previous occasion [42], often judgement of a comparatively good CNL has been made on the

basis of curve steepness alone. Achieving a large CNL ratio should be of prime concern during future development of dielectric materials for this application since this increases the quality of oscillation, peak voltage amplification and frequency, and according to simulation data may even aid extraction from a single line to a single resistive load (section 5.3 and figure 6.18).

Changes in CNL steepness are in principle equivalent to changes in input pulse amplitude, and as such mirror that influence on frequency and the overdrive limitation.

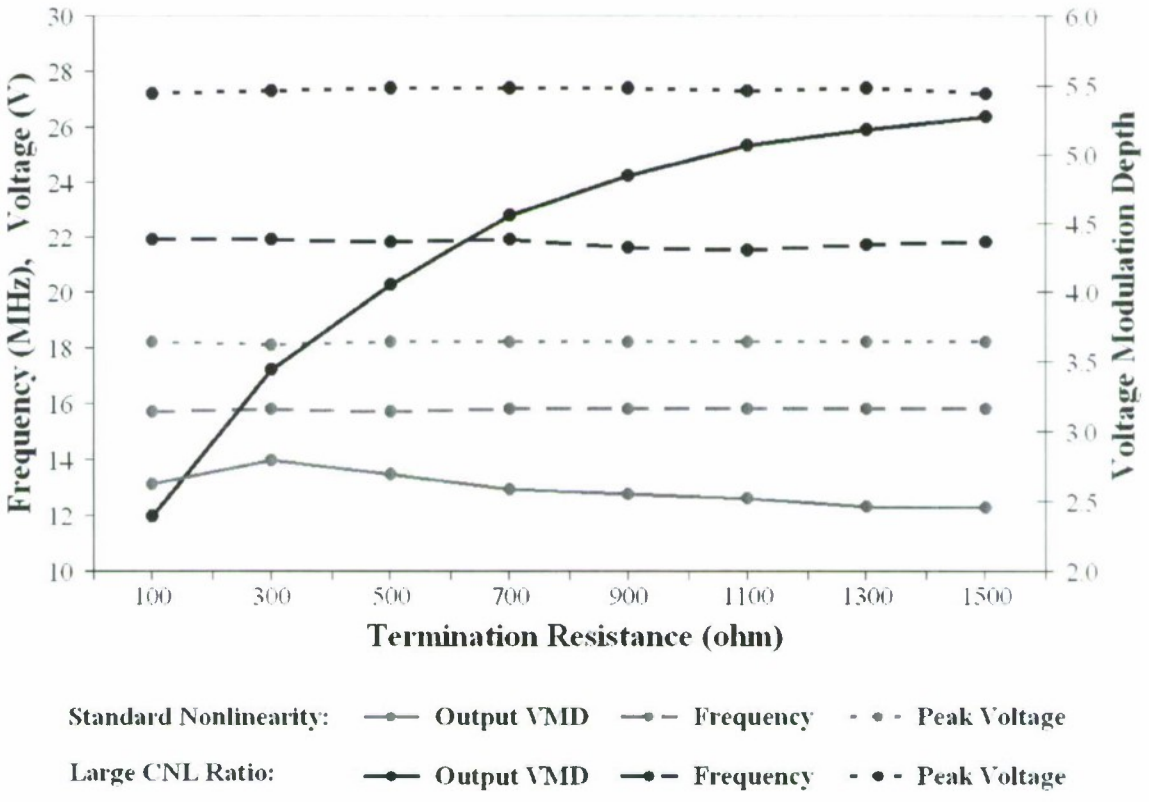

Figure 6.18: Under currently achievable CNL conditions (ratio of around 10, grey lines) each of output VMD, mid-line frequency and peak voltage amplification are invariant with the value of a resistive load. According to this simulation data, a much larger CNL ratio (around 25, black lines) increases frequency as noted already, but also facilitates a significant improvement in output VMD to larger loads.

6.3.4 ESR Loss

The numerical simulation tool allows loss in the form of capacitive equivalent series resistance (ESR) to be studied, and indicative results have also been obtained experimentally by comparing various high voltage capacitive elements and the low voltage BB212 diodes (chapter 8). It is currently thought that loss is the factor limiting experimental results to 250 MHz (and 80 MHz at high voltage) and this key result was reported in more detail in section 5.4. Decreasing inductance and or nominal capacitance is an intuitive means of increasing frequency but this approach is limited because at some point oscillation dies away, and the frequency at which this occurs is strongly dependent on ESR loss. This form of loss has no effect on frequency, a fact considered likely to be the case in past work [42]. But it should be noted that stray inductance and capacitance would be expected to decrease frequency in practice, and should design of higher frequency NLETLs become feasible it could become necessary to make every effort to minimise strays via compact construction, subject of course to voltage strength requirements. This is particularly relevant due to the discrete nature of the oscillation effect and is considered further in chapter 7.

6.3.5 End L Values

A discrete transmission line can be viewed as a series of T elements each comprising one capacitor with half the stage inductance on each side. Following this configuration the input and output end inductances would be half those throughout the interim line stages. Unexpected initial experimental and numerical results implied that using this value for end inductors gives slightly improved output oscillation in terms of modulation depth than using the full mid-line inductance. The difference is not very great and extracted waveforms from single lines to single loads are still typically very poor, but figure 6.19 illustrates the trend over a range of end inductance values. There is also some indication that this precise value of inductor on the input end of a NLETL results in the fastest development of the pulse burst waveform but, although interesting to note, once again the difference is relatively small.

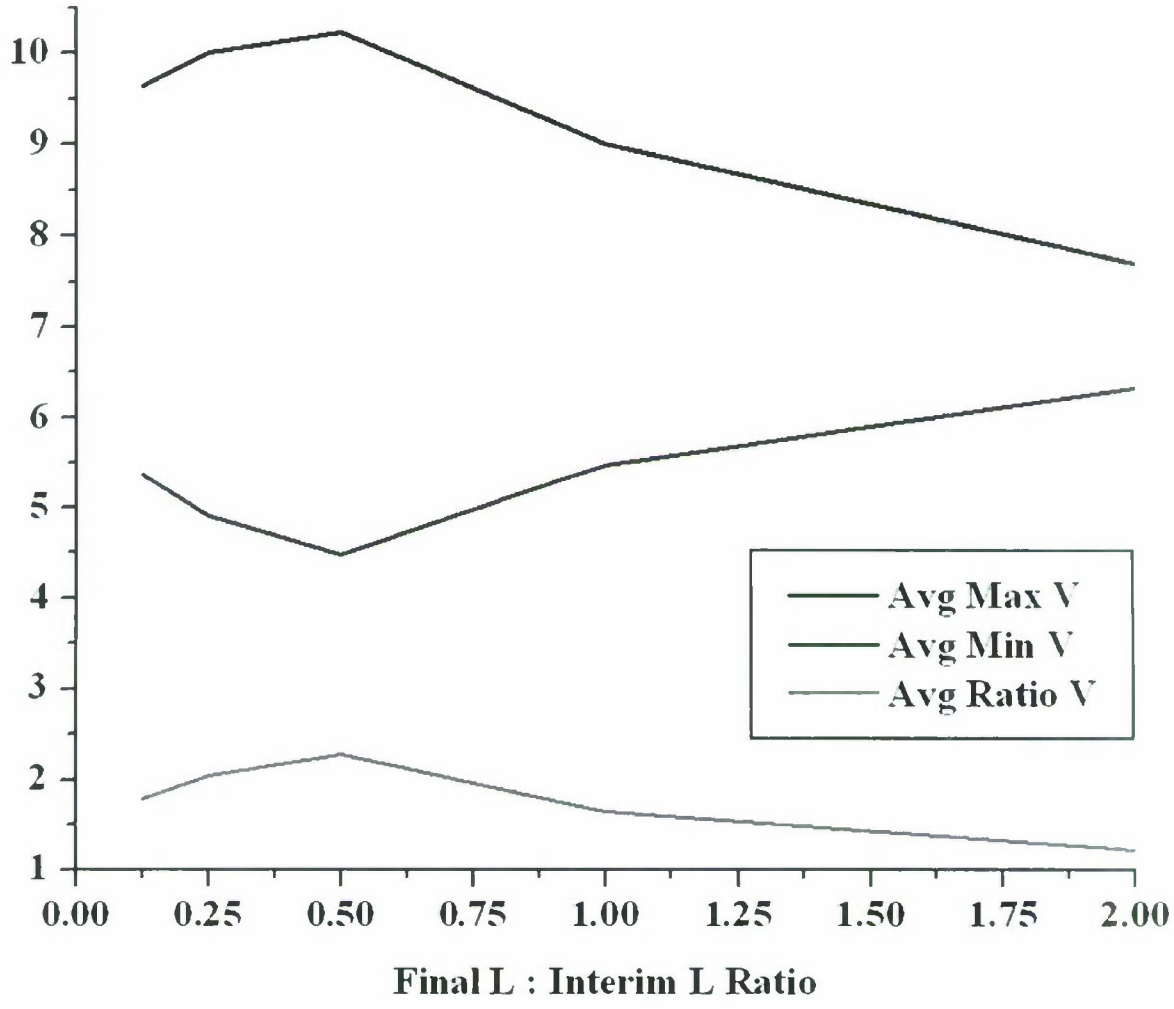

Figure 6.19: Output waveform averaged peak to trough voltage ratio is maximised with end inductor values equal to half those within the NLETL.

6.3.6 Termination and Extraction

It is not straightforward to extract the RF energy from the NLETL system—this issue has been acknowledged and tackled quite successfully during work on the project. A suitably large inductive termination minimises mid-line disruption and as seen in figure 6.20 can maintain good oscillation but does not consume real power since the load is purely reactive. The nature of energy propagation along the line with regards the high frequency RF component is considered

further in chapter 7. In the following section the loss of oscillation associated with the presence of a resistive load is noted and feasible explanations suggested, along with some novel ideas for improving extraction and thus enabling practical application of the technology for pulsed RF generation.

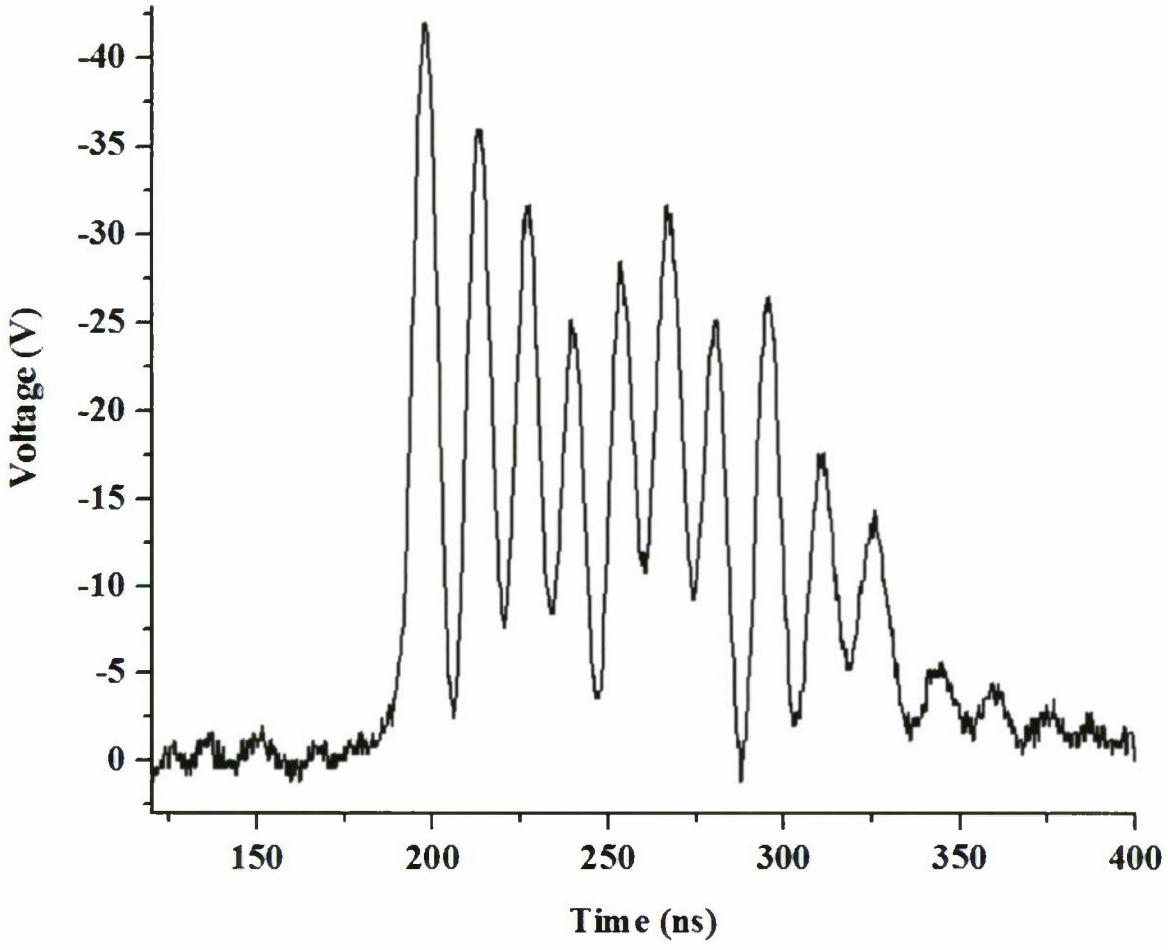

Figure 6.20: Output waveform delivered to a 22 μH inductor load is comparable to that generated mid-line, from an 18 stage BB212 NLETL with 1 μH of inductance per stage which oscillates at 70 MHz.

6.4 The Extraction Problem and Ideas for its Solution

6.4.1 Resistive Terminations

In figure 6.6 and figure 6.7 complete line progression data for an experimental NLETL terminated in relatively low and high value resistors demonstrated the extraction problem in both cases. It is necessary for a power consuming (resistive) load to be connected to a line in order to extract and make effective use of the RF energy, but any resistive or even open circuit interference with the periodic nonlinear structure results in a significant decrease in oscillation. Noted previously in section 5.3 and figure 5.6, the loss of a single pulse per stage progressing from the load end is just about visible in these figures and may be attributed to a backwards reflection component according to the fixed wavelength of two discrete stages. In this way a resistive termination leads to disruption earlier in the line, over as many stages as there are pulses in the burst. This disruption is minimal when the resistor value approximates the nominal line impedance with reduced mismatch; then the RF component decays more uniformly over the final few stages.

Extraction is sometimes not such an issue where the waveform comprises a small number of (for example two or three) soliton pulses, but is a serious limitation when more useful extended pulse bursts are generated as per the potential capabilities of the NLETL. The extraction problem is often visible in past reported data (no evidence has been seen of successful extraction of more than a few pulses of RF energy) but oddly had yet to be fully acknowledged or tackled. An exception is provided by the numerical work of Lin Liu et. al. in 1991 [90] which concluded that the absorption of energy by a resistive termination could be very good with less than one percent reflection for certain resistor values. Output waveforms or comparative frequency spectra with those mid-line were not presented however, and even if a reasonably large amount of extracted energy was at the high frequency of oscillation it is possible that extraction was improved in this case by the "strong nonlinearity" used according to the effect noted in section

5.3. Also it was noted that "some oscillation was lost ... certainly due to the transition from a nonlinear to a linear system".

Although not supported by experimental results from longer lines, simulations here have suggested that very long lines of several hundred stages may be able to deliver improved output waveforms, if still relatively poor in comparison with those generated earlier in the line. Such a NLETL is inevitably subject to quite significant spreading though, and the extraction problem tends to be slightly less bad at lower frequencies for a given CNL ratio. It has been found that purely inductive loads can sustain good oscillation if the reactance at the frequency of operation is sufficiently large, typically several kΩ. This potentially offers a good termination where minimal disruption is desired but of course the power is not real and no energy is being removed from the system by such a load.

Some ideas are suggested by way of explanation for the problem. Figure 4.4 showed the extraction of single solitons to a resistive termination and an accompanying decrease in amplitude and corresponding increase in width. This appears to occur for a single soliton pulse unless the resistor value is very much greater than the nominal characteristic line impedance. Given the fixed time of arrival at the load between solitons within an extended burst of many such pulses, it is reasonable to associate a widening of each pulse with some overlap between neighbours and a loss of modulation depth. Some of the Direct method work detailed in section 4.3 obtained multiple soliton solutions to the KdV equation with identical pulses and varying peak to peak distances in order to investigate the influence of co-propagating solitons on one another (figure 4.8 and figure 4.9). The impression so obtained is that small changes in spacing or in pulse width can have a strong effect on the modulation depth of a pulse train. The behaviour of single NLETL pulses at a load of reasonable value suggests that this process may be playing a role in limiting extracted RF energy, but a high load or an open circuit gives only a slight improvement and the poor extraction is then unlikely to be solely accounted for by interaction between pulses.

Considering the final few stage voltage waveforms before and at a resistive load, it is interesting to note a change in delay between the arrival of adjacent waveforms, which earlier in the line is half a wavelength period. With reference to the stage numbering convention of figure 3.1, generally the delay between stage N and stage $N+1$ (the output) is significantly reduced from that between stage $N-1$ and stage N and all previous neighbouring stages. Simulation and experimental results imply that the delay before the output decreases further with increasing load, and is roughly unchanged if the load is very small as seen in figure 6.21 and figure 6.22. However, output oscillation to small loads is virtually nil, due to pulse spreading and overlap if nothing else. A loss of the key anti-phase relationship can be linked to disrupted oscillation on other occasions also, behind a reflected component travelling through an otherwise uniform pulse train. An experiment was carried out to try and increase the delay before the load in order to possibly improve extraction via suitable lengths of cable, but the measured waveforms at the resistor terminals were not improved. The addition is effectively an inductance to each side of the load; whilst this can improve oscillation over the series of elements a quick analysis reveals most of the impedance to be imaginary at the given frequency of oscillation, and as such a negligible RF component is delivered to the resistor. Indeed, with higher frequency lines particular care was taken throughout these experiments in choosing measurement points to obtain the most faithfully representative output waveform results possible in the circumstances.

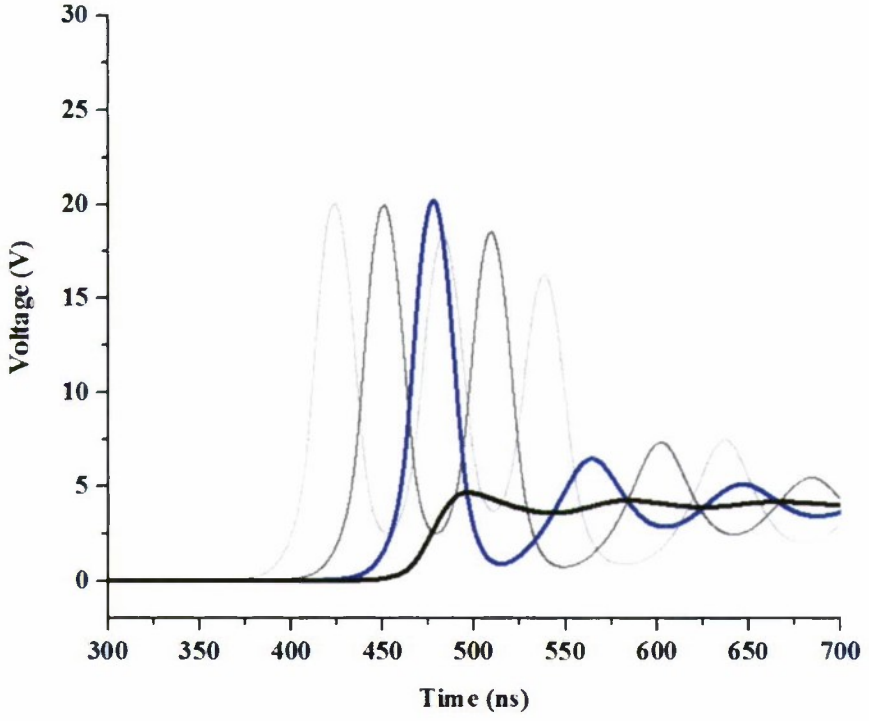

Figure 6.21: Final four stage simulated waveforms, including output, to a relatively low value resistive load.

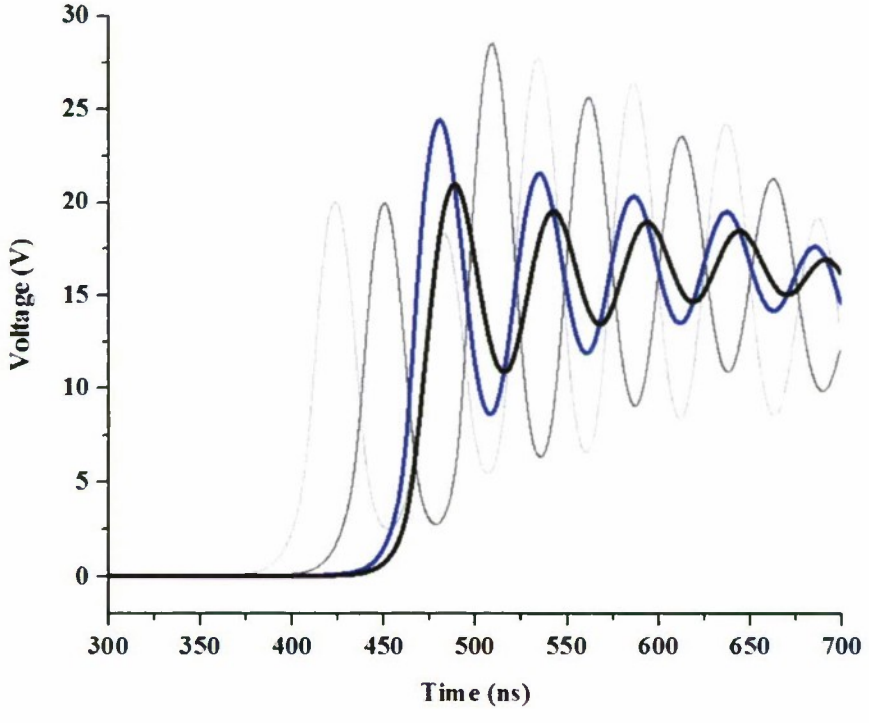

Figure 6.22: Final four stage simulated waveforms, including output, to a relatively high value resistive load.

Simulated NLETLs were run with resistive loads being exactly matched to the instantaneous line characteristic impedance according to $\sqrt{L/C(V)}$ but this did not improve extraction and the delay effect was evident. Although it was not possible to replicate this setup in practice, a rough experiment along similar lines used zener diode loads whose effective resistance increases with increasing voltage: up to the zener cut-off voltage results were similar to those with normal resistors. In fact it is now thought that the issue with any resistive termination may indeed be related to a phase interruption, in that for real RF power to be extracted the current and voltage waveforms have to be pulled into phase, a condition not met mid-line where they possess similar waveforms to one another which oscillate with a $\pi/2$ phase shift.

Chapter 7 includes additional ideas along the lines of symmetry, resistive snubbing of an inductive kick effect and the fundamental nature of a standing RF wave of zero group velocity, the latter bearing relevance to the most successful method of extraction proposed during this work, via distributed periodic loading.

6.4.2 Colliding Solitons and Parallel NLETL Approach

The increase in instantaneous amplitude created by a head-on collision between two solitons (and decrease during an overtaking interaction) was noted in chapter 4 in accordance with both nonlinear dispersive wave theory and numerical modelling of the NLETL system. In theory the resultant peak amplitude can be slightly greater than their sum and arranging a head-on collision between individual soliton pulses at a load could be expected to counter the broadening effect described above. A 1997 paper by Ibuka et. al. [91] posed the question "can the energy of a soliton, that can exist only in a nonlinear media, be extracted from a nonlinear transmission line?". They were concerned with single pulses only, not RF pulse burst waveforms generated via longer input pulse durations, but in itself this mode of NLETL operation has potential value for pulse compression. Due to the symmetrical sech^2 waveform the extended tail generated by continuous nonlinear shock wave generators is not present, and all the pulse energy is delive-

rable in a short time period. By driving two NLETLs in parallel and connecting the outputs of both to a common resistive load, it was indeed possible to achieve voltage amplification and pulse sharpening. That effect was reproduced here with two low voltage BB212 lines and a narrow single soliton generating input pulse (figure 6.23).

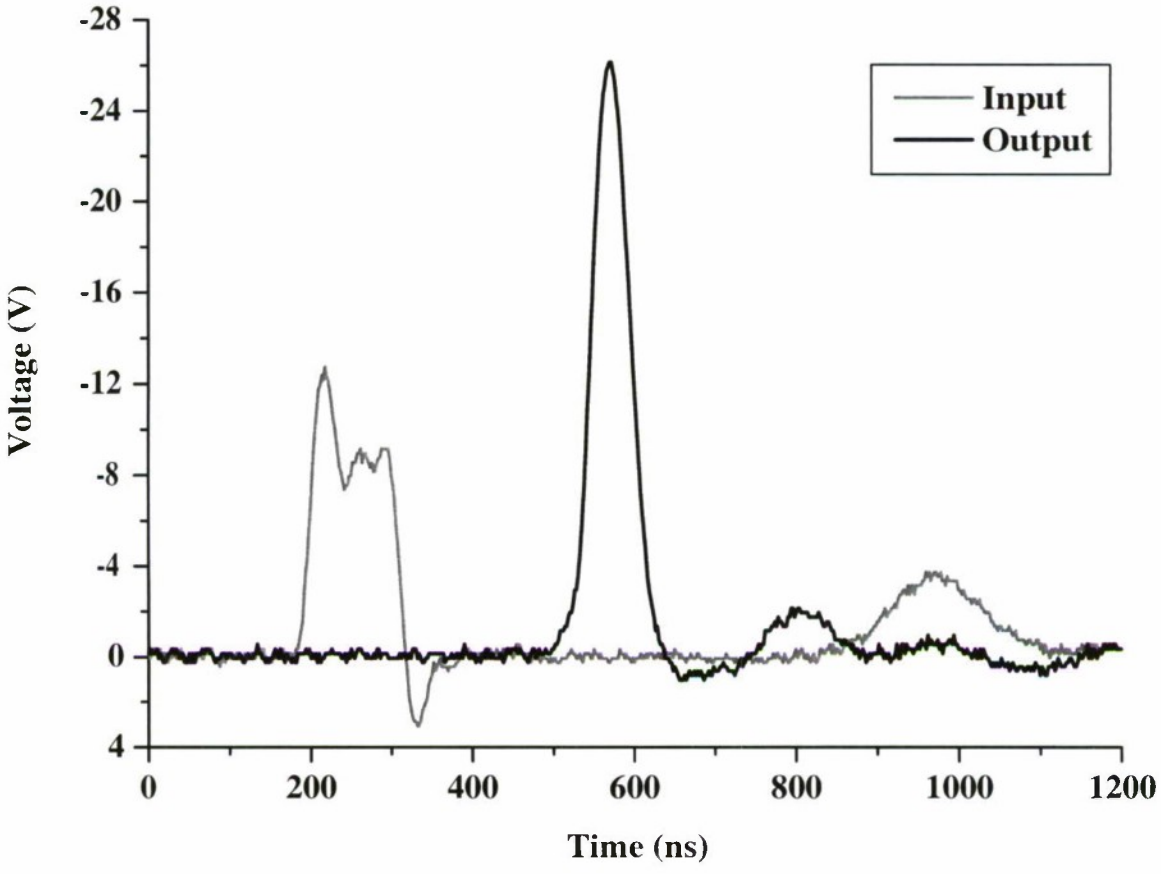

Figure 6.23: Single pulse compression and voltage amplification with two lines in parallel.

In attempting to extend this approach to pulse bursts experiments were carried out with a range of line designs and using up to five in parallel, and the simulation tool was developed to incorporate up to four lines in various configurations. Extraction to larger loads can be somewhat improved with the parallel line configuration but remains limited by comparison with the potential RF energy generated mid-line, and it was not possible to reproduce any significant improvement during high voltage experiments on parallel lines. A brief overview of

these results is presented in section 6.5. It is also potentially feasible to increase the effective pulse burst duration if several lines of different length are driven in parallel such that each pulse burst generated by the same input pulse arrives one after the other at the load. But the differences in line lengths must at least accommodate a single pulse burst duration and where many lines are used the frequency can decrease notably due to spreading, and of course the system drive impedance quickly becomes very low.

6.4.3 Asymmetric Parallel Configuration

As a reasonably effective solution to the extraction problem, based on the anti-phase property now associated with NLETL oscillation, the asymmetric parallel (ASP) configuration has been conceived and demonstrated during this work. Two lines whose lengths differ by a single discrete stage are driven in parallel and their outputs connected to opposite terminals of the resistive load, as illustrated in figure 6.24. By virtue of the anti-phase property, in principle the differential output voltage waveform would be expected to oscillate strongly. Encouraging results at low and high (chapter 8) voltages will be presented, with the ASP configuration facilitating greatly improved extraction of RF energy to single resistive loads, and the first indication of realistic application potential.

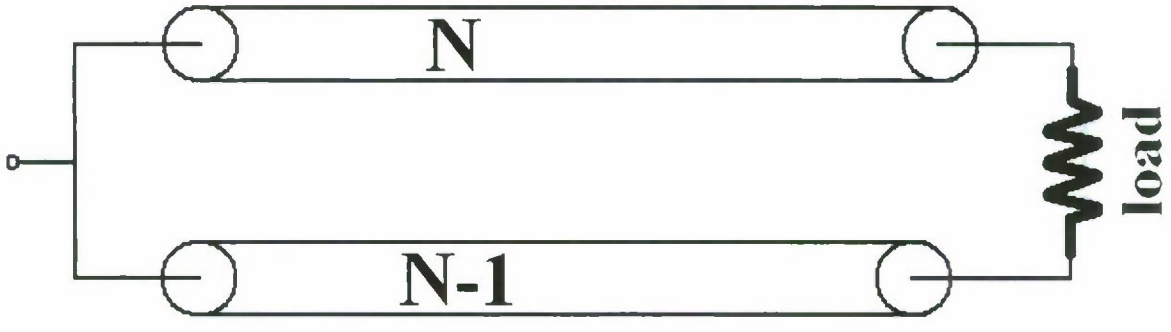

Figure 6.24: Circuit diagram of the asymmetric parallel (ASP) NLETL configuration, designed to enhance extraction of RF energy to resistive loads.

Attempts were made to simulate ASP NLETL operation, but the numerical scenario turns out to be particularly unstable which limited the results at useful frequencies (section 5.3). Accurate experimental measurement required pairs of matched probes in order to establish instantaneous differential voltage (this method was also used along higher frequency single unbalanced lines where the 'earth' side typically possessed significant inductance in itself). Some low voltage results are presented in section 6.5, along with a refinement in the form of cross-links between the two lines. Good results have been obtained with a wide range of lines, and frequency agility demonstrated in one case between 56 and 75 MHz through a DC bias of 0 to 5 V.

6.4.4 Alternative Ideas for Improving Extraction

Various other ideas have been contemplated upon gaining a proper full appreciation of the extraction problem: in some cases results were unimpressive and others have not been tried out at this time but are mentioned here for reference. Using the numerical model it was possible to gradually vary frequency along a simulated line by tapering inductance or nominal capacitance values. A taper of nonlinearity such that the NLETL becomes linear for the final few stages was also used to establish whether this might remove any issues with the interface between the nonlinear line and linear resistive load. However, within a stage or two of the propagation medium become linear the oscillations were found to immediately collapse and so this approach was not successful, although the evidence of immediate sensitivity to reduced nonlinearity was insightful at the time.

Increasing the output voltage to counter soliton broadening and overlap, which motivated the head-on collision of pulses with parallel lines, could potentially be achieved with a Blumlein NLETL configuration, perhaps with a taper to linearity at the far end of the open circuit line for good clean reflection of energy. This would require accurate timing and well matched lines but is feasible in practice, along with a range of other special square pulse forming networks

designed to boost output voltage [92]. They are relatively complicated to construct and remain ideas for future study, but a different approach using converging rings on a central load was carefully tested, unfortunately with poor results. The idea was based on speculation that branching of lines at the highest order, as in after every stage, could force a large number of successive collisions and strong oscillation. This followed experiments on feeding two lines into one, sometimes repeatedly, but in a fractal type pattern often associated with nonlinear physical systems. A series of six branches was arranged in rings with 124 BB212 capacitive elements over a flat copper sheet earth plan, seen in figure 6.25. In hindsight it is perhaps not surprising that such a system should not oscillate as per a uniform NLETL since the phenomenon is now thought to rely on its symmetry between neighbouring stages in accordance with the anti-phase property (chapter 7).

Following the chronological order of work on the project, one remaining method of effective RF extraction (periodic loading) developed and successfully demonstrated at high voltage is left to chapter 8, with preliminary discussion in chapter 7.

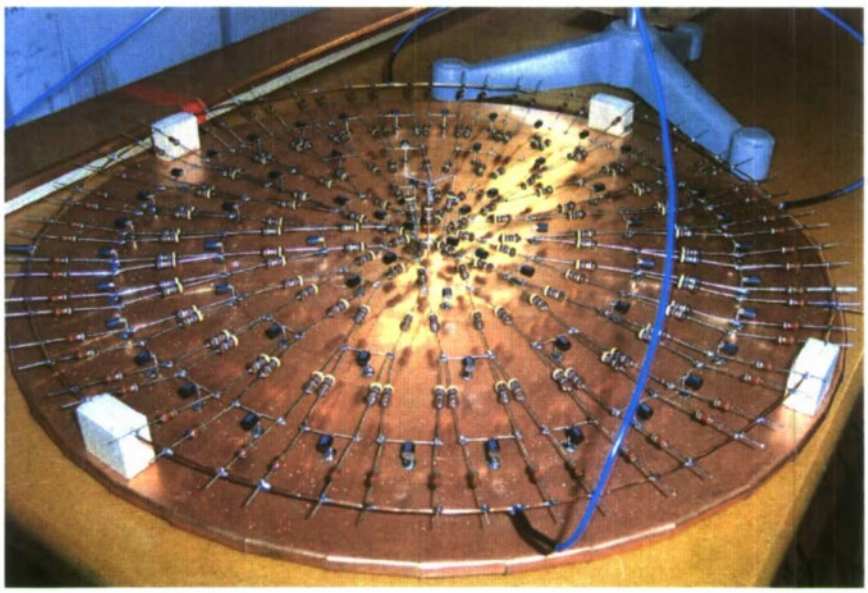

Figure 6.25: Experimental testing of the converging rings configuration.

6.5 Parallel and ASP Configuration Results

A sample of pulse burst waveforms delivered to low inductance resistive loads are presented in this section. Further ASP results may be found in the following section on low voltage propagation work, and also from the high voltage lines of chapter 8.

With two parallel lines some improvement in output waveform may be observed in figure 6.26, but to larger loads only and for a relatively small number of cycles. There is typically significant disruption to waveform uniformity with premature pulse shortening in comparison tp the mid-line waveform, and a lack of reproducibility since results are better with certain lines and poor with others. Simulation results suggest that increasing the number of lines in parallel beyond two should improve output modulation depth (figure 6.27) but experiments with up to six lines failed to generate any significant improvement over the double arrangement.

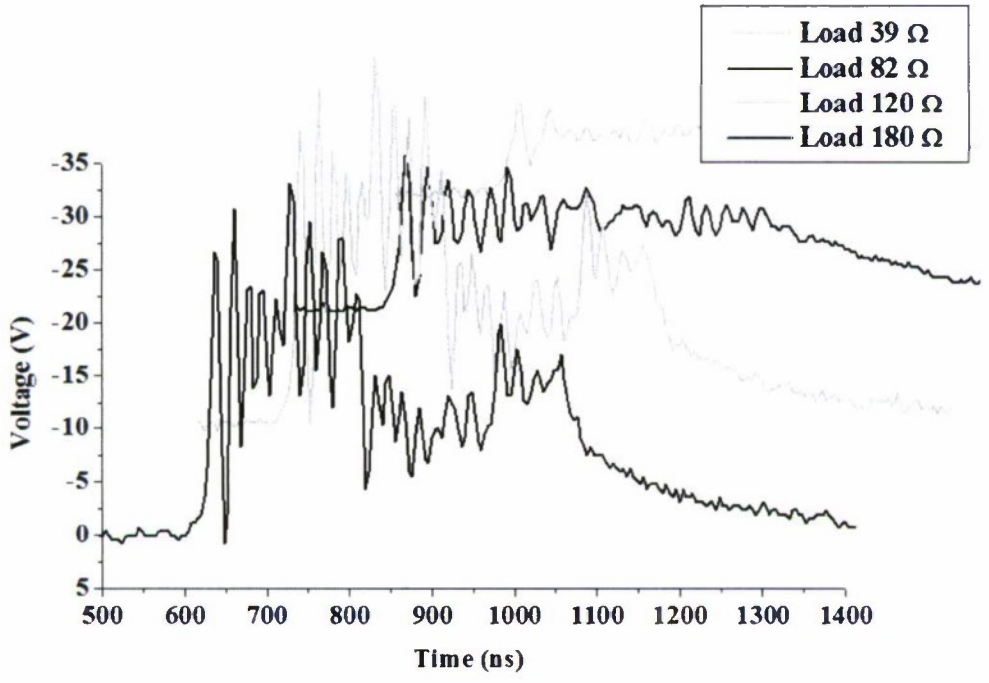

Figure 6.26: On occasion the use of two lines in parallel has improved experimental output waveforms, to larger value load resistors.

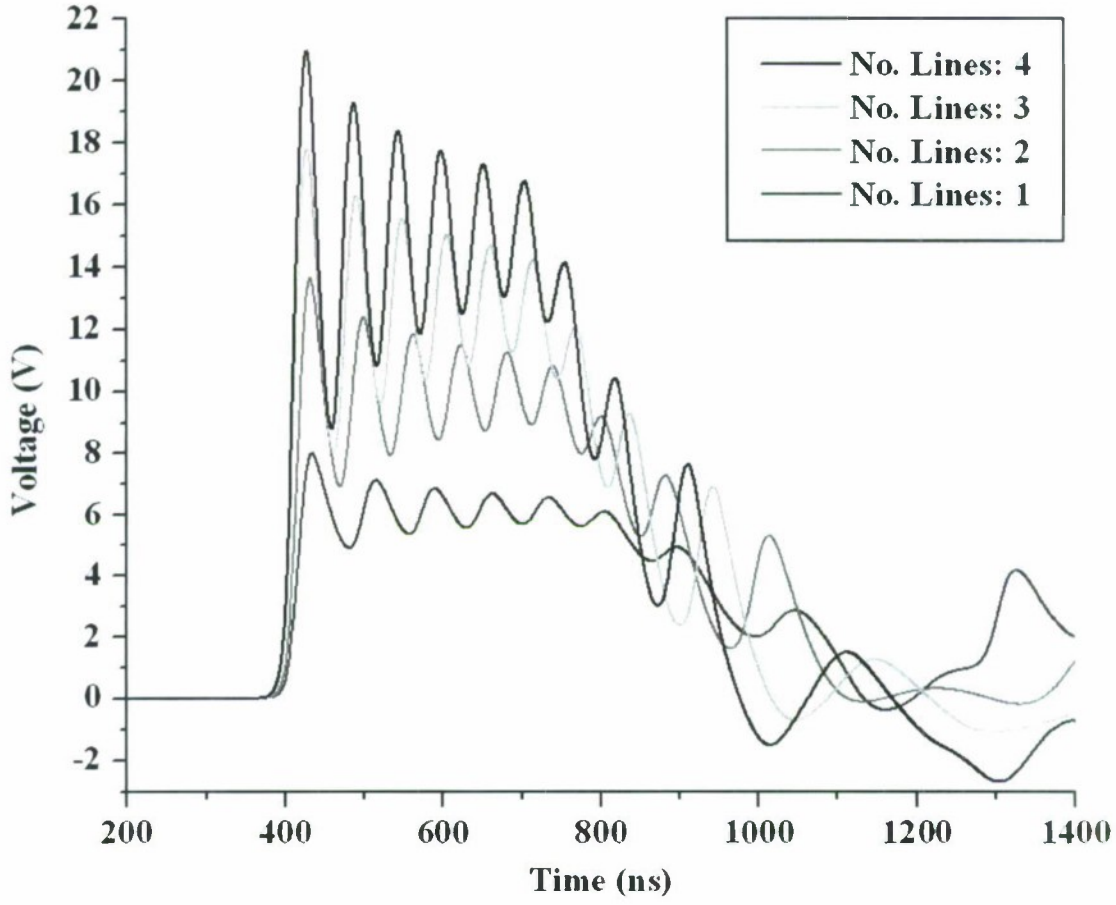

Figure 6.27: Output waveforms of simulations run with up to four lines in parallel.

Figures 6.28 through 6.33 provide some ASP results from a range of low voltage NLETLs. In all cases where an equivalent single line was terminated with a resistive load the output waveform was, as expected, a reconstructed form of the input pulse containing negligible RF energy, albeit with a sharpened leading edge. Whilst the load resistance doesn't have to be particularly large, where it falls well below the nominal impedance of each NLETL the output waveform collapses. Typical ASP output characteristics are represented in these selected examples, including a reduction in pulse duration but good peak to peak power delivery for a pulse duration that is reasonable for many applications.

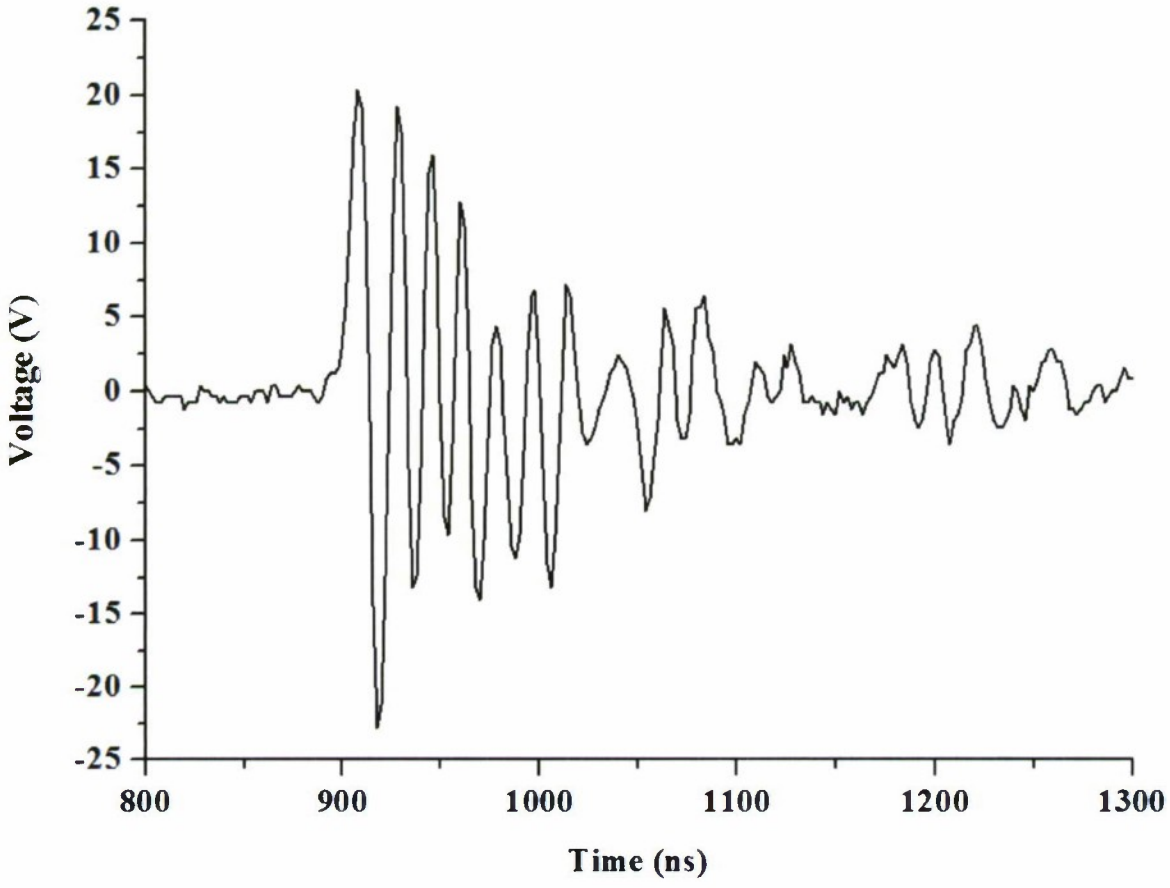

Figure 6.28: One of the first experimental ASP output waveforms, largely representative of those obtained from a range of different NLETL designs. Two BB212 1 μH ferrite cored commercial inductor lines (termed number 6) of lengths 20/21 stages were used to deliver this 62 MHz pulse burst to a 680 Ω resistor.

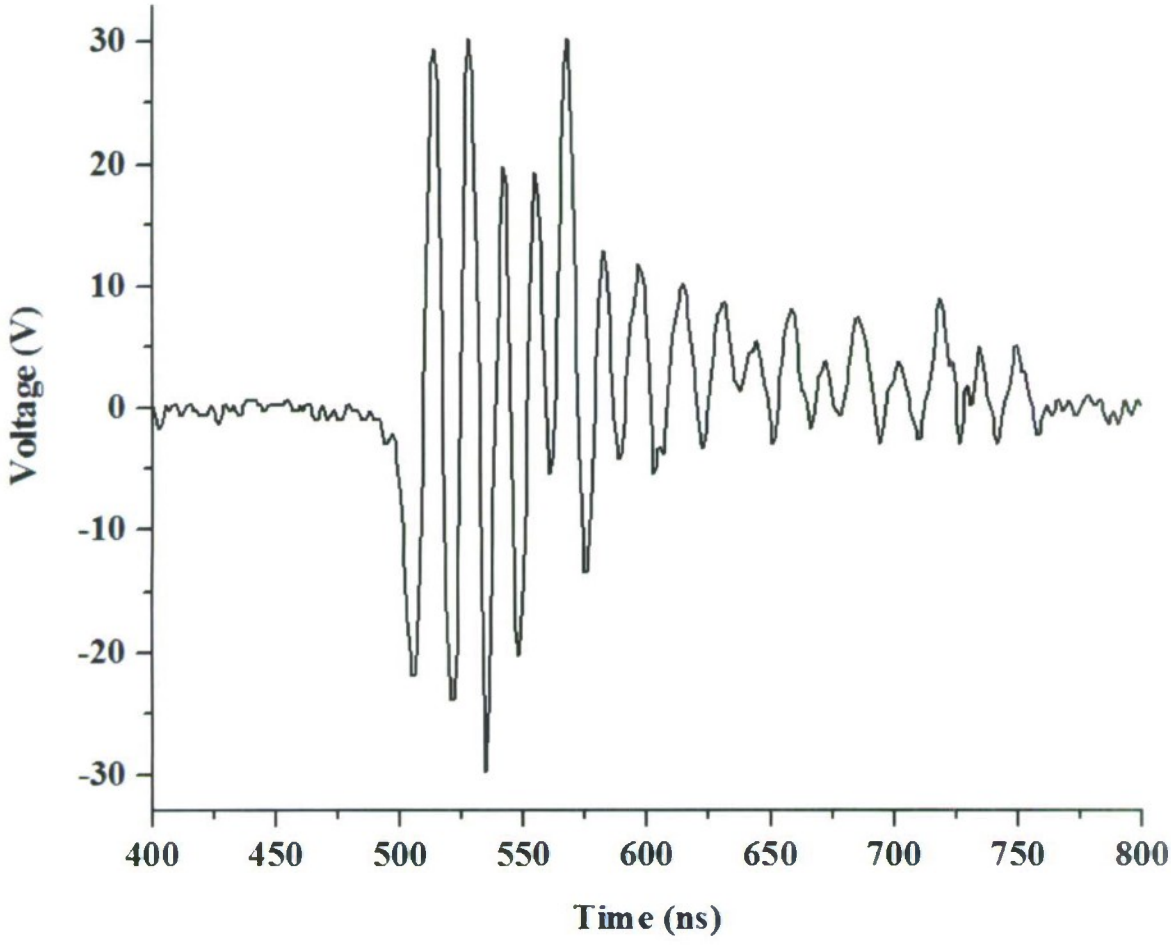

Figure 6.29: The system of figure 6.28, based on line 6, was subsequently driven with a larger amplitude input pulse from the KSM 50 V pulse generator unit, with a resulting output frequency of 76 MHz.

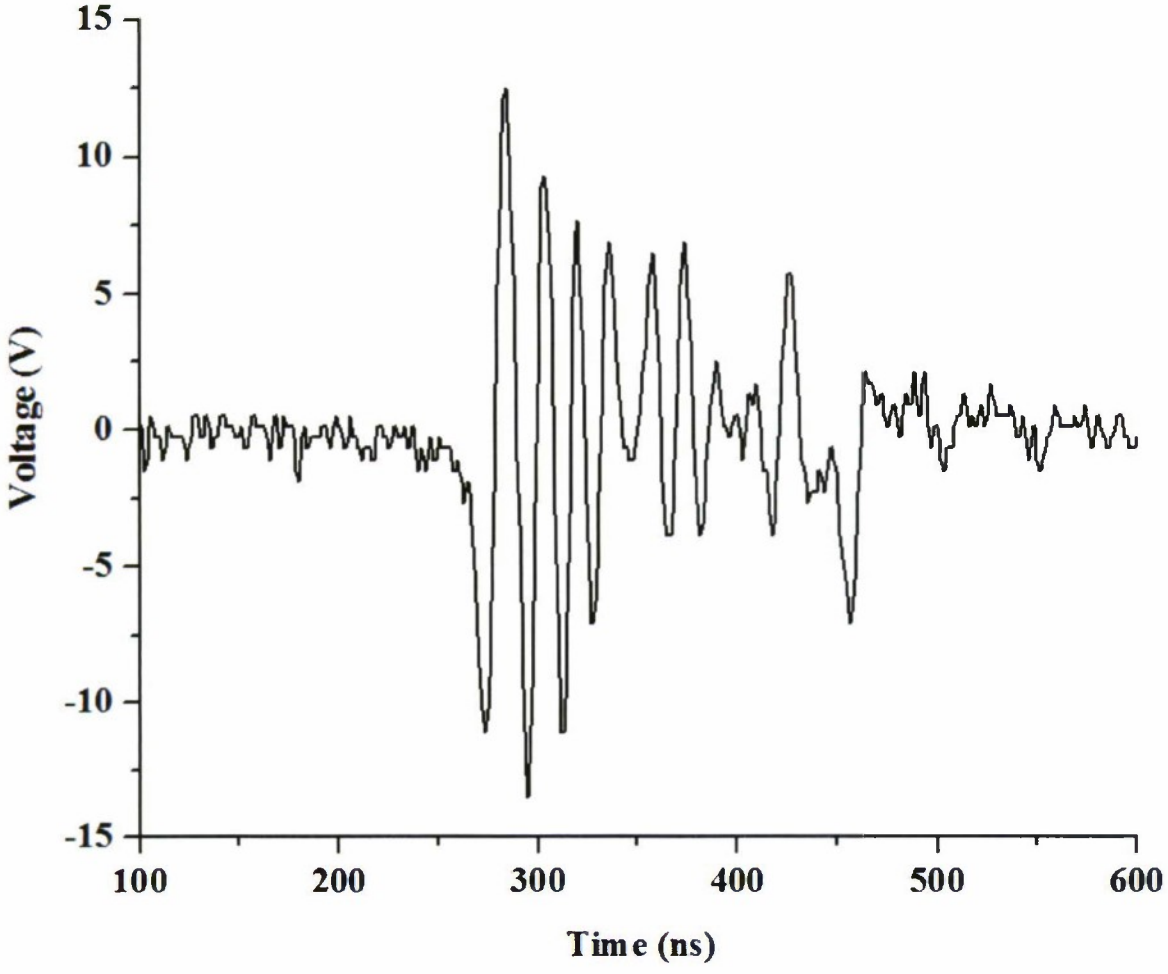

Figure 6.30: Output of line 6 in ASP mode to a 180 Ω load.

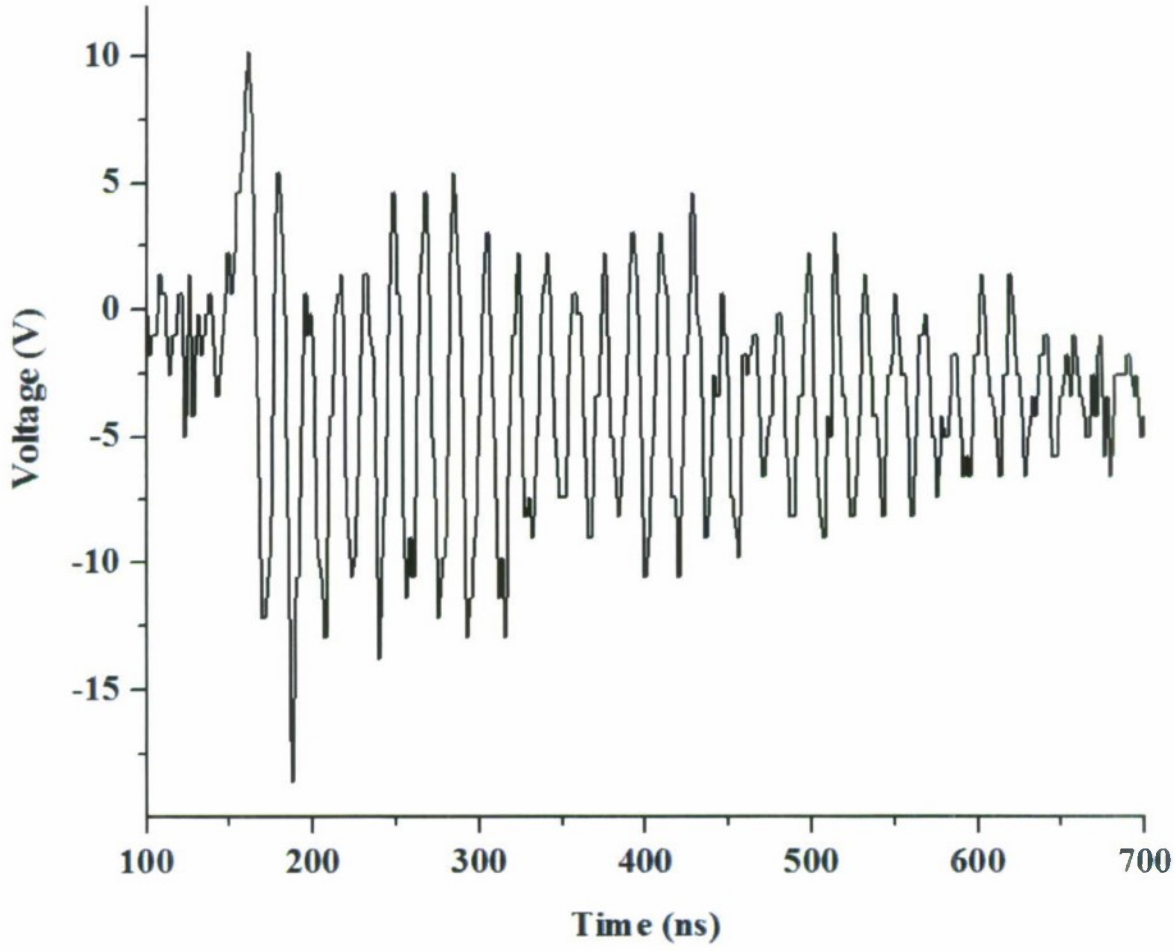

Figure 6.31: A relatively short ASP configuration of 10/11 stages with line design number 8 oscillating at around 60 MHz to 80 Ω.

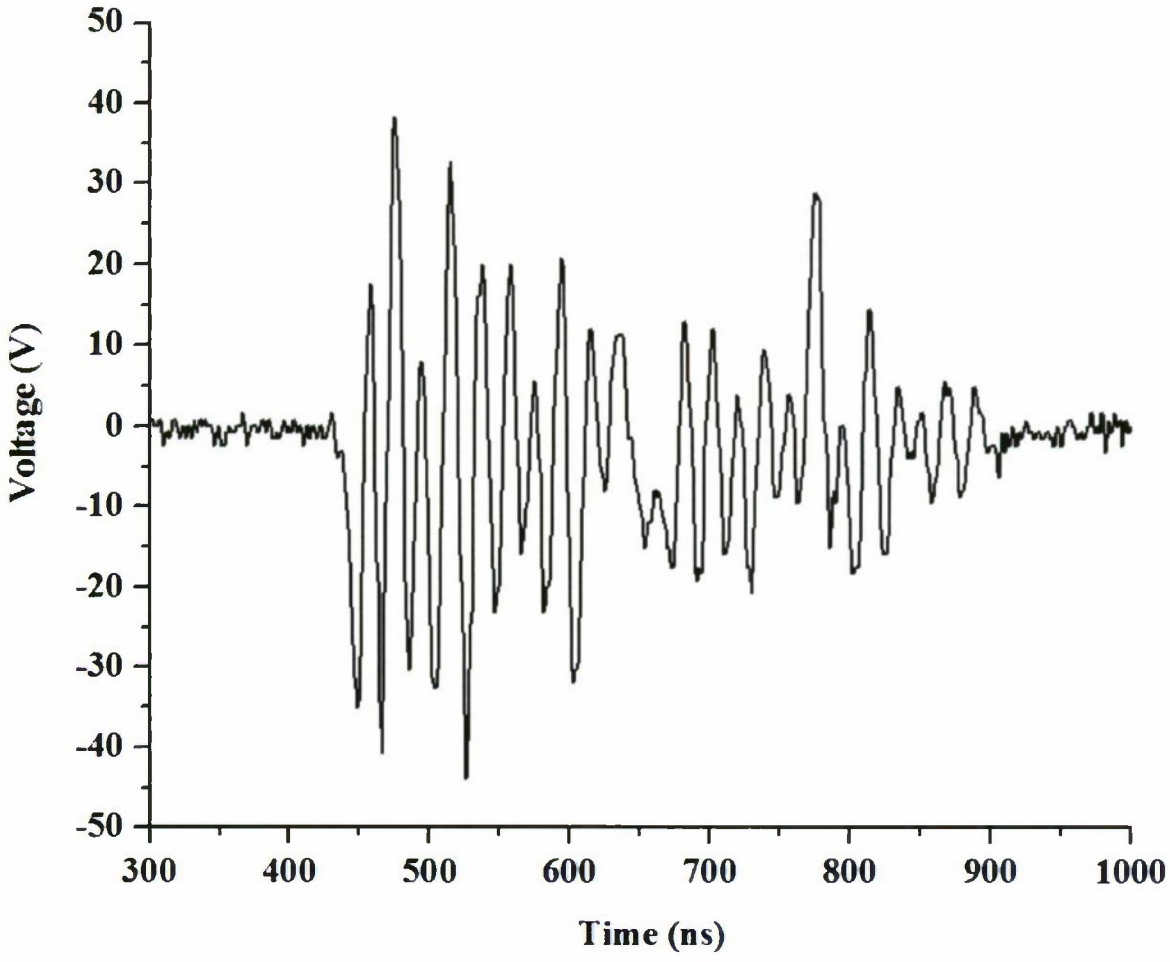

Figure 6.32: Line number 9 incorporating 24/25 BB212 diode stages and self-wound air cored 2 μH inductors delivers a 50 MHz pulse burst to a 680 Ω load.

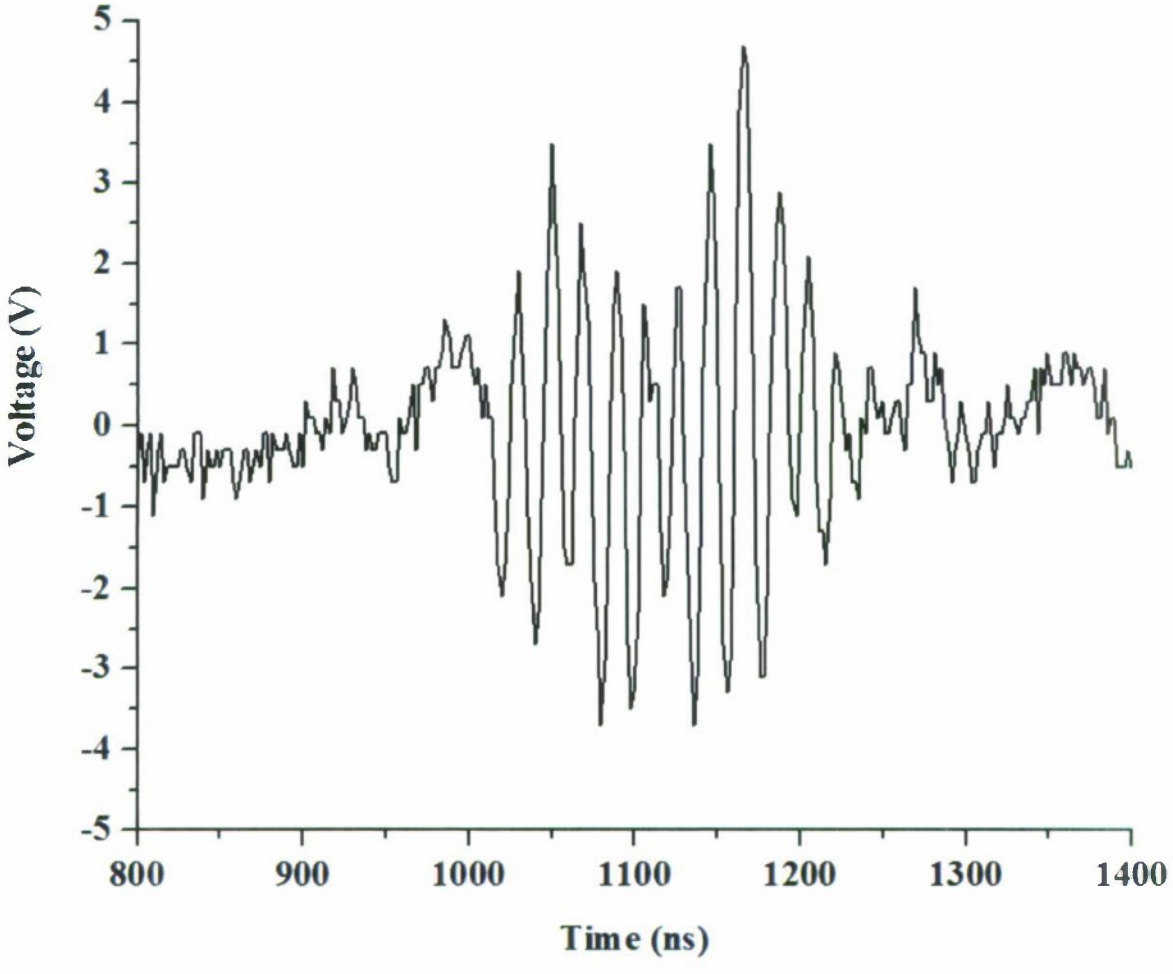

Figure 6.33: Line number 9 in ASP mode as per figure 6.32 with a lower value 68 Ω load.

The loss of output oscillation with lower loads, and also that leading to the pulse shortening evident in these examples, is manifest in a drift of phase at the output ends of each line such that the required anti-phase is compromised. Sometimes the two lines in an ASP configuration are not precisely matched which limits operation; although the phase difference does not need to be perfect to establish a strong differential waveform it is quite possible for phase to drift by a half wavelength over a reasonably modest length of line. This was sometimes the case with the stacked diode arrangement described in section 6.1, and a method of generally improving the phase relationship between a pair of ASP lines has been conceived. One or more short circuit or capacitive cross links are used to connect corresponding stages of each NLETL at the output end, as illustrated in figure 6.34. The addition of these cross caps has on occasion been helpful (figure 6.35 and figure 6.40) but whilst they are capable of effectively dealing with line mismatch, assuming well matched lines their ability to control the forced phase drift associated with pulse shortening is limited. Of course, at very high frequencies they should be used with caution unless very compact since the extra stray inductance can impair the quality of link and by itself inhibit the output waveform, which was indeed the case where frequencies reached 250 MHz.

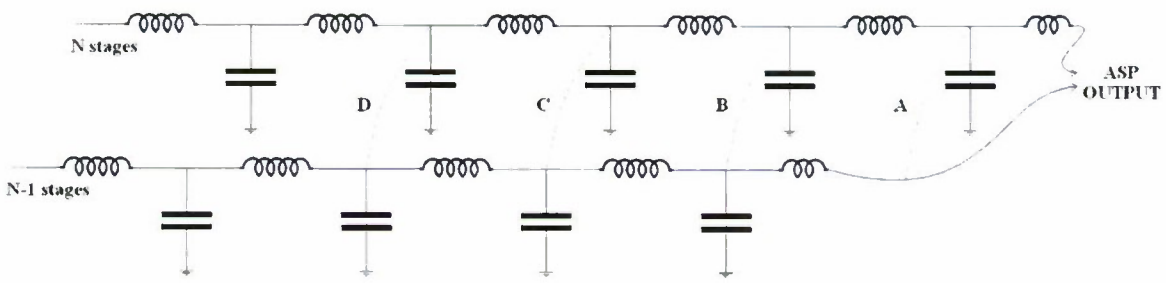

Figure 6.34: The addition of one or more cross links 'A', 'B', 'C', 'D' etc. between two ASP lines can improve phase stability and hence the quality of the differential output voltage waveform.

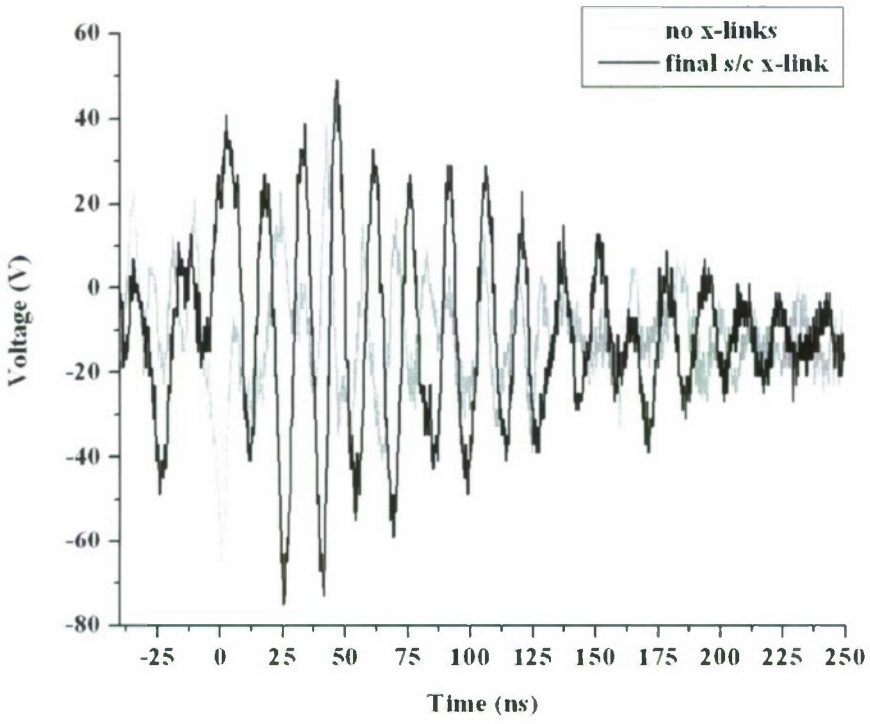

Figure 6.35: Comparison of ASP output waveforms to 68 Ω with and without a cross link in position 'B'.

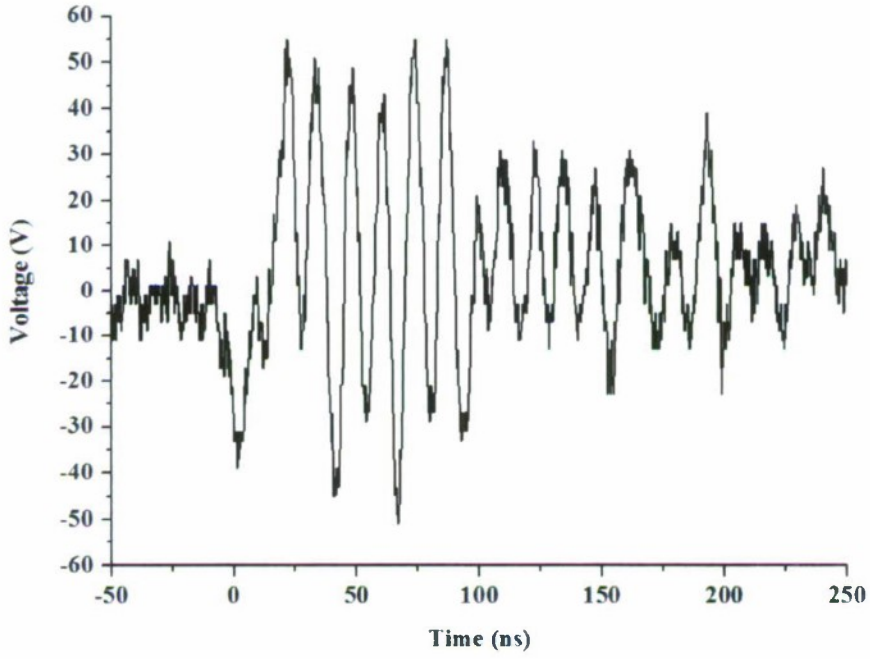

Figure 6.36: The ASP performance of the stacked diode lines described in section 6.1 was improved by the addition of cross link capacitors, with this example delivering a 74 MHz pulse burst to 680 Ω at a peak to peak voltage of around 90 V.

6.6 Propagation with Low Voltage NLETL Systems

Certain applications involving the propagation of RF waveforms, to which NLETL technology may be suited, suggest motivation for attempting to drive antenna type loads using these experimental lines, particularly in ASP mode. As this stage of work progressed it fell into two parts: the initial interest was in driving a transmitting antenna and detecting effective propagation, but when it became necessary to suppress a relatively strong component radiating directly from the NLETL the feasibility of enhancing and exploiting this effect was also considered. Results presented here were obtained with the 80–100 MHz stacked lines and also at 200–250 MHz from the high frequency lines described in section 6.1.

Antennas for transmission and reception were either simple dipole wires or more sophisticated directional or broadband designs supplied by CPC [2]. The latter included two log-periodic VHF and UHF arrays, a Triax five element FM antenna on 87–108 MHz and a Scanmaster omnidirectional discone [32] offering reception over a very large bandwidth of tens of MHz to GHz frequencies, nominally 50 Ω devices. The ASP NLETL outputs were fed to the antenna via a pair of 50 Ω coaxial cables. Detected waveforms were fed directly to the 1 GHz oscilloscope via a 50 Ω attenuator whose response was confirmed to be very uniform over the frequency ranges of interest. The conditions for such experiments were poor due to a cluttered path of around 10 m between transmitting and receiving antennas within the laboratory environment, but sufficient to generate qualitative results of interest.

Faithful measurements of voltages on antennas are difficult to make, but it was nonetheless clear that the waveforms extracted to these antennas were poor despite the extended pulse bursts typically radiated and received (figure 6.37). By way of explanation the load impedances were thought to be too low for best ASP operation from the NLETLs being used at the time, and in order to improve the situation a series of paired unbalanced unsymmetrical 4:1 impedance

[2]CPC, Faraday Drive, Preston, PR2 9PP. 08701 202530, http://cpc.farnell.com

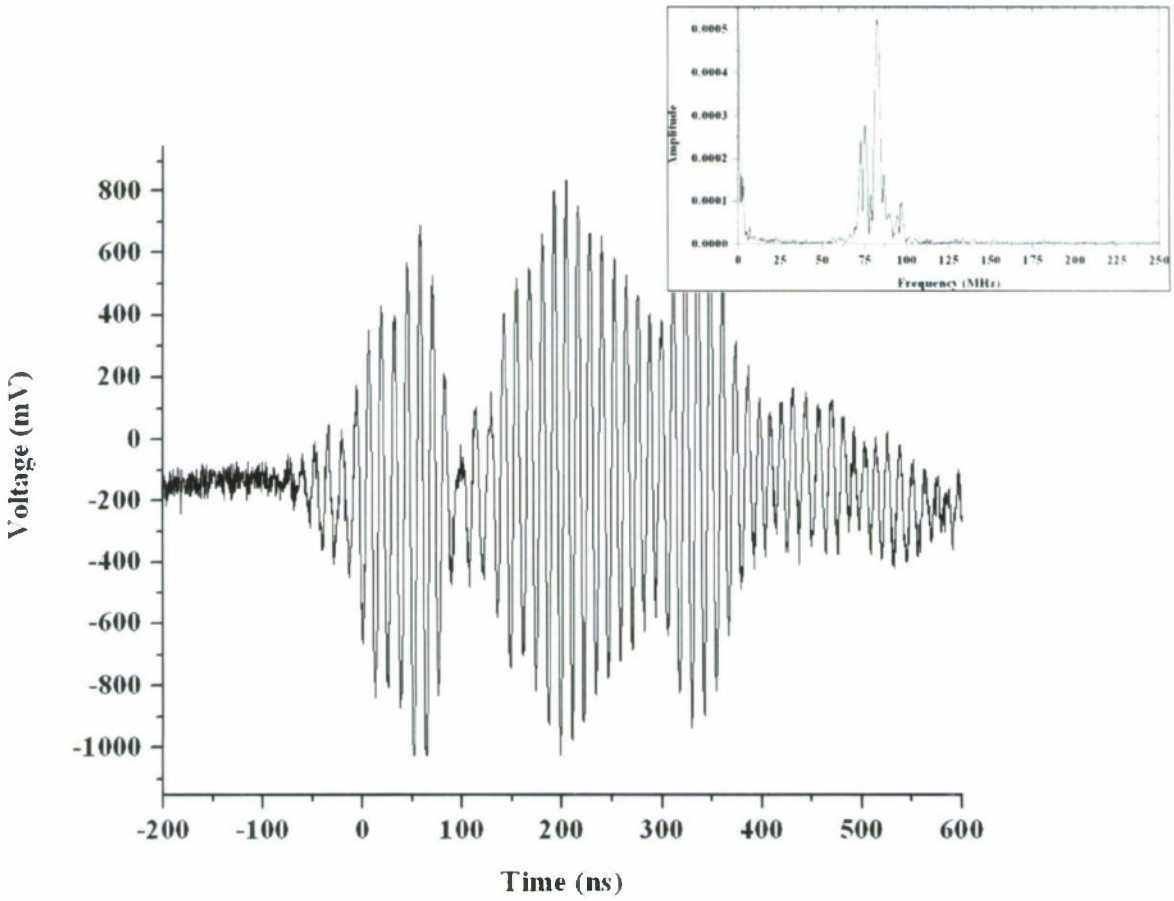

Figure 6.37: Typical pulse burst received during propagation experiments, in this case on a log-periodic antenna.

transformers [93] were designed specifically with compact windings on very small magnetic cores to operate effectively up to 100 MHz. The idea was to increase the terminal resistance presented to the NLETL and after careful design, response testing and minor modifications it became possible to deliver much improved ASP waveforms to the transmitting antenna (figure 6.38), or indeed to any resistive load (figure 6.40 and figure 6.41). Whilst many encouraging results were obtained from experiments carried out with impedance transformers between the NLETL system and various loads, they are only mentioned in passing in order to focus on the primary technology under consideration. Their practicality at very high powers and frequencies is questionable due to fundamental design requirements and compromise—attempts were made to reproduce the effect with high voltage lines without success.

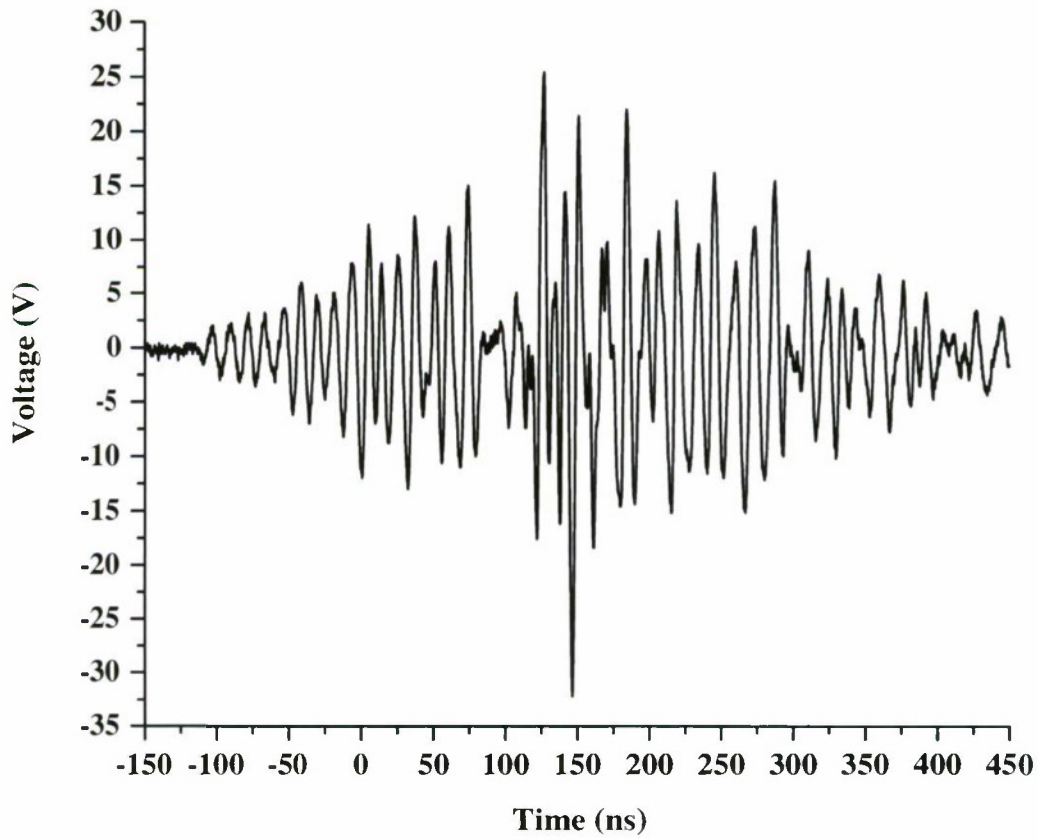

Figure 6.38: 90 MHz waveform delivered to yagi transmitting antenna by 39/40 stage stacked diode ASP lines via twin 50 Ω coaxial cables with impedance transformers, measured with high impedance probes.

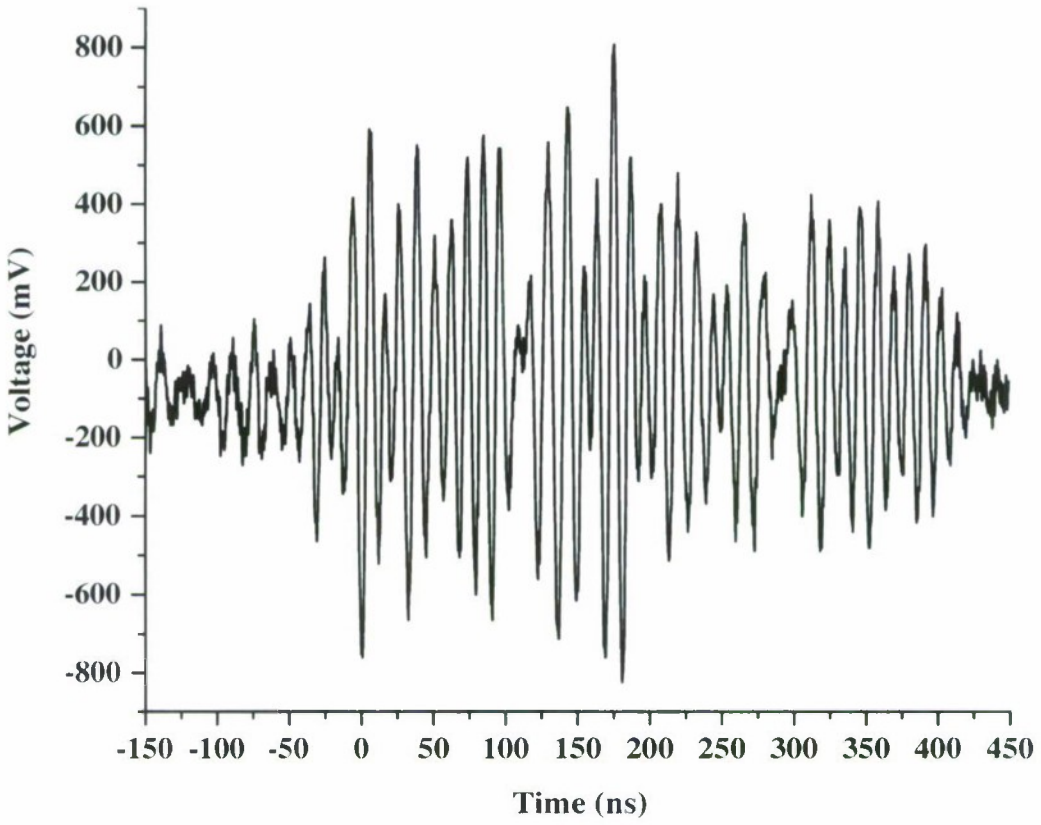

Figure 6.39: Received waveform on discone antenna corresponding to that of figure 6.38, where the NLETL section was foil shielded. The features of this waveform may be compared with the transmitting antenna signal.

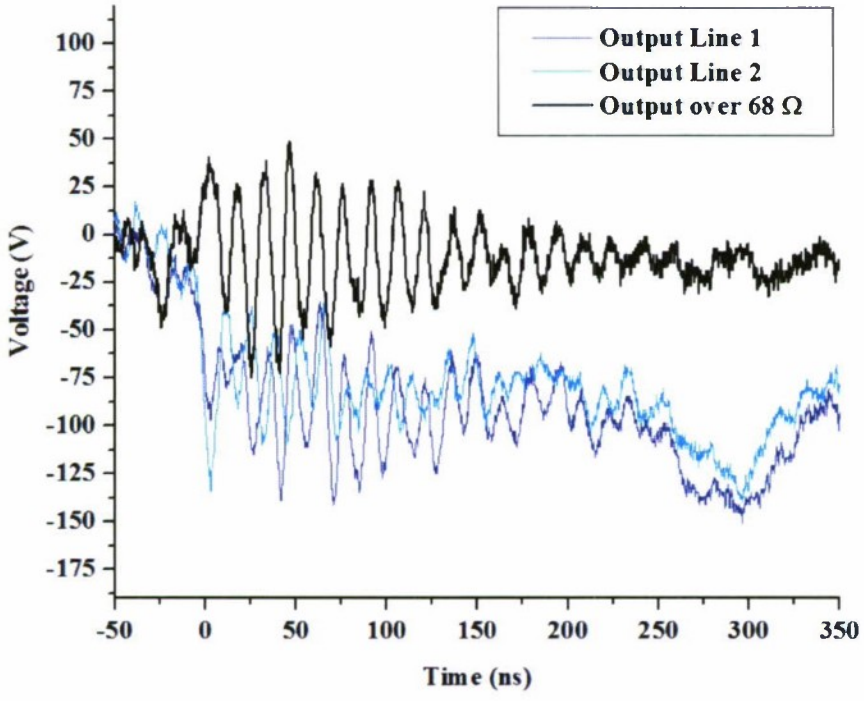

Figure 6.40: ASP output from 39/40 stage stacked diode lines to 68 Ω load, with cross links but no impedance transformers.

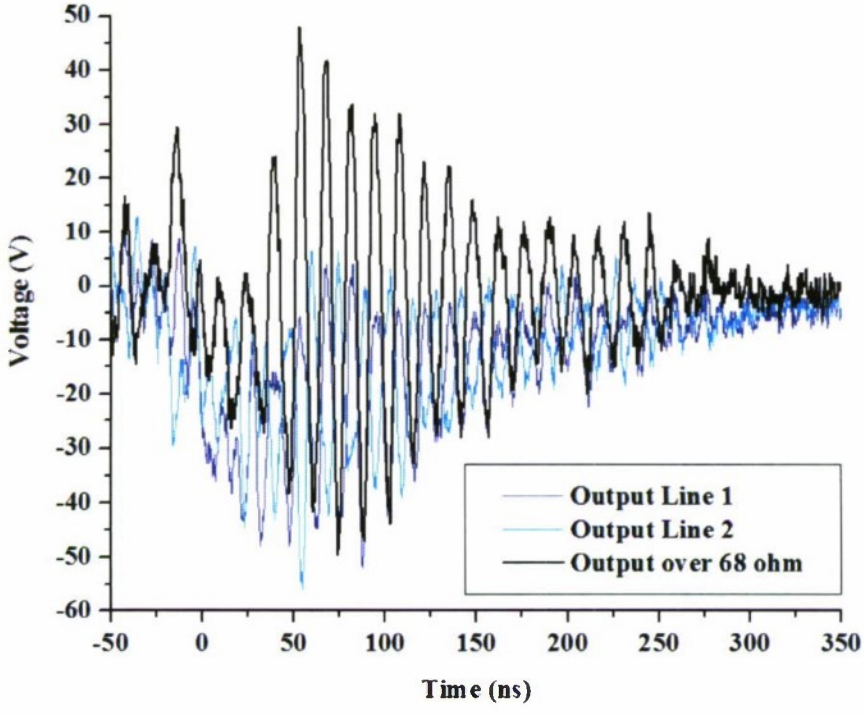

Figure 6.41: Improved antiphase and ASP output to 68 Ω with the addition of a single pair of high frequency impedance transformers between the NLETLs and the load.

It soon became clear that results such as figure 6.37 are due largely to radiation directly from the NLETL structure, with removal of the transmitting antenna altogether making a relatively minor difference. By progressively removing components it was confirmed that this was not associated with any other parts of the complete system such as the pulse forming network, trigger and switch circuit or even mains feed. An earthed shield of foil and silver tape applied to the NLETL part of the system effectively suppressed this radiated component and allowed the degree of antenna to antenna propagation to be ascertained. Then, for example, it was possible to observe an increase in received power with the addition of impedance transformers and to make the rough comparison between transmitted and received waveforms (figure 6.38 and figure 6.39). Checks were carried out throughout these experiments to verify detected waveforms, in terms of frequency, adjustments in propagation distance and the temporary addition of a large blocking foil screen.

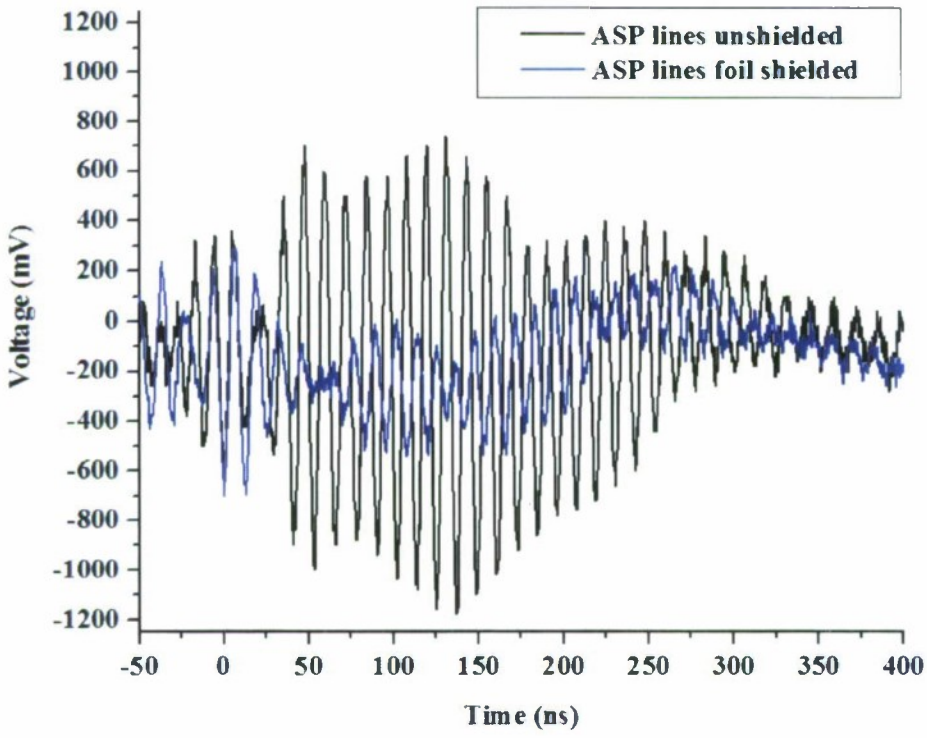

Figure 6.42: Detected waveform radiated from the stacked diode NLETL with and without earthed foil shielding in place.

Direct propagation and that with a dipole transmitting antenna load was also demonstrated with the high frequency low voltage lines, to beyond 200 MHz. Changes to the relative orientation of the NLETL and receiving antenna has a significant effect on the amplitude of the detected waveform, the main implication being that radiation from the NLETL structure is strongest in the plane of inductor loops and weakest in the normal directions. Multiple mechanisms are no doubt present but it seems that the primary means of radiation in this case was from the inductor loops which were presenting small (diameter less than $\lambda/10$) antenna loops [31] excited by the strongly oscillating stage-to-stage differential signal. Further consideration is given to self propagation and its enhancement in chapter 7, and the experiments of chapter 8 with high voltage lines.

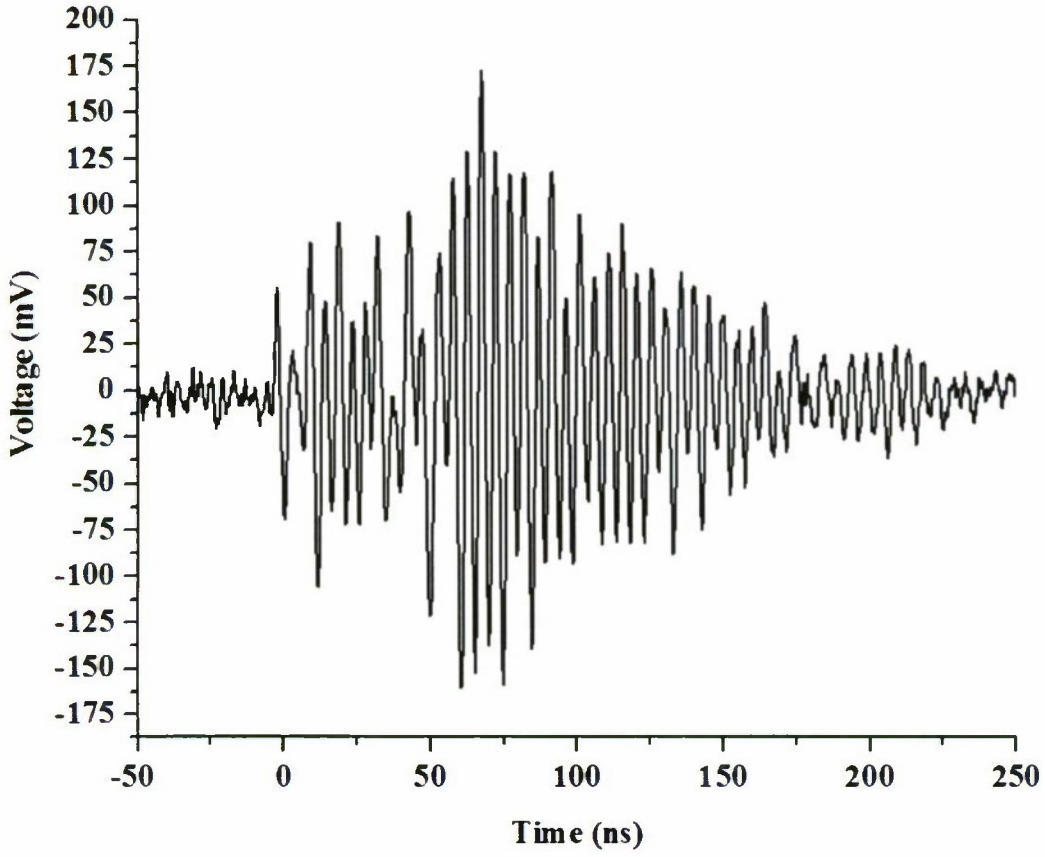

Figure 6.43: Radiation from the high frequency BB212 lines described in section 6.1 at 210 MHz.

Chapter 7

Perceptions of NLETL Oscillation

7.1 Relevance of Continuous Soliton Wave Theory

Past research into the use of nonlinear lumped element transmission lines of the type illustrated in figure 3.1 for RF applications has consistently referred to the individual pulses thus generated as solitons. This understanding is based on the presence of nonlinearity and dispersion, the latter inevitably accompanying the former and also due to the discrete nature of the propagation medium. The counter balance of the two influences is noted in accordance with the mathematical description of the soliton as a stable nonlinear dispersive wave, covered in chapter 4. That direct link to continuous soliton wave theory has been queried for the reasons mentioned in section 4.2, and adjusted to consider more specifically the soliton in discrete lattice breather form. NLETL pulses are now understood to be fundamentally discrete in nature, and comparison with approximately continuous waves on discrete lines, whose wavelength exceeds several discrete stages, is perhaps misleading.

Despite this the well established link to soliton theory in general is still considered relevant, which is fitting given the observation of soliton pulse shape properties and propagation characteristics. Soliton behaviour for individual pulses and cnoidal pulse trains (figure 4.12 and figure 4.13) is perhaps coincidental, given the variable nature of line capacitance and discrete stage time constant with respect to voltage, but any physical realisation of a mathematical phenomenon must have some practical mechanism which may be viewed as coincidental. The practical discussion which follows in section 7.3 serves to offer an explanation of NLETL operation from a less abstract perspective.

The discrete lattice breather has close links to certain physical phenomena but is associated with a rather complex field of theory [83] [94]. Further mathematical investigation and clarification with respect to electrical nonlinear lumped element transmission lines may prove insightful, although from a practical perspective other issues of materials science such as dielectric loss and CNL ratio are more immediate concerns for future work.

Section 7.2 continues briefly the discussion began in section 4.4 with the review of alternative aspects of nonlinear dispersive wave theory, with specific relevance to the periodic loading method of extraction introduced in section 7.4 by way of concept and experiment.

7.2 Summary of New Observations and Implications

The design trends established via extensive experimental and numerical studies have clear value in the optimisation of performance of a potential NLETL pulse burst generator with respect to application requirements. These have already been summarised in section 6.3 and considered during the design of subsequent experimental lines such as those which follow in chapter 8. But an additional awareness of the importance of certain issues such as loss (section 3.3, section 5.4 and section 8.5) and extraction has also been gained.

Observing the anti-phase property has been relevant to further understanding the generation of high frequency oscillation, and leads to questions of a theoretical limit on frequency before the continuous limit and associated infinite frequency is reached. Certainly there would be physical limits imposed by stray inductance and capacitance, loss and dielectric relaxation properties at comparable frequencies. Also this observation has led to ideas such as the ASP configuration to enable some extraction of RF energy to resistive loads, and gradual extraction with phased power combining as per the direct NLETL antenna or periodic loading concepts (section 7.4).

The new term NLETL emphasises the specific reliance on discreteness and nonlinearity, but in addition the importance of uniformity (section 7.3.1), or "discrete translational symmetry" [83] [94] suitable for breather formation has become clear. Further interpretation of a wavelength equal to two discrete stages in terms of the Brillouin limit of zero characteristic impedance and group velocity (section 4.4) suggests a form of resonance or standing wave with no actual propagation of energy along the line at the frequency of the superposed RF component. Perhaps

therefore problems with its extraction at the output end of the line should not be unexpected. Continuous solitons are considered unusual in part because they shift energy (for example tidal bores transport water unlike conventional surface waves), but discrete breathers generally aren't thought to move energy [94].

The NLETL scenario, depicted in figure 7.1, is more complex than might initially be thought, and involves more than a delicate counter balance between nonlinear and dispersive influences. In itself, that would probably be applicable to a far narrower range of line design parameters than those on which good oscillation has been demonstrated during this work. An increased awareness of the factors described above is progressive and has led to advancements in terms of tackling issues such as the extraction problem.

7.3 Inductive Kick Effect

7.3.1 Physical Explanation for Strong Oscillation

An appreciable reduction in capacitance with increasing voltage may be thought of as an opening switch to fast transients, in that its high frequency impedance increases. Within the NLETL it is possible to envisage an inductive kick effect [95] as explanation for the initial voltage amplification. If a switch flowing current through an inductor suddenly opens, the inductor resists the change in current without a large spike in voltage according to the equation $V_L = L\ \mathrm{d}I/\mathrm{d}t$. If in the corresponding equation for the nonlinear capacitor, $I = C(V)\ \mathrm{d}V/\mathrm{d}t$, the reduction in capacitance is not countered completely by the increase in voltage gradient to the shock front limit, then a sudden drop in current through that capacitor to earth is imposed, rather like an opening switch to high frequency signals.

With a careful analysis of simulation voltage and current waveforms (such as those of figure 7.1), the inductive kick reasoning may be applied to the NLETL on a stage by stage basis

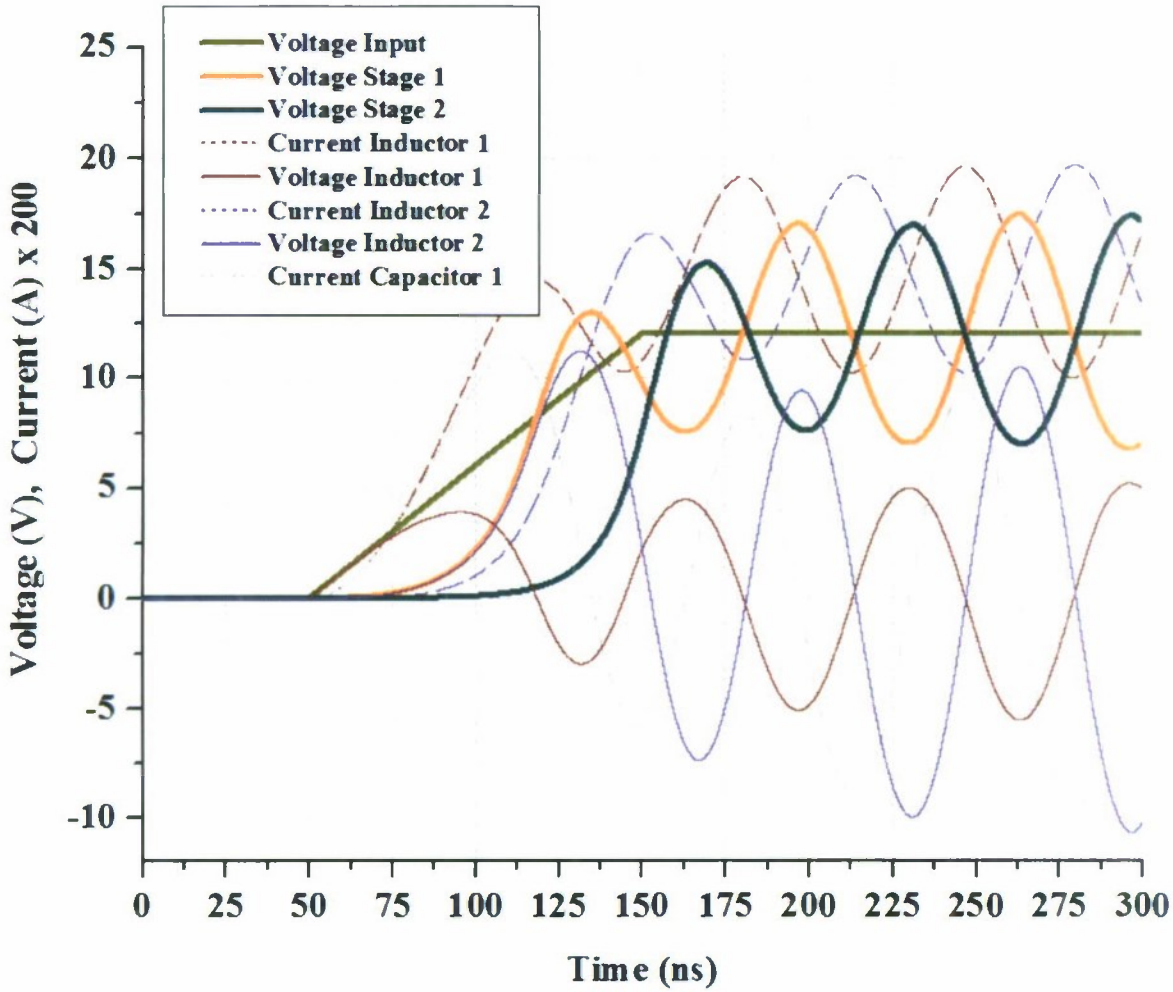

Figure 7.1: Selected voltage and current waveforms at the input end of a simulated NLETL undergoing the onset of soliton type oscillation. Dark red corresponds to the current through and voltage across the first inductor, violet the second. The first three stage voltages and current through the first nonlinear capacitor are also shown.

where incoming current feeds both the capacitor 'switch' and the subsequent inductor. This is with regard to both the anti-phase property and the need for an equally rapid voltage reduction to form the symmetrical soliton pulse shape within a repeating pulse train. In figure 7.2 below, voltage levels along a series of stages are illustrated at three time periods as oscillation progresses in a see-saw fashion down the line.

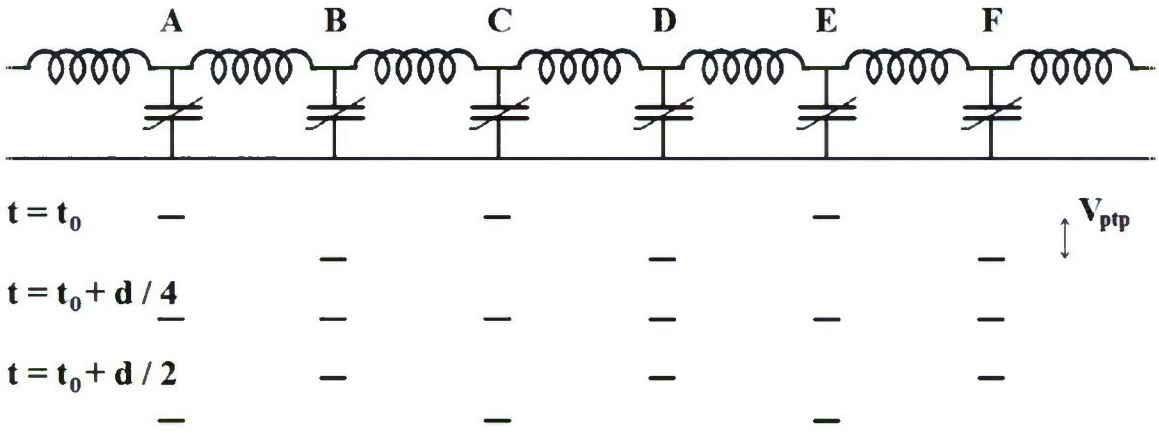

Figure 7.2: Voltage levels on a series of stages at three moments in time, where d is the period of high frequency oscillation. Twice per period all voltages are instantaneously approximately equal and at the input pulse amplitude, represented by the grey line.

As the voltage on a given stage, for instance stage B in figure 7.2, rises to that of the input pulse, and if this voltage sufficiently saturates the nonlinear capacitor, then by an inductive kick effect it may be presumed that the voltage at B should have to increase further. But if all inductor values are identical the inductive kick acts equally on inductors AB and BC, demanding voltage fluctuations across them of reversed polarities. In effect, the drop in capacitor current may be satisfied by a decrease in that through inductor AB and also by an increase in that through BC. Within the NLETL, and during the time frame of the input pulse period, each inductor is at a floating voltage about the input pulse level, and at the instant under consideration voltage B is pulled up while A and C are pulled down.

Subsequent to the inductive kick voltage requirement being satisfied and the capacitor current approaching zero, the voltage gradient and capacitor current become negative as per figure 7.1. It is interesting to note that negligible charge remains stored on each capacitor during the time of the main pulse body passing its point on the line except at the RF pulse burst frequency—a sensible observation when the saturated capacitance value is instantaneously very small and unable to store much charge at higher voltages, and the higher capacitance value accumulates charge at times of lower voltage. On a linear line, a positive pulse of capacitor current is seen on the leading edge of the main pulse body, reversed on the trailing edge, perhaps with some low frequency and amplitude ringing in between, as each capacitor is temporarily charged during the pulse period. Parallels may be drawn with the operation of a backward wave oscillator and its periodic slow wave structure (section 2.3.2), in terms of the forward and backward interaction between stages associated with the floating nature of each inductor and the anti-phase property, although this observation is based on speculation only.

The speed of propagation of the pulse body down the line is set by the shock transition time to which its leading edge is sharpened by the strong capacitive nonlinearity. This voltage rise time is also applicable to the leading edge of a given pulse burst cycle and, since the inductive kick acts symmetrically on forward and backward inductors on a uniform line, to the trailing edge. Thus each high frequency pulse is symmetrical, roughly according to the hyperbolic secant soliton form, and the anti-phase property is necessarily maintained.

The loss of oscillation associated with the presence of a terminating resistance, or indeed a single resistive load at any point on the line, may be attributed to a snubber effect, as per the technique used to reduce undesirable voltage spikes associated with inductors subject to sudden changes in current [95]. Furthermore, by replacing the subsequent nonlinear capacitor switching action by a resistor, the uniformity necessary to maintain the delicate balance between pulse burst rise and fall times and propagation velocity, and the corresponding full modulation

depth, is disrupted. The inductive kick suggestion can hence go some way towards explaining the extraction problem, from an alternative perspective to that offered in section 6.4.1. Overdriving a given NLETL has been associated here with a reduction in oscillation (section 6.3), which makes sense if the incoming voltage front amplitude becomes sufficient to fully meet the inductive kick voltage spike requirement, which can only rise at the same gradient. NLETL oscillation is superposed about the input pulse body amplitude voltage, and in an overdrive condition it seems reasonably to suppose that no further rise in voltage beyond that of the driving input pulse is required to satisfy the initial current transient experienced by each inductor.

This explanation also places emphasis on the discrete nature of the NLETL, in terms of presenting a sufficiently large inductance to induce the effect at each discrete stage, and a reasonable nominal capacitance to initiate current flow with a small saturated capacitance to properly simulate the effect of an actual opening switch. The analogy of a mechanical system with nonlinear interactions (section 4.4), along the lines of a series of masses with displacements and nonlinear interconnecting springs, is perhaps more intuitive if the voltage and voltage derivative dependence of capacitor current is taken into account in the inductor equations, whereby their values assume a complicated nonlinearity dependent on voltage.

7.3.2 Fuse Line Experiment

Some time was dedicated to pursuing this idea further, by building and testing a high voltage line incorporating the standard series inductors but with nonlinear capacitors replaced by exploding wires in the form of domestic fuses. This allowed a comparison to be made between conventional NLETL operation and any oscillation which might occur on such a line with one time opening switches.

The fuse line (figure 7.3) was 10 stages in length, with 800 nH air cored inductors at each stage and series resistors typically around 20 Ω with each fuse in order to establish an initial current.

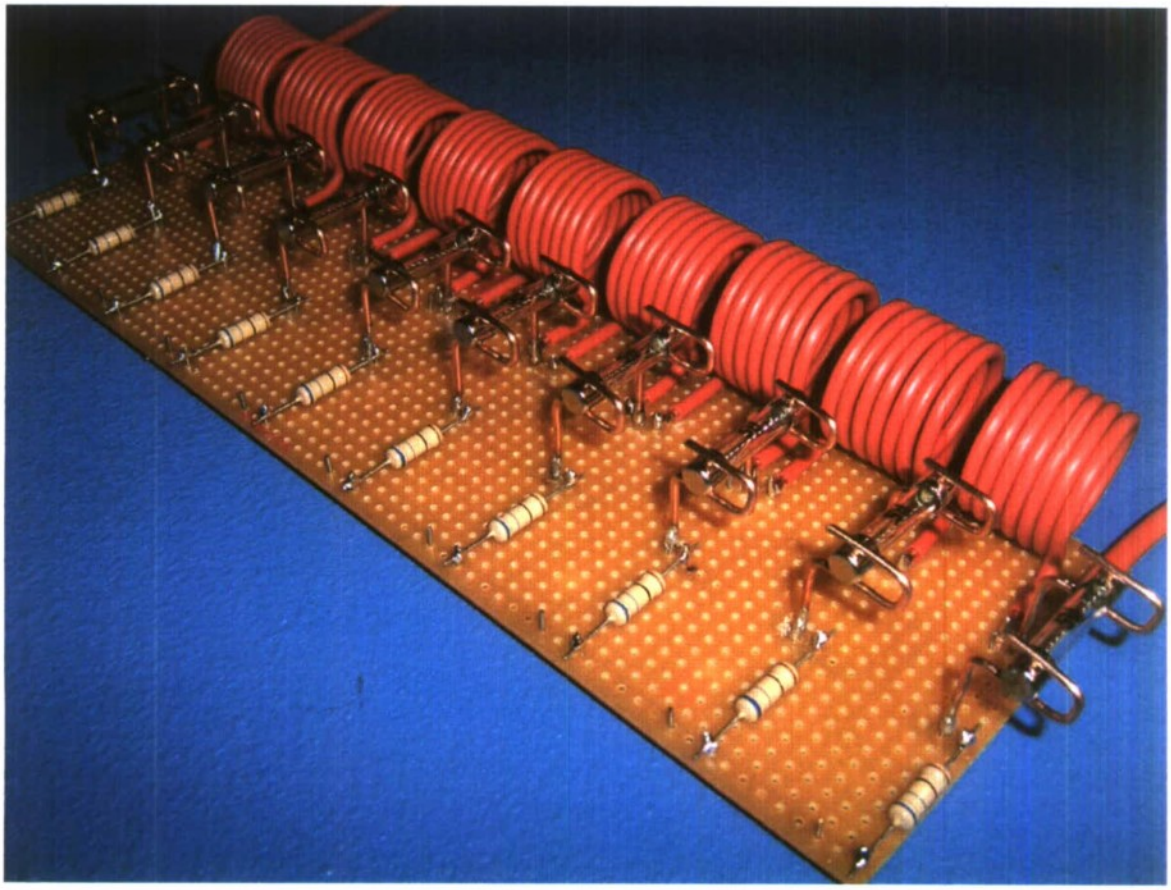

Figure 7.3: Discrete line incorporating exploding wire nonlinearity.

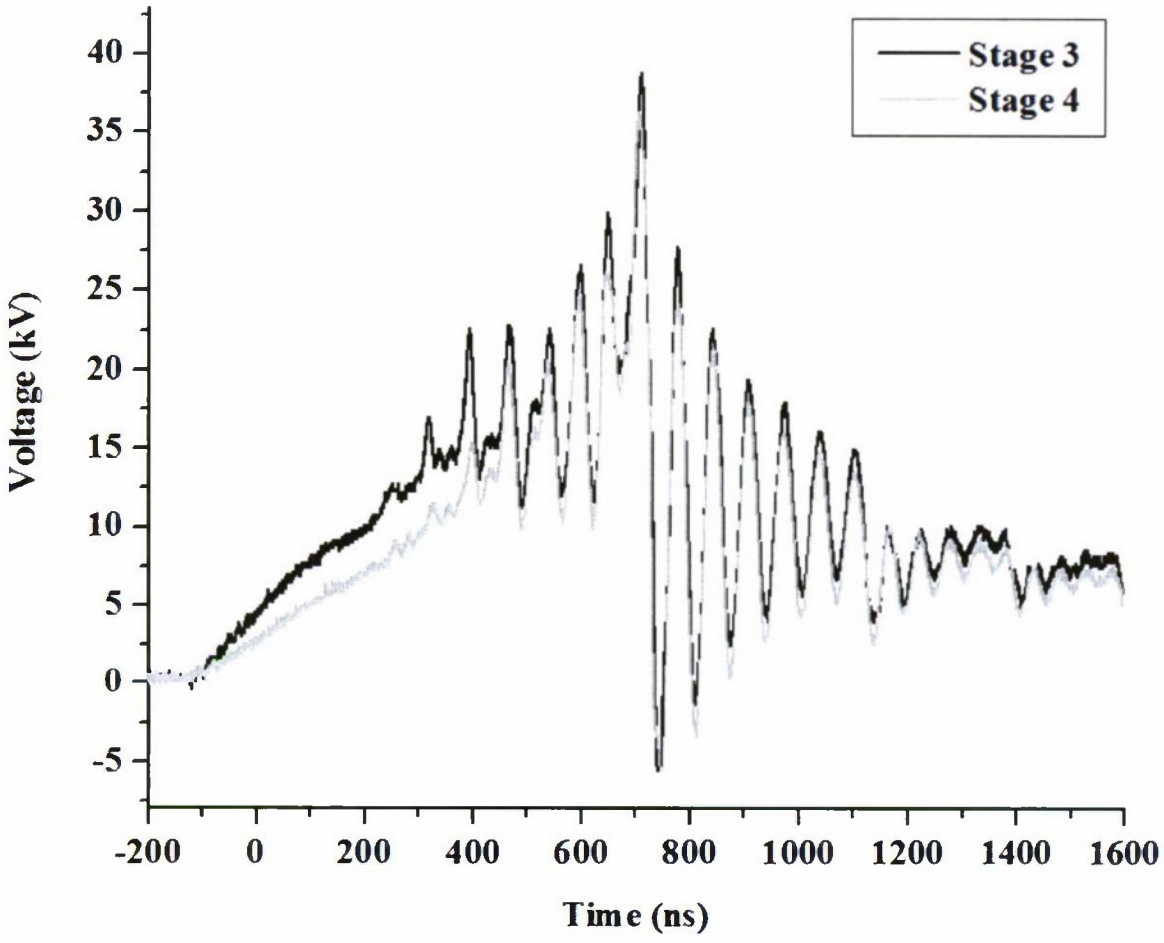

Figure 7.4: Waveforms developed on the fuse line, in this case with 100 mA quick blow fuses and a 15 kV input pulse amplitude.

Compact fuse holders were made up with rigid copper wire for good contact but also ease and speed of replacement; several hundred fuses were blown during tests on the line. Input pulses up to around 20 kV were applied, and only the lower value fuses were found to all consistently blow despite the high voltages to which they were subjected. This was due to the short time durations involved—in fact a significant property of the NLETL topology is the very fast reaction time of the CNL dielectric at frequencies below those characteristic of relaxation effects. An exploding wire undergoes the processes of ohmic heating, fragmentation and vaporisation which leads to a rapid increase in resistance and eventual cut-off to current flow, which under optimum conditions can be expected to take at least 50 ns [20].

The fuse wire switch is not frequency selective, and remains permanently open after its initial transition, without the subsequent closing action associated with a reduction in voltage increasing capacitance as described above. So for several reasons, whilst it is interesting to note oscillation such as that of figure 7.4, it being different in some aspects to that generated on a NLETL isn't unexpected. The frequency in this example is 15 MHz, which is relatively low, and adjacent stage waveforms were not found to oscillate in anti-phase with one another, a property now considered to be a defining characteristic of NLETL soliton type oscillation.

7.4 Periodic Loading for Extraction of RF Energy

Further to the ASP concept first mentioned in section 6.4.3, an alternative approach to solving the extraction problem is proposed in this section. It can be used as an extension of the ASP configuration, as demonstrated experimentally in section 8.6.1, and is in any case an even more promising development for many RF applications which could benefit from NLETL technology. This idea, termed periodic loading, was first publicly presented at the 2nd Euro-Asian Pulsed Power Conference in Vilnius during the summer of 2008 [3], with experimental confirmation of its potential made in the following months.

The predictable stage by stage phase relationship along a NLETL suggests the feasibility of incorporating transmitting antenna components directly into the transmission line structure, rather than attempting to deliver RF energy to a single antenna load for propagation applications. An array of dipoles spaced along the line may in theory propagate constructively, but subject to the loading of adjacent or regularly spaced stages of the line not severely disrupting either oscillation quality or phase.

The effect that this form of periodic loading might have was first investigated on a low voltage varactor diode line with a range of low inductance solid carbon resistor values applied at various stage intervals. A resistor loading a given stage is connected in parallel with the nonlinear capacitor, from the stage voltage measurement point to earth. This was undertaken with the fragile nature of the oscillations in mind: a single resistor loading any point on a NLETL severely disrupts the waveform at that point. The result is therefore perhaps unexpected but encouraging for the direct NLETL antenna concept and other applications potentially utilizing phased extraction on an incremental basis. Where several resistors loaded a series of stages along the line, good waveforms were observed after an initial disruption, with the quick re-establishment of full modulation and the anti-phase property. The travelling pulse train appears to adjust to the new line conditions, but only if every consecutive stage is loaded. Trying to load, say, every other stage, or every third stage, leads to disruption and unpredictable phase relationships between extracted waveforms. In this configuration, the resistor values need to be reasonably large—in this case at least around 500 Ω—but the result is RF power extraction at each resistor far exceeding that achievable with a single resistor (wherever it be connected along the line) without a significantly compromised pulse duration. The waveforms in figure 7.5 are driving 1 kΩ resistors in this way.

The potential for coherent extraction from the multiple stages loaded in this configuration exists by virtue of the NLETL anti-phase property being maintained after the initial disruption. The

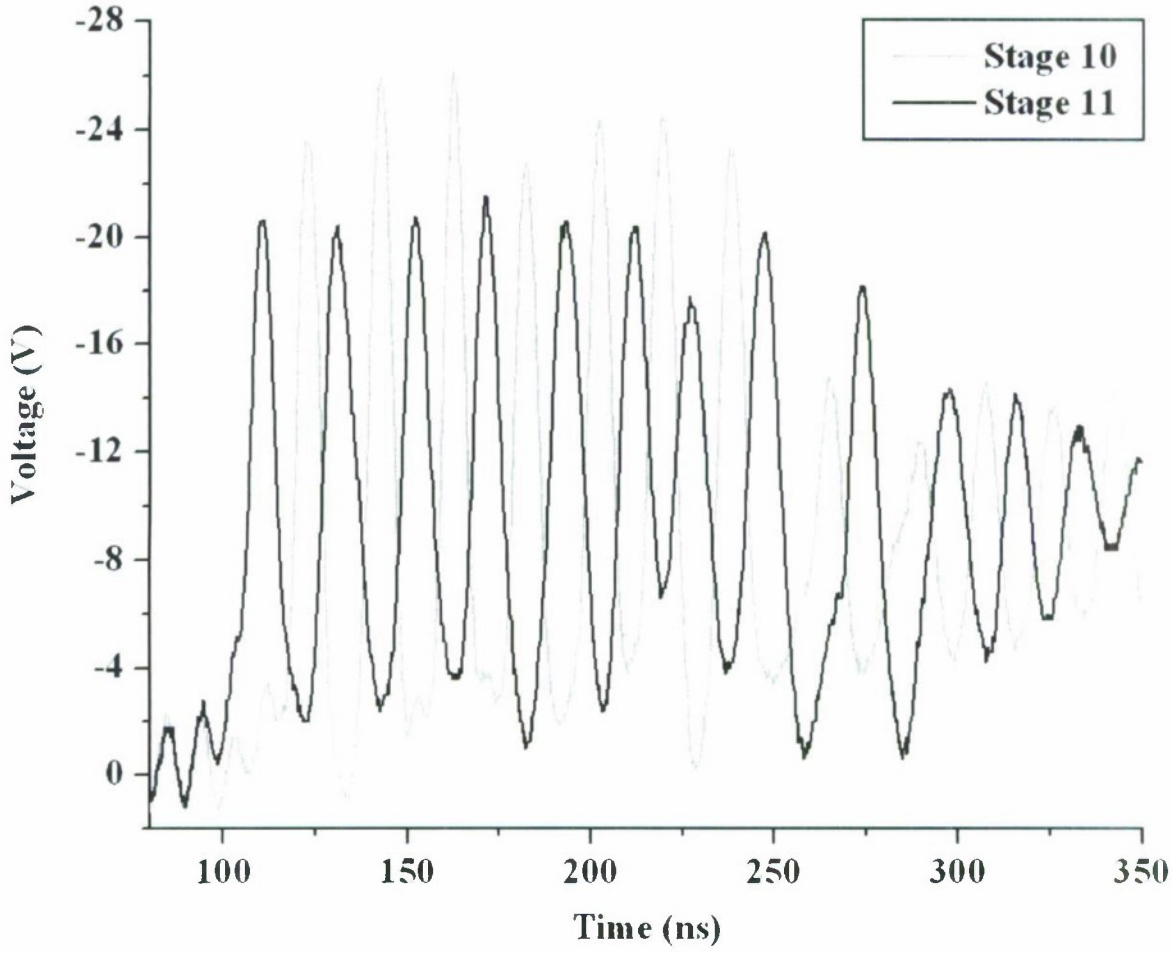

Figure 7.5: Low voltage periodic loading. Waveforms on stages 5 and 6 of the NLETL, with 1 kΩ low inductance resistors loading stages 3, 4, 5, 6, 7 and 8 of the line.

periodic loading approach may also be applied to the ASP configuration, with a series of resistors connected between singly offset stages of two lines, with similar results. The output to each resistor is also improved slightly over that to a single ASP load. It is apparent that lower values of resistor may suitably be used in this fashion, increasing feasible power delivery, and a high voltage ASP demonstration has extracted 63 MW peak power via seven 100 Ω resistors (section 8.6.1). During experiments with high voltage lines the direct NLETL antenna concept was also demonstrated (section 8.6.2).

Spatially distributed loading along a section of line maintains the uniformity and symmetry mentioned in section 7.3 and appears to be capable of interacting with the Brillouin limit oscillation, which may be thought of as a standing wave, without major disruption. The requirement of loading every adjacent stage means at frequencies of a few hundred MHz an end-fire dipole array is probably not feasible due to a relatively small inter-element spacing, but with a suitable connection arrangement and phased excitation a broad-side array factor may be created (section 2.5). Antenna design is an involved field and it is likely that more sophisticated structures could be optimised for the efficient radiation of NLETL energy by periodic loading.

Should a large number of stages be loaded with antenna elements then some extension of radiated pulse duration would be expected, as the pulse body travels one stage at a time along this section of the NLETL. Either by the spreading property (section 6.3.1) or by a gradual taper of inductor or capacitor values it may be possible to achieve chirping (section 2.1.3). The results described here are very encouraging and along with the ASP technique suggest realistic application of the technology. Without measures such as these the potential to exploit its capabilities seems to be limited by the extraction problem.

Chapter 8

High Voltage Experiments

8.1 Introduction to High Voltage NLETL Work

The NLETL concept has been applied at high voltage, with a series of test lines designed to investigate a range of capacitive nonlinearity options and various aspects of design relating to electrical strength etc. On the basis of this experience a couple of longer and more robust demonstrator lines were designed and built. Most high voltage lines were designed to operate at relatively modest frequencies well below 100 MHz, since the primary motivation was to demonstrate the formation of good quality—in terms of modulation depth, uniformity and duration—soliton type oscillation at MW levels such that available measurement techniques may be used reliably. A higher frequency NLETL was also designed, at which point should the high voltage probe data become unreliable an alternative method of detecting radiated waveforms could be used as per the experimental work of section 6.6.

Measurements of capacitive nonlinearity characteristics for a given material may be used, in conjunction with the design trends outlined in section 6.3, to establish suitable dimensions for custom blocks of dielectric material based on barium strontium titanate ferroelectric in ceramic form. However, the decision was made to use commercially manufactured (although generally not still readily available) capacitors, or the disc cores thereof, to construct the high voltage lines on this occasion. After obtaining initial CNL data from a range of commercial capacitors it was thought that further significant improvements in nonlinearity ratio were unlikely to be feasible with this type of material. For example, the MuRata DE121205F103Z2K 2 kV 10 nF capacitor, sourced once again via obsolete component supplier Kingsbeech Ltd, typically has an excellent CNL ratio of 12.5, and the 6.3 kV rated 1 nF DE1110E102Z6K has a useful ratio of 10. Initial contact was made with specialist electrical material suppliers able to manufacturer barium titanate based dielectric blocks, such as Morgan Matroc Electroceramics. It then also became clear that even if they felt they could expect to produce a CNL ratio of 10 or higher, which they basically did not, the remaining budget and time available on this project was by no means sufficient to proceed down the custom materials route. The modulated strip line

topology [57] is in itself probably too continuous anyway, with insufficient discrete inductance between stages for the development of strong soliton type oscillation. Capacitor manufacturers generally try to ensure reasonably good linearity with respect to working voltage; the limited selection found to possess the full nonlinearity potential of a ferroelectric material fall within the category of those designed to offer high capacitance values in small volumes (section 8.3). Although most of the time manufacturers use dopants to successfully remove very strong nonlinearity at room temperature, there is a correlation between a high dielectric constant, nonlinearity and loss at and around the Curie temperature which was discussed in chapter 3. Stacking of capacitors was used to increase power and frequency, but the latter was always going to be limited by the relatively large capacitance value per discrete stage. As it turned out, a lower ceiling on frequency was enforced by the increased ESR type loss associated with these high voltage lines anyway.

The realistic target was to reach tens of MW of peak RF power, and to investigate high power extraction to resistive loads (section 8.5 and section 8.6) following the success of low voltage experiments. The maximum mid-line peak power achieved was 175 MW, an approximation of available RF power based on the nominal line impedance, the value found to provide the best termination match of minimal reflection disruption. The impression is that power should be quite scalable with thicker dielectric elements and a higher voltage input pulse generator, at moderate frequencies below 100 MHz where stray effects are manageable with increasing dimensions. The highest frequency reached was around 90 MHz, with both simulation and experimental results highlighting the important influence of capacitor ESR loss on the maximum frequency which may be achieved via a reduction in L and or C before oscillation collapses, for a given CNL ratio. Ferroelectric hysteresis loss is minimised, but atomic displacement is highest at the temperature of maximum nonlinearity (room temperature when the useable dielectric constant has been maximised); small improvements could potentially be achieved with the dielectric to conductor interface contribution on some of the lines built here but the individual

capacitor loss was found to be greater than on a typical BB212 low voltage NLETL (section 8.3).

Encouraging results were obtained on lines using a range of different CNL elements from 10 to 90 MHz, with more extended pulse durations and modulation depths than reported on previous occasions. Based on ideas conceived and developed during the low voltage phase of work on this project, and the further idea of periodic loading resulting from an improved understanding of the discrete nature of the NLETL oscillation (chapter 7), extraction of useful waveforms to resistive loads has also been successfully demonstrated at over 60 MW.

8.2 Equipment and Procedures

Prior to describing the construction and testing of selected NLETL systems, the equipment typically used to enable their operation at high voltages will be introduced along with some of the procedures followed. Power supplies or capacitor charging units such as the Hartley Measurements Ltd Model 411 provided the necessary DC charge to 30 kV; reliable operation of apparatus, accurate measurement and ensuring a reasonably safe working environment were of particular concern throughout the high voltage experimental work. Initially the NLETL input pulse was generated by a simple high voltage pulse generator circuit [96] consisting of a capacitor charged to the point of self break of an air spark gap. In order to permit more control over pulse rise time and flat top duration a pulse forming network (PFN) was then built and used to drive most of the lines described here. The basic PFN accumulates energy during the charging period and releases it as a reasonably square pulse in a short time duration, using a ladder network of discrete inductors and capacitors to increase energy density and pulse shape control in comparison to a length of continuous cable. A matched load fed by a single PFN receives around half the charging voltage, the arrangement used to drive some of the low voltage NLETL systems of chapter 6, but it was now necessary to deliver the full charging voltage to the NLETL and so a Blumlein PFN configuration [97] was used whereby two lines are effectively charged in parallel and discharged in series. Twenty 40 kV TDK N470/202M/001B

capacitors were used and each measured at 2.09 to 2.10 nF—with the capacitance value fixed it was possible to vary the inductance of self wound coils to provide approximate matching to a given NLETL load and an appropriate pulse rise time and duration. The Blumlein PFN was first tested with resistor loads of various values where results accorded well with design expectations, and proved effective at driving the NLETLs built here. The high voltage Blumlein PFN circuit is illustrated in figure 8.1.

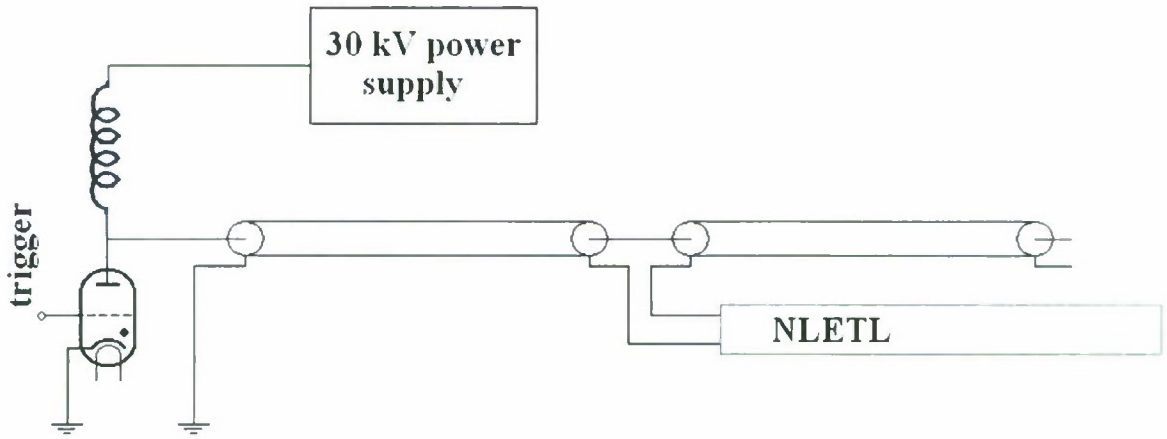

Figure 8.1: High voltage pulse generation apparatus for driving the NLETL, with DC power supply charging the Blumlein PFN which is switched via a hydrogen thyratron. The arrangement may be seen in the background of the photo of figure 8.22.

A basic self break air spark gap with adjustable electrode spacing was first used as the necessary switch. Its inductance and switching time was reduced by operation under transformer oil, although this was further improved by the use of a hydrogen thyratron switch [20] [98], which also enabled better control over charging voltage and trigger timing without the generation of potentially harmful noise levels, UV and ozone. The 35 kV 5 kA CX1785 8623 thyratron (figure 8.2) was manufactured by e2v [1] and is suitable for use in a Blumlein circuit by virtue of its ability to flow some reverse current because it has a hollow anode. Switching action is achieved

[1] e2v Technologies PLC, 106 Waterhouse Lane, Chelmsford, Essex, CM1 2QU. 01245 493493, http://www.e2v.com

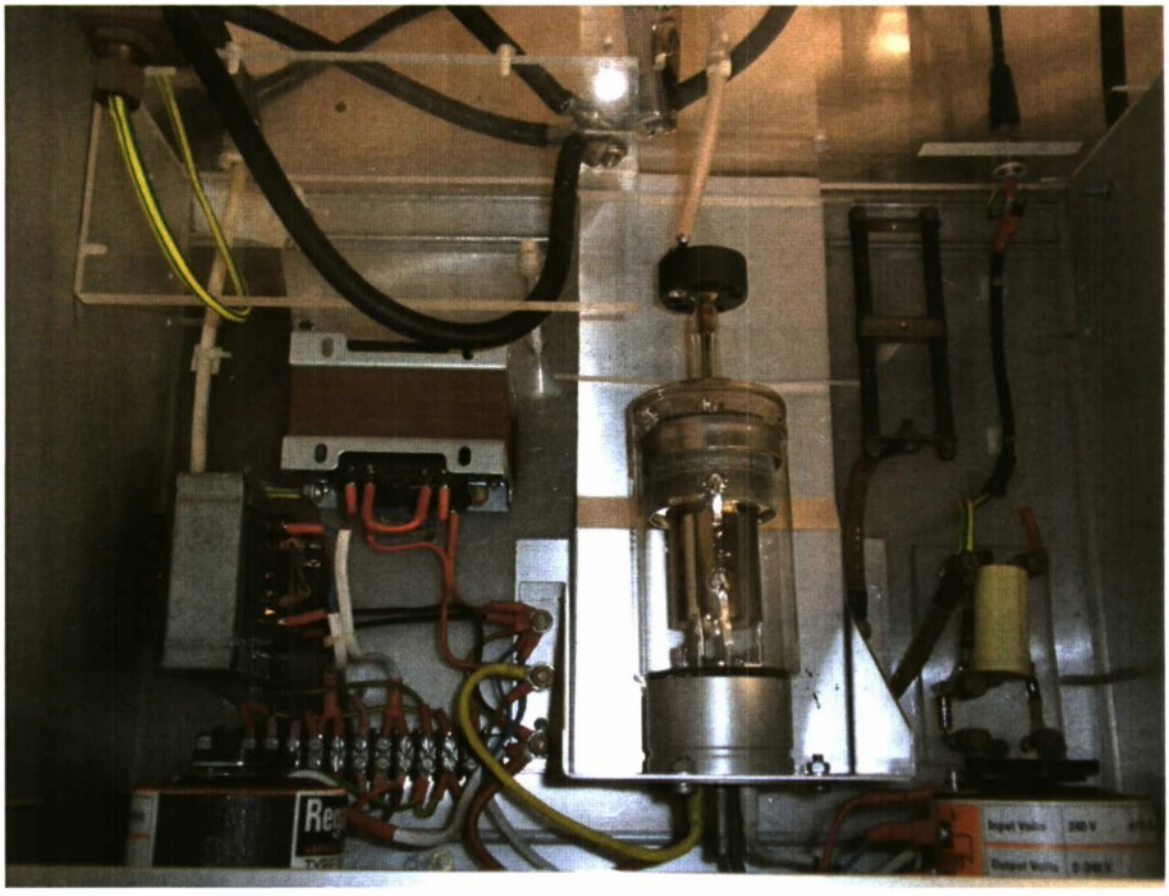

Figure 8.2: CX1785 thyratron and supporting circuitry for cathode and hydrogen reservoir heating, with the trigger unit housed separately.

by the rapid transition from an insulating neutral medium to a conducting ionised plasma, and initiated by the application of a 700 V trigger pulse to a grid connection. By careful control of the cathode heater and hydrogen reservoir voltages (typically 6.28 and 4.00 V respectively) rise times of around 100 ns were achieved.

Often mention will be made of equipment operation under oil—at more than 10 kV per mm this has a greater electrical strength than air so long as bubbles are not present [65]—and here Shell 148 electrical insulation oil specified to BS148-98 class I and II is used. High voltage measurements were generally made with the 1000:1 North Star PVM-5 probe which is rated to 60 kV DC, 100 kV pulsed and 100 MHz with noise suppression resistor removed. An additional

two of these probes were supplied by PPM Power [2] so four were available in total such that two simultaneous differential voltage measurements could be made. The low voltage responses of these probes were tested and found to exceed their frequency specifications, and the two new units were specified and found to be accurately matched which was necessary for the method of CNL measurement described in section 8.3. Sufficient bandwidth and reliable operation was provided by a Tektronix DPO 4104 1 GHz digital oscilloscope. Under zero voltage bias, accurate measurements of resistance, capacitance and inductance values were made with a Tinsley 6401 LCR Databridge meter.

Appropriate health and safety precautions were adhered to during high voltage experiments, with rigorous attention to the procedure of residual charge removal via an earthing stick before handling of the apparatus, and maintaining appropriate working distances from live voltages. Multiple earth points and high current capacity connections were used throughout and their condition regularly checked. Standard procedure was to wear UV goggles since arcing at the spark gap switch or upon insulation or NLETL failure was fairly common, and these also offered eye protection against fragmenting capacitors when certain lines were tested to their limits.

8.3 Ceramic Capacitive Nonlinearity and Strength Measurement

With the discussion of section 3.3 in mind specific attention was paid to the problem of measuring nonlinearity under high voltage bias, and investigating the typical electrical strength that suitably nonlinear capacitive elements may be expected to possess. In addition to a rough idea of the strength limitations of BST ceramics, the opportunity was taken to compare a range of silicone insulating compounds designed to prevent breakdown and surface flashover. Data from

[2] Pulse Power and Measurement Ltd, 65 Shrivenham Hundred Business Park, Watchfield, Swindon, Wiltshire, SN6 8TY. 01793 784389. http://www.ppm.co.uk

these tests were useful in the design of high voltage NLETLs, which were then based on the more robust commercial capacitors which also possessed suitably large CNL ratios.

Measuring capacitive nonlinearity under high voltage proved to be more tricky than first imagined: first attempts used a basic circuit incorporating a large value linear capacitor as isolation between a standard capacitance meter and the applied DC bias, whose series contribution to the resultant total capacitance measured was relatively small. This circuit was unable to provide consistent results, primarily because it consistently damaged capacitance meters due to relatively large transients propagating through the isolation capacitor. A review of such techniques brought to light an alternative, generally termed electrochemical impedance spectroscopy (EIS) [99] [100] and often applied to the impedance measurement of such things as Li-Ion cell packs, where DC voltages can reach several hundred volts. A small amplitude sinusoidal excitation (from a 20 V signal generator in this case) is applied to the component under test via an isolation capacitor and a resistor of low value typically a few ohms. Accurate measurement of the voltage at the subject and the differential voltage across the resistor along with its precise value allows complex voltage, current and impedance data to be obtained. Here the method was extended to much higher voltages according to the circuit of figure 8.3 which generated waveforms such as those of figure 8.4 from which impedance and thus capacitance could be established. Low inductance and very stable thick film resistors manufactured by Caddock and specifically intended for current sense applications were used and, since the specimen side of the isolation capacitor is at high voltage, the two new PVM-5 high voltage probes were used to measure the necessary voltage signals. In order to minimise the risk of breakdown and associated transients the capacitor(s) under test were generally placed under transformer oil.

The circuit and data analysis methods were tested and refined on a range of linear capacitors, inductors and low inductance resistors and the results presented here in figures 8.5 through 8.12 are considered representative of the nonlinear capacitors under test. In many cases the nonli-

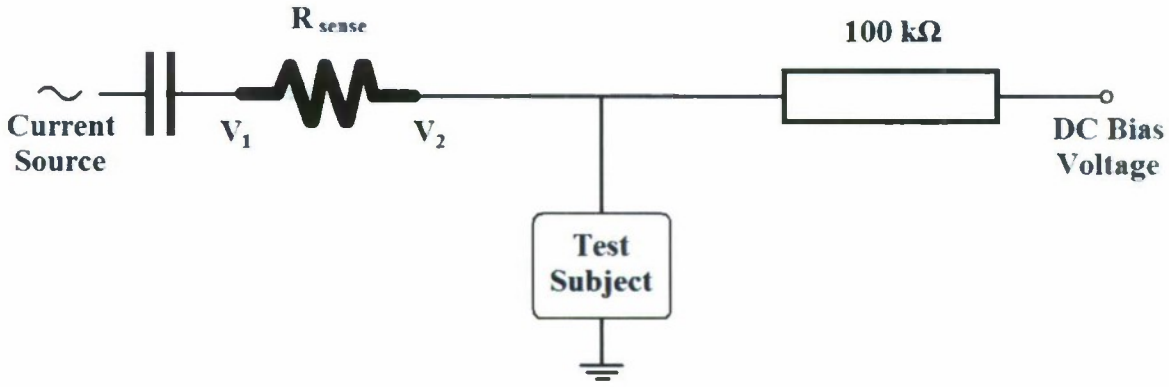

Figure 8.3: EIS method of impedance measurement used to characterise capacitive nonlinearity under high voltage.

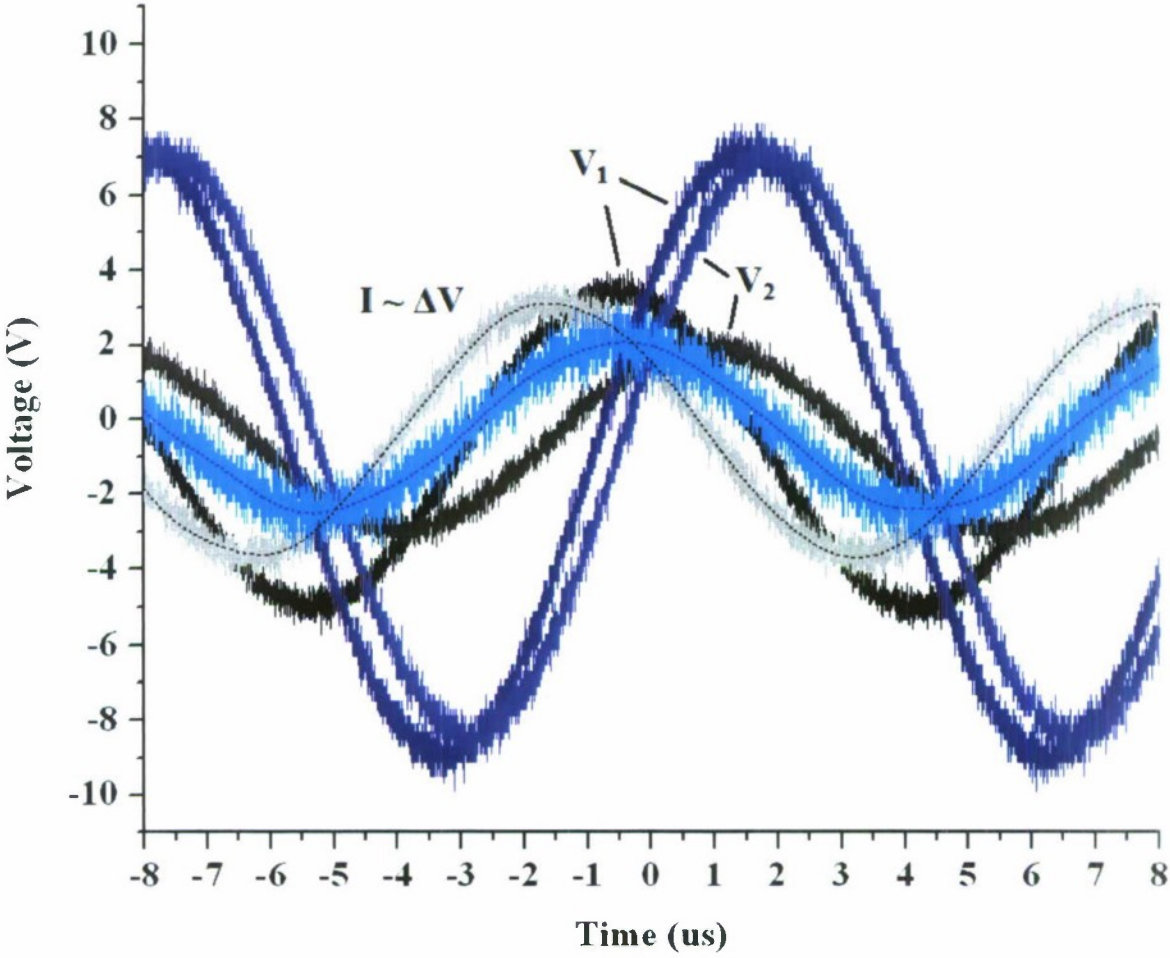

Figure 8.4: Example EIS waveforms under zero (black/grey) and 1 kV (blue/aqua) charge, with the two voltage waveforms and inferred current for each case, the latter subject to a low pass filter which can be helpful when dealing with the very low currents corresponding to higher impedances.

nearity ratio was found to be quite satisfactory for NLETL use, often reaching a value of 10 and so matching that of the BB212 tuning diode. These particular capacitors represent a minority whose nonlinearity is not by design and which weren't easy to identify, and it has previously been suggested that "high voltage nonlinear capacitors are as yet not available commercially" [101] for advanced snubber circuits. In addition to the capacitance voltage waveforms which follow, CNL data are summarised for a range of selected capacitors in table 8.1.

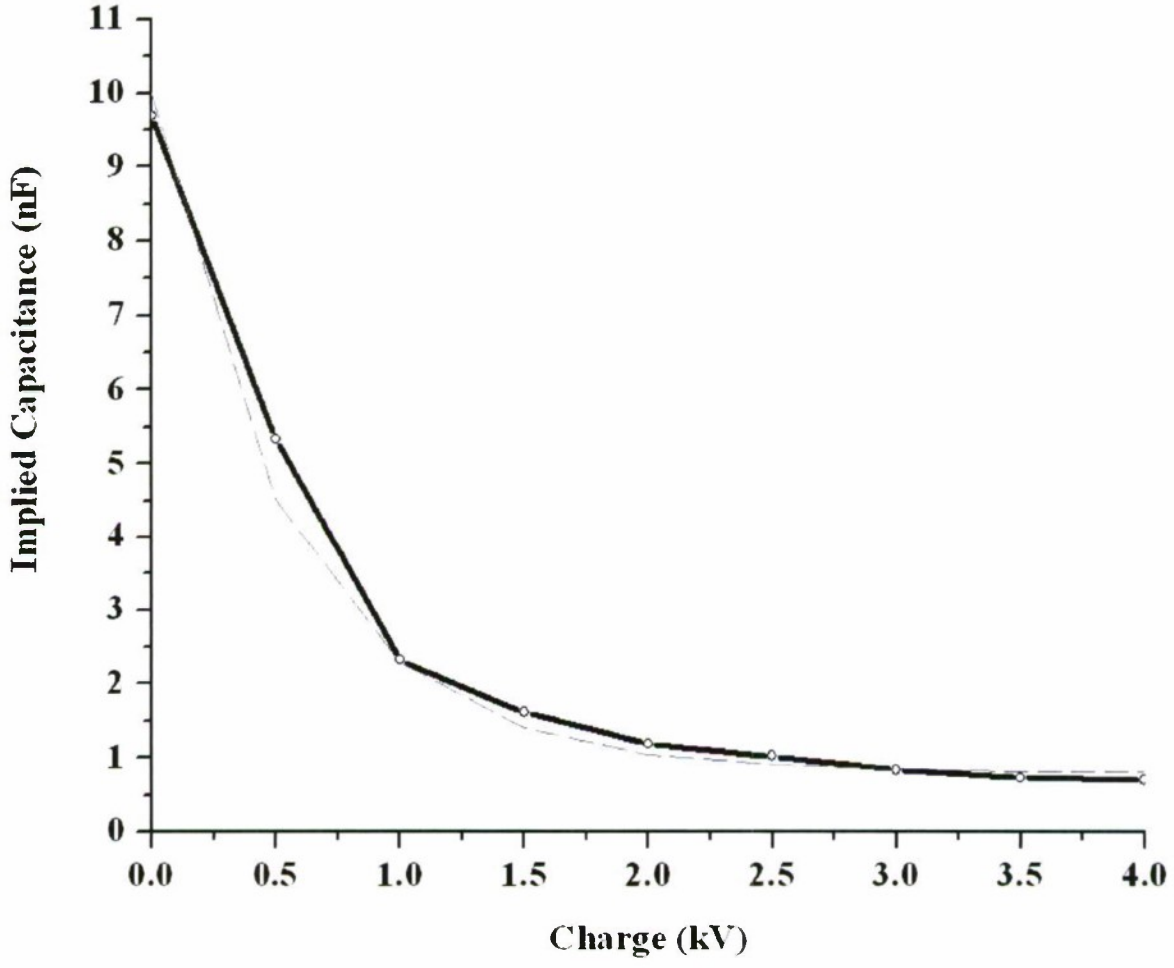

Figure 8.5: Capacitive nonlinearity characteristic of the obsolete 10 nF DE121205F103Z2K capacitor manufactured by MuRata, rated voltage 2 kV.

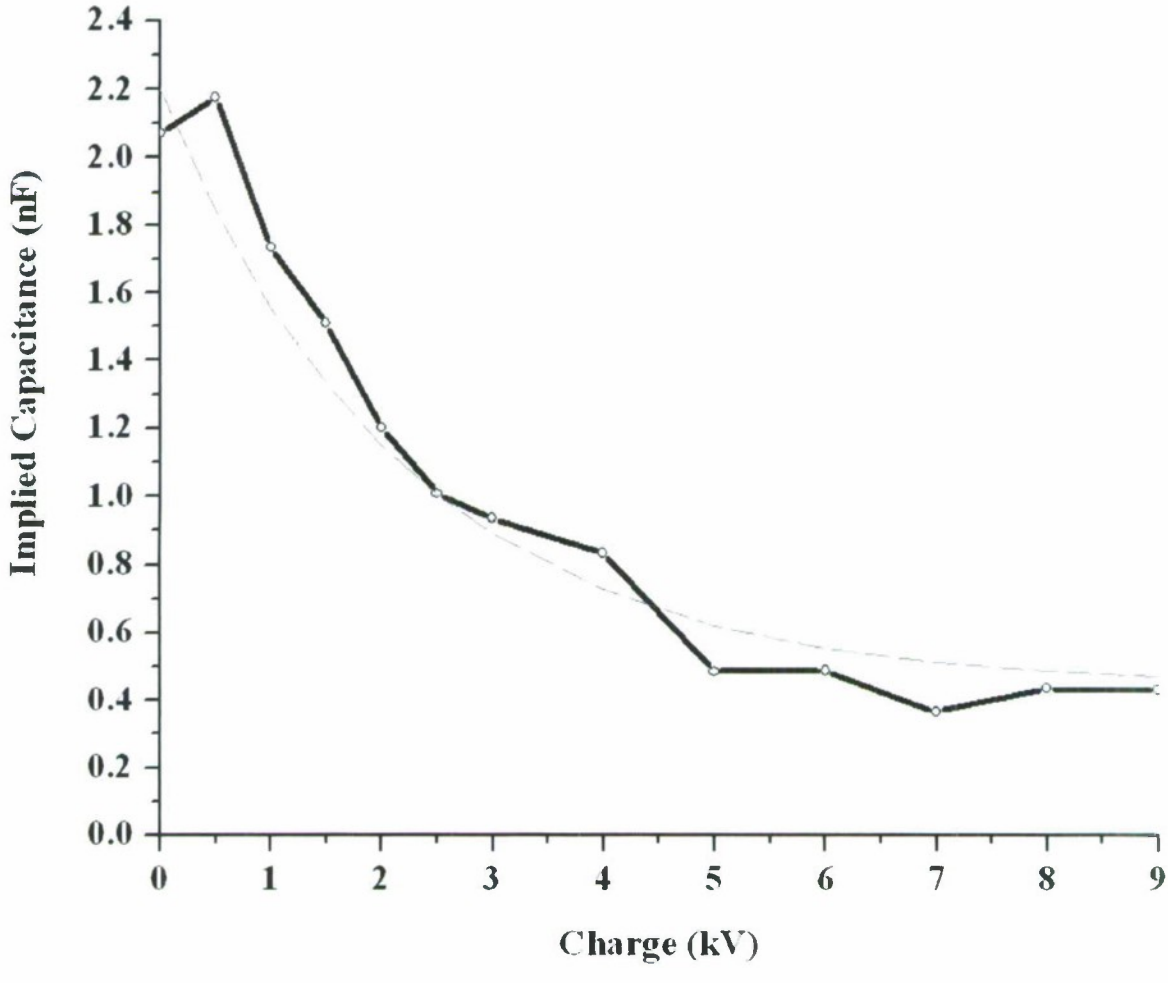

Figure 8.6: CNL measurement for three DE121205F103Z2K capacitors stacked in series.

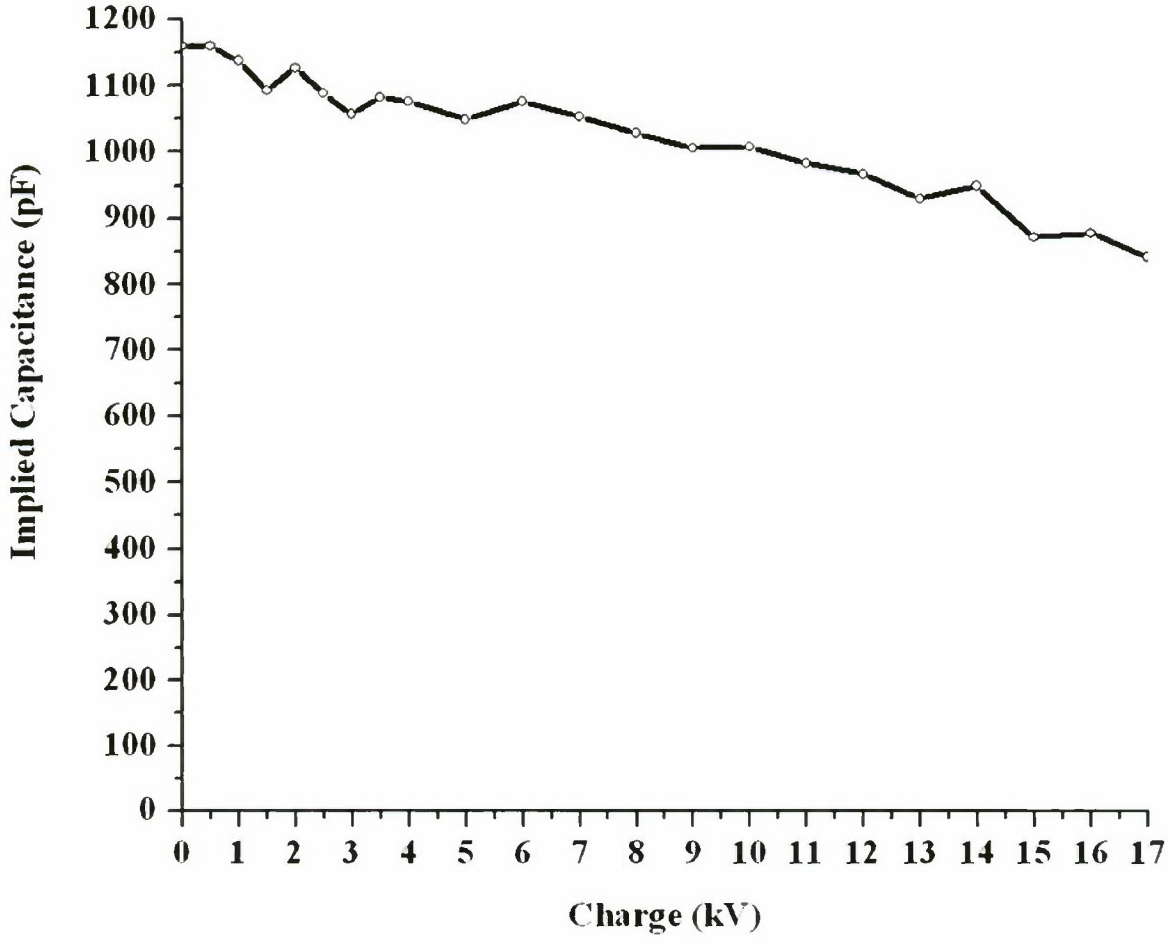

Figure 8.7: CNL measurement for relatively linear 15 kV rated ECK series capacitor.

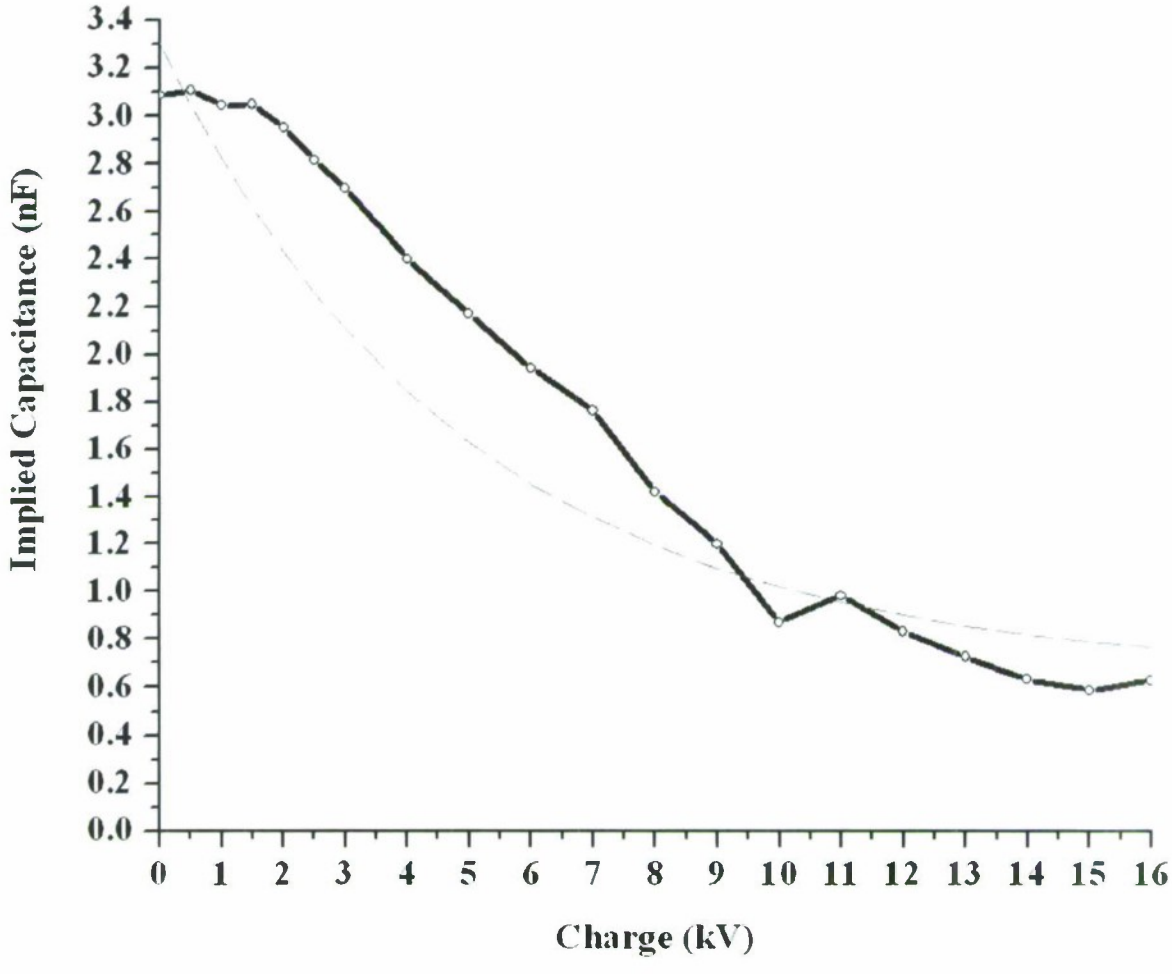

Figure 8.8: CNL measurement for unknown capacitor originally manufactured by Beck with inscription CHV 418P 03N3 ZDV.

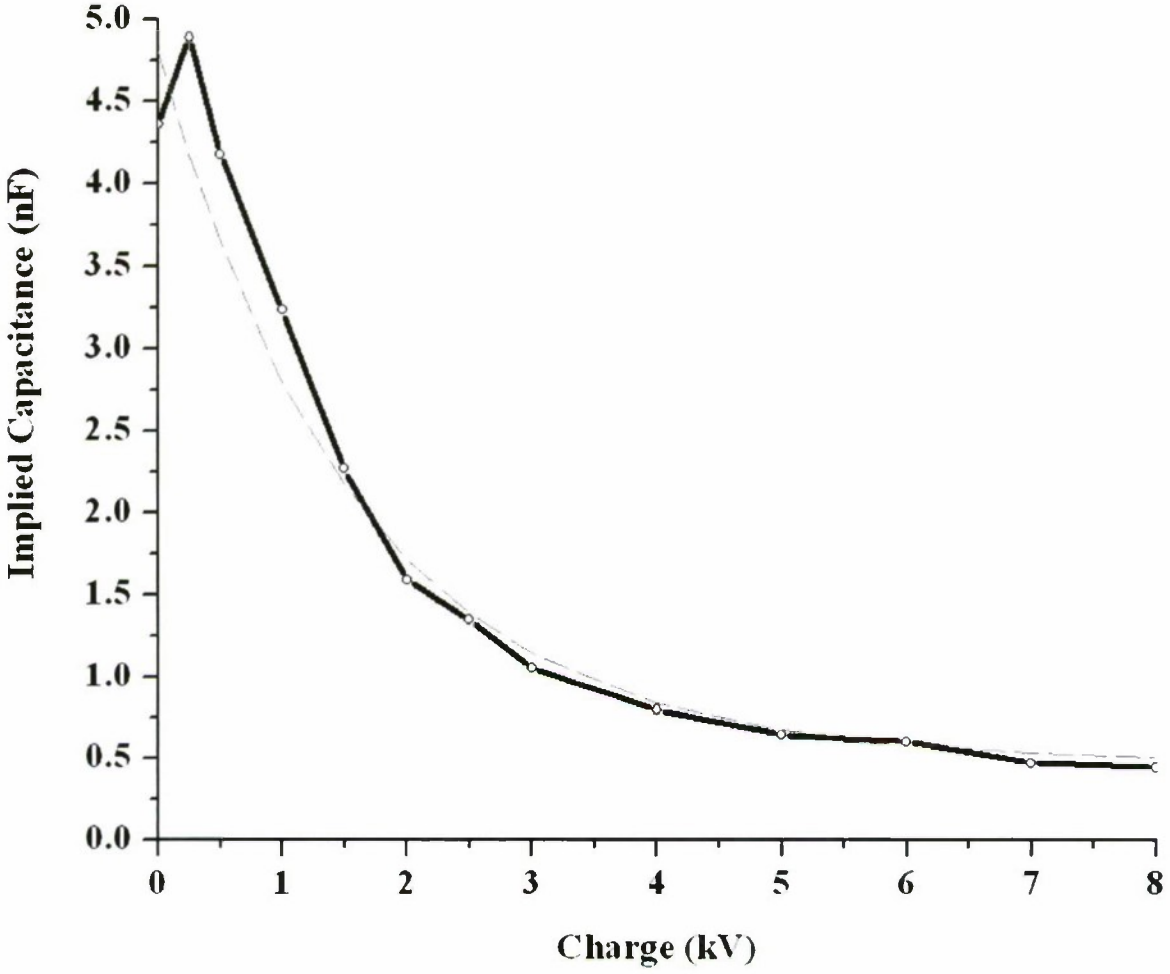

Figure 8.9: CNL measurement for unusually nonlinear 4.7 nF AVX 472 SUM capacitor currently available from Farnell under part number 1216394 and rated to 4 kV.

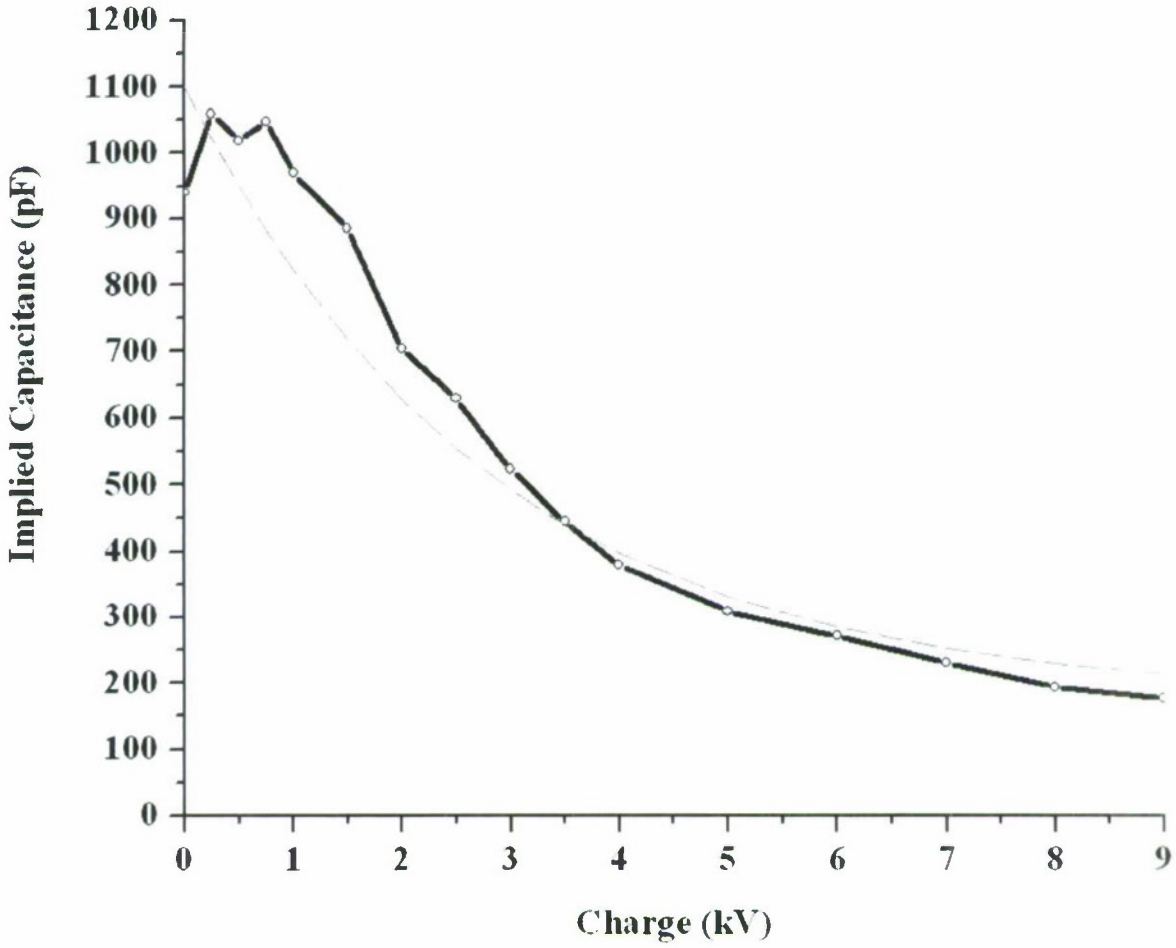

Figure 8.10: CNL measurement for obsolete MuRata 1 nF 6.3 kV DE1110E102Z6K capacitor.

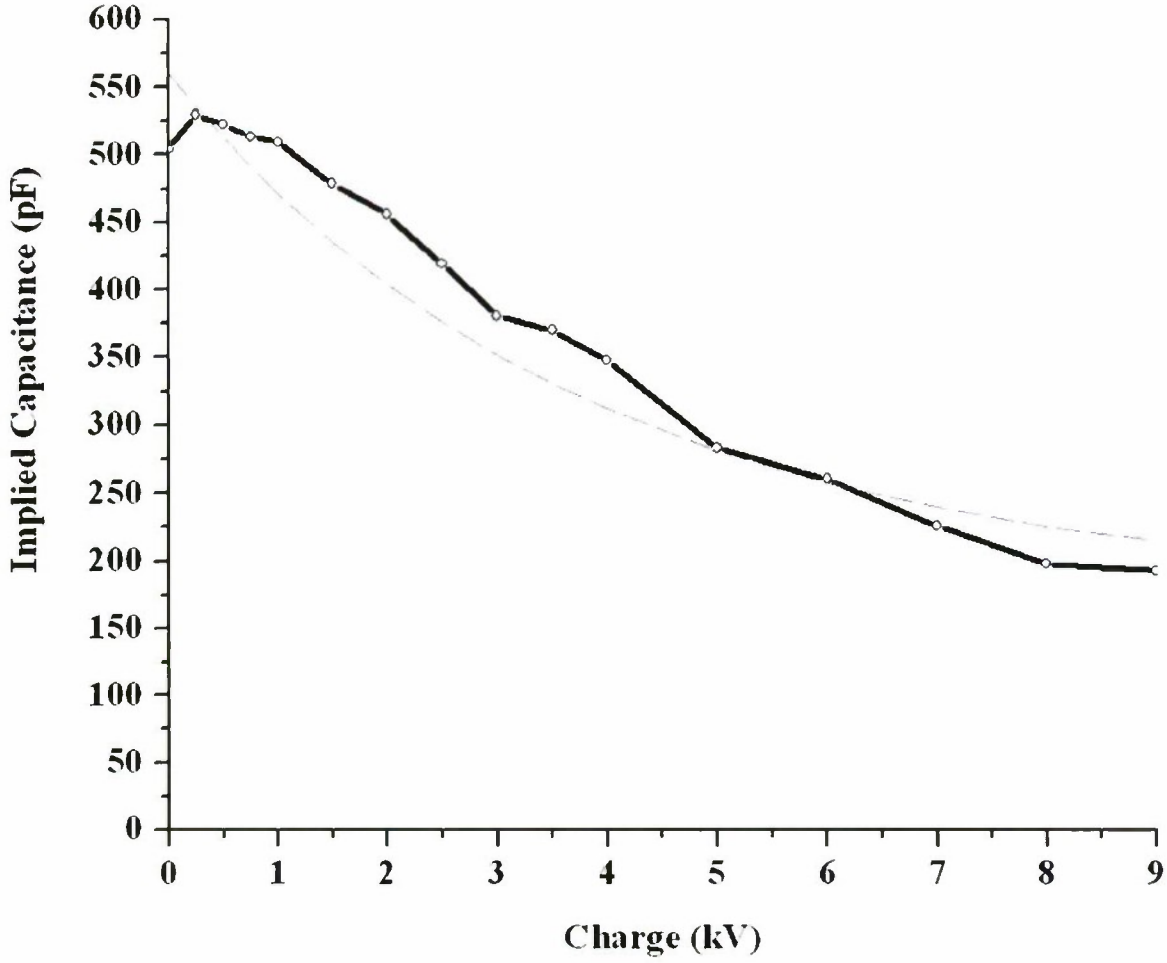

Figure 8.11: CNL measurement for DECB33J471KC4B, in an equivalent package to the capacitor of figure 8.10 but showing the reduced nonlinearity ratio generally associated with lower nominal capacitance values.

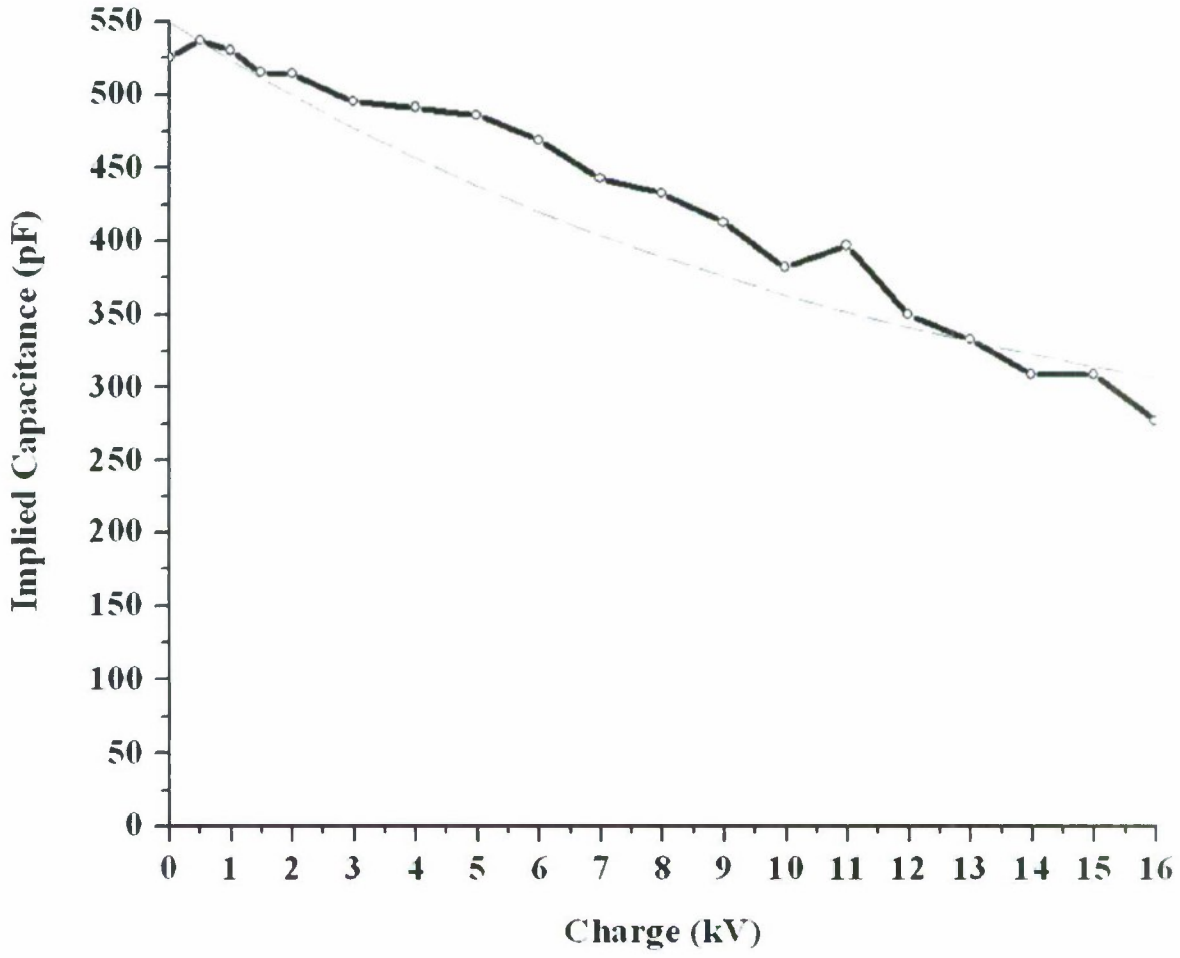

Figure 8.12: CNL measurement for a 500 pF higher voltage 15 kV rated MuRata capacitor, with poor ratio.

Manufacturer	Capacitor Designation	Nominal Capacitance	Implied cnl_a	Implied cnl_b	Rated Voltage
MuRata	DE121205F103Z2K	10 nF	0.08	750	2.0 kV
MuRata	DE121205F103Z2K x3	3.3 nF	0.20	2200	6.0 kV
MuRata	DHRB5AD221M1CB3	220 pF	0.35	9200	7.5 kV
Beck	CHV 418P 03N3 ZDV	3.3 nF	0.20	5000	-
AVX	472SUM Farnell 1216394	4.7 nF	0.10	1600	4.0 kV
MuRata	DE1110E102Z6K	1.0 nF	0.10	3200	6.3 kV
MuRata	DE1510E222Z6K	2.2 nF	0.11	3400	-
MuRata	RS 652-9709	220 pF	0.35	9200	7.5 kV
MuRata	DECE33J102ZC4B	1.0 nF	0.16	2800	6.3 kV
MuRata	DECB33J471KC4B	470 pF	0.32	3800	6.0 kV

Table 8.1: Some representative results from EIS testing of capacitive nonlinearity. A smaller cnl_a implies a larger CNL ratio; a smaller cnl_b implies a steeper CNL curve.

Several capacitors and their disc cores were also subject to DC and pulsed strength testing. Initial impressions from a selection of large unspecified barium titanate based ceramic blocks suggested that the first failure mode in air is surface flashover at only around 2 kV/mm, a process enhanced at discontinuities such as cracks, chips, sharp corners and previous tracking marks. Clearly the presence of the coating material added by the manufacturer is effective at suppressing surface tracking, but there are potential advantages to being able to remove the ceramic disc from its original casing and leads for incorporation into a NLETL structure. It becomes possible to clamp the relatively flat block of dielectric material between inductor planes in order to reduce the stray inductance associated with the discrete capacitive elements, which may be expected to affect the discrete pulse waveforms at frequencies of several hundred MHz. The general indication from experiments with many high voltage lines is that commercial

capacitors tend to fail along the line of lead attachment (solder) to the ceramic disc surface (figure 8.13). This sometimes occurs at quite low voltage and generally causes lead separation and structural failure of the ceramic. It is sensible to assume that a well designed arrangement incorporating the disc by itself should remove points of weakness such as this. As such a further motivation for this aspect of the work was to ascertain the relative effectiveness of a range of options for re-coating the ceramic dielectric material alongside that applied by the capacitor manufacturer.

Test ID	Manufacturer	Description	Rated V (kV/mm)	Farnell Part No
A	Dow Corning	DC4 Electrical Compound	16	537-019
B	Servisol	Silicone Grease	-	382-1559
C	ACC	SGM 494 Silicone Grease	19	166-7365
D	Dow Corning	732 Single Compound Silicone Sealant	24	101-701
E	Dow Corning	9161 RTV Silicone Base + N9162 Catalyst	22	101-778

Table 8.2: Details of the five silicone compounds tested for electrical strength and ceramic surface coating properties under DC and pulsed conditions.

If necessary the original coating was removed by submersion in paint stripper for a couple of days, whereupon it was found to be softened and easily peeled away. Three main tests were used to compare the performance of air, oil, the original coating and five different electrical compounds with and without oil. The first test simply looked at the strength of the material against a DC voltage over a 1.75 mm gap between two rounded electrodes to the point of electrical breakdown (manufacturer coatings not included on this occasion). Then the DC voltage required to initiate a surface track breakdown across a 2.5 mm thick, 5 mm radius disc from the MuRata DE12 capacitor was established for the different coating options. Finally pulsed strength in a similar arrangement (three different discs compared) was investigated subject to

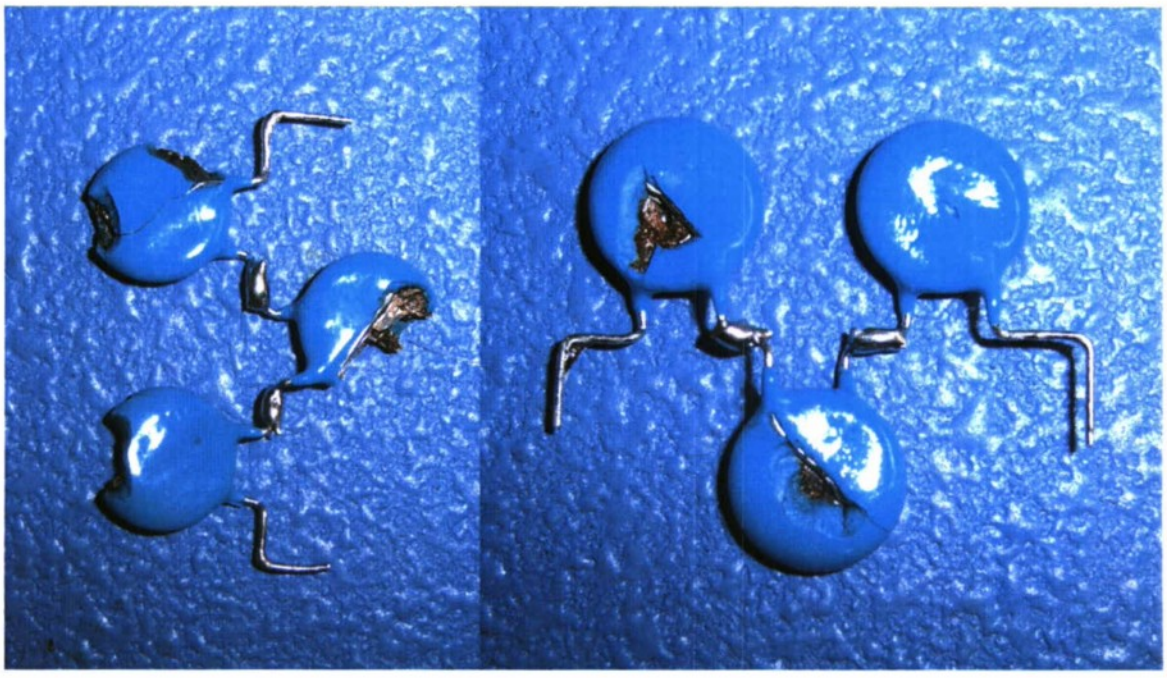

Figure 8.13: High voltage ceramic capacitors such as the MuRata DE121205F103Z2K (figure 8.5) tend to fail along the line of solder connecting leads to the metallised surface.

a 600 ns duration, 200 ns rise and fall time pulse delivered from the Blumlein PFN switched by the thyratron. As well as the highest pulse amplitude held off before any tracking failure occurred, note was made of the nature of any permanent damage to the ceramic discs. The capacitor under test was connected in parallel to a resistor which ensured an approximate match to the Blumlein to avoid repeat pulses due to reflections, and four shots were applied at incrementing voltages. Where an electrical compound was used, the coating was subject to a partial vacuum during application in order to remove as many air bubbles as possible and ensure a fair test. The five electrical silicone compounds are detailed in table 8.2, and these generally outperformed oil by a clear margin in terms of absolute DC breakdown strength. Compound B was notably poor in preventing surface tracking when applied against the ceramic under DC conditions, but in most other cases performance reached that of the OEM coating material. The pulsed strength of a given test subject tends to be much lower than its DC strength (by about 50 percent, comparing DE15 results between tests) and the original coating just about proves strongest under these conditions.

Whilst under pulsed test conditions, with the original coating removed but original leads still in place and used to apply the test voltage, none of the silicone compounds quite reached the performance of the original coating, but a DECE33J disc under D survived 20 shots at 35 kV peak voltage when parted from its leads and separated from clamping copper discs by thin layers of graphite felt. There was the odd incidence of surface tracking from 16 kV but, whereas previously complete structural failure was the immediate result, this disc survived to a much higher voltage. Electrostrictions (section 3.3.4) are known to be an issue for the survivability of dielectric materials (section 3.3.4) and it appears that the provision of some shock absorption, along with a non-brittle coating compound, could be beneficial.

Flashover between capacitor terminals is often associated with its structural failure, and the various silicone compounds also had potential use within the NLETL structure where original coatings were to be retained, especially for operation in air as opposed to oil (section 8.6). The line of section 8.5 used compound D in addition to oil to safeguard a particularly compact arrangement of stacked capacitors. Compounds D and E were found to be the strongest and both were used on occasion with the former offering a single pack transparent gel which is easy to apply where some structural rigidity is required during the 24 hour setting period. The latter requires mixing with a suitable catalyst to form a white liquid which may be brushed on as a coating or set in a mould. In being completely opaque this option makes the process of locating and repairing failure points on a long line relatively difficult.

Further to dedicated strength testing, the initial phase of high voltage experimentation with a range of test lines did single out several capacitors which were simply too weak to operate well in a NLETL, despite possessing excellent CNL characteristics. Some were markedly stronger though, and even more so when careful attention was paid to the design and build of subsequent demonstrator lines.

8.4 High Voltage Test Lines 1 Through 9

Nine relatively short high voltage NLETL systems were constructed in order to gain an indication of the actual effectiveness of various capacitance options which had demonstrated good CNL characteristics under EIS testing. Table 8.3 provides an outline summary of this stage of the work. In several cases two lines were built and the NLETLs tested in ASP mode, although output waveforms were not spectacular primarily because these test lines suffered from multiple failures before sufficient input amplitudes were reached. With special attention paid to certain aspects of the line design and construction (section 8.5), strength and reliability were subsequently improved. Two modest sized tanks (figure 8.14) were fabricated from mild steel, for reasonable conductivity but also ease of welding. The tanks were used to contain the transformer oil under which the NLETLs were generally operated and, these being asymmetric single-sided lines, to act as the low inductance plane. It is important to note that this plane is not at earth potential given the floating differential nature of the Blumlein output, and potentially has non-negligible inductance of its own, so voltage measurements were taken relative to the local voltage on this plane. In all cases the fundamental problem of extracting the high frequency energy from a single NLETL to a terminating resistive load was confirmed.

The waveforms which follow in this section are representative of experimental results from high voltage test lines 1 through 9. More refined work was subsequently carried out on longer and carefully designed demonstration lines and is described in the following section, but several of these waveforms offer good examples of high voltage NLETL soliton type oscillation in themselves. The line numbers refer to those used in table 8.3.

Being very short, driven by a capacitor and spark gap and subject to arcing due to operation in air, line 1 only supported rather poor waveforms of just a few pulses, but they demonstrated first the defining antiphase characteristic of the oscillation which was encouraging. This is also clear from the waveforms on line 2, which were reasonably uniform and extended at around 30

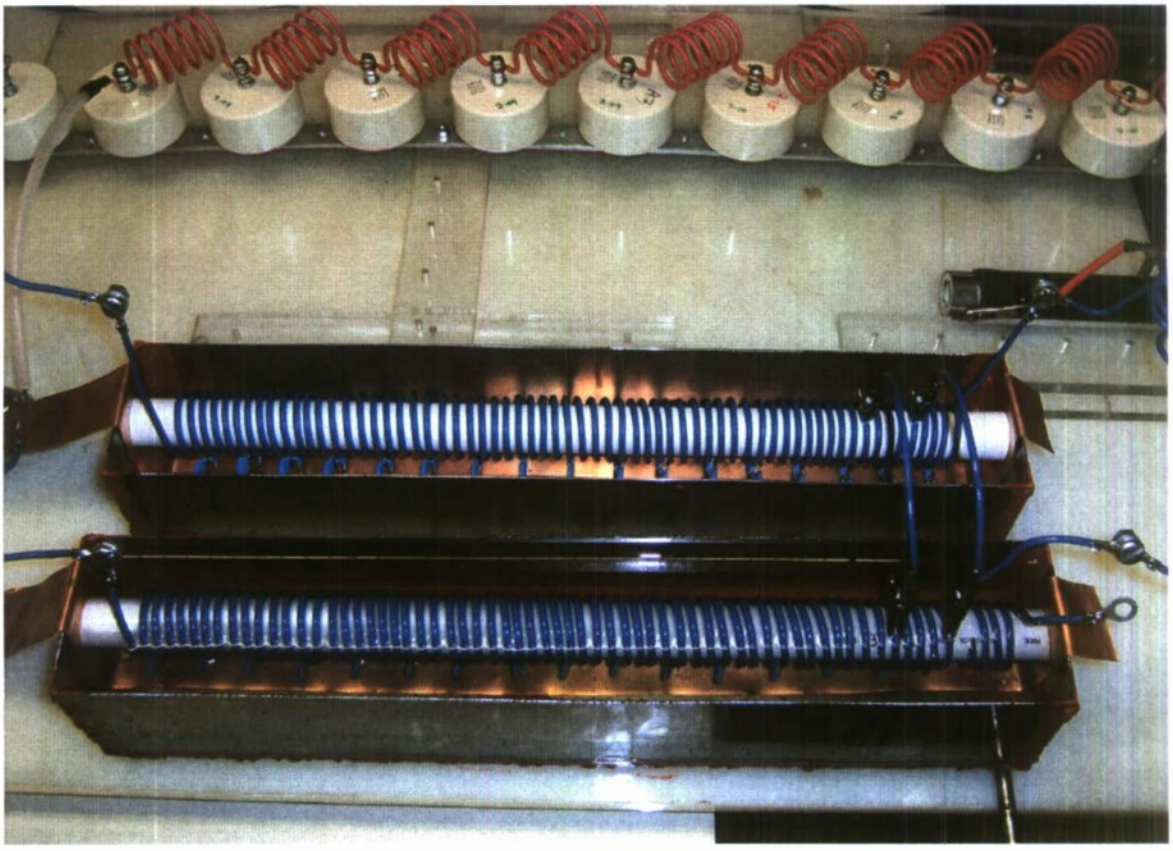

Figure 8.14: Two mild steel tanks for the initial high voltage test NLETLs operated under oil, with some stages of the Blumlein PFN visible in the background.

NLETL No	Capacitive Elements	Nominal C	Stage L	Nominal Z (Ω)	Rated V (kV)	Length (stages)	Max F (MHz)	Max ptp V (kV)
1	DE12	10 nF	1 nH	10.0	2.0	6	13	8
2 ⇉	DE12 x3	3.3 nF	400 nH	11.5	6.0	16/17	37	37
3	DHRB5A	220 pF	400 nH	42.6	7.5	17	63	15
4	DHRB34	470 pF	400 nH	29.2	15	17	52	40
5	CHV 418P	3.3 nF	650 nH	14.0	-	12	18	30
6 ⇉	AVX 472	4.7 nF	400 nH	9.23	4.0	16/17	20	12
7 ⇉	DE11	1.0 nF	400 nH	20.0	6.3	16/17	41	12
8 ⇉	DECE33J	1.0 nF	400 nH	20.0	6.3	16/17, 33	45	20
9 ⇉	DE15	2.2 nF	400 nH	13.5	6.3	16/17	28	16

Table 8.3: Summary of initial high voltage test NLETL results. ⇉ These lines tested in ASP mode. Rated voltage of the Beck CHV 418P is not known but likely to be around 15-20 kV.

MHz (figure 8.15). This NLETL incorporated a stacked arrangement of three DE12 capacitors per stage for a resultant capacitance of around 3 nF, and thick 2.5 mm diameter solid copper wire wound to give a 400 nH stage inductance. By driving the line harder, to its point of failure, a 37 kV peak-to-peak pulse train at 37 MHz was obtained giving an implied available RF power of 120 MW. Implied RF power is based on the nominal line impedance, which is of course a minimum value but does give the termination resistance offering best indication of a match in terms of amplitude disruption. An ASP output to 10 Ω was initially impressive at 72 MW, but deliverable only to a relatively inductive wire wound resistor. A quite small series inductance can significantly improve an ASP output waveform and at these frequencies it is easy to obtain misleading figures for the actual power being extracted from the system. ASP performance of the initial test lines with purely resistive loads was poor, probably because of their relatively short lengths and line failures occurring before the necessary input amplitude could be reached.

With its lower nominal capacitance, line 3 oscillated at 63 MHz. The capacitance was perhaps a bit low, and the line too short which explains a relatively poor modulation depth. Results from line 4, based on much higher rated capacitors, were rather poor and it was apparent that insufficient input amplitude could be supplied despite repeated failures at full Blumlein charge. The capacitors used in line 5 are of particular interest because they were found to possess a good CNL characteristic along with a relatively high voltage strength. They were manufactured by Beck and are now obsolete: unfortunately extensive attempts, with the help of Kingsbeech Ltd and others, to source more over the ten or so found in the lab proved unsuccessful. Nonetheless, on the 12 stage line built here good quality peak-to-peak oscillation of 30 kV was demonstrated before failure, as seen in figure 8.17. With a line of around 25 or more stages using two of these capacitors per stage, the implication is that a mid-line RF power approaching 250 MW would immediately be achievable.

Line 6 (figure 8.18) was built with currently available capacitors that were found by chance to have terrible linearity and hence to be well suited to this application, with a CNL ratio exceeding 10. Their nominal capacitance is high at 4.7 nF which resulted in relatively low frequency operation, and they were found to be quite weak and incapable of surviving many, if any, discharge events where their nonlinearity was exploited fully. The capacitors of line 7 were also clearly too weak, although good mid-line pulse burst waveforms were obtained from a single NLETL. Results from line 8, some of which are shown in figures 8.19 through 8.21, were encouraging and demonstrated the effect at 45 MHz, 22 kV peak-to-peak due to a low nominal capacitance and reasonably good CNL and strength. This line was also run in longer single mode, with 33 stages giving improved performance and a clear indication of reflection effects from a full progression of stage voltage waveforms. Finally, line 9 once again demonstrated a suitable capacitive element by providing bursts of around 10 pulses at up to 28 MHz, 16 kV peak-to-peak under short test line conditions.

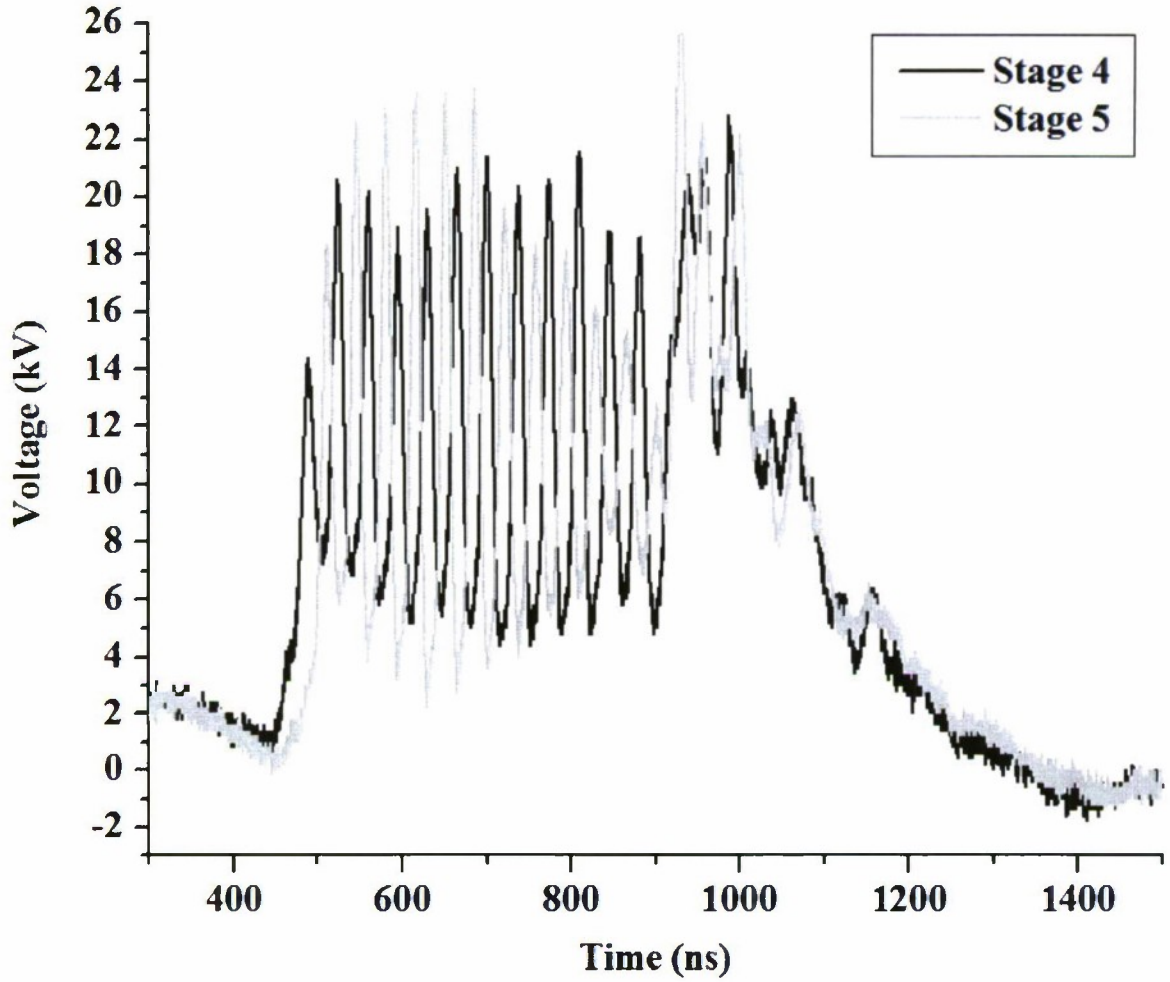

Figure 8.15: Voltage waveforms on stages 4 and 5 of high voltage test NLETL number 2, demonstrating good modulation depth and the characteristic anti-phase property between adjacent stages.

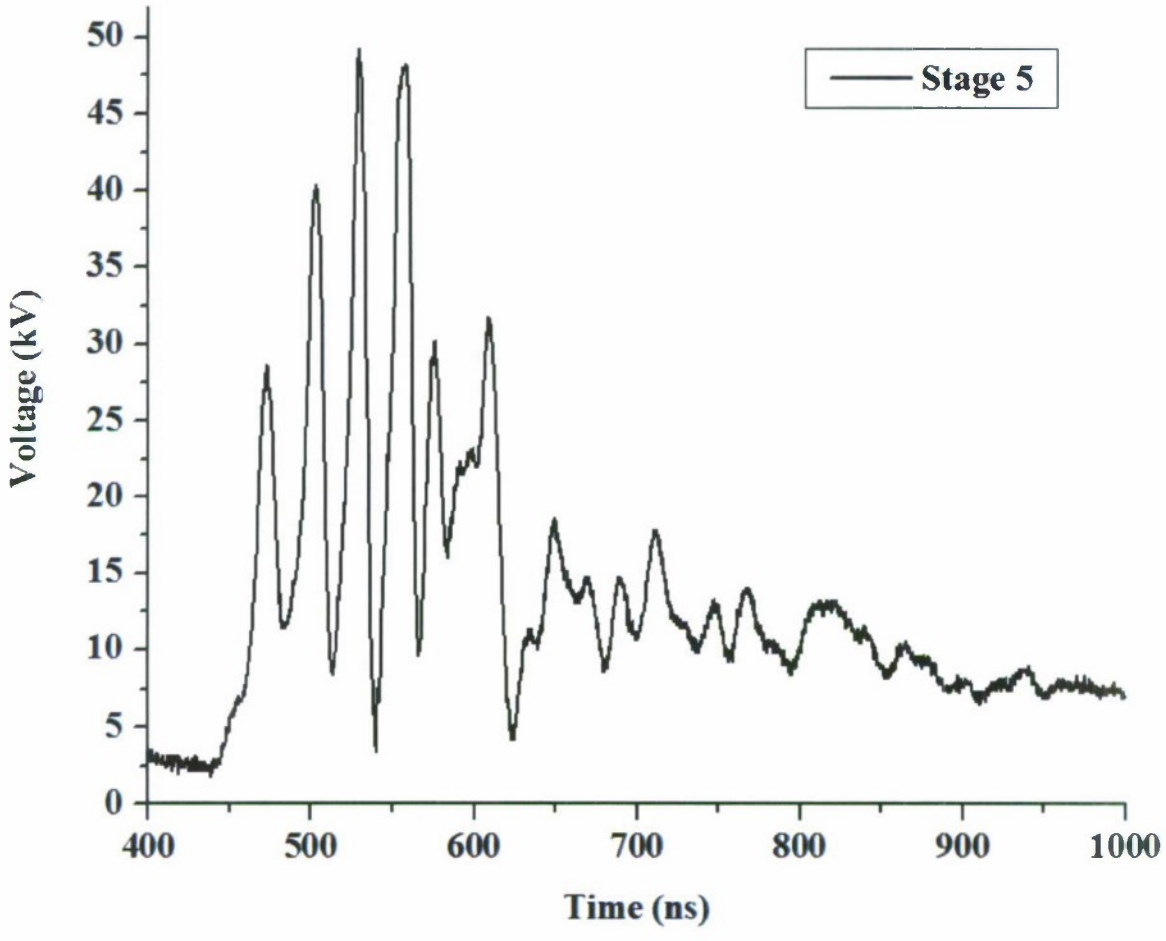

Figure 8.16: Higher amplitude mid-line pulse burst generated on line 2. Subsequent increase in input pulse amplitude resulted in the failure of multiple capacitors within the line.

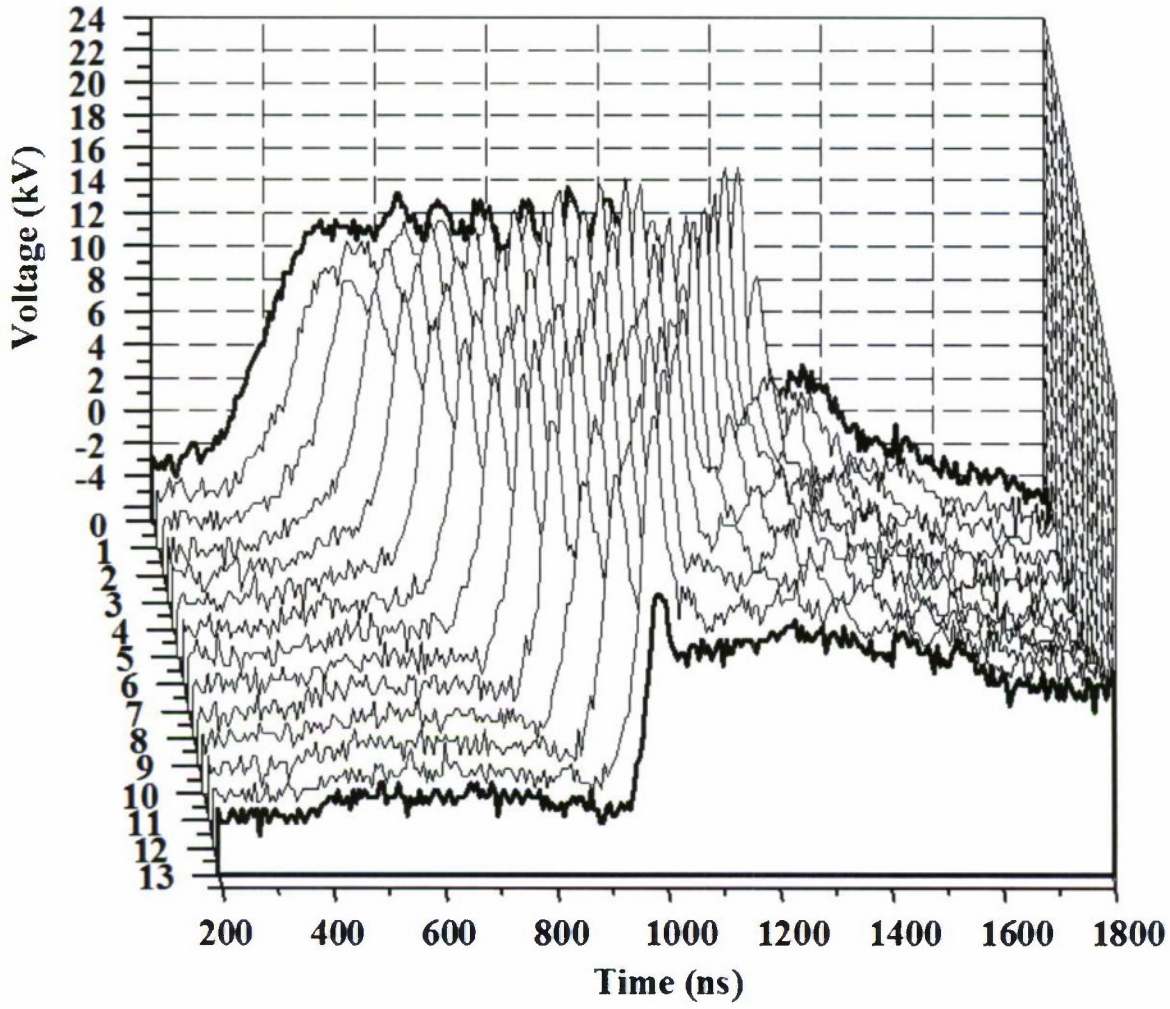

Figure 8.17: Line progression of voltages at each stage along test line number 5, with input at the back and output to the front. The extraction problem and associated disruption in the loss of a single pulse per stage can clearly be seen, along with leading edge sharpening.

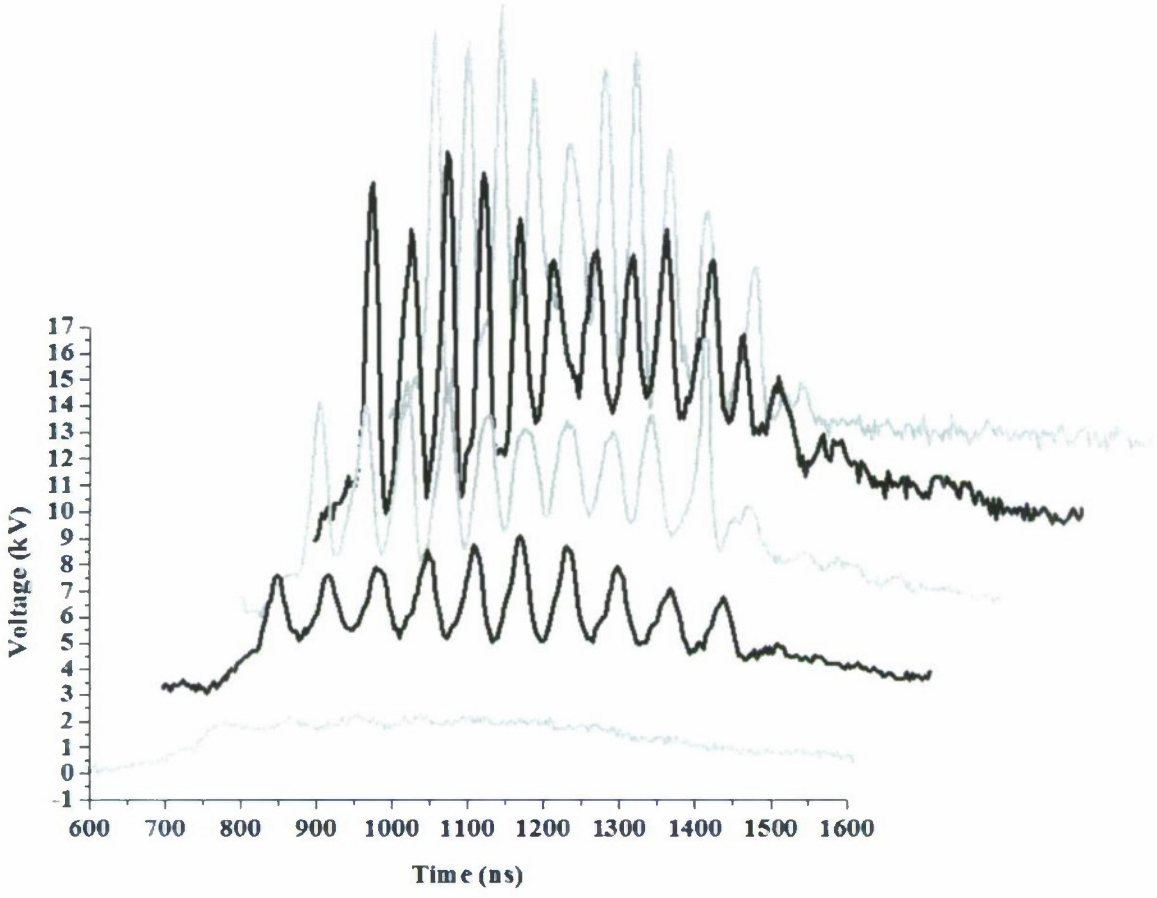

Figure 8.18: Mid-line pulse burst waveforms on test NLETL 6 when driven with various input pulse amplitudes.

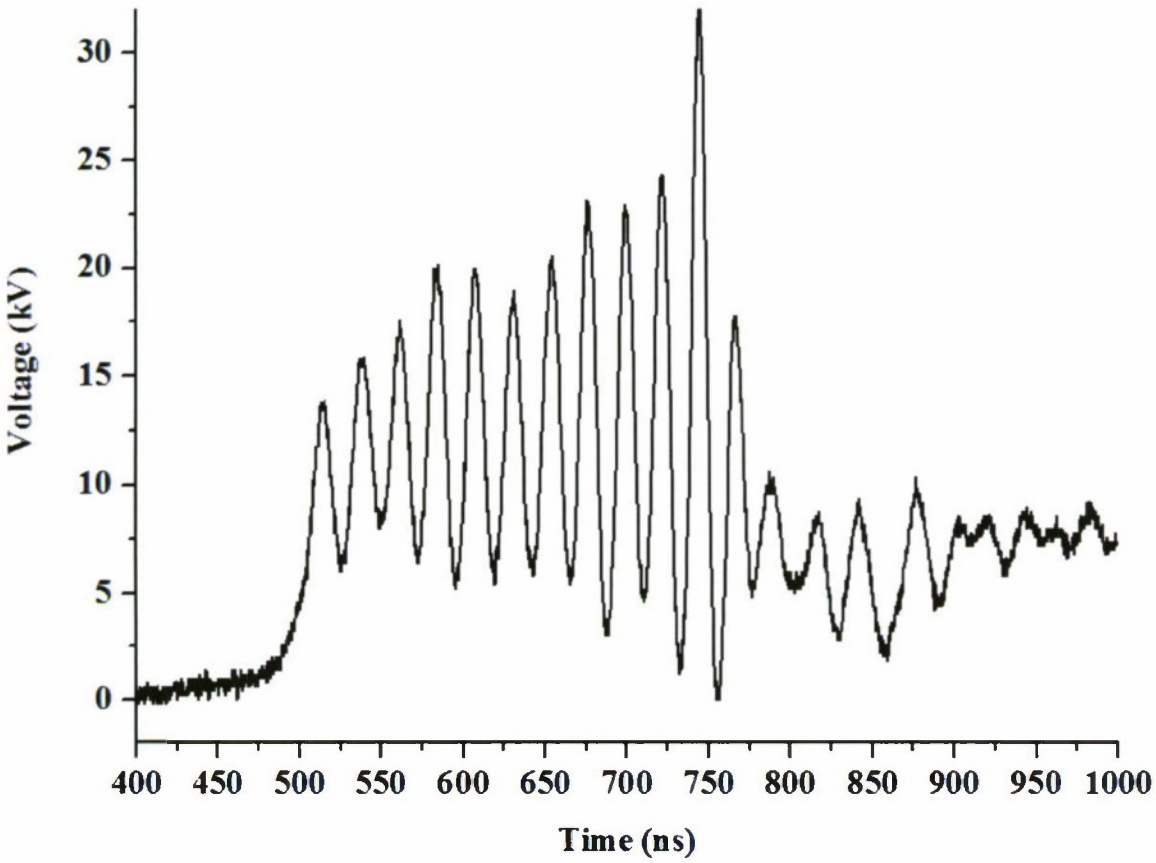

Figure 8.19: Typical waveform generated by test line 8 with 16 stages, oscillating at around 45 MHz.

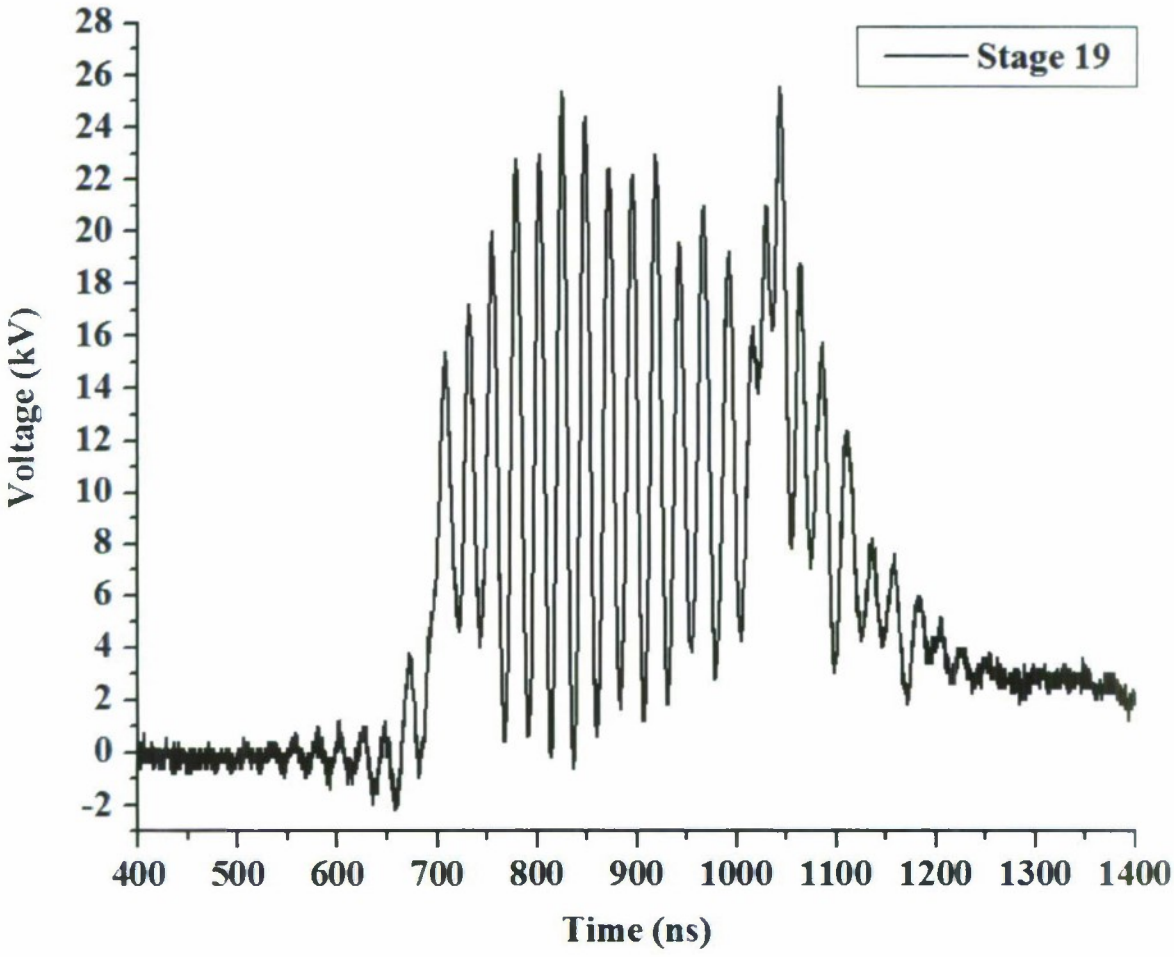

Figure 8.20: Mid-line waveform with NLETL number 8 extended to 33 stages in length.

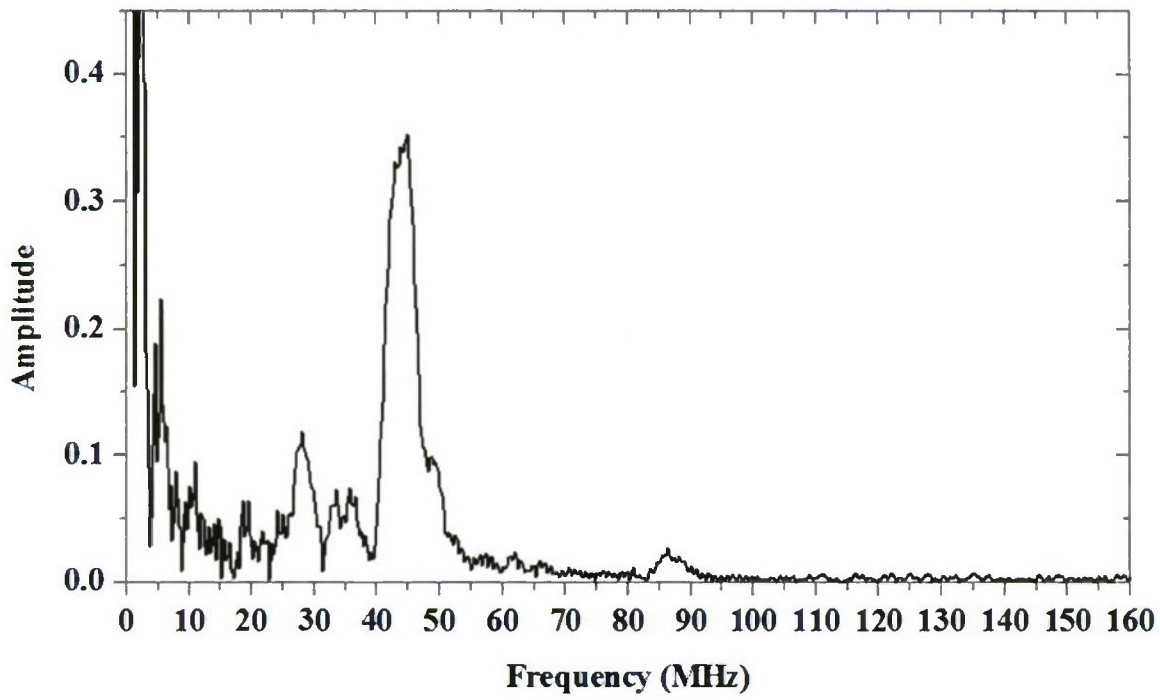

Figure 8.21: Fast Fourier transform spectral analysis of a typical mid-line pulse burst on test line number 8.

The phenomenon of NLETL soliton type oscillation has been demonstrated—over extended pulse bursts of more than just a few cycles—with a completely different mechanism of capacitive nonlinearity to that of the varactor diode lines, and in doing so waveforms generated at much higher voltages. The defining anti-phase property has consistently been observed, and the characteristics of high voltage results accord well to corresponding simulation and low voltage NLETL data. Alongside the process of building and testing these lines, the high voltage input pulse generation equipment has been developed and refined to incorporate a 30 kV Blumlein PFN and hydrogen thyratron switch and its supporting circuitry.

8.5 Demonstration ASP Lines

A pair of NLETLs each of 38 stages in length were constructed and operated within specially fabricated larger mild steel tanks around a metre in length. They were carefully designed to be well matched and of maximum strength. The MuRata DE121205F103Z2K capacitor (referred

to as "DE12", figure 8.5), now long obsolete, has an excellent CNL ratio and is reasonably strong beyond its rated voltage of 2 kV, and four of these were stacked per stage for a resultant nominal capacitance of approximately 2.5 nF. They were stacked very tightly and co-axially, with the transparent silicone compound D used to provide additional insulation between the terminal points over the oil in which the whole assembly was submersed. Each of the 320 or so capacitors were first measured so that, despite inevitable variations, well matched values are found in each stack to optimise voltage sharing and the two lines were well matched for parallel or ASP operation. Nominal capacitance was found to vary from 8.7 to 10.3 nF. The opportunity was taken to try and improve inductive coupling between odd and even stages, and reduce it between adjacent stage inductors, by winding odd number inductors on one plastic support tube and even ones on a different tube placed on the other side of the capacitive elements.

Four turns of the thick copper wire were used to provide a stage inductance of around 300 nH, which maintained a reasonably high NLETL drive impedance of the order of 10 Ω and supported good quality oscillation at a measurable frequency of 35-40 MHz. The total rated capacitance stack voltage was 8 kV but NLETL strength exceeded expectations with no failures or repairs required up to an input pulse amplitude of 20 kV, and corresponding mid-line peak voltages of close to 50 kV. Prior to the lines being tested to destruction a large amount of data was obtained in single, parallel, ASP and periodic loading configurations, the latter described in section 8.6. The extraction problem was once again observed as per figure 8.24 and operation of two lines in parallel did not in this case much improve output waveforms to resistive loads. Mid-line implied peak RF power levels of around 175 MW were measured on several occasions (a larger amplitude pulse burst example waveform is shown in figure 8.25), and the strength of the line construction proved valuable for ASP operation. When driven sufficiently hard the ASP configuration was successfully demonstrated at high voltage with 38/39 stages delivering, for example, 10 MW to a 100 Ω low inductance carbon resistive load and 29 MW to 12 Ω (figure 8.26 and figure 8.27). On occasion, such as figure 8.27, there was some evidence of

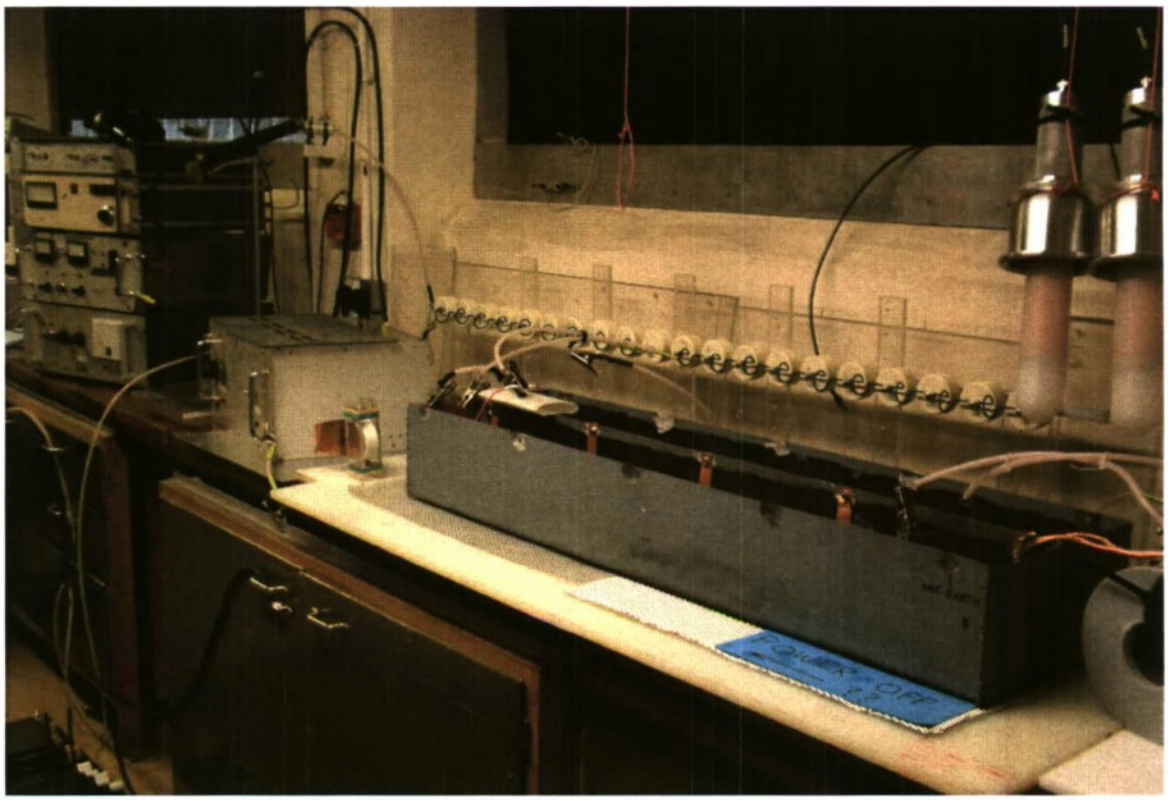

Figure 8.22: High voltage experimental apparatus: from left, power supplies and thyratron with trigger unit, Blumlein PFN and two NLETL oil tanks containing the lines under test, two PVM-5 high voltage oscilloscope probes.

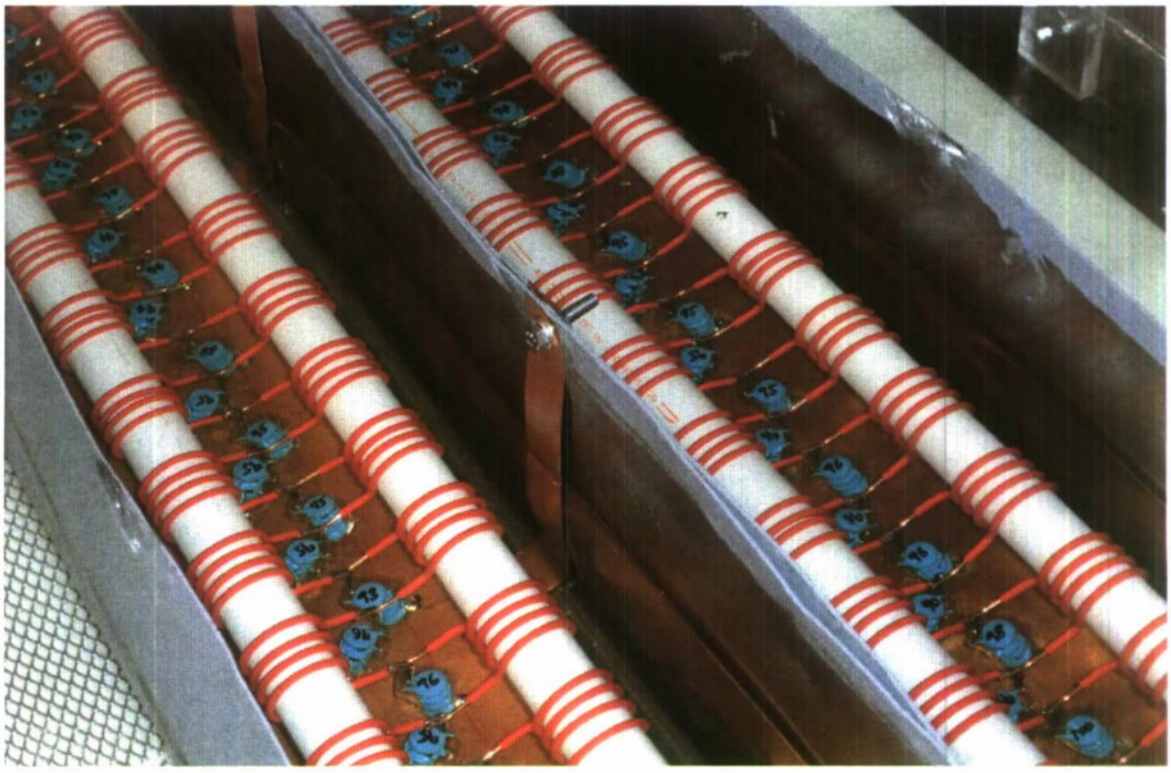

Figure 8.23: Construction of demonstration NLETL stages with self wound air cored inductors, four stacked DE12 capacitors per stage encased in silicone compound D and the whole arrangement under transformer oil.

coupling between the two channels or probes used to take the ASP output differential voltage measurements, which led to a slight frequency doubling effect and reduction in peak values. The implication is that the actual peak extracted RF power is likely to have been even higher than those stated figures.

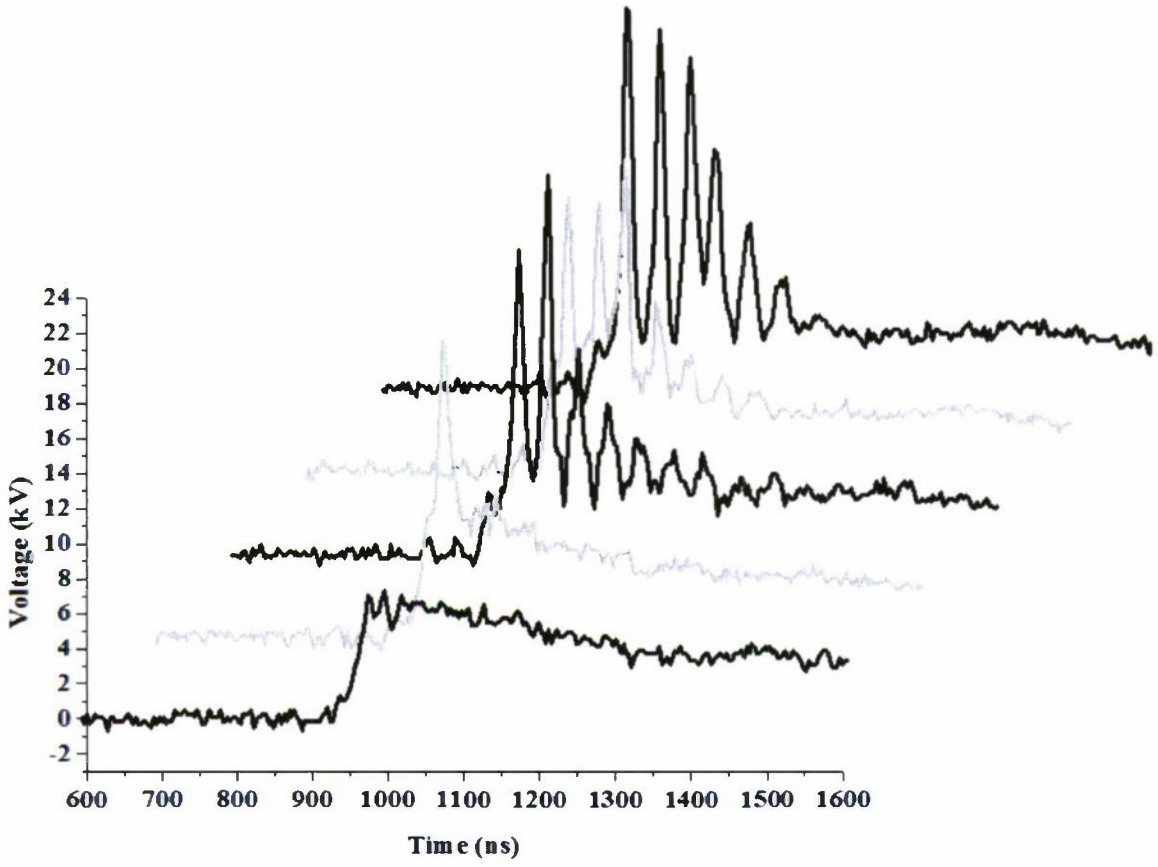

Figure 8.24: Typical single line output waveform, along with the three preceding stage waveforms, illustrating the loss of a single pulse per stage progressing back from a relatively low value resistance load.

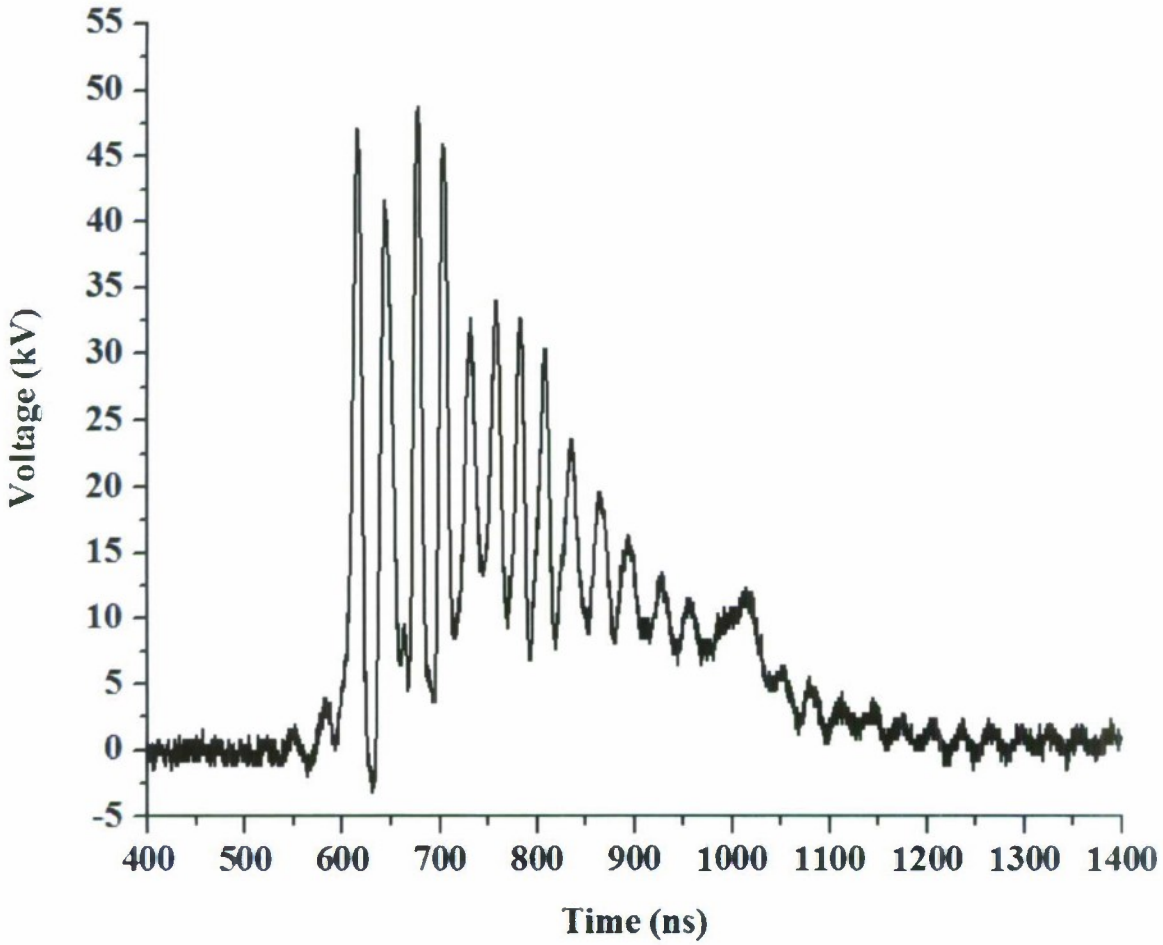

Figure 8.25: Mid-line waveform at maximum input pulse amplitude sustained before NLETL failure.

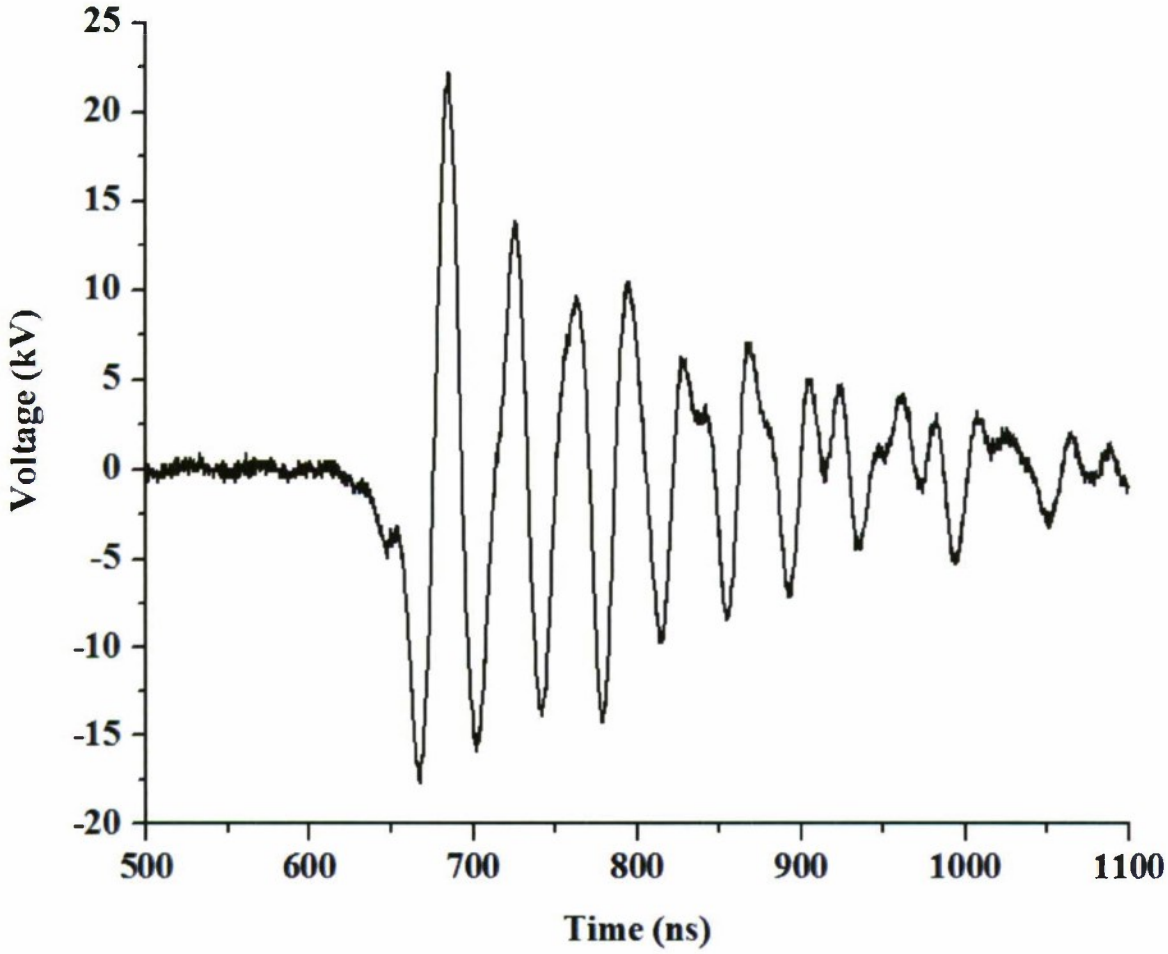

Figure 8.26: ASP output to a resistive 100 Ω load delivering approximately 10 MW peak power averaged over the leading three cycles.

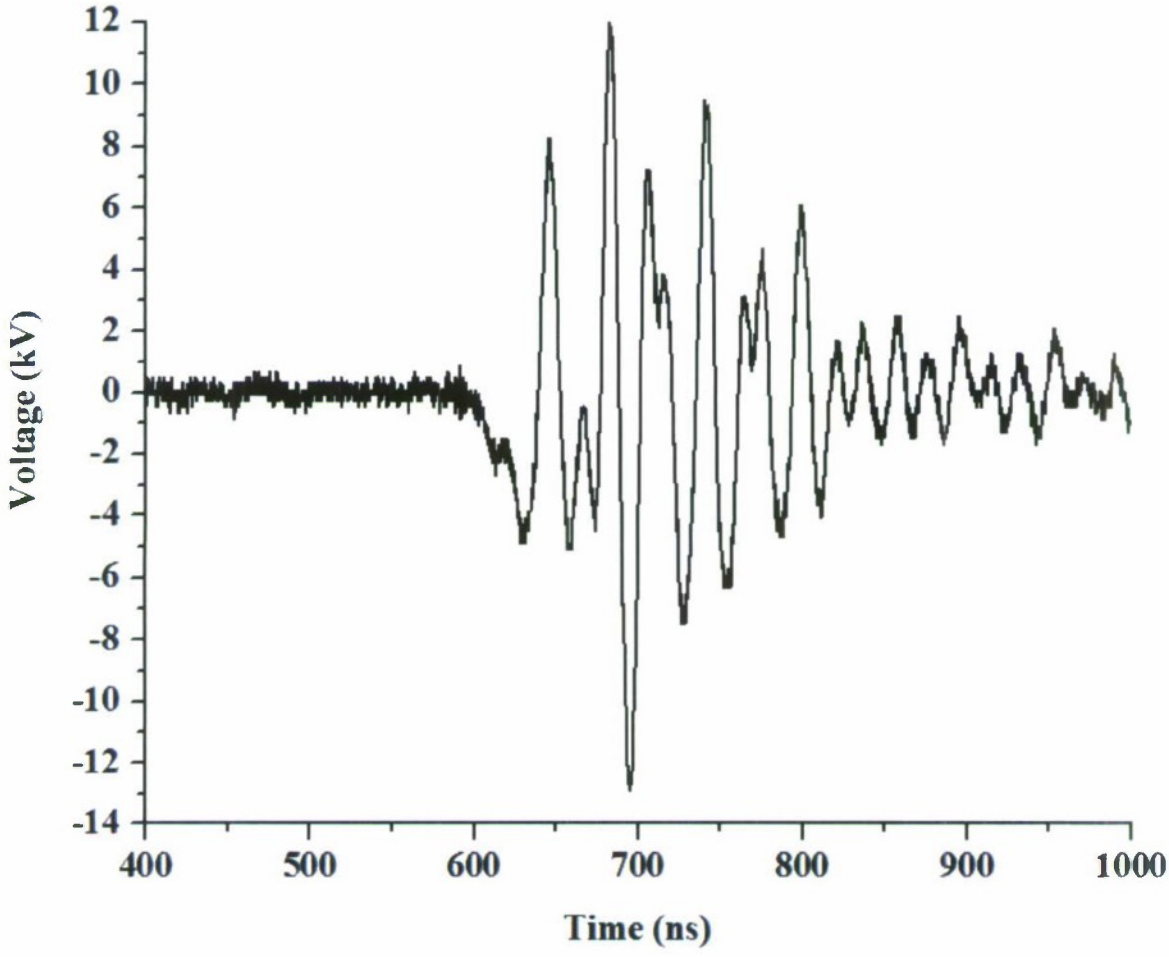

Figure 8.27: 29 MW ASP output to a resistive 12 Ω load.

These demonstration lines were somewhat stronger and better matched than their preceding test lines and, although not designed to push the limits of frequency or power, they generated useful duration pulse burst waveforms at quite substantial power levels and allowed the ASP method of RF extraction to be proved at high voltage. The actual extraction of RF energy to tens of MW is a progressive achievement but in addition further progress has been made by the alternative method of periodically loading this high voltage NLETL at multiple adjacent stages. Results from those experiments are presented in the following section.

High voltage lines were also built for higher frequency oscillation, although the maximum reached was 90 MHz with 1 nF nominal capacitance and a single small loop of inductance. This was lower than expected and is likely due to the increasing influence of stray inductance and capacitance, but also further reductions in inductance led to a loss of oscillation in accordance with the low voltage high frequency work. It is thought that the limit on frequency is due in part to a larger loss equivalent to capacitor ESR, by virtue of Q factor measurements and the lack of oscillation on a separate NLETL based on stacked capacitor discs and designed for high frequency operation. Each stage of this line consisted of three ceramic discs taken from DECE33J capacitors whose coating had been softened with paint stripper for relatively easy removal. The solder connections were carefully removed with emery paper, silver paint applied in their place and the discs stacked with a very thin layer of carbon felt in between. This was introduced to offer some potential shock absorption against piezoelectric and electrostrictive vibrations after initial pulsed strength tests hinted at a small increase in robustness. The dielectric discs were gently clamped between the heads of brass screws which had been ground flat and fitted in small perspex blocks, fixed together on each side by nylon bolts. This line was intended for operation in air as opposed to under oil with the propagation experiments of section 8.6.2 in mind: three coats of silicone compound E were applied by paint brush to the exposed ceramic surfaces, along with a thicker layer of compound D to fill in the remaining space. Fifty such stages were constructed with a total physical length of around 1.5 m, but no

oscillation was observed with low inductance values, even several loops. Whilst ESR loss does not influence frequency, further simulation data subsequently revealed its role in setting the low L and or C limit before oscillation collapses (described in section 5.4). Relative indications of ESR for the various capacitance options were found by Q factor measurements in parallel with a suitable wire wound air cored inductance. For this latest line based on stacked ceramic discs the loss was definitely high, as in greater than 1 Ω, and the single capacitor used in the 90 MHz NLETL described in the next section also had a greater loss than that of the BB212 tuning diode, at around 400 mΩ versus 200 mΩ.

8.6 High Voltage Periodic Loading Results

8.6.1 Resistive Periodic Loading in ASP Configuration

The value in connecting multiple resistive loads to adjacent stages along a section of NLETL for RF extraction was introduced in section 7.4. Periodic loading may be applied to a single line or to two lines in an ASP type configuration, the latter supporting lower values of resistors according to low voltage results. This method, with a series of resistors connected between singly offset stages of the two 35 MHz demonstration lines, was used to increase the total power extracted from the NLETL system. The restoration of symmetry between stages leads to a big improvement in the quality of output waveforms with a single line, and in the ASP case there is also sometimes a notable improvement in the uniformity of each load waveform over that delivered to a single load connected in standard ASP mode. The fact that the predictable phase relationship is maintained between adjacent loaded stages means it is feasible to envisage coherent extraction of RF energy from multiple points along the NLETL, for propagation (section 8.6.2) and other types of application.

When nine 1 kΩ ceramic resistors loaded stages 14/15 through 22/23 of the two lines described in section 8.5 the effectiveness of ASP periodic loading was demonstrated at high voltage, with

several MW of total peak power extraction and good anti-phase between adjacent waveforms. A rough estimate of conversion efficiency when seven 100 Ω resistors were used, via calculations of the energy stored in the Blumlein PFN and appropriate integration of the output waveforms, was over 20 percent. On this occasion the total average peak power output delivered to the seven resistor loads was 63 MW. A typical waveform at one of these 100 Ω loads may be seen in figure 8.28.

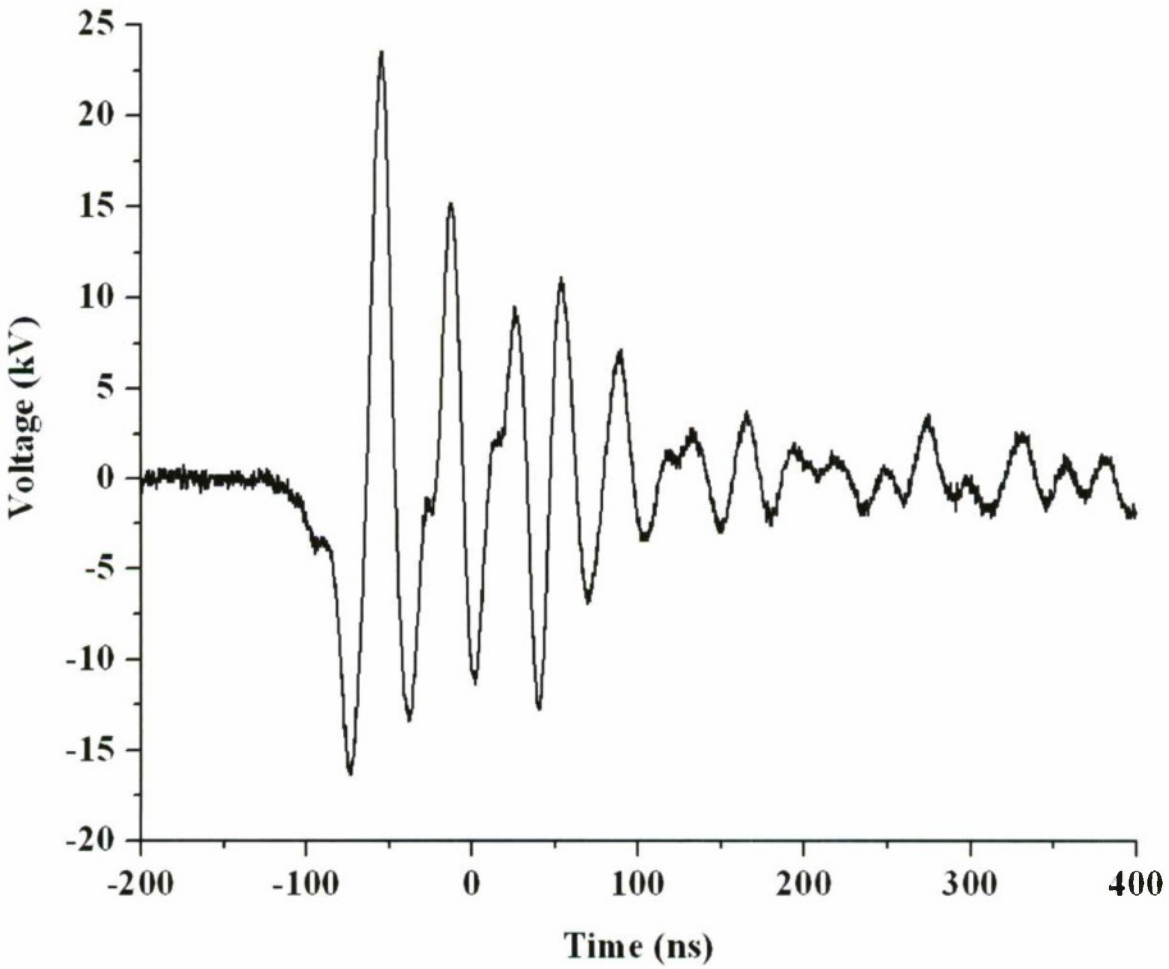

Figure 8.28: Example pulse burst waveform delivered to one of several 100 Ω resistor loads connected in an ASP periodic loading configuration.

8.6.2 Direct NLETL Antenna Propagation

The direct NLETL antenna concept was conceived during work on this project and also introduced in chapter 7, alongside the underlying principle of periodic loading and the anti-phase property on which it relies. A qualitative experiment was carried out to test the effect of dipole loading on the high voltage NLETL mentioned in section 8.5, which oscillated well at around 90 MHz, and to establish whether radiation from such a line could be enhanced and thus energy effectively extracted by a dipole array. Subject to the antenna design considerations outlined previously in section 2.5, the frequency was sufficiently high for the practical construction of centre fed dipoles with 3 mm diameter rigid copper rods of around 1.5 m in length. Since in the loaded section of NLETL it is necessary to load every stage and the wavelength is still relatively long, the connections were alternated at each stage to ensure phased excitation of the dipole elements and a broadside array factor. It was not practical to operate this line under oil and so silicone compound D was used in its place, equally capable of preventing arcing so long as care was taken to avoid air gaps during its application.

Of the 33 stages, 18 through 26 were loaded with the nine dipoles in an arrangement which is shown in figure 8.30. With the dipole array in place the amplitude and duration of the pulse burst waveform received over a propagation distance of around 10 m was greatly increased (figure 8.29). Also the directionality of the array factor pattern was checked by rotating the line and dipole array, with nulls observed in perpendicular directions as expected. This indicates effective extraction of RF energy via the dipole array—it is now possible to envisage more sophisticated antenna structures optimised further for incorporation with a discrete nonlinear transmission line pulse burst generator.

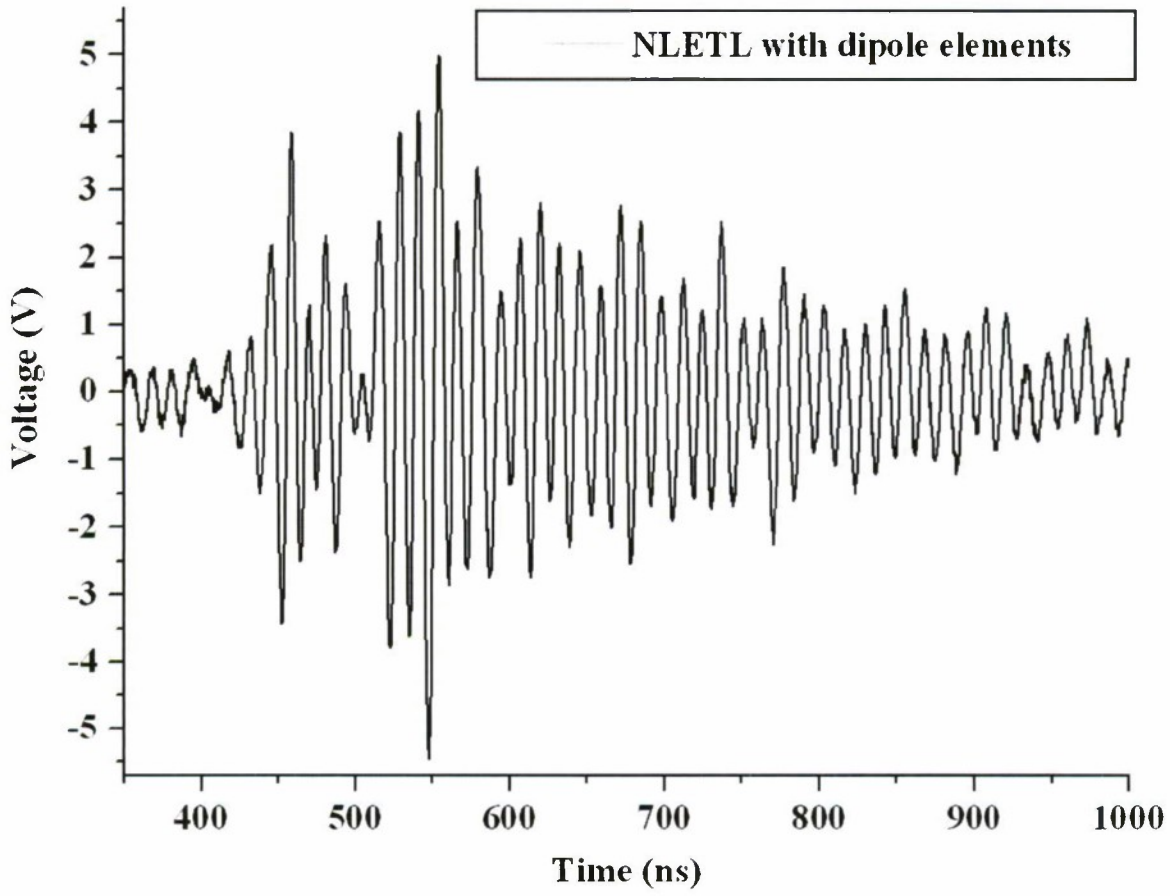

Figure 8.29: Detected waveform, direct to oscilloscope within a shielded enclosure via 50 Ω coaxial cable and a 50 Ω attenuator.

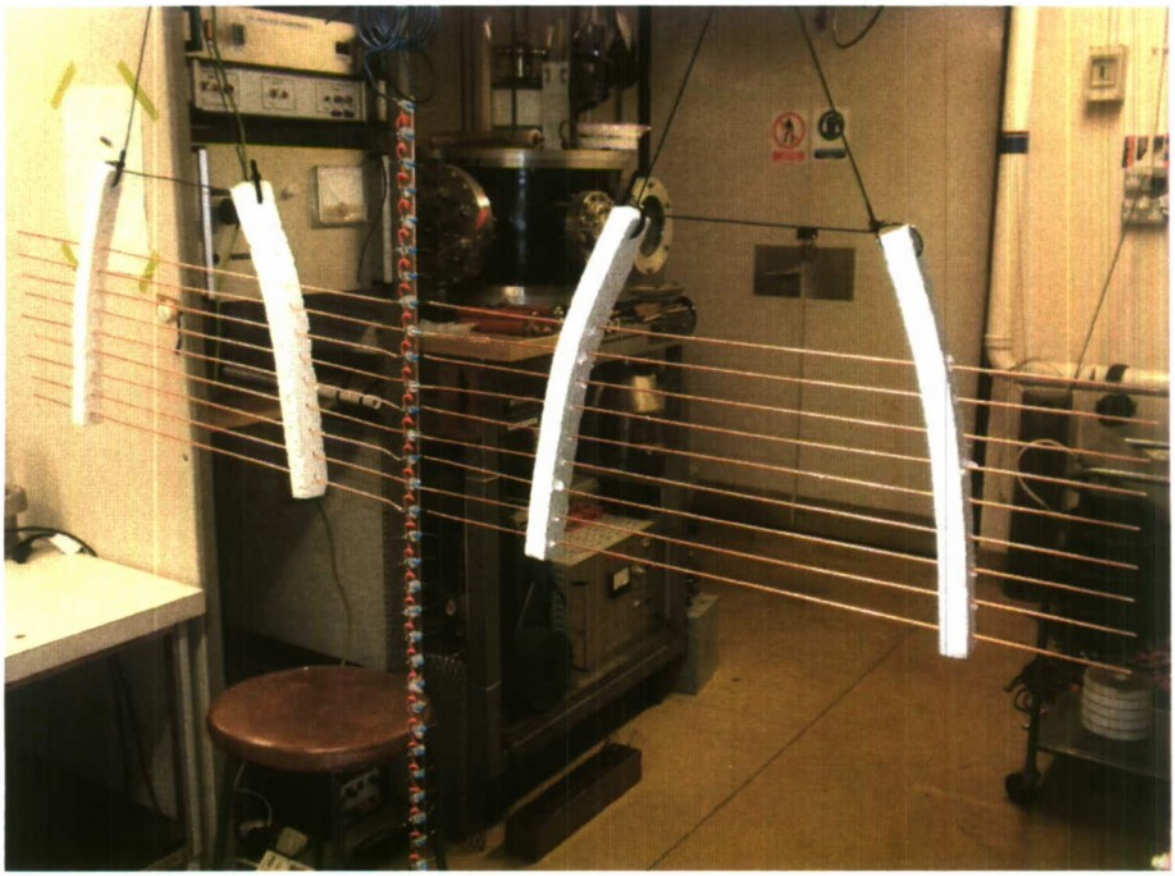

Figure 8.30: Direct NLETL antenna radiator.

Chapter 9

Conclusions

9.1 Nonlinear Lumped Element Transmission Line Technology for RF Applications

The specific term nonlinear lumped element transmission line, NLETL, has been introduced for use alongside the more general term NLTL, a convention which has since been adopted elsewhere in the industry. The importance of distinguishing the NLETL topology from other more continuous nonlinear transmission line systems is emphasised, and an awareness of the fundamentally discrete nature of its soliton type oscillation has now been established. The strong oscillation which may be observed over a very wide range of line design parameters is probably not simply the result of a delicate counter balance between nonlinear and dispersive effects. It is, however, possibly a physical realisation of the breather soliton, a limiting oscillatory state of minimum wavelength enforced where the CNL ratio is sufficiently large. Breathers, like conventional sinusoidal water waves, tend not to transmit energy, and indeed the progression of a pulsed RF waveform along a NLETL may be interpreted as a standing wave situation where the group velocity is zero.

The somewhat curious ability of nonlinear transmission lines to create high frequency pulse burst waveforms has been acknowledged since 1967, with reference to RF applications since 1988. Several published studies of the topic were summarised in chapter 3, where interesting and valuable contributions to pulsed power research formed the basis for this phase of work to begin. However, practical development of NLETL technology has been limited and after two decades has yet to fulfil its acclaimed promise as a novel high power RF source. Several issues that inhibit immediate application to practical systems have been identified and assessed. Issues which may be taken on board from the range of results presented here include the relatively high dielectric loss generally associated with ferroelectric ceramics (and its crucial influence on the maximum frequency achievable by a reduction in line inductance or nominal capacitance), and the extraction problem. NLETL operation may now be better understood

according to the discussions of chapter 6 and chapter 7. An awareness of the nature of the oscillation has inspired certain novel ideas arising from the problem of extracting RF energy to resistive loads. Significant progress has now been made in this area, which was necessary for practical application of the technology.

The soliton phenomena was introduced and reviewed in chapter 4, where also the nonlinear dispersive KdV equation was solved analytically in an attempt to investigate the behaviour of, and interactions between, continuous soliton pulses. Further aspects of soliton theory with respect to discrete systems were also briefly introduced—these selected outcomes from a wider review of nonlinear dispersive applied mathematics should, it is thought at this time, be associated with NLETL operation.

A high voltage ceramic line subject to advanced industrial fabrication techniques, such that losses relating to the dielectric–conductor interfaces are minimised, could quite possibly operate at several hundred MHz as per the low voltage BB212 results in chapter 6. Further significant increases in frequency are unlikely without the progressive research in dielectric materials science stipulated in section 9.3. Some applications do require high power pulse burst generation at frequencies down to a hundred MHz or so, and an effective NLETL system operating at a few hundred MHz, with its associated frequency agility, is in itself a valuable prospect. In comparison with alternative MVED and SSPA technologies the NLETL concept has several potential advantages which were summarised in section 3.4. Initially, it may simply be the case that in an environment where the requirements of a given application are often strictly constrained, it is appealing to have an additional viable option for consideration. Of course, with the basic NLETL system, this is first reliant upon the extraction of mid-line RF energy to power consuming loads.

9.2 Concluding Remarks

Our understanding of NLETL oscillation and our ability to utilise it for RF applications has been substantially improved, and several research groups around the world continue to work on the problem. In addition to the observation and appreciation of discreteness and the antiphase property, extensive experimental and numerical data have revealed various design trends, noted in chapter 6. Some are not immediately obvious but represent important outcomes. For example, the overdrive limit on input voltage amplitude should be taken into account alongside CNL steepness and voltage strength during design for a given power level. Accordingly, it has become necessary to distinguish between CNL ratio and steepness, the former of which should be as large as possible but the latter perhaps relatively shallow assuming sufficient voltage strength and the desire to operate at maximum power. The structure of barium titanate ferroelectric ceramic is such that electrical failure tends to occur soon after full dielectric saturation has been reached, before any loss of oscillation due to an excessively large input voltage. But on occasion, particularly in the event of new stronger NLETL dielectrics being introduced, the overdrive limit could be more directly relevant to system design. An explanation for the initiation of strong NLETL oscillation has been suggested, in terms of the inductive kick effect, and this supports the overdrive observation if the sharpened leading edge shock transient amplitude becomes sufficient to fully satisfy any voltage spike requirement.

A versatile NLETL simulation tool is now available, whose development time has been justified by the ability to quickly run tests on a variety of different lines and to investigate a range of parameter values outside those available experimentally. The BB212 varactor diode has in the past been used to demonstrate soliton behaviour on electrical transmission lines, and here the performance of over 900 such devices was investigated in a large number of NLETL systems. Their loss is relatively low and the maximum frequency achievable with this CNL characteristic is around 250 MHz. A modest increase could possibly be achieved with a lower nominal capacitance, certainly with any increase in CNL ratio, and this result suggests value in pursuing a

high voltage solid state approach at moderate power levels, despite the potentially high cost. The construction and testing of long discrete transmission lines is somewhat time consuming but at low voltage was a convenient way of testing line designs and novel configuration ideas. The high voltage phase of experimental work was more involved, with greater expense and consideration necessarily paid to equipment requirements, safety, input pulse generation and accurate measurement. The useful result is a demonstration of the effect, with its unusual defining characteristics noted during low voltage work, under the completely different mechanism of nonlinearity and at greatly increased power levels approaching 200 MW. A range of pulsed RF waveforms at tens of kV and frequencies from around 10 MHz to 90 MHz have been obtained mid line, typically exhibiting useful pulse uniformity and durations of around ten cycles. A review of many different commercial capacitors turned up a small selection whose measured capacitive nonlinearity ratio was surprisingly large and suited to NLETL application. The majority of currently available commercial high voltage barium titanate ceramic capacitors were not found to be sufficiently nonlinear in this respect; successful results were obtained using capacitors now obsolete. As with the low voltage BB212 diodes, Kingsbeech obsolete component finders were extremely helpful throughout the project in this respect.

The extraction problem has been consistently observed, and is unfortunate given the possibility, especially at higher frequencies, of converting a wide input pulse to an extended burst of RF energy containing a large number of cycles mid line. Series load inductance can dramatically improve output oscillation but at the RF frequency a negligible portion of energy is consumed by the resistive load component. The issue is obviously important but had yet to be addressed and so much of the work on this project focused on generating ideas for the delivery of NLETL RF energy to resistive loads. The asymmetric parallel (ASP) and periodic loading ideas are two successful examples, of several considered, which exploit the antiphase property between neighbouring discrete stages. Pulse burst waveforms up to 30 MW have been extracted to resistive loads of around 10 Ω using high voltage lines in the ASP configuration,

following many encouraging results at low voltage. Extraction of reasonable duration pulse bursts is possible by this method but the output tends to be limited by a pulse shortening effect, without more than around ten cycles typically observed. An additional refinement in the form of cross links sometimes helped to mitigate phase drift between two lines not well matched.

The discussion of chapter 7 on the standing wave nature of the discrete propagating waveform perhaps offers some reasoning for the very good results at low and high voltage using periodic NLETL loading. The idea was conceived on the basis of the predictable stage by stage phase relationship and the resulting possibility of driving multiple elements of a propagating antenna array from successive discrete stages. However, given the disrupting influence of a single resistive load connected to any point along a line, there was no reason to think that simply adding a larger number of loads should work well at all. Despite this, initial experiments used resistors to test the loading effect that a series of dipole antenna elements might have on NLETL waveforms, with promising results provided that every adjacent stage is loaded and spatial uniformity is preserved. At the discontinuity between unloaded and loaded sections of line it was interesting to observe a disruption and loss of oscillation as per the extraction problem to single loads. With periodic loading at high voltage a total power of 60 MW has been extracted from the NLETL, and this figure could be scaled up with a larger number of high voltage resistors and ceramic dielectric blocks designed specifically for higher power operation. On the basis of initial experimental results, the periodic loading idea is suggested as possibly the most efficient way of extracting RF energy from a NLETL pulse burst generator. This applies either to multiple resistive loads able to combine phased power components, or to the direct connection of antenna components to the NLETL as illustrated in figure 8.30.

9.3 Future Directions

At this stage of concluding the current work on NLETL technology development several new avenues for specific future activity have become clear, and research could prove beneficial in

the following areas. Assuming that the RF waveforms deliverable by the ASP and or periodic loading configurations are able to satisfy some application requirements, the next phase of work should certainly be concerned with dielectric materials science research. If lifetime can be substantially increased, and frequency limiting loss reduced, there is every indication that a versatile, compact low cost pulse burst generator delivering hundreds of MW at hundreds of MHz is feasible.

Justification for improving dielectric nonlinear materials is offered by the encouraging experimental and numerical waveforms obtained on a wide range of different lines, and by demonstration of the ASP and periodic loading ideas for actually extracting RF energy from the NLETL system. It may be the case that the capabilities of ceramic ferroelectric materials are fundamentally limited under conditions of strong nonlinear exertion; research dedicated to the topic could consider completely different dielectric options, alternative materials or even the development of high power solid state equivalents to the varactor diodes used here. In any case, given the strong interest which exists throughout the pulsed power community in nonlinear transmission line technology, the provision of a robust and sufficiently nonlinear dielectric material is likely to be very welcome. The nonlinearity that appears to be available with well prepared barium titanate ceramic, in terms of CNL ratio, is just about good enough, although an increase would be valuable should a significant increase in frequency beyond a couple of hundred MHz be desired. It is necessary to decrease loss if high power NLETLs based on this material are to reach such frequencies however. The fundamental limits on bulk dielectric loss should be considered alongside that associated with the conductor interfaces. ESR type loss directly limits the maximum frequency that may be reached by a reduction in inductance and or capacitance, and may be an important motivation for looking at alternative materials or solid state CNL options. Simulation data have suggested that a larger nonlinearity ratio can increase this frequency limit for a given loss, should it be feasible to implement. In addition to reducing dielectric loss and increasing CNL ratio if possible, developing a robust material

with a much longer lifetime when fully saturated under pulsed conditions is a future priority for specialist materials science research. The issue to be tackled in the case of ferroelectric ceramics is the coincidence of maximum loss and electrostrictive mechanical strains with the operating conditions of maximum nonlinearity. Progress may be made in these areas with appropriate materials science expertise and the provision of specialised facilities supporting the manufacture of ceramics and possibly alternative materials, but it would also be interesting to simply scale up the power of experimental lines similar to those developed here. Dielectric blocks built to suitable dimensions could be used to demonstrate discrete soliton type oscillation at increased power levels, specifically to further improve ASP and periodic loading output figures. This would require higher voltage power supplies, pulse forming components and switching, since the pulse forming network and hydrogen thyratron were operated here to maximum voltage.

A greater number and range of values of high voltage resistors would allow more periodic loading experiments to be carried out. For propagation applications consideration should subsequently be given to the optimal design of a more advanced direct NLETL antenna, and to establish its feasibility as a reasonably efficient directed energy radiator. The incorporation of a phased dipole element array was found by qualitative experiment to effectively load a high voltage NLETL (in agreement with similar resistor tests) but there are far more specialised and complex radiating antenna structures which are likely to be suitable. Furthermore, the concept could perhaps be extended to a range of NLETL layouts such as, for example, a two dimensional arrangement forming a scanning array or high impedance surface type of antenna. Similar to the future work in materials science discussed above, this is a specialist field of research which would benefit from the involvement of appropriate expertise and facilities.

The numerical model capabilities have been sufficient to support this experimental work, but to simulate much higher frequency lines the further modifications described in section 5.3 would be required. Alternative transmission line topologies, incorporating for example magnetic as

well as dielectric nonlinearity, may be interesting to consider. The mathematical review of soliton wave theory and in particular breathers has been insightful, and further understanding of the phenomenon from this perspective would be likely to aid future system design and optimisation. For example, the periodic loading idea brings great potential to NLETL research. Its effectiveness, in spatially distributing loading along a line so as to maintain uniformity, is probably closely related to the standing wave nature of discrete lattice breather solitons.

Bibliography

[1] J.D.C. Darling and P.W. Smith. High power RF generation from nonlinear delay lines. In 16^{th} *IEEE International Pulsed Power Conference*, volume 1, pages 472–475, 2007.

[2] J.D.C. Darling and P.W. Smith. High power pulsed RF extraction from nonlinear lumped element transmission lines. *IEEE Transactions on Plasma Science*, 36(5):2598–2603, 2008.

[3] J.D.C. Darling and P.W. Smith. High power RF generation and delivery from nonlinear lumped element transmission lines. In 2^{nd} *Euro-Asian Pulsed Power Conference*, 2008.

[4] J.D.C. Darling and P.W. Smith. High power pulse burst generation by soliton type oscillation on nonlinear lumped element transmission lines. In 17^{th} *IEEE International Pulsed Power Conference*, 2009.

[5] D.V. Giri. *High–power electromagnetic radiators: nonlethal weapons and other applications*. Harvard University Press, Dec 2004.

[6] R.J. Barker, N.C. Luhmann, J.H. Booske, and G.S. Nusinovich. *Modern microwave and millimeter–wave power electronics*. Wiley–VCH, Apr 2005.

[7] Defense Advanced Research Projects Agency. http://www.darpa.mil/.

[8] M.G. Hussain. Ultra–wideband impulse radar—an overview of the principles. IEEE AES Systems Magazine, Sep 1998.

[9] R.J. Fontana. Recent system applications of short pulse ultra–wideband (UWB) technology. *IEEE Transactions On Microwave Theory and Techniques*, 52(9), Sep 2004.

[10] J.O. Rossi, M. Ueda, C.B. Mello, and G. Silva. Short repetitive pulses of 50–75 kV applied to plasma immersion implantation of aerospace materials. In 16^{th} *IEEE International Pulsed Power Conference*, volume 2, 2007.

[11] H. Bluhm, R. Bohme, W. Frey, H. Giese, P. Hoppe, G. Kessler, G. Muller, N. Neubert, D. Rusch, C. Schultheiss, G. Schumacher, M. Sohner, H. Strassner, D. Strauss, V. Vath, F. Zimmermann, V. Engelko, A. Dulson, and V.I. Kurets. Industrial applications of high voltage pulsed power techniques: developments at forschungszentrum karlsruhe (FZK). In 11^{th} *IEEE International Pulsed Power Conference*, volume 1, pages 1–12, 1997.

[12] K. Yatsui. Progress of pulsed power commercial applications in Japan. In 11^{th} *IEEE International Pulsed Power Conference*, volume 1, pages 13–24, 1997.

[13] S.H. Gold and G.S. Nusinovich. Review of high power microwave source research. *Review of Scientific Instruments*, 68(11):3947–3974, Nov 1997.

[14] P.A. Rizzi. *Microwave engineering: passive circuits*. Prentice Hall, Feb 1988.

[15] R.H. Varian and S.F. Varian. A high frequency oscillator and amplifier. *Journal of Applied Physics*, 10(5):321–327, 1939.

[16] Y. Carmel, J. Ivers, R.E. Kribel, and J. Nation. Intense coherent cherenkov radiation due to the interaction of a relativistic electron beam with a slow wave structure. *Physical Review Letters*, 33(21):1278–1282, 1974.

[17] S.F. Adam. *Microwave theory and applications*. Mei Ya Publications Inc., Jan 1969.

[18] J.A. Nation. On the coupling of an high current electron beam to a slow wave structure. *Applied Physics Letters*, 17:491–494, 1970.

[19] J. Schneider. Stimulated emission of radiation by relativistic electrons in a magnetic field. *Physical Review Letters*, 2(12):504–505, 1959.

[20] S.T. Pai and Q.I. Zhang. *Introduction to high power pulse technology*. World Scientific Publishing Co. Pte. Ltd., Jul 1995.

[21] P. Persephonis, K. Vlachos, C. Georgiades, and J. Parthenios. The inductance of the discharge in a spark gap. *Journal of Applied Physics*, 71(10):4755–4762, May 1992.

[22] N. Seddon, J.E. Dolan, and C.R. Spikings. RF pulse formation in nonlinear transmission lines. In 34^{th} *IEEE Conference on Plasma Science*, pages 678–681, 2007.

[23] A.M. Belyantsev and A.B. Kozyrev. Generation of high frequency oscillations by electromagnetic shock wave at its synchronism with backward harmonic of periodic transmission line based on multilayer heterostructure. *International Journal of Infrared and Millimeter Waves*, 19(11):1571–1586, Nov 1998.

[24] A.M. Belyantsev and A.B. Kozyrev. Direct transformation of a video pulse into a radio pulse in coupled transmission lines with normal and anomalous dispersion. *Radiophysics and Quantum Electronics*, 44(11):892–899, 2001.

[25] A.M. Belyantsev and A.B. Kozyrev. Multilayer heterostructures with asymmetric barriers as new components for nonlinear transmission lines to generate high frequency oscillations in the 100–300 GHz range. *International Journal of Infrared and Millimeter Waves*, 23(10):1475–1500, Oct 2002.

[26] A.B. Kozyrev and D.W. van der Weide. Trains of envelope solitons in nonlinear left–handed transmission line media. *Applied Physics Letters*, 91(25):254111, Dec 2007.

[27] R.J. Trew, J.W. Mink, and U. Varshney. The role of government support for research in US academic institutions. *IEEE Transactions on Microwave Theory and Techniques*, 50(3):1028–1033, 2002.

[28] C.R. Smith, C.M. Armstrong, and J. Duthie. The microwave power module: a versatile RF building block for high power transmitters. *Proceedings of the IEEE*, 87(5):717–737, May 1999.

[29] J. Gaudet, E. Schamiloglu, J.O. Rossi, C.J. Buchenauer, and C Frost. Nonlinear transmission lines for high power microwave applications—a survey. In *IEEE International Power Modulators and High Voltage Conference*, pages 131–138, 2008.

[30] C.A. Balanis. *Antenna theory: analysis and design*. Longman Higher Education, Jul 1982.

[31] J.J. Carr. *Practical antenna handbook*. McGraw–Hill / TAB Electronics, 4 edition, May 2001.

[32] D.S. Evans and G.R. Jessop. *VHF–UHF manual*. RSGB, 3 edition, 1976.

[33] F. Kouril and K. Vrba. *Nonlinear and parametric circuits—principles, theory and applications*. Ellis Horwood, 1988.

[34] J.J. Stoker. *Nonlinear vibrations in mechanical and electrical systems*. Wiley–Interscience, 1 edition, Jan 1992.

[35] P.W. Smith. *Transient electronics—pulsed circuit technology*. John Wiley and Sons Inc., Jul 2002.

[36] H. Ikezi, J.S. de Grassie, Y.R. Lin-Liu, and J. Drake. High power pulse burst generation by magnetically segmented transmission lines. *Review of Scientific Instruments*, 62(12):2916–2922, 1991.

[37] N. Seddon and E. Thornton. A high voltage, short risetime pulse generator based on a ferrite pulse sharpener. *Review of Scientific Instruments*, 59(11):2497–2498, 1988.

[38] S. Ibuka, T. Miyazawa, A. Ishii, and S. Ishii. Fast high voltage pulse generator with nonlinear transmission line for high repetitive operation. In 10^{th} *IEEE International Pulsed Power Conference*, volume 2, pages 1365–1370, 1995.

[39] C.R. Wilson, M.M. Turner, and P.W. Smith. Pulse sharpening in a uniform LC ladder network containing nonlinear ferroelectric capacitors. 19^{th} *IEEE Power Modulator Symposium*, 38(4):204–207, Apr 1991.

[40] M.M. Turner, G. Branch, and P.W. Smith. Methods of theoretical analysis and computer modeling of the shaping of electrical pulses by nonlinear transmission lines and lumped element delay lines. *Electron Devices, IEEE Transactions on*, 38(4):810–816, 1991.

[41] R. Hirota and K. Suzuki. Theoretical and experimental studies of lattice solitons in nonlinear lumped networks. *Proceedings of the IEEE*, 61(10):1483–1491, Oct 1973.

[42] G. Branch. *Nonlinear pulsed power technology*. PhD thesis, University of Oxford, Mar 1994.

[43] M.P. Brown. *High voltage soliton production in nonlinear transmission lines and other pulsed power applications*. PhD thesis, University of Oxford, Sep 1997.

[44] M. Toda. Wave propagation in anharmonic lattices. *Journal of the Physical Society of Japan*, 23(3):501–506, 1967.

[45] M. Toda. Vibration of a chain with nonlinear interaction. *Journal of the Physical Society of Japan*, 22(2):431–436, 1967.

[46] J.A. Kolosick, D.L. Landt, H.C.S. Hsuan, and K.E. Lonngren. Properties of solitary waves as observed on a nonlinear dispersive transmission line. *Proceedings of the IEEE*, 62(5):578–581, May 1974.

[47] K. Daikoku, Y. Mizushima, and T. Tamama. Computer experiments on new lattice solitons propagating in Volterra's system. *Japanese Journal of Applied Physics*, 14(3):367–376, 1975.

[48] H. Nagashima and Y. Amagishi. Experiment on the toda lattice using nonlinear transmission line. *Journal of the Physical Society of Japan*, 45(2):680–688, 1978.

[49] K.E. Lonngren. Observation of solitons on nonlinear dispersive transmission lines. In *Workshop on Solitons, Alabama, GA*. Academic Press New York, 1977.

[50] E. Infeld and G. Rowlands. *Nonlinear waves, solitons and chaos*. Cambridge University Press, Jul 2000.

[51] D. Jager. Soliton propagation along periodic–loaded transmission line. *Applied Physics A: Materials Science and Processing*, 16(1):35–38, 1978.

[52] D. Jager. Experiments on KdV solitons. *Journal of the Physical Society of Japan*, 51(5):1686–1693, 1982.

[53] H. Ikezi, S.S. Wojtowicz, R.E. Waltz, and D.R. Baker. Temporal contraction of solitons in a non–uniform transmission line. *Journal of Applied Physics*, 64(12):6836–6838, 1988.

[54] H. Ikezi, S.S. Wojtowicz, R.E. Waltz, J.S. deGrassie, and D.R. Baker. High power soliton generation at microwave frequencies. *Journal of Applied Physics*, 64(6):3277–3281, 1988.

[55] H. Ikezi, Y.R. Lin-Liu, T. Ohkawa, and J.S. deGrassie. Electrostrictions in high–power soliton generator. *Journal of Applied Physics*, 64(9):4717–4719, 1988.

[56] H. Ikezi, J.S. DeGrassie, and J. Drake. Soliton generation at 10 MW level in the very high frequency band. *Applied Physics Letters*, 58(9):986–987, 1991.

[57] M.P. Brown and P.W. Smith. High power, pulsed soliton generation at radio and microwave frequencies. In 11^{th} *IEEE International Pulsed Power Conference*, volume 1, pages 346–354, 1997.

[58] A.A. Balyakin and N.M. Ryskin. Chaotic oscillations in a nonlinear lumped parameter transmission line. *Radiophysics and Quantum Electronics*, 44(8):637–644, Aug 2001.

[59] D.S. Ricketts, L. Xiaofeng, and H. Donhee. Taming electrical solitons—a new direction in picosecond electronics. In *IEEE Radio Frequency Integrated Circuits (RFIC) Symposium*, pages 24–27, 2006.

[60] R.E. Waltz, M.N. Rosenbluth, and H Ikezi. Nonlinear reflection in a bandpass filter. *Journal of Applied Physics*, 67(9):4327–4332, 1990.

[61] F. Jona and G. Shirane. *Ferroelectric crystals—Int. series of monographs on solid state physics Vol. 1.* Pergamon Press, 1962.

[62] J. Cross. *Electrostatics: principles, problems and applications.* Institute of Physics Publishing, Jan 1987.

[63] A. Wood. *Acoustics.* Blackie and Son Ltd., 1960.

[64] R.W. Whatmore. Electronic ceramics. *Physics in Technology*, 19:58–66, 1988.

[65] E. Peschke and R. von Olshausen. *Cable systems for high and extra-high voltage.* Wiley-VCH, Feb 2000.

[66] J. Cieminski. High-signal electrostriction in ferroelectric materials. *Journal of Physics D: Applied Physics*, 24:1182–1186, 1991.

[67] H. Kawai. The piezoelectricity of polyvinylidene fluoride. *Japanese Journal of Applied Physics*, 8(7):975, 1969.

[68] M.T. Domonkos, P.J. Turchi, J.V. Parker, T.C. Grabowski, C.W. Gregg, C.E. Roth, and K. Slenes. A ceramic loaded polymer blumlein pulser for compact, rep-rated pulsed power applications. In 15^{th} *IEEE International Pulsed Power Conference*, pages 1322–1325, 2005.

[69] P.G. Drazin and R.S. Johnson. *Solitons: an introduction.* Cambridge University Press, 2 edition, Mar 1989.

[70] A.B. Pippard. *Response and stability.* Cambridge University Press, Nov 1985.

[71] J. Scott Russell. Report of the committee on waves. 7^{th} *meeting of the British Association for the Advaneement of Science, Liverpool*, pages 417–496, 1837.

[72] J. Scott Russell. Report on waves. 14^{th} *meeting of the British Association for the Advancement of Science, York*, pages 311–390 and plates 47–57, 1844.

[73] D.J. Korteweg and G. de Vries. On the change of form of long waves advancing in a rectangular canal, and on a new type of long stationary waves. *Philosophical Magazine*, 39:422–443, 1895.

[74] N.J. Zabusky and M.D. Kruskal. Interaction of "solitons" in a collisionless plasma and the recurrence of initial states. *Physical Review Letters*, 15(6):240–243, 1965.

[75] R. Hirota. *The direct method in soliton theory.* Cambridge University Press, english translation edition, Aug 2004.

[76] C. Rogers and W.K. Schief. *Backlund and darboux transformations—geometry and modern applications in soliton theory.* Cambridge University Press, 1 edition, Aug 2002.

[77] J.E. Allen. The early history of solitons (solitary waves). *Physica Scripta*, 57(3):436–441, 1998.

[78] R.L. Merlino. Experimental investigations of dusty plasmas. In 4^{th} *International Conference on the Physics of Dusty Plasmas*, volume 799, pages 3–11, Oct 2005.

[79] S. Ghosh, A.K. Bera, and S. Das. Evidence for nonlinear capacitance in biomembrane channel system. *Journal of Theoretical Biology*, 200(3):299–305, Oct 1999.

[80] A. Pekcan. The hirota direct method. Master's thesis, Bilkent University, Jul 2005.

[81] A.V. Slyunyaev and E.N. Pelinovski. Dynamics of large amplitude solitons. *Journal of Experimental and Theoretical Physics*, 89(1):173–181, Feb 2006.

[82] M. Remoissenet. *Waves called solitons: concepts and experiments*. Springer–Verlag, Feg 1996.

[83] S. Aubry. Breathers in nonlinear lattices: existence, linear stability and quantization. *Physica D: Nonlinear Phenomena*, 103(4):201–250, 1997.

[84] S. Lippman, J. Lajoie, and B. Moo. *C++ primer*. Pearson Education, 4 edition, 2005.

[85] B.H. Flowers. *An introduction to numerical methods in C++*. Clarendon Press, 1995.

[86] J. Smiley. *Learn to program Visual Basic objects*. Muska and Lipman, Jan 2001.

[87] P. Snaith. *The complete idiot's guide to C++*. Que Corp., Nov 1998.

[88] N. Kockler. *Numerical methods and scientific computing*. Oxford University Press, 1994.

[89] G.B. Ferraris and D. Manca. Bzzode: a new C++ class for the solution of stiff and non–stiff ordinary differential equation systems. *Computers and Chemical Engineering*, 22(11):1595–1621, 1998.

[90] Y.R. Lin-Liu, V.S. Chan, J.S. Degrassie, and H. Ikezi. Characteristic impedance of a soliton–bearing nonlinear transmission line. *Microwave and Optical Technology Letters*, 4:468–471, Oct 1991.

[91] S. Ibuka, M. Ohnishi, T. Yamada, K. Yasuoka, S. Ishii, and K. Kwang-Cheol. Voltage amplification effect of nonlinear transmission lines for fast high voltage pulse generation. In 11^{th} *IEEE International Pulsed Power Conference*, volume 2, pages 1548–1553, 1997.

[92] G.H. Rim, E.P. Pavlov, H.S. Lee, and J.S. Kim. Pulse forming lines for square pulse generators. In *Pulsed Power and Plasma Science Conference*, volume 2, pages 1225–1228, 2001.

[93] C.L. Ruthroff. Some broadband transformers. *Proceedings of the IRE*, 47:1337–1342, 1959.

[94] S Flach and C.R. Willis. Discrete breathers. In *eprint arXiv:patt-sol/9704004*, pages 4004–4066, 1997.

[95] P. Horowitz and W. Hill. *The art of electronics*. Cambridge University Press, 2 edition, Jul 1989.

[96] J. Kuffel, E. Kuffel, and W.S. Zaengl. *High voltage engineering: fundamentals*. Newnes, 2 edition, Jul 2000.

[97] J.O. Rossi and M. Ueda. Design of a 150 kV 300 A 100 Hz Blumlein coaxial pulser for long pulse operation. In 13^{th} *IEEE International Pulsed Power Conference*, volume 2, pages 1225–1228, 2001.

[98] E2V Technologies Hydrogen Thyratrons Preamble. http://www.e2v.com/assets/media/files/d

[99] Gamry Instruments Electrochemical Impedance Spectroscopy Application Note. http://www.gamry.com/app_notes/eis_primer/eis_primer_2007.pdf.

[100] P. Agarwal, M.E. Orazem, and L.H. Garcia-Rubio. Measurement models for electrochemical impedance spectroscopy. *Journal of the Electrochemical Society*, 139:1917–1927, July 1992.

[101] C.K. Campbell, J.D. van Wyk, M.F.K. Holm, J.J.R. Prinsloo, and J.J. Schoeman. Relaxation effects in high voltage barium titanate nonlinear ceramic disc capacitors. *IEEE Transactions on Components, Hybrids, and Manufacturing Technology*, 16:418–423, June 1993.

Appendix A

Matlab Implementation of Direct Method on KdV Equation

```
% N soliton solution to the KdV equation
% Based on the Direct Method by Hirota
% Jamie Darling, March 2008
% Pulsed Power and Plasma Physics Group
% Department of Engineering Science
% University of Oxford

% There will be 2^N main exponential terms

syms x;    % symbolic space
syms t;    % symbolic time

N = 4;

p = [0.8 1.0 1.2 1.4];
o = -1  (p.^3);
% syms n;
% syms q;
% syms f;
u = [-7.5 -2.5 2.5 7.5];
n1 = 0;
n2 = 0;
n3 = 0;
n4 = 0;
q = 0;
f = 0;
w = 0;



m = [0 0 0 0 0 0 0 0 1 1 1 1 1 1 1 1;
     0 0 0 0 1 1 1 1 0 0 0 0 1 1 1 1;
     0 0 1 1 0 0 1 1 0 0 1 1 0 0 1 1;
     0 1 0 1 0 1 0 1 0 1 0 1 0 1 0 1];


% m = m';

a = [0 0 0 0; 0 0 0 0; 0 0 0 0; 0 0 0 0];
A = [0 0 0 0; 0 0 0 0; 0 0 0 0; 0 0 0 0];

n1 = (p(1) * x) + (o(1) * t) + u(1);
n2 = (p(2) * x) + (o(2) * t) + u(2);
n3 = (p(3) * x) + (o(3) * t) + u(3);
n4 = (p(4) * x) + (o(4) * t) + u(4);



for i = 1:N
    % n_sm(i) = (p(i) * x) + (o(i) * t) + u(i);
    % n_sm = (p(i) * x) + (o(i) * t) + u(i);
    for j = 1:N
        a(i, j) = ((p(i) - p(j))^2) / ((p(i) + p(j))^2);
        if a(i, j) > 0
            A(i, j) = log(a(i, j));
        end
    end
end


A = m * A;



for k= 1:2^N

     q = 0;

     for i= 1:N
          % q = q + (m(i, k) * n_sm);
          if i== 1
              q = q + (m(i, k) * n1);
          end
```

```
    if i == 2
        q = q + (m(i, k) * n2);
    end
    if i == 3
        q = q + (m(i, k) * n3);
    end
    if i == 4
        q = q + (m(i, k) * n4);
    end
    for j = 1:N
        if i < j
            q = q + (m(i, k) * m(j, k) * A(i, j));
        end
    end
    end

    f = f + exp(q);

end


w = log(f);
w = diff(w, x);
w = diff(w, x);
w = 2 * w;

w

ezsurf(w)
```

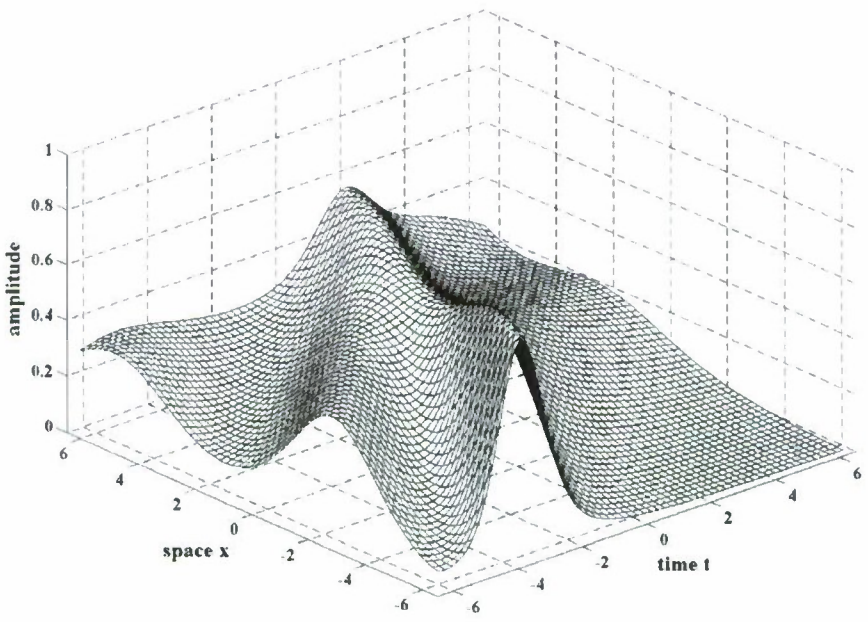

Appendix B

Periodic Cnoidal Wave Train Solution of KdV Equation with Elliptic Integrals

This appendix contains material relevant to chapter 4, specifically equation 4.23 and the graphs of figure 4.12 and figure 4.13, where a comparison is made between typical NLETL pulse burst waveforms and the strongly nonlinear periodic wave solution to the KdV equation. It is appropriate to consider periodic solutions given the NLETL generation of multiple pulse wave trains. Here the concept of elliptic integrals is introduced and their application to the KdV equation is mentioned, to offer some further explanation for the terminology seen in equation 4.23. A full and comprehensive analysis leading to this cnoidal solution is quite extensive and available in [82] and [69].

The periodic soliton solution is termed cnoidal due to the cn Jacobi elliptic integral function employed in its derivation. Elliptic integrals are often applied to the solution of nonlinear partial differential equations and may be defined as inverses of the elliptic integral

$$u(\phi) = \int_0^{\phi} \frac{\mathrm{d}\theta}{\sqrt{1 - m\sin^2\theta}} \tag{B.1}$$

where m is known as the 'parameter' and ϕ is the 'modulus'. From equation B.1 a total of 12 elliptic integral functions may be defined, such as sn $u = \sin\phi$ and cn $u = \cos\phi$. Given their dependence on u and m these are often written sn(u, m) and cn(u, m). For $m = 0$ this pair become equal to the trigonometric functions sin u and cos u, to which they may generally be considered analagous. This case will be seen below to give a periodic KdV solution in the linear limit, of purely sinusoidal profile. The nonlinear limiting wave is a single soliton arising when $m = 1$ and sn u and cn u become equal to tanh u and sech u respectively.

Equation 4.23 was written in a form derived in [69], by starting with the KdV equation in one of its convenient standard forms, where subscripts indicate differentiation

$$\psi_t - 6\psi\psi_x + \psi_{xxx} = 0. \tag{B.2}$$

Assuming standard travelling wave solutions $\psi(x, t) = f(\xi)$ where $\xi = x - ct$ the KdV equation

may be written in the following form [?], where A, B are constants of integration

$$\frac{1}{2}(f')^2 = f^3 + \frac{1}{2}cf^2 + Af + B = F(f). \tag{B.3}$$

It turns out that three zeros of $F(f)$ exist: f_1, f_2, f_3, and these terms appear in the periodic cnoidal solution of equation 4.23, repeated here as equation B.4.

$$f(\zeta) = f_2 - (f_2 - f_3)\mathrm{cn}^2\left[(\zeta - \zeta_3)(\frac{f_1 - f_3}{2})^{1/2}, m\right]. \tag{B.4}$$

Once again, it should be noted that when the modulus m is given a value of 1 the period of this solution becomes infinite. The familiar sech^2 soliton pulse profile results. For $m = 0$ the solution is a linear sinusoidal wave, but with intermediate values of modulus the cnoidal wave and its characteristic dependence of frequency on amplitude may be observed. This method of KdV solution is an alternative to that considered in more detail in section 4.3, is subject to fewer assumptions and may be extended to look at the infinitely periodic wave train solution corresponding to $m < 1$. Its implementation in Matlab is actually very straightforward thanks to `ellipj(u, m)` which returns an array [SN, CN, DN] containing the sn, cn and dn functions respectively:

```
% Periodic, as opposed to solitary, wave solution to the KdV
% equation using Jacobi elliptic integral functions

% Jamie Darling
% Pulsed Power and Plasma Physics Group
% Department of Engineering Science
% University of Oxford
% October 2008


u = linspace(0, 30, 1000);
m = linspace(0.95, 0.95, 1000);

f1 = 12;
f2 = 10;
f3 = 4;
f2v = linspace(f2, f2, 1000);

u_ = u + 5;
u_ = u_ * (((f1 - f3) / 2) ^ 0.5);

[SN, CN, DN] = ellipj(u_, m);

f = CN .* CN;
f = f * (f2 - f3);
f = f2v - f;

plot(u, -f);
```

Appendix C

Selected NLETL Simulation C++ Code

C.1 Outline and Naming Conventions

An object oriented (OOP) C++ numerical model of the NLETL system has been created in Microsoft Visual Studio 6.0 with the user interface illustrated in figure 5.1. The OOP approach facilitated ongoing development during the course of work on this thesis; code presented here corresponds to the latest application version, called nll_4. It is not practical to include certain extensive dialogue implementation code, and that corresponding to routine tasks such as data validation, nor a range of support files such as bitmap graphics. Objects are given a defining class structure, and a functional implementation, in .h header and .cpp source files respectively. Some of the files listed below form the overall application (`nll_4`, `stdafx`, `nll_4_dlg`) and handle data retrieval from the user, as well as declaring instances of the `nletl` object. The application supports parallel and ASP mode simulation and up to four instances of `nletl` are created for a given simulation. Each of these objects contain the data defining their line and its simulation environment, and functions to carry out incremental calculations of voltages and currents at each discrete stage position.

A fourth order Runge-Kutta method is employed and due to the large numbers of time steps typically required a range of data management capabilities were introduced. For example, an interval between data points being written to disc may be specified in order to generate binary output files of moderate size. A special time block array data type was also defined whereby 500 calculations are carried out between disc write operations; with a large number of stages there was too great a risk of memory overflows with all the data stored in array variables but a write to disc operation on every time step was far too time consuming. Where feasible memory pointers were preferred over passing huge amounts of data from function to function, and the naming conventions used to distinguish pointers, member variables etc. may be seen in the code below (comments begin with //). In addition to the binary output files, information including a date stamp and all simulation parameters is output to a series of text files.

C++ source files were converted to LaTeX format for inclusion in this thesis document using the cpp2latex 2.3 application available at http://cpp2latex.geodar.com.

C.2 Code Listing

C.2.1 nll_4.h

```
001 // nll_4.h : main header file for the NLL_4 application
002
003 #if !defined(AFX_NLL_4_H__D8FAF8DE_E187_4E9C_A5A6_3039A67BA108__INCLUDED_)
004 #define AFX_NLL_4_H__0BFAF80E_E1B7_4E9C_A5A6_3039A67BA108__INCLUOED_
005 #if _MSC_VER > 1000
006 #pragma once
007 #endif // _MSC_VER > 1000
008
009 #ifndef __AFXWIN_H__
010   #error include 'stdafx.h' before including this file for PCH
011 #endif
012
013 #include "resource.h"
014
015 class nll_4 : public CWinApp
016 {
017   public:
018     nll_4();
019   public:
020     virtual BOOL InitInstance();
021   OECLARE_MESSAGE_MAP()
022 };
023
024 #endif // !defined(AFX_NLL_4_H__0BFAF80E_E1B7_4E9C_A5A6_3039A67BA108__INCLUOED_)
```

C.2.2 nll_4.cpp

```
001 // nll_4.cpp : Defines the class behaviors for the application
002
003 #include "stdafx.h"
004 #include "nll_4.h"
005 #include "nll_4_dlg.h"
006
007 #ifdef _DE8UG
008 #define new OEBUG_NEW
009 #undef THIS_FILE
010 static char THIS_FILE[] = __FILE__;
011 #endif
012
013 BEGIN_MESSAGE_MAP(nll_4, CWinApp)
014 ON_COMMANO(ID_HELP, CWinApp::OnHelp)
015 ENO_MESSAGE_MAP()
016
017 nll_4::nll_4()    // nll_4 construction
018 {
019 }
020
021 nll_4 theApp;     // The one and only nll_4 object
022
023 800L nll_4::InitInstance()
024 {
025   AfxEnableControlContainer();
026
027 #ifdef _AFXDLL
028   Enable3dControls();
029 #else
030   Enable3dControlsStatic();
031 #endif
032
```

```
033   nll_4_dlg dlg;
034   m_pMainWnd = &dlg;
035   int nResponse = dlg.DoModal();
036   if (nResponse == IDOK)
037   {
038   }
039   else if (nResponse == IDCANCEL)
040   {
041   }
042   return FALSE;
043 }
```

C.2.3 stdafx.h

```
001 // stdafx.h : include file for standard system include files,
002 // or project specific include files that are used frequently, but
003 // are changed infrequently
004
005 #if !defined(AFX_STDAFX_H__89299502_0DD6_48B5_83A4_639EBABD6D69__INCLUDED_)
006 #define AFX_STDAFX_H__89299502_0DD6_48B5_83A4_639EBABD6D69__INCLUDED_
007
008 #if _MSC_VER > 1000
009 #pragma once
010 #endif // _MSC_VER > 1000
011
012 #define VC_EXTRALEAN        // Exclude rarely-used stuff from Windows headers
013
014 #include <afxwin.h>         // MFC core and standard components
015 #include <afxext.h>         // MFC extensions
016 #include <afxdisp.h>        // MFC Automation classes
017 #include <afxdtctl.h>       // MFC support for Internet Explorer 4 Common Controls
018 #ifndef _AFX_NO_AFXCMN_SUPPORT
019 #include <afxcmn.h>         // MFC support for Windows Common Controls
020 #endif // _AFX_NO_AFXCMN_SUPPORT
021
022 #endif // !defined(AFX_STDAFX_H__89299502_0DD6_48B5_83A4_639EBABD6D69__INCLUDED_))
```

C.2.4 stdafx.cpp

```
001 // stdafx.cpp : source file that includes just the standard includes
002 // nll_4.pch will be the pre-compiled header
003 // stdafx.obj will contain the pre-compiled type information
004
005 #include "stdafx.h""
```

C.2.5 nletl.h

```
001 #ifndef NLL_4H
002 #define NLL_4H
003
004 /*
005   m__ => member variable
006   p__ => pointer (possibly also a member variable)
007
008   Jamie Darling
009   2007 - 2008
010   Pulsed Power & Plasma Physics Group
011   Department of Engineering Science
012   University of Oxford
013
014   NLETL Line Class Definition
015
016   Incorporating the ability to run as part of a single line,
017   parallel or ASP mode simulation
018 */
019
020 namespace Soliton {
```

```
021
022 class nl_line {
023
024   typedef double tba[501];    // see pointers to multidimensional time block arrays
025
026   enum {FAIL, SUCCESS, COMPLETE} stepex;
027
028   public:
029
030     // constructor ('par_number' identifies line in multi-line simulations)
031     nl_line(int par_number, int par_c_stages, const double *par_cap, const double *par_res, const double
*par_ind,
032         const double *par_cnl_a, const double *par_cnl_b,
033         const double *par_lnl_a, const double *par_lnl_b, double par_r_term);
034
035     void set_scenario(double par_total_time, long par_no_t_steps, int par_write_interval, bool par_asp,
036       double par_gen_opi, const double *par_gen_ti, const double *par_gen_vi,
037       double par_bias_v, double par_bias_f);
038
039     // initiate simulation sequence under current line conditions (returns a stepex)
040     double vi_run(long time_step_tot, double external_vi);
041
042     // destructor
043     ~nl_line(void);
044
045   private:
046
047     // disable access to default constructor
048     nl_line(void);
049
050     int m__number;              // line identification number (1 to 4)
051     int m__c_stages;            // number of stages (capacitors) to this line
052     double m__total_time;       // actual time in seconds
053     long m__no_t_steps;         // number of processing steps to compute
054     int m__write_interval;      // interval between steps actually written to file
055     int m__write_int_cnt;       // object level counter for write interval purposes
056     bool m__asp;                // indicates whether or not line is part of an asp simulation
057     double m__bias_v;           // bias level amplitude to line in volts
058     double m__bias_f;           // bias frequency in rad per second based on cosine
059     double m__gen_opi;          // generator output impedance in ohms
060     double m__r_term;           // termination resistance in ohms
061
062     double m__r_ind;            // inductors series nonlinear resistance component
063     double m__r_ind_a;          // resistive nonlinearity factor a for above
064     double m__r_ind_b;          // resistive nonlinearity factor b for above
065
066     const double *p__cnl_a;     // capacitive nonlinearity factor a
067     const double *p__cnl_b;     // capacitive nonlinearity factor b
068     const double *p__lnl_a;     // inductive nonlinearity factor a
069     const double *p__lnl_b;     // inductive nonlinearity factor b
070
071     // these member pointers refer to variables provided upon object construction,
072     // assignment within the object being a pointer copy operation
073     const double *p__capacitors;
074     const double *p__resistors;
075     const double *p__inductors;
076
077     bool m__use_exploding_wires;// replace capacitors with opening switches
078     double m__blow_current;     // current at which switches open
079     bool *p__open;              // trip variable indicating stage wire has blown
080
081     // these member pointers refer to variables dynamically allocated and populated
082     // entirely within nl_line object procedures, pointing to an array of 501 doubles
083     // (see typedef double tba[501] above)
084     tba *p__line_voltage;
085     tba *p__line_current;
086
087     tba *p__write_v;
088     tba *p__write_i;
089
090     // input generator voltage waveform parameters, pointers to start of array
091     const double *p__gen_ti;    // up to 12 time points
092     const double *p__gen_vi;    // up to 12 voltage values
```

```
093
094
095     // private line functions for use by v_run:
096
097     // v_progression modified to return value for current or voltage to permit parallel and
098     // asp mode scenarios, current if parallel and voltage if asp
099     double vi_progression(long time_step_total, int time_step_block, double external_vi);
100
101     void initialise_io(bool info_header, bool column_titles);
102
103     void save_data(int from_level, int up_to_level, long prev_blocks);
104
105     double v_charge(double time_step, double time = -1);
106
107     double v_pulse(double pulse_time, double pulse_amp, double rise_time, double top_duration,
108                 double fall_time);
109
110     double linear_int(double t_low, double t_high, double t_actual,
111                 double v_low, double v_high);
112
113     double capacitance(double v, double i, double nom_cap, double a, double b,
114                 double cap_res, double step);
115
116     double nl_line::inductance(double i, double nom_ind);
117
118     double rk_analysis(double v_n_minus, double v_n, double v_n_plus, double i_n,
119                 double i_n_plus, double r_n, double l_n, double l_n_plus,
120                 double nom_cap, double a, double b, double step);
121
122     double diff_analysis(double v_n_minus, double v_n, double v_n_plus, double i_n,
123                 double i_n_plus, double r_n, double l_n, double l_n_plus,
124                 double nom_cap, double a, double b, double step);
125
126     double line_bias(double time_step);
127
128 };  // end of class nl_line
129
130 }   // end of namespace Soliton
131
132 #endif
```

C.2.6 nletl.cpp

```
001 // #pragma hdrstop
002 // #include <precomp.h>
003
004 /*
005   Jamie Darling
006   2007 - 2008
007   Pulsed Power & Plasma Physics Group
008   Department of Engineering Science
009   University of Oxford
010
011   NLETL Line Class Implementation
012 */
013
014 #include "stdafx.h"
015 #include "nletl.h"
016 #include "nll_4.h"
017 #include <iostream>
018 #include <fstream>
019 #include <stdlib.h>
020 #include <stdio.h>
021 #include <string>
022 #include <math.h>
023 #include <time.h>
024
025 using namespace std;
026
027 // #pragma package(smart_init)
028
```

```
029 namespace Soliton {
030
031 nl_line::nl_line(int par_number, int par_c_stages, const double *par_cap, const double *par_res, const double
*par_ind,
032         const double *par_cnl_a, const double *par_cnl_b,
033         const double *par_lnl_a, const double *par_lnl_b, double par_r_term)
034 {
035   // -+- nl_line object constructor -+-
036
037   m__number = par_number;
038
039   m__c_stages = par_c_stages;
040
041   p__capacitors = par_cap;
042   p__resistors = par_res;
043   p__inductors = par_ind;
044
045   p__cnl_a = par_cnl_a;
046   p__cnl_b = par_cnl_b;
047   p__lnl_a = par_lnl_a;
048   p__lnl_b = par_lnl_b;
049
050   m__r_term = par_r_term;
051
052   m__r_ind = 0;           // NLR capability
053   m__r_ind_a = 1;
054   m__r_ind_b = 1e99;
055 }
056
057
058 nl_line::~nl_line(void)
059 {
060   // -+- nl_line object destructor -+-
061
062   delete [] p__line_voltage;
063   delete [] p__line_current;
064 }
065
066
067 void nl_line::set_scenario(double par_total_time, long par_no_t_steps, int par_write_interval, bool par_asp,
068                double par_gen_opi, const double *par_gen_ti, const double *par_gen_vi,
069                double par_bias_v, double par_bias_f)
070 {
071   // -+- part of process of initialising a given line object, with some further parameters not
072   // previously set within constructor and standard initial values -+-
073
074   m__total_time = par_total_time;
075   m__no_t_steps = par_no_t_steps;
076   m__write_interval = par_write_interval;
077   //m__write_int_cnt = -1;
078   m__asp = par_asp;
079
080   m__gen_opi = par_gen_opi;
081   p__gen_ti = par_gen_ti;
082   p__gen_vi = par_gen_vi;
083
084   m__bias_v = par_bias_v;
085   m__bias_f = par_bias_f;
086
087   m__write_int_cnt = 0;
088
089   m__use_exploding_wires = 0;   // option to replace CNL with opening switch
090   m__blow_current = 100;
091
092   // dynamically allocate an array of pointers, each pointing to an array of 501 doubles,
093   // for voltage and current data corresponding to a single time block
094   // allocate an array of (par_c_stages + 2) tba's and return pointer to first element,
095   // each tba is an array of 501 pointers
096   // dereference as follows:
097   //
098   //    (*(p__line_voltage + stage))[timestep];
099   //
100   p__line_voltage = new tba[m__c_stages + 2]();
```

```
101   p__line_current = new tba[m__c_stages + 2]();
102
103   p__write_v = new tba[m__c_stages + 2]();
104   p__write_i = new tba[m__c_stages + 2]();
105
106   p__open = new bool[m__c_stages]();
107
108
109   int tmp_time_step, tmp_stage;
110
111   for(tmp_stage = 0; tmp_stage < m__c_stages + 2; tmp_stage++)
112   {
113     for(tmp_time_step = 0; tmp_time_step < 501; tmp_time_step++)
114     {
115       (*(p__line_voltage + tmp_stage))[tmp_time_step] = 0.0;
116       (*(p__line_current + tmp_stage))[tmp_time_step] = 0.0;
117
118       (*(p__write_v + tmp_stage))[tmp_time_step] = 0.0;
119       (*(p__write_i + tmp_stage))[tmp_time_step] = 0.0;
120
121       *(p__open + tmp_stage) = 0;    // set all stage wires to not blown
122     }
123   }
124
125   (*(p__line_voltage + 0))[0] = v_charge(0);
126
127   initialise_io(true, false);
128 }
129
130
131 double nl_line::vi_run(long time_step_tot, double external_vi)
132 {
133   // -+- run vi_progression for the actual time step, time_step_tot, and return current status of simulation
134   // via outcome for error catching and to terminate upon completion, also here manage time step blocks
135   // which are filled with data between disc write operations -+-
136
137   if(time_step_tot < 1 || time_step_tot > m__no_t_steps) return(-1E9);  // stepex enumeration FAIL
138
139   static int time_step_blk[4] = {1, 1, 1, 1};// zeroth block time step is intermediate initial condition
140   static int blk_count[4] = {0, 0, 0, 0};    // number of data blocks previously processed & written to file
141
142   static int write_tsb[4] = {1, 1, 1, 1};
143   static int write_blc[4] = {0, 0, 0, 0};
144
145   if(time_step_tot == 1)
146   {
147     blk_count[m__number - 1] = 0;        // n.b. static declarations
148     write_blc[m__number - 1] = 0;
149   }
150
151   int tmp_stage = 0;
152
153   m__write_int_cnt++;
154   if(m__write_int_cnt == m__write_interval) m__write_int_cnt = 0;
155
156   // see nl_line::v_progression for details of what 'outcome' might contain
157   double outcome = vi_progression(time_step_tot, time_step_blk[m__number - 1], external_vi);
158
159   if(m__write_int_cnt == 0)
160   {
161     for(tmp_stage = 0; tmp_stage <= m__c_stages + 1; tmp_stage++)
162     {
163       (*(p__write_v + tmp_stage))[write_tsb[m__number - 1]] = (*(p__line_voltage +
tmp_stage))[time_step_blk[m__number - 1]];
164       (*(p__write_i + tmp_stage))[write_tsb[m__number - 1]] = (*(p__line_current +
tmp_stage))[time_step_blk[m__number - 1]];
165     }
166
167     write_tsb[m__number - 1]++;
168
169     if(write_tsb[m__number - 1] == 501)  // time block is full; write data to disc and reset
170     {
171       write_tsb[m__number - 1] = 1;
```

```
172
173       save_data(0, 499, write_blc[m__number - 1]);
174
175       write_blc[m__number - 1]++;
176
177       for(tmp_stage = 0; tmp_stage <= m__c_stages + 1; tmp_stage++)
178       {
179         (*(p__write_v + tmp_stage))[0] = (*(p__write_v + tmp_stage))[500];
180         (*(p__write_i + tmp_stage))[0] = (*(p__write_i + tmp_stage))[500];
181       }
182     }
183   }
184
185   time_step_blk[m__number - 1]++;
186
187   if(time_step_blk[m__number - 1] == 501)  // next process step would overflow time block array array;
188   {                                        // need to save this data block and overwrite data in memory
189     time_step_blk[m__number - 1] = 1;
190
191     // append o/p data (final entry saved with subsequent data block)
192     // save_data(0, 499, blk_count[m__number - 1]);
193
194     // increment count of data blocks processed
195     blk_count[m__number - 1]++;
196
197     // copy final entries in time block array to start positions stage by stage
198     for(tmp_stage = 0; tmp_stage <= m__c_stages + 1; tmp_stage++)
199     {
200       (*(p__line_voltage + tmp_stage))[0] = (*(p__line_voltage + tmp_stage))[500];
201       (*(p__line_current + tmp_stage))[0] = (*(p__line_current + tmp_stage))[500];
202     }
203   }
204
205   // if this is the final time step, write remaining data in time block array to files
206   if(time_step_tot == m__no_t_steps && write_tsb[m__number - 1] != 1){
207                     // i.e. still some data left to be output from arrays
208                     // partially occupied final (or indeed only) time block
209     // save_data(0, m__no_t_steps - ((blk_count[m__number - 1]) * 500), block_count[m__number - 1]);
210     save_data(0, write_tsb[m__number - 1] - 1, write_blc[m__number - 1]);
211     return(+1E9);     // stepex enumeration COMPLETE
212   }
213   else if(time_step_tot == m__no_t_steps)
214                     // running time exact multiple of 500 steps, but
215   {                 // final entry wasn't written
216     save_data(500, 500, write_blc[m__number - 1] - 1);
217     return(+1E9);     // stepex enumeration COMPLETE
218   }
219   else
220   {
221     return(outcome); // stepex enumeration SUCCESS
222   }
223 }
224
225
226 double nl_line::vi_progression(long time_step_total, int time_step_block, double external_vi)
227 {
228   // -+- populates line_voltage array for all nletl stages at time (step) given
229   // but not for 0th (initial condition) time step -+-
230
231   int tmp_stage = 0;
232   double time_int = m__total_time / m__no_t_steps;
233   double v_ind = 0.0;     // used to take into account effect of series nonlinear resistor
234   double r_ind = 0.0;     // calculation of above value, currently only fixed value for whole line
235
236   // const double GEN_POW = 8.0;
237
238   // input before first inductor (stage 0) and before any line bias isolation
239   (*(p__line_voltage + 0))[time_step_block] = v_charge(time_step_total) -
240                 ((*(p__line_current + 1))[abs(time_step_block - 1)] * m__gen_opi);
241
242   for(tmp_stage = 1; tmp_stage <= m__c_stages; tmp_stage ++)          // stages (1 to N)
243   {
244     //(*(p__line_voltage + tmp_stage))[time_step_block] = line_bias(time_step_total);
```

```
245
246     if(!m__use_exploding_wires)
247     {
248       (*(p__line_voltage + tmp_stage))[time_step_block] =
249         rk_analysis((*(p__line_voltage + tmp_stage - 1))[time_step_block - 1],
250           (*(p__line_voltage + tmp_stage    ))[time_step_block - 1],
251           (*(p__line_voltage + tmp_stage + 1))[time_step_block - 1],
252           (*(p__line_current + tmp_stage    ))[time_step_block - 1],
253           (*(p__line_current + tmp_stage + 1))[time_step_block - 1],
254           *(p__resistors + tmp_stage - 1),
255           inductance((*(p__line_current + tmp_stage    ))[time_step_block - 1], *(p__inductors + tmp_stage -
1)) * 1E-9,
256           inductance((*(p__line_current + tmp_stage + 1))[time_step_block - 1], *(p__inductors + tmp_stage))
* 1E-9,
257           *(p__capacitors + tmp_stage - 1) * 1E-12,
258           *(p__cnl_a + tmp_stage - 1), *(p__cnl_b + tmp_stage - 1),
259           time_step_total);
260     }
261     else
262     {
263       if(*(p__open + tmp_stage - 1))
264       {
265         // switch opens / fuse blows
266         // to avoid numerical problems model this as a large increase in resistance i.e. not perfect switch
267         (*(p__line_voltage + tmp_stage))[time_step_block] = 1e2 * *(p__resistors + tmp_stage - 1) *
268               ((*(p__line_current + tmp_stage))[time_step_block - 1] - (*(p__line_current + tmp_stage +
1))[time_step_block - 1]);
269       }
270       else
271       {
272         (*(p__line_voltage + tmp_stage))[time_step_block] = *(p__resistors + tmp_stage - 1) *
273               ((*(p__line_current + tmp_stage))[time_step_block - 1] - (*(p__line_current + tmp_stage +
1))[time_step_block - 1]);
274       }
275     }
276
277     // offset in rnl set here to 1 amp
278     // if((*(p__line_current + tmp_stage))[time_step_block - 1] < 1)
279     // {
280       r_ind = m__r_ind;
281     // }
282     // else
283     // {
284     //   r_ind = m__r_ind * (m__r_ind_a + ((1 - m__r_ind_a) * exp(-1 * fabs(((*(p__line_current +
tmp_stage))[time_step_block - 1] - 1) / m__r_ind_b))));
285     // }
286
287     v_ind = (*(p__line_voltage + tmp_stage - 1))[time_step_block - 1] - (*(p__line_voltage +
tmp_stage))[time_step_block - 1] - ((*(p__line_current + tmp_stage))[time_step_block - 1] * r_ind);
288
289     (*(p__line_current + tmp_stage))[time_step_block] =  (*(p__line_current + tmp_stage))[time_step_block -
1] + (time_int * v_ind /
290                                 (inductance((*(p__line_current + tmp_stage))[time_step_block - 1],
*(p__inductors + tmp_stage - 1)) * 1E-9));
291
292     // if((*(p__line_current + tmp_stage))[time_step_block - 1] - (*(p__line_current + tmp_stage +
1))[time_step_block - 1] > m__blow_current)
293     // {
294     //   *(p__open + tmp_stage - 1) = 1;
295     // }
296   }
297
298   // option to drive line from both ends
299   // (*(p__line_voltage + m__c_stages + 1))[time_step_block] = v_charge(time_step_total);
300
301   // output after last inductor (stage N + 1) and after any line bias isolation,
302   // taking into account any other parallel or asp connected lines
303
304   // - - - - - - - - -
305
306   // normal linear resistive termination:
307   //(*(p__line_voltage + m__c_stages + 1))[time_step_block] =  (*(p__line_current + m__c_stages +
1))[time_step_block - 1] * m__r_term;
```

```
308
309   // nonlinear resistive termination to match nletl characteristic impedance:
310   /*double z_ch = sqrt(inductance((*(p__line_current + m__c_stages + 1))[time_step_block - 1], *(p__inductors +
m__c_stages) * 1E-9)
311     / capacitance((*(p__line_voltage + m__c_stages + 1))[time_step_block - 1],
312     (*(p__line_current + m__c_stages - 1))[time_step_block - 1] - (*(p__line_current +
m__c_stages))[time_step_block - 1],
313     *(p__capacitors + m__c_stages - 1) * 1E-12, *(p__cnl_a + m__c_stages - 1), *(p__cnl_b + m__c_stages - 1),
314     *(p__resistors + m__c_stages - 1), time_step_total));*/
315   // double z_ch = *(p__inductors + m__c_stages) * 1E-9; // or use this
316   /*z_ch = z_ch / capacitance((*(p__line_voltage + m__c_stages + 1))[time_step_block - 1],
317       (*(p__line_current + m__c_stages - 1))[time_step_block - 1] - (*(p__line_current +
m__c_stages))[time_step_block - 1],
318       *(p__capacitors + m__c_stages - 1) * 1E-12, *(p__cnl_a + m__c_stages - 1), *(p__cnl_b + m__c_stages -
1),
319       *(p__resistors + m__c_stages - 1), time_step_total);
320   z_ch = sqrt(z_ch);*/
321
322   // normal termination:
323   z_ch = m__r_term;
324
325   (*(p__line_voltage + m__c_stages + 1))[time_step_block] = (*(p__line_current + m__c_stages +
1))[time_step_block - 1] * z_ch;
326
327   // - - - - - - - - -
328
329   if(m__asp)
330   {
331     (*(p__line_voltage + m__c_stages + 1))[time_step_block] += external_vi;
332   }
333   else
334   {
335     (*(p__line_voltage + m__c_stages + 1))[time_step_block] += (external_vi * m__r_term);
336   }
337
338   // don't apply nlr to final inductor
339   //r_ind = m__r_ind * (m__r_ind_a + ((1 - m__r_ind_a) * exp(-1 * fabs((*(p__line_current + m__c_stages +
1))[time_step_block - 1] / m__r_ind_b))));
340
341   v_ind = (*(p__line_voltage + m__c_stages))[time_step_block - 1] - (*(p__line_voltage + m__c_stages +
1))[time_step_block - 1]; //- ((*(p__line_current + m__c_stages + 1))[time_step_block - 1] * r_ind);
342
343   (*(p__line_current + m__c_stages + 1))[time_step_block] =  (*(p__line_current + m__c_stages +
1))[time_step_block - 1] + (time_int * v_ind /
344                               (inductance((*(p__line_current + m__c_stages + 1))[time_step_block - 1],
*(p__inductors + m__c_stages)) * 1E-9));
345
346   // return the voltage or current value required for any other lines in the simulation
347   if(m__asp)  // other asp line requires voltage
348   {
349     return((*(p__line_voltage + m__c_stages + 1))[time_step_block]);
350   }
351   else    // any other parallel lines require current, may as well return even if single line
352   {
353     return((*(p__line_current + m__c_stages + 1))[time_step_block]);
354   }
355 }
356
357
358 void nl_line::initialise_io(bool include_info, bool include_columns)
359 {
360   // -+- deletes any old data files in working directory, creates new files and
361   //     appends header information and / or column titles as appropriate -+-
362
363   // delete any existing data files and create appropriate string name for
364   // data and information output files
365   std::string ofile_v = "";
366   std::string ofile_i = "";
367   std::string ofile_x = "";
368
369   switch(m__number)
370   {
371   case 1:
```

```
372     remove("nll4_data_v_1.dat");
373     remove("nll4_data_i_1.dat");
374     remove("nll4_data_info_1.txt");
375     ofile_v = "nll4_data_v_1.dat";
376     ofile_i = "nll4_data_i_1.dat";
377     ofile_x = "nll4_data_info_1.txt";
378     break;
379   case 2:
380     remove("nll4_data_v_2.dat");
381     remove("nll4_data_i_2.dat");
382     remove("nll4_data_info_2.txt");
383     ofile_v = "nll4_data_v_2.dat";
384     ofile_i = "nll4_data_i_2.dat";
385     ofile_x = "nll4_data_info_2.txt";
386     break;
387   case 3:
388     remove("nll4_data_v_3.dat");
389     remove("nll4_data_i_3.dat");
390     remove("nll4_data_info_3.txt");
391     ofile_v = "nll4_data_v_3.dat";
392     ofile_i = "nll4_data_i_3.dat";
393     ofile_x = "nll4_data_info_3.txt";
394     break;
395   case 4:
396     remove("nll4_data_v_4.dat");
397     remove("nll4_data_i_4.dat");
398     remove("nll4_data_info_4.txt");
399     ofile_v = "nll4_data_v_4.dat";
400     ofile_i = "nll4_data_i_4.dat";
401     ofile_x = "nll4_data_info_4.txt";
402     break;
403   }
404
405   // stream object bound to given o/p file, with output in append mode
406   //cout << " ---> stage voltages...";
407   ofstream outfile_v(ofile_v.c_str(), ios::out | ios::binary | ios::app);
408   ofstream outfile_i(ofile_i.c_str(), ios::out | ios::binary | ios::app);
409   ofstream outfile_x(ofile_x.c_str(), ios::out | ios::app);
410   //cout << "  0";
411
412   // check i/o successful this far
413   if(!outfile_v || !outfile_i || !outfile_x)
414   {
415   }
416
417   // get the current time and date (will still require conversion for string output)
418   time_t raw_time;
419   time(&raw_time);
420
421   int tmp_stg;
422   int tmp_gmk;
423
424   outfile_x  << "nll_4.cpp (gui app via class nl_line) Numerical Simulation ~ Nonlinear Soliton-Generating
Delay Line\n"
425         << "- - - - - - - - - - - - - - - - - - - - - - - - - - - - - - - - - - - - - - - - - - - - - - - -
- \n\n\n";
426   outfile_x  << "LINE NUMBER : " << m__number << "\n\n\n";
427
428   outfile_x   << "Voltage data (nll4_data_v_x.dat), Current data (nll4_data_i_x.dat)\n created as of "
429         << ctime(&raw_time) << "\n\n"
430         << "This nletl was initialised with...\n\n\n";
431
432   outfile_x  << "Number of discrete stages : " << m__c_stages << "\n";
433   outfile_x  << "Total simulation running time : " << m__total_time << " seconds" << "\n";
434   outfile_x  << "Number of time steps processed : " << m__no_t_steps << "\n";
435   outfile_x  << "Write Interval : " << m__write_interval << "\n";
436   outfile_x  << "Part of asp simulation? : " << m__asp << "\n\n";
437
438   outfile_x  << "Discrete inductor values (" << m__c_stages + 1 << ", nH) :\n\n";
439
440   for(tmp_stg = 0; tmp_stg <= m__c_stages; tmp_stg++)
441   {
442     outfile_x << "St." << tmp_stg << " " << *(p__inductors + tmp_stg);
```

```
443     if(tmp_stg != m__c_stages) outfile_x << "; ";
444   }
445
446   outfile_x  << "\n\n";
447   outfile_x  << "Discrete nominal capacitor values (" << m__c_stages << ", pF) :\n\n";
448
449   for(tmp_stg = 0; tmp_stg < m__c_stages; tmp_stg++)
450   {
451     outfile_x << "St." << tmp_stg << " " << *(p__capacitors + tmp_stg);
452     if(tmp_stg != m__c_stages - 1) outfile_x << "; ";
453   }
454
455   outfile_x  << "\n\n";
456   outfile_x  << "Discrete capacitor esr values (" << m__c_stages << ", ohm) :\n\n";
457
458   for(tmp_stg = 0; tmp_stg < m__c_stages; tmp_stg++)
459   {
460     outfile_x << "St." << tmp_stg << " " << *(p__resistors + tmp_stg);
461     if(tmp_stg != m__c_stages - 1) outfile_x << "; ";
462   }
463
464   outfile_x  << "\n\n";
465   outfile_x  << "Capacitive nonlinearity factor a : " << *p__cnl_a << "\n";
466   outfile_x  << "Capacitive nonlinearity factor b : " << *p__cnl_b << "\n";
467   outfile_x  << "Inductive nonlinearity factor a : " << *p__lnl_a << "\n";
468   outfile_x  << "Inductive nonlinearity factor b : " << *p__lnl_b << "\n\n";
469
470   outfile_x  << "Input waveform time markers :\n\n";
471
472   for(tmp_gmk = 1; tmp_gmk <= 12; tmp_gmk++)
473   {
474     outfile_x << "No." << tmp_gmk << " " << *(p__gen_ti + tmp_gmk - 1);
475     if(tmp_gmk != 12) outfile_x << "; ";
476   }
477
478   outfile_x  << "\n\n";
479   outfile_x  << "Input waveform voltage markers :\n\n";
480
481   for(tmp_gmk = 1; tmp_gmk <= 12; tmp_gmk++)
482   {
483     outfile_x << "No." << tmp_gmk << " " << *(p__gen_vi + tmp_gmk - 1);
484     if(tmp_gmk != 12) outfile_x << "; ";
485   }
486
487   outfile_x  << "\n\n";
488   outfile_x  << "Generator output impedance : " << m__gen_opi << " ohm\n\n";
489   outfile_x  << "Line termination : " << m__r_term << " ohm\n\n";
490   outfile_x  << "- - - -";
491
492   if(include_columns)    // include column titles prior to data
493   {
494     int tmp_col;
495
496     outfile_v << "time ";
497
498     for(tmp_col = 0; tmp_col <= m__c_stages; tmp_col++)
499     {
500       outfile_v << "Vstage" << tmp_col << " ";
501     }
502
503     outfile_v << "Vstage" << m__c_stages + 1 << endl;
504
505     outfile_i << "time, ";
506
507     for(tmp_col = 0; tmp_col <= m__c_stages; tmp_col++)
508     {
509       outfile_i << "Istage" << tmp_col << " ";
510     }
511
512     outfile_i << "Istage" << m__c_stages + 1 << endl;
513   }
514 }
515
```

```
516
517 void nl_line::save_data(int from_level, int to_level, long prev_blocks)
518 {
519   // -+- saves voltage and current data to appropriate binary files -+-
520
521   // string name of data o/p file
522   std::string ofile_v = "";
523   std::string ofile_i = "";
524
525   switch(m__number)
526   {
527   case 1:
528     ofile_v = "nll4_data_v_1.dat";
529     ofile_i = "nll4_data_i_1.dat";
530     break;
531   case 2:
532     ofile_v = "nll4_data_v_2.dat";
533     ofile_i = "nll4_data_i_2.dat";
534     break;
535   case 3:
536     ofile_v = "nll4_data_v_3.dat";
537     ofile_i = "nll4_data_i_3.dat";
538     break;
539   case 4:
540     ofile_v = "nll4_data_v_4.dat";
541     ofile_i = "nll4_data_i_4.dat";
542     break;
543   }
544
545   // stream object bound to given o/p file, with output in append mode
546   ofstream outfile_v(ofile_v.c_str(), ios::out | ios::binary | ios::app);
547   ofstream outfile_i(ofile_i.c_str(), ios::out | ios::binary | ios::app);
548
549   // check i/o successful this far
550   if(!outfile_v || !outfile_i)
551   {
552     cerr << "I/O Error: Unable to open file(s) for Output" << endl << endl;
553   }
554
555   int tmp_dline = 0;
556   int tmp_stage = 0;
557
558   double time = 0.0;    // we will include a time column, in seconds
559
560   for(tmp_dline = from_level; tmp_dline <= to_level; tmp_dline++)
561   {
562     time = ((tmp_dline + (prev_blocks * 500)) / m__no_t_steps) * m__total_time;  // n.b. priority forced with
numerical conditioning in mind
563
564     time = tmp_dline + (500 * prev_blocks);
565     time /= m__no_t_steps;
566     time *= m__total_time;
567
568     time *= m__write_interval;
569
570     outfile_v << time << " ";
571     outfile_i << time << " ";
572
573     // generator output (only include column if gen opi is not zero)
574     if(m__gen_opi > 0)
575     {
576       outfile_v << v_charge(0, time) << " ";
577       outfile_i << (*(p__write_i + 0))[tmp_dline] << " ";
578     }
579
580     // stage 0 is line input after generator output impedance
581     for(tmp_stage = 0; tmp_stage <= m__c_stages; tmp_stage++)
582     {
583       outfile_v << (*(p__write_v + tmp_stage))[tmp_dline] << " ";
584       outfile_i << (*(p__write_i + tmp_stage))[tmp_dline] << " ";
585     }
586
587     outfile_v << (*(p__write_v + m__c_stages + 1))[tmp_dline] << endl;
```

```
588     outfile_i << (*(p__write_i + m__c_stages + 1))[tmp_dline] << endl;
589   }
590
591   outfile_v.close();
592   outfile_i.close();
593 }
594
595
596 double nl_line::v_charge(double time_step, double time)
597 {
598   // -+- returns charging voltage as supplied by pulse input to line for real time t -+-
599
600   double time_actual = 0;
601
602   if(time == -1)
603   {
604     time_actual = m__total_time * time_step / m__no_t_steps;
605   }
606   else
607   {
608     time_actual = time;
609   }
610
611   // generate aribrary waveform via linear interpolation between from 1 to 12
612   // time-voltage points supplied
613   // m__gen_ti are set to -1 if not used, meaning final else statement will be
614   // executed when all used markers have been covered
615   if(*(p__gen_ti + 0) >= time_actual)
616   {
617     return(linear_int(0, *(p__gen_ti + 0), time_actual, 0, *(p__gen_vi + 0)));
618   }
619
620   for(int tmp = 1; tmp <= 11; tmp++)
621   {
622     if(*(p__gen_ti + tmp) >= time_actual)
623     {
624       return(linear_int(*(p__gen_ti + tmp - 1), *(p__gen_ti + tmp), time_actual,
625                         *(p__gen_vi + tmp - 1), *(p__gen_vi + tmp)));
626     }
627     else if(*(p__gen_ti + tmp) == -1)
628     {
629       return(linear_int(*(p__gen_ti + tmp - 1), m__total_time, time_actual,
630                         *(p__gen_vi + tmp - 1), 0));
631     }
632   }
633
634   return(0);
635 }
636
637
638 double nl_line::linear_int(double t_low, double t_high, double t_actual,
639                            double v_low, double v_high)
640 {
641   // -+- return voltage value from linear line joining two data points -+-
642
643   return(v_low + ((v_high - v_low) * ((t_actual - t_low) / (t_high - t_low))));
644 }
645
646
647 double nl_line::v_pulse(double pulse_time, double pulse_amp, double rise_time, double top_duration,
648                         double fall_time)
649 {
650   // -+- returns a linear ramp rise and fall time charging voltage from leading edge
651   // time of a single pulse -+-
652
653   double v_p;
654   double const PI = 3.14159;
655   double const large = 5E7;
656
657   if(pulse_time < rise_time) {
658     v_p = (pulse_time / rise_time) * pulse_amp;
659   } else if(pulse_time < rise_time + top_duration) {
660     v_p = pulse_amp;
```

```
661
662     // v_p += (pulse_amp * 0.5) * sin(8 * PI * (pulse_time - rise_time) / top_duration);
663
664   } else if(pulse_time < rise_time + top_duration + fall_time) {
665     v_p = pulse_amp - (((pulse_time - (rise_time + top_duration)) / fall_time) * pulse_amp);
666   } else {
667     v_p = 0;
668   }
669
670   return(v_p);
671 }
672
673
674 double nl_line::capacitance(double v, double i, double nom_cap, double a, double b,
675                 double cap_res, double step)
676 {
677   // -+- returns a capacitance value for a given voltage, and current through RC combination
678   // accounts for nonlinear function with voltage -+-
679
680   v = v + line_bias(step);                    // add on any line bias present
681
682   double v_cap = v - (i * cap_res);           // voltage actually across capacitor
683
684   return(nom_cap * (a + ((1 - a) * exp(-1 * fabs(v_cap / b)))));  // a is one means no nonlin
685 }
686
687
688 double nl_line::inductance(double i, double nom_ind)
689 {
690   // -+- returns an inductance value for a given current, accounts for nonlinear function with current -+-
691
692   double a = *(p__lnl_a + 0);
693   double b = *(p__lnl_b + 0);
694
695   return(nom_ind * (a + ((1 - a) * exp(-1 * fabs(i / b)))));    // a is one means no cnl
696 }
697
698
699 double nl_line::rk_analysis(double v_n_minus, double v_n, double v_n_plus, double i_n,
700                 double i_n_plus, double r_n, double l_n, double l_n_plus,
701                 double nom_cap_n, double a, double b, double step)
702 {
703   // -+- returns fourth order runge-kutta approximation for voltage at new time step -+-
704
705   double time_int = m__total_time / m__no_t_steps;
706
707   double k1, k2, k3, k4;
708
709   k1 = time_int * diff_analysis(v_n_minus, v_n      , v_n_plus, i_n, i_n_plus, r_n, l_n, l_n_plus, nom_cap_n,
a, b, step);
710
711   k2 = time_int * diff_analysis(v_n_minus, v_n + (k1 / 2)  , v_n_plus, i_n, i_n_plus, r_n, l_n, l_n_plus,
nom_cap_n, a, b, step);
712
713   k3 = time_int * diff_analysis(v_n_minus, v_n + (k2 / 2)  , v_n_plus, i_n, i_n_plus, r_n, l_n, l_n_plus,
nom_cap_n, a, b, step);
714
715   k4 = time_int * diff_analysis(v_n_minus, v_n + k3    , v_n_plus, i_n, i_n_plus, r_n, l_n, l_n_plus,
nom_cap_n, a, b, step);
716
717   return(v_n + (k1 / 6) + (k2 / 3) + (k3 / 3) + (k4 / 6));
718 }
719
720
721 double nl_line::diff_analysis(double v_n_minus, double v_n, double v_n_plus, double i_n,
722                 double i_n_plus, double r_n, double l_n, double l_n_plus,
723                 double nom_cap_n, double a, double b, double step)
724 {
725   // -+- returns a value for delta-vn / delta-t via the appropriate differential difference eqn -+-
726
727   double diff = (i_n - i_n_plus) / capacitance(v_n, i_n - i_n_plus, nom_cap_n, a, b, r_n, step);
728
729   diff += r_n * (v_n_minus - v_n) / l_n;
```

```
730   diff -= r_n * (v_n - v_n_plus) / l_n_plus;
731
732   return(diff);
733 }
734
735
736 double nl_line::line_bias(double time_step)
737 {
738   // -+- returns a value in volts for bias on line given specified amplitude, frequency and time -+-
739
740   double const PI = 3.14159;
741   double time_actual = m__total_time * time_step / m__no_t_steps;
742
743   return(m__bias_v * cos(2 * PI * m__bias_f * time_actual));
744 }
745
746
747 }  // end of namespace Soliton
```

C.2.7 nll_4_dlg.h

```
001 // nll_4_dlg.h : header file
002
003 #if !defined(AFX_NLL_4_DLG_H__31C1A78B_AC80_437A_B6E2_D1175A773A94__INCLUDED_)
004 #define AFX_NLL_4_DLG_H__31C1A78B_AC80_437A_B6E2_D1175A773A94__INCLUDED_
005
006 #if _MSC_VER > 1000
007 #pragma once
008 #endif // _MSC_VER > 1000
009
010 // nll_4_dlg dialog
011
012 class nll_4_dlg : public CDialog
013 {
014 // Construction
015 public:
016   nll_4_dlg(CWnd* pParent = NULL);  // standard constructor
017
018 // Dialog Data
019   //{{AFX_DATA(nll_4_dlg)
020   enum { IDD = IDD_NLL_4_DIALOG };
021
022     // **** EXTENSIVE DIALOGUE IMPLEMENTATION CODE NOT INCLUDED ****
023
024   //}}AFX_DATA
025
026   // ClassWizard generated virtual function overrides
027   //{{AFX_VIRTUAL(nll_4_dlg)
028   protected:
029   virtual void DoDataExchange(CDataExchange* pDX);  // DDX/DDV support
030   //}}AFX_VIRTUAL
031
032 // Implementation
033 protected:
034   HICON m_hIcon;
035
036   // Generated message map functions
037   //{{AFX_MSG(nll_4_dlg)
038
039     // **** EXTENSIVE DIALOGUE IMPLEMENTATION CODE NOT INCLUDED ****
040
041   //}}AFX_MSG
042   DECLARE_MESSAGE_MAP()
043
044 private:
045
046   CBitmap bmp_noline, bmp_single, bmp_double, bmp_triple, bmp_quadru, bmp_asp;
047
048   double *p__capacitors_1;
049   double *p__inductors_1;
050   double *p__resistors_1;
```

```
051   double *p__capacitors_2;
052   double *p__inductors_2;
053   double *p__resistors_2;
054   double *p__capacitors_3;
055   double *p__inductors_3;
056   double *p__resistors_3;
057   double *p__capacitors_4;
058   double *p__inductors_4;
059   double *p__resistors_4;
060
061   //bool *p__open_1;
062   //bool *p__open_2;
063   //bool *p__open_3;
064   //bool *p__open_4;
065
066   double *p__cnl_a_1;
067   double *p__cnl_b_1;
068   double *p__lnl_a_1;
069   double *p__lnl_b_1;
070   double *p__cnl_a_2;
071   double *p__cnl_b_2;
072   double *p__lnl_a_2;
073   double *p__lnl_b_2;
074   double *p__cnl_a_3;
075   double *p__cnl_b_3;
076   double *p__lnl_a_3;
077   double *p__lnl_b_3;
078   double *p__cnl_a_4;
079   double *p__cnl_b_4;
080   double *p__lnl_a_4;
081   double *p__lnl_b_4;
082
083   double gen_ti[12], gen_vi[12];
084   double *p__gen_ti;
085   double *p__gen_vi;
086
087   int component_stage;
088   int component_line;
089   int component_type;
090
091   void nll_4_dlg::Simulate(const double *c_1, const double *r_1, const double *i_1,
092              const double *ca_1, const double *cb_1, const double *la_1, const double *lb_1,
093              const double *c_2, const double *r_2, const double *i_2,
094              const double *ca_2, const double *cb_2, const double *la_2, const double *lb_2,
095              const double *c_3, const double *r_3, const double *i_3,
096              const double *ca_3, const double *cb_3, const double *la_3, const double *lb_3,
097              const double *c_4, const double *r_4, const double *i_4,
098              const double *ca_4, const double *cb_4, const double *la_4, const double *lb_4);
099
100   bool nll_4_dlg::error(char* message);
101   bool nll_4_dlg::user_alert(char* message);
102   bool nll_4_dlg::ValidateSetup();
103   bool nll_4_dlg::SaveCompValue();
104 };
105
106 #endif // !defined(AFX_NLL_4_DLG_H__31C1A78B_AC80_437A_B6E2_D1175A773A94__INCLUDED_))
```

C.2.8 nll_4_dlg.cpp

```
001 // nll_4_dlg.cpp : implementation file
002
003 #include "stdafx.h"
004 #include "nll_4.h"
005 #include "nll_4_dlg.h"
006 #include "nletl.h"
007 #include <stdlib.h>
008 #include <string>
009 #include <iostream>
010 #include <fstream>
011 #include <iterator>
012 #include <stdio.h>
```

```
013 #include <math.h>
014
015 using namespace std;
016
017 #ifdef _DE8UG
018 #define new DEBUG_NEW
019 #undef THIS_FILE
020 static char THIS_FILE[] = __FILE__;
021 #endif
022
023 // nll_4_dlg dialog
024
025     // **** EXTENSIVE DIALOGUE IMPLEMENTATION CODE NOT INCLUDED ****
026
027 void nll_4_dlg::Simulate(const double *c_1, const double *r_1, const double *i_1,
028             const double *ca_1, const double *cb_1, const double *la_1, const double *lb_1,
029             const double *c_2, const double *r_2, const double *i_2,
030             const double *ca_2, const double *cb_2, const double *la_2, const double *lb_2,
031             const double *c_3, const double *r_3, const double *i_3,
032             const double *ca_3, const double *cb_3, const double *la_3, const double *lb_3,
033             const double *c_4, const double *r_4, const double *i_4,
034             const double *ca_4, const double *cb_4, const double *la_4, const double *lb_4)
035             //const bool *o_1, const bool *o_2, const bool *o_3, const bool *o_4)
036 {
037   // -+- set up and run simulation -+-
038
039   m__prgProgress.SetRange(0, 1000);
040
041   SetDlgItemText(m__lblState.GetDlgCtrlID(), "Current Simulation State:    establishing line scenario(s).");
042
043   bool run_asp = false;
044   if(m__chkASP_val == 1) run_asp = true;
045
046   Soliton::nl_line LINE_1(1, atoi(m__txtNoStages1_val), c_1, r_1, i_1, ca_1, cb_1, la_1, lb_1,
atof(m__txtLoadR_val));
047
048   LINE_1.set_scenario(atof(m__txtTime_val) * 1E-6, atoi(m__txtSteps_val), atoi(m__txtWriteSteps_val),
run_asp,
049                 atof(m__txtGenOPI_val), p__gen_ti, p__gen_vi, atof(m__txt8iasAmp1_val),
atof(m__txt8iasFreq1_val));
050
051   Soliton::nl_line LINE_2(2, atoi(m__txtNoStages2_val), c_2, r_2, i_2, ca_2, cb_2, la_2, lb_2,
atof(m__txtLoadR_val));
052
053   LINE_2.set_scenario(atof(m__txtTime_val) * 1E-6, atoi(m__txtSteps_val), atoi(m__txtWriteSteps_val),
run_asp,
054                 atof(m__txtGenOPI_val), p__gen_ti, p__gen_vi, atof(m__txtBiasAmp2_val),
atof(m__txt8iasFreq2_val));
055
056   Soliton::nl_line LINE_3(3, atoi(m__txtNoStages3_val), c_3, r_3, i_3, ca_3, cb_3, la_3, lb_3,
atof(m__txtLoadR_val));
057
058   LINE_3.set_scenario(atof(m__txtTime_val) * 1E-6, atoi(m__txtSteps_val), atoi(m__txtWriteSteps_val),
run_asp,
059                 atof(m__txtGenOPI_val), p__gen_ti, p__gen_vi, atof(m__txtBiasAmp3_val),
atof(m__txtBiasFreq3_val));
060
061   Soliton::nl_line LINE_4(4, atoi(m__txtNoStages4_val), c_4, r_4, i_4, ca_4, cb_4, la_4, lb_4,
atof(m__txtLoadR_val));
062
063   LINE_4.set_scenario(atof(m__txtTime_val) * 1E-6, atoi(m__txtSteps_val), atoi(m__txtWriteSteps_val),
run_asp,
064                 atof(m__txtGenOPI_val), p__gen_ti, p__gen_vi, atof(m__txtBiasAmp4_val),
atof(m__txtBiasFreq4_val));
065
066   long step = 1;
067
068   double outcome_1 = 0.0;
069   double outcome_2 = 0.0;
070   double outcome_3 = 0.0;
071   double outcome_4 = 0.0;
072   double input_1 = 0.0;
073   double input_2 = 0.0;
```

```
074   double input_3 = 0.0;
075   double input_4 = 0.0;
076
077   SetDlgItemText(m__lblState.GetDlgCtrlID(), "Current Simulation State:    running.");
078
079   for(step = 1; step <= atoi(m__txtSteps_val); step++)
080   {
081     m__prgProgress.SetPos(1000 * step / atoi(m__txtSteps_val));
082
083     if(m__chkLine1_val) outcome_1 = LINE_1.vi_run(step, input_1);
084     if(m__chkLine2_val) outcome_2 = LINE_2.vi_run(step, input_2);
085     if(m__chkLine3_val) outcome_3 = LINE_3.vi_run(step, input_3);
086     if(m__chkLine4_val) outcome_4 = LINE_4.vi_run(step, input_4);
087
088     input_1 = outcome_2 + outcome_3 + outcome_4;
089     input_2 = outcome_1 + outcome_3 + outcome_4;
090     input_3 = outcome_1 + outcome_2 + outcome_4;
091     input_4 = outcome_1 + outcome_2 + outcome_3;
092   }
093
094   SetDlgItemText(m__lblState.GetDlgCtrlID(), "Current Simulation State:    complete.");
095
096   user_alert("Simulation process completed successfully");
097
098   //LINE_1.~nl_line();
099   //LINE_2.~nl_line();
100   //LINE_3.~nl_line();
101   //LINE_4.~nl_line();
102 }
```